ZONATION AND EMPLACEMENT OF THE NEWRY IGNEOUS COMPLEX, NORTHERN IRELAND

by

Paul Anderson

A thesis submitted to the University of Birmingham for the degree of DOCTOR OF PHILOSOPHY

School of Geography, Earth and Environmental Sciences
College of Life and Environmental Sciences
University of Birmingham
August 2014

ACKNOWLEDGEMENTS

I am firstly grateful to Carl Stevenson for remembering me when this PhD opportunity came along, after previously having been in correspondence. As a result Carl became my main supervisor and has provided much guidance and support throughout my time of study.

I would also like to thank my other supervisors, Mark Cooper (from the Geological Survey of Northern Ireland) and Rob Ellam (from the Scottish Universities Environmental Research Centre), for their input in deciding the initial aims of the project. Mark has additionally spent many days in the field with me, along with Ian Meighan, from which the resulting discussions have proved invaluable in bringing me up to speed with an intrusion that is rightfully referred to as a 'complex'! I am grateful as well to James Inman and Murray Hoggett, who enthusiastically helped me in the field as MSci students on successive years. My work has been aided greatly also by the field notebooks of Colm Hurley, kindly provided through John Reavy at University College Cork.

I would like to thank all the staff within the University of Birmingham Earth Sciences department for making me feel at home from early on. Many individuals have been particularly helpful, including Aruna Mistry for her technical assistance; Paul Hands for guidance in sample preparation and Andy Chambers for his opinions on my geochemistry results.

In addition I am very happy and grateful to have made many good friends during my time as a PhD student. Of these Plamen Andreev and Ed Fleming started on the same week and so have shared all the ups and downs. Other friends who started their projects before me (and thus provided guidance) include Ken McDermott, Craig Magee, Sarah King, Andrew Storey, Andy Rees and Ben Slater. Those who started after me (to whom I probably provided no guidance!) in turn include Joanne Murray, Carlos D'Apolito, Rosemary Dartnall, Ban To, Mahmoud Ja, Simiao Sun, Gary Clarke, Roland Sookias, Martin Ezcurra and again Murray Hoggett.

I am grateful always to my mum and dad. To my dad for inspiring me to want to learn more about the world from an early age and to my mum for still wanting to hear all about it! They were both keen to read a draft of my thesis, but unfortunately became stuck somewhere around 'Streckeisen (1976)'

Finally I am grateful to my fiancée, Holly Merrill, who has successfully taken over the practical side of my life during my time of 'writing up'. As well as this she has been an incredible support throughout and has been hugely helpful in forcing me to work evenings and weekends to get finished in time, against my poorer judgement!

ABSTRACT

The Newry Igneous Complex (NIC) in Northern Ireland comprises three largely granodioritic plutons, together with an intermediate-ultramafic body at its northeast end. Geochronology shows that the NIC becomes broadly younger to the southwest and towards the centres of individual plutons. Geophysical results from the recent Tellus Survey of Northern Ireland have been combined with petrology and geochemistry to establish 17 distinct zones within the NIC, which are interpreted to represent separately intruded magma pulses. A combination of Anisotropy of Magnetic Susceptibility (AMS), petrographical and field data shows that the NIC was emplaced as a series of laccoliths into a tension-releasing bend on a strike-slip fault. This regime is proposed to have been facilitated by two deep-seated crustal lineaments. Inflation is suggested to have occurred due to magma pressure during emplacement of each individual zone. At least five constituent parts of the NIC are interpreted to have been emplaced separately at successively higher crustal levels. Thus the intrusion is thought to represent a series of stacked laccoliths, produced by a southwestward migrating source.

CONTENTS

LIST OF FIGURES

LIST OF TABLES AND PHOTOGRAPHS

Tables

Photographs

CHAPTER 1: INTRODUCTION

1.1 'Granite'

1.1.1 An Overview

James Hutton first confirmed that granite was a once molten rock (Hutton, 1788). However, since then there has been much debate over how granitic bodies came to occupy sites within the Earth's crust. Theories on the origin of granites have ranged from the wholesale replacement of host rocks, termed *granitisation* (Egan, 1872; Nolan, 1877; Hull, 1881; Reynolds, 1942), to the now accepted idea of melting, upward transport and ultimate stalling of material from a lower source area (e.g., Nockolds, 1940; Atherton, 1993; Petford et. al., 2000; Brown, 2013). These processes can be broadly categorised as magma *generation*, *segregation*, *ascent* and *emplacement* (e.g., Petford et. al., 2000). The granite composition is also often the result of a process termed fractional crystallisation, whereby more basic components solidify and are removed from the molten rock, leaving an acidic melt (Bowen, 1919). This is possible at various stages prior to and during final emplacement (e.g., Meighan and Neeson, 1979).

1.1.2 Classifying granite

Pitcher (1997, p. 20) commented on the difficulty of classifying rocks of the "granite family" due to the vast number of possible processes and source rock compositions contributing to their current form. However, numerous classification attempts have been made. The most enduring of these was originally proposed by Streckeisen (1976) and Le Bas and Streckeisen (1991)

(see fig 1.1), which has been incorporated into the more recent British Geological Survey (BGS) (see Gillespie and Styles, 1999) and International Union of Geological Sciences (IUGS) (see Le Maitre et. al., 2002) classifications (fig. 1.1). Unlike many other schemes (e.g., Didier and Lameyre, 1969; Chappell and White, 1974; Ishihara, 1977), Streckeisen's considers only observed mineral proportions, without the complexities of rocks' petrogenetic relationships. The compositions included within this classification are broadly referred to as '*granitoids*' (see fig 1.1).

Within both Streikeisen's (1976) and the most recent BGS/IUGS classifications (Gillespie and Styles, 1999; Le Maitre et. al., 2002) the term *granite* applies to a very specific set of compositions, consisting of mainly quartz (20 – 60%) and alkali feldspar (35 – 90%), along with lesser plagioclase. Other categories, such as, *granodiorite*, *quartz monzonite* and *alkali feldspar granite*, etc, are in turn distinguished based on differing relative proportions of these minerals. However, the *granite* classification is often applied more loosely, incorporating all of the above, in order to simply distinguish these from more mafic igneous rocks (i.e., it can be interchangeable with the term 'granitoid'). As a very general rule, the term is used loosely when referring to felsic rocks of non-specific composition en mass (i.e., granite *sensu lato*) (e.g., Pitcher, 1997); whereas when detailed mineral proportions are brought into consideration the more specific classifications (i.e., Streikeisen, 1976; Gillespie and Styles, 2002; Maitre et. al., 2002) are applied.

1.1.3 From melt generation to emplacement: An overview of granite formation

Melt generation represents the earliest part of a magma's evolution (see Atherton, 1993; John and Stunitz, 1997; Weinberg, 1999; Petford et. al., 2000). This term refers to the initial process of melt production, which occurs by partial melting of a source area within the continental crust or underlying upper mantle (e.g., Meighan and Neeson, 1979; Petford et. al., 2000). *Segregation* in turn relates to how this melt is separated from other material within the source region. Such has been suggested to take place by gravity-driven compaction (e.g., McKenzie, 1984) and due to localised deformation, for example through deeply penetrating shear zones (e.g., Jacques and Reavy, 1994; Keleman and Dick, 1995; Petford et. al., 2000)

Ascent represents the stage during which magma rises through the crust and/or upper mantle. This can culminate in either final emplacement, or in the temporary storage of magma prior to further ascent (e.g., Reid, 2003). The process is affected by numerous factors, including buoyancy and rheological properties of the magma and host rock; together with tectonic forces (Bateman, 1984; Weinberg, 1996; Petford et. al., 2000;).

Finally, *emplacement* refers to how an intrusive igneous rock comes to be accommodated in its current crustal position (i.e., put *in place)*, following the point at which the previous controls prevent further ascent. Many granite studies focus on this stage, although it has increasingly been demonstrated that determining emplacement requires at least some understanding of how the preceding processes operated.

For a start, the separation between ascent and emplacement may not always be straightforward. For example, igneous rock preserved as a dyke reflects both ascent *and* emplacement, as the dyke is *emplaced* simply when magma ascent halts (Petford, 1996; Clemens, 1998). However, in the case where upper crustal igneous rock comprises discrete *plutons* it is unlikely that the original melt ascended in exactly this form (Leake, 1978). Numerous studies (e.g., Harry and Richey, 1963; Pitcher, 1979; Petford 1996) suggest that plutons in the upper part of the crust are most likely to have been fed by dykes or at least smaller magma batches (i.e., diapirs – see Paterson and Vernon, 1995). Therefore, emplacement can be considered separately from ascent (e.g., Leake, 1978).

Nevertheless, other studies have suggested that all four of the processes involved in granite formation are closely linked. This has been explained through structural connectivity of the magma source area and site of intrusion (e.g., D'Lemos et. al., 1992; Jacques and Reavy, 1994; Hutton and Alsop, 1996; Stevenson et. al., 2006; Weinberg et. al., 2009; Cooper et. al., 2013). Such has been inferred through the interaction of recognised shear zones with deep-seated, geophysically-detected crustal lineaments (see Chapter 1.3) (e.g., Jacques and Reavy, 1994; Cooper et. al., 2013). The resulting transcrustal connection has been suggested to facilitate magma melting and segregation, promote ascent and control the sites in which emplacement takes place (see Jacques and Reavy, 1994).

1.2 The petrogenesis of granite

In the context of this study the term *petrogenesis* relates to how an igneous rock was originally formed (see Wilson, 1989). Hence, this encompasses the process of magma generation, along with any other influences on the composition of the melt prior to its final crystallisation within the emplacement site.

1.2.1 Magma generation

Since the source regions of granitic intrusions can be located in the continental crust or upper mantle, the processes through which melt generation occurs are highly variable. However, geothermal gradients dictate that melting in these locations is unlikely in the absence of other influences (Tatsumi, 1986; Thompson, 1999; Petford et. al., 2000; Conder et. al., 2002). In the crust melting can occur in the form of heat advection by intruded or underplated basic magmas (e.g., Huppert and Sparks, 1988; Koyaguchi and Kaneko, 1999). Conversely, in the the upper mantle melting has been suggested to result from the presence of volatiles originating from a subducted slab (Tatsumi, 1986) or more recently from decompression melting as a result of local mantle dynamics (Conder et. al., 2002).

Within the continental crust generated melts can potentially be granitic in composition (e.g., Thompson, 1999; Petford et. al., 2000; Searle, 2010). This is largley due to the abundance of quartz in the continental crust, as well as relatively high proportion of hydrous minerals (micas and amphiboles), which have been experimentally shown to produce significant acidic melt fractions at temperatures of ca. 800 – 950°C (Vigneresse et. al., 1996; Petford et. al., 2000). On the other hand, the ultramafic composition of the upper mantle, means that production of primary

granitic melts from here is extremely unlikely (see McBirney, 1993; Hall, 1996). In some cases partial melting of this source area can yield andesites (e.g., Tatsumi, 1982; Hirose, 1997; Grove et. al., 2002; Carmichael, 2002; Parman and Grove, 2004), but otherwise the resulting magmas are dominantly basaltic (e.g., Crawford et. al., 1987). Granite production from mantle melts will therefore require the operation of one or more *secondary* processes.

1.2.2 Secondary processes influencing magma composition

A number of different processes have been shown to alter the composition of primary, basic magmas, including fractionational crystallisation; liquid immiscibility; zone refining; contamination from crustal material and mixing with other magmas (e.g., Bowen, 1919; Gamble, 1979; Meighan and Neeson, 1979). For the purposes of the current study crystal fractionation and magma mixing are the most relevant of these.

The former occurs during crystallisation of magma, whereby the composition of crystals removed from the melt differs to that of the remaining liquid (e.g., Bowen, 1919; Meighan and Neeson, 1979). Since silica-poor components (olivine and clinopyroxene) are often the first to crystallise (at highest temperatures), the process will generally lead to progressive silica enrichment within the melt (i.e., it becomes more acidic). This is termed magmatic *evolution*. It takes place to a larger extent if crystals are continuously removed from the magma: a process specifically referred to as *fractional crystallisation* (Bowen, 1919; Meighan and Neeson, 1979).

The process of mixing involves the partial or total homogenisation of two or more separate magma compositions (e.g., Gamble, 1979). This is most likely to occur in basic melts and is rarer in acidic melts due to their comparatively high viscosities. However, numerous authors have proposed that some intermediate magmas may be the products of mixing between respective basic and acidic end members (e.g., Yoder, 1973; Eichelberger, 1975, Reid et al., 1983, Frost and Mahood, 1987 and Ratajeski et al., 2001). Nevertheless, much recent work shows that the processes controlling such inferred mixing relationships are either poorly understood (e.g., Ratajeski et al., 2001, Eichelberger et al., 2006; Reubi and Blundy, 2009) or require specific conditions (Farner et. al., 2014). For example Frost and Mahood (1987), together with Paterson et. al. (2004) suggested that the rapid cooling of basic material within a acidic host would preclude mechanical mixing. On the other hand, the work of Farner et. al. (2014) implied that the latter was possible, but only during an extended low temperature cooling phase of a magma body. Therefore, whilst crystal fractionation represents a likely control on the composition of an acidic melt, this is not necessarily the case for magma mixing.

1.2.3 Magma pulses and pluton construction: the overlap between petrogenesis and emplacement

Whereas some early studies (e.g., Walker, 1924; Grantham, 1928) assumed that compositional variation in magmas took place mainly within the emplacement site, more recent work shows that variation can occur extensively during any of the preceeding stages (e.g., Huppert and Sparks, 1988; Sawyer, 1996; Koyaguchi and Kaneko, 1999; Annen et. al., 2006; Ruprecht et. al., 2012; Solano et. al., 2012). This means that many zoned plutons do not represent the result of in situ differentiation,

but are instead the end products of a more complex magmatic history. Abrupt changes in composition within these have in turn been shown to reflect periodic intrusion of magmas (i.e., magma *pulses*) that have differentiated in an underlying location, for example by fractional crystallisation (e.g., Meighan and Neeson, 1979; Coleman et. al., 2004; Glazner et. al., 2004).

As a result, it is proposed that even secondary petrogenetic processes may not be significant within a magma's final emplacement site. Nevertheless, as has been previously mentioned, the events of magma generation, segregation, ascent and emplacement of a granitic body may be linked on a larger scale through related structural controls. (see Hutton, 1982, 1988; D'Lemos et. al., 1992; Jacques and Reavy, 1994; Hutton and Alsop, 1996; Weinberg et. al., 2004; Stevenson, 2006; Cooper et. al., 2013). Therefore, in order to fully understand the present form of an igneous complex, it is necessary to adopt a holistic approach, whereby a complete structural and petrological history is considered.

1.3 Modelling the emplacement of granite

Recognition of what has now become known as the granite '*space problem*' was first documented in 1835 (Pitcher, 1997). The basis of such is that explanation is required for how the vast amounts of granites observed in the crust came to be accommodated. For example, the Dinkey Creek Pluton, part of the Sierra Nevada Batholith, California, has an areal extent of 800 km^2 (Petford et. al., 2000). Early theories which neatly resolved the space problem through the wholesale replacement (*granitisation*) of host rocks (e.g., Reynolds, 1942) have been shown to be energetically implausible for the majority of settings (see Pitcher, 1997). Hence, accommodation requires generation of space within the crust.

1.3.1 Forceful and Passive emplacement

The terms *forceful* and *passive* emplacement classically relate to the way in which space for an intrusion is generated. During passive emplacement magma flows into tectonically generated fractures and/or voids due to the negative pressure gradient resulting from opening of these spaces (e.g., Pitcher and Berger, 1972; Hutton, 1988; Paterson and Fowler, 1993; Pitcher, 1997; Stevenson, 2009). On the other hand, forceful emplacement represents the generation of space through magma-driven pressures, which will cause deformation and/or displacement of the magma itself and the surrounding host rocks (e.g., Johnson and Pollard, 1973; Hutton, 1988; McCaffrey and Petford, 1997; Molyneux and Hutton, 2000; Stevenson, 2009).

However, the above represent end member scenarios, whereas in reality an intrusion will often show evidence for both tectonic facilitation and forceful emplacement of magma (e.g., Hutton, 1988; Brun et. al., 1990; Stevenson, 2009; De Saint Blanquat et. al., 2011). The relative importance of each is controlled by the interplay between the rate of tectonic space creation and the magma *body forces*. Hutton (1997) listed the latter as buoyancy; confining pressure; pressure due to volume increase on melting and regional tectonic stress at the source. These forces have been shown to cause compressional stress within magma at the emplacement site, resulting in strong, often contact-parallel foliations in this (e.g., Cloos 1925; Hutton, 1988; Paterson et. al., 1989; Cruden, 1990; Molyneux and Hutton, 2000; Yan et. al., 2011). The displacement of host rocks surrounding a forcefully emplaced pluton will also result in ductile and/or brittle deformation (e.g., Pollard and Johnson, 1973; Petford et. al., 2000; Stevenson et. al., 2007a).

Although this deformation is a key element of the forceful emplacement model, it has been shown that the space created from such is often not resolvable in terms of the extent of deformation (e.g., Hutton and Siegesmund, 2001; Stevenson et. al., 2007a; Magee et. al., 2013). This may be partly due to displacement occurring in an orientation that is not recorded in the field (e.g., vertically, when the overlying host rocks have been removed by erosion – Hutton and Siegesmund, 2001; Stevenson et. al., 2007a). Other authors have additionally shown that volume loss from the host material can occur due to thermal metamorphism (e.g., Yoshinobu and Girty, 1999) or fluid expulsion from poorly lithified sediments (Magee et. al., 2013).

On the other hand, passive emplacement is traditionally associated with limited deformation of the host rocks and subtle deformation of the magma relating only to its flow towards the generated space (e.g., Kingsley, 1931; Richey, 1932; Chapman and Chapman, 1940). Resulting fabrics within the intrusion will thus usually be discordant to the regional structures displayed within the host rocks (see Richey, 1932). However, this idealised scenario assumes that the magma is not affected by regional tectonics. As is elaborated subsequently, numerous more recent studies have shown that fabrics and regional structures are often intimately related (e.g., Pitcher and Berger, 1972; Hutton, 1982, 1988; Hutton and McErlean, 1991; Hutton and Reavy, 1992; McCaffrey, 1992; Jacques and Reavy, 1994; Stewart et. al., 2001; Stevenson, 2006; Stevenson, 2009; Cooper et. al., 2013; Rabillard et. al., 2014).

1.3.2 Emplacement and regional tectonics

Since the advent of plate tectonics there has been much further scope for understanding the tectonic facilitation of emplacement of igneous intrusions. In particular this has revealed the close relationship between shear zones and magma ascent/intrusion (e.g., Hutton, 1982; Guineberteau et. al., 1987; Brun et. al., 1990; Petford et. al., 2000; Rabillard et. al., 2014). For example, Hutton (1982) suggested that the Caledonian Main Donegal Granite in Ireland was emplaced synchronously with operation of a major sinistral shear zone. The presence of granite melt within the shear zone was interpreted to cause the shear zone to bend and split lengthways, in turn

resulting in a local extensional regime (see fig. 1.2). This facilitated final emplacement of the granite as a pluton. Due to the synchronisity between tectonic and magmatic events, such an intrusion is referred to as *syn-tectonic*.

Stevenson et. al. (2006) further showed that the Main Donegal Batholith as a whole is also related to a deeper-seated crustal structure, termed the *Donegal Lineament* (see Cooper et. al., 2013). The structure is thought to represent a Pre-Caledonian fault, which was reactivated along with 6 smaller basement faults, leading to the creation of dilational space. This provided a conduit for magma to ascend and ultimately be emplaced within the main shear zone.

Numerous other authors have suggested the importance of *transcrustal* structures such as this in terms of facilitating emplacement (e.g., Hutton, 1992; Hutton and Reavy, 1992; Jacques and Reavy, 1994; Hutton and Alsop, 1996; Dehls et. al., 1998; Chernicoff et. al., 2002; Weinberg et. al., 2004; Chew and Stillman, 2009; Cooper et. al., 2013). Much of this work relates to transcrustal structures within the UK and Ireland, which will be accounted for which the subsequent Geological Setting chapter.

Hutton (1997) suggested that these structures may allow confining pressure at the source to be transferred to the emplacement site through the ascending magma. Hence, magma pressure would in this case largely be a component of the regional stress, rather than an independent factor. In this sense emplacement could never truly be a *passive* event (Pitcher, 1997).

Within some syn-tectonic granites magma pressure seems to have been a major influence. This has been observed through tectonically accommodated intrusions that have additionally been forcefully enlarged (Brun and Pons, 1981; Brun et. al., 1990; Guineberteau et. al., 1987; Petford et. al., 2000; Morgan et. al., 2013), as well as those emplaced into compressional areas, for which space creation will often be dominantly forceful (e.g., Blumenfeld and Bouchez, 1988; Hutton, 1992, 1997; Ingram and Hutton, 1994; Simancas et. al., 2000; Miller and Paterson, 2001; Mahan et. al., 2003; Ferre et. al., 2012). Hence, although tectonic facilitation and forceful emplacement may be fundamentally linked, the relative importance of each in terms of their influence at the site of emplacement of a syn-tectonic intrusion can be highly variable.

1.3.3 Classical emplacement models

Several classical models are still used to account for emplacement, although it is important to note that these were developed before establishment of modern plate tectonic theory. Hence these largely represent simplified scenarios that do not consider the tectonic regime in great detail. Nevertheless, when combined with the information on the tectonic regime such models can assist in determining a more holistic view of emplacement. Four commonly proposed traditional emplacement models are outlined below:

Cauldron subsidence

This represents the classic mechanism for passive emplacement, being essentially the plutonic equivalent of caldera collapse (e.g., Clough et.

al., 1909). The model thus involves fracturing and subsidence of a large (km-scale), subterranean block into an underlying magma chamber (fig. 1.3a) (e.g., Kingsley, 1931; Richey, 1932; Chapman and Chapman, 1940). Displacement of the block creates a pressure gradient so that magma is drawn up the steep surrounding fractures and into the space created above it, resulting in a thick, steep-sided, *stock*-shaped intrusion. Because magma body forces play little role here, cauldron subsidence is considered to be a passive emplacement mechanism.

The mechanism of cauldron subsidence has also been invoked more recently (e.g., Oldershaw, 1974; Myers, 1975; Ewart et. al., 2002; Emeleus et. al., 2012; Burchardt et. al, 2012). However, it has additionally been subjected to much criticism. Firstly, Stevenson et. al. (2007a) used field evidence and anisotropy of magnetic susceptibility results to show that the Eastern Mournes Granite, Ireland, which has been thought to represent one of the type-examples of cauldron subsidence (Richey, 1932), was more likely inflated as a laccolith (see below). Other work additionally casts doubt on the overall viability of the cauldron subsidence mechanism. For example, the classic scenario requires an underlying magma chamber of even larger proportions than the pluton created from the process, which is unaccounted for in the model (Anderson, 1936). Furthermore, suitable candidates for subsided blocks are rarely identified (Stevenson et. al., 2007a).

Ballooning

The original form of the *ballooning* model was termed *laccolithic* (or *lopolithic*) *inflation* (fig. 1.3b). This involved an initially subhorizontal sheet-like body doming upwards (or downwards in the case of a lopolith) as further magma is added from a central feeder dyke (e.g., Gilbert, 1877; Johnson and Pollard, 1973; McCaffrey and Petford, 1997; Kerr and Pollard, 1998; Petford et. al., 2000). This doming (termed *inflation*) causes uplift and shouldering aside of the surrounding host rocks, which is typically recorded through their ductile and/or brittle deformation. The mechanism is therefore a forceful one, as it is the body forces of the magma that determine its intrusion and interaction with the host rocks (see Hutton, 1997). A key distinguishing property of this mechanism is the fact that inflation occurs in situ, due to the addition of magma via a stationary feeder dyke (e.g., Gilbert, 1877; Johnson and Pollard, 1973; McCaffrey and Petford, 1997).

Unlike the previous model, clear evidence for laccolithic inflation can be observed in the field. For example, the classical model of Gilbert (1877) was based on clear field data from the Henry Mountains in Utah. Johnson and Pollard (1973) elaborated on this work to infer how magma was intruded along near-horizontal bedding planes, before either crystallising as sills or expanding vertically to produce the laccoliths observed in this area.

However, many recent studies use the term *ballooning* to refer to more generalised in situ inflation of plutons (e.g., Holder, 1979; Brun and Pons, 1981; Ramsey, 1989; Brun et. al., 1990; Clemens, 1998; Molyneux and

Hutton, 2000; Shan et. al., 2004; Morgan et. al., 2013). This avoids the assumption that the intrusion initiates as a sub-horizontal sheet. For example, the Flamanville Granite in northwest France is considered to represent a ballooning type pluton, although this is thought to have dominantly inflated outwards following relatively steep initial intrusion (Brun et. al., 1990).

Evidence for the ballooning process in general includes the presence of concentric igneous foliations. These are caused by addition of magma to the centre of the pluton, which flattens earlier intruded material against its edges (e.g., Molyneux and Hutton, 2000; Pons et. al., 2006; Stevenson 2007a; Plissart et. al., 2012; Roni et. al., 2014). The forceful nature of the mechanism also means that host rock displacement will occur, resulting in brittle and/or ductile deformation surrounding a pluton (see above). The corcordance of host rock bedding/cleavage with the boundaries of a pluton also provides evidence of the ballooning process. This shows that the former features have been brought into alignment with the expanding pluton (e.g., Gilbert, 1877; Johnson and Pollard, 1973; Holder, 1979; Molyneux and Hutton, 2000; Pownall et. al., 2012).

However, interpretation of the ballooning process may be complicated by the fact that some work suggests a potential crossover between this and other emplacement mechanisms. For example, Cruden (1998) and Cruden and McCaffrey (2001) argued that the intrusion of many tabular intrusions (i.e., laccoliths and lopoliths) is facilitated by ‘floor subsidence’, thus providing parallels with the passive mechanism of cauldron subsidence described

above. As a result, it is important to note that traditional emplacement models presented here represent end member scenarios only.

Diapirism

Magmatic diapirism (or simply *diapirism*) represents another forceful emplacement mechanism, through which similar features to those outlined above could potentially be produced. Diapirism involves a body of magma ascending from deeper in the crust by displacing overlying rocks (e.g., Mrazec, 1927; Grout, 1945; Ramberg, 1981; Bateman, 1984) (fig. 1.3c). The magma body is termed a *diapir*, which is derived from Greek word meaning 'to pierce through', describing its relationship to the host rocks. This therefore differs from ballooning in that the resulting pluton is not produced in situ.

Experimental modelling by Cruden (1990) revealed a variety of ascent-related strain patterns that would be specific to diapirs. These included the concentric foliations discussed above, but also near-vertical linear fabrics within the centre of the pluton. Other authors (e.g., Clemens et. al., 1997) infer that plutonside-up shear structures should also be observed, due to the relative movement between the diapir and its host rocks.

However, diapirism is strictly only an ascent mechanism, meaning that subsequent emplacement of the magma body could represent a potentially separate structural event (e.g., England, 1990; Paterson and Vernon, 1995; Paterson et. al., 1998; Miller and Paterson, 1999; Galadí-Enríquez et. al., 2003; He et. al., 2009). In this case, it has been suggested that the typical

fabric characteristics of a diapir may be overprinted by processes that occur during emplacement (Paterson and Vernon, 1995; Paterson et. al., 1998; Miller and Paterson, 1999; He et. al., 2009).

Despite this, the traditional ('*Hot Stokes*') diapirism model as a whole has been heavily criticised by many authors (e.g., Marsh, 1982; Schwerdtner, 1990; Clemens and Mawer, 1992; Petford, 1996; Clemens, 1998). This is largely due to the relatively low ductility of host rocks throughout most of the crust. Marsh (1982) suggests that a single diapir would reach a point about halfway through the lithosphere where its own heating of the host rocks would be insufficient to reduce the viscosity of these by the required amount to allow further ascent.

The diapir model has in turn been defended from such criticisms by the suggestion that diapirs may ascend along pre-heated pathways (Miller and Paterson, 1999). Furthermore, ascent of multiple magma batches within these pathways has been proposed to produce the observed incremental assembly of some plutons (Bateman, 1985; Paterson and Vernon, 1995; Miller and Paterson, 1999; He et. al., 2009). In this case the final intrusion has been termed a *nested diapir* (e.g., Paterson and Vernon, 1995).

Here there may again be a crossover between processes. Millar and Paterson (1999) suggest that ascending diapirs may only differ from dykes in terms of their length to width ratios. They regarded a length:width of less than 100 as being representative of a diapir, with anything larger representing a

dyke. Furthermore, proponents of the nested diapir model acknowledge that such intrusions may show a degree of in situ inflation (e.g., Bateman, 1985; Paterson and Vernon, 1995); whilst some (e.g., Van den Eeckhout (1986, p. 162; Vernon and Paterson, 1993) suggested that some could show a "non-piercing" (concordant) relationship with their host rocks. Hence, a ballooning, dyke-fed pluton may not significantly differ from one that has been fed by multiple, very small-scale diapirs.

Stoping

This process involves magma rising through the crust by shattering and incorporating the overlying rocks (Daly, 1903; Marsh, 1982). Therefore, in its traditional form the stoping model is again effectively an ascent mechanism, although some authors have suggested that the process could also have a significant influence on final emplacement (e.g., Daly, 1933; Marsh, 1982; Miller et. al., 2009; Burchardt et. al, 2012).

The incorporation of host rocks can be seen to have occurred in numerous igneous intrusions around the world. However, there are several theoretical problems with the process of stoping being a primary process in the ascent and emplacement of magma. Glazner and Bartley (2006) identified five of these problems, which are as follows:

1) A lack of xenoliths within studied plutons, which would be expected to be abundant if magma had arrived at its emplacement sites by stoping.

2) A large amount of incorporated host rock material would be likely to trap magma from within the chamber, producing pluton-scale ‘magmatic breccias’. This would prevent further ascent of magma, making the stoping process inefficient. More importantly, though, these ‘magmatic breccias’ are not seen in the field.
3) The distribution of fragmented xenoliths within a magma chamber would be expected to be fractal, with small particles settling more slowly within the body, making these abundant at the pluton edge. However, most plutons do not exhibit numerous xenoliths at their contacts.
4) Although the geochemistry of some plutons indicates that they have assimilated large amounts of crustal material, others have geochemical signatures that imply very little crustal contamination. Stoping cannot be the primary process responsible for the ascent and emplacement of these plutons.
5) For intrusions that have been emplaced as pulses, where there is a time gap between intruded pulses (as can often be demonstrated) classical stoping cannot be a significant process as only a relatively small volume of magma will be molten at any one time, and it is only this molten materal that can facilitate the setttling of stoped blocks.

As a result, Glazner and Bartley (2006, p. 1185) concluded that stoping is not likely to be a “volumetrically significant” process in the emplacement of

plutons. Instead the authors argued that plutons with abundant xenoliths reflect incremental intrusion between now isolated fragments of wall-rock.

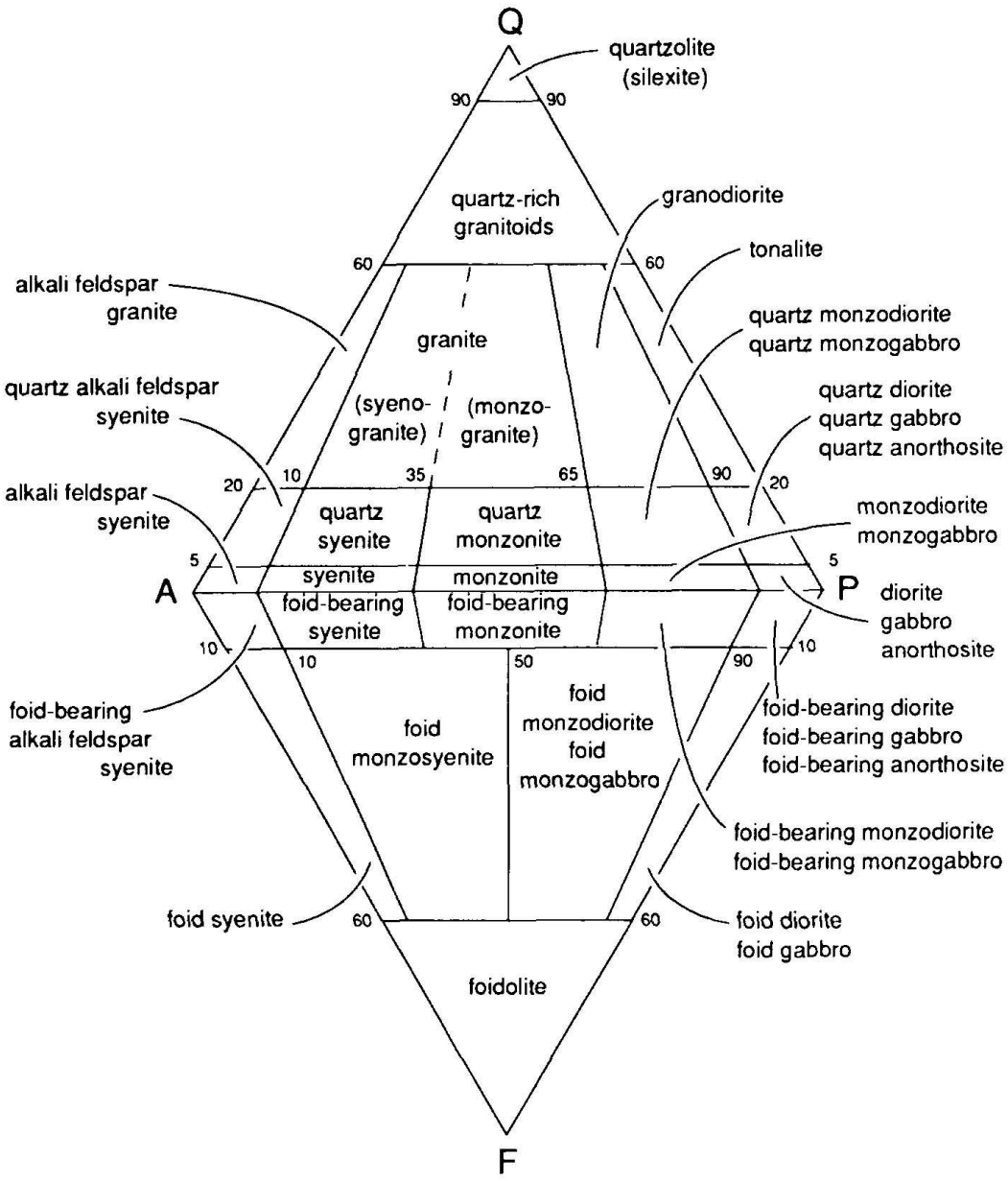

Fig 1.1: Classification of granitoids based on original by Strekeisen (1976) (Le Bas and Streckeisen, 1991)

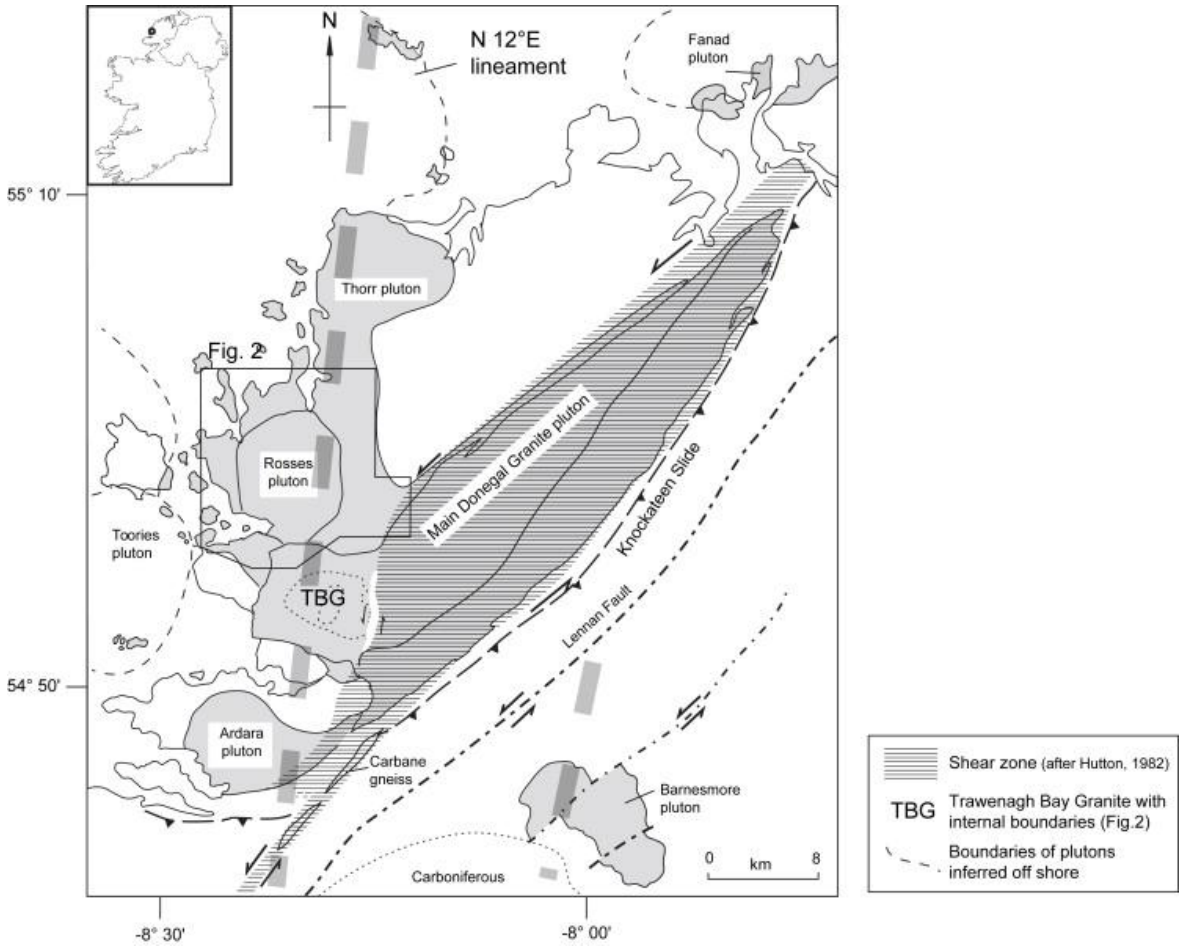

Fig 1.2 (above): Plutons within the Donegal Batholith, highlighting the relationship of the local shear zone and N-S trending Donegal Lineament (Stevenson et. al., 2006; modified from Hutton, 1982)

Fig 1.3 (right): Three classical models for emplacement of a pluton: **a**: Cauldron subsidence (after Richey, 1932)
b: Laccolithic inflation (after Gilbert, 1877)
c: Diapirism (after Ramberg, 1981)

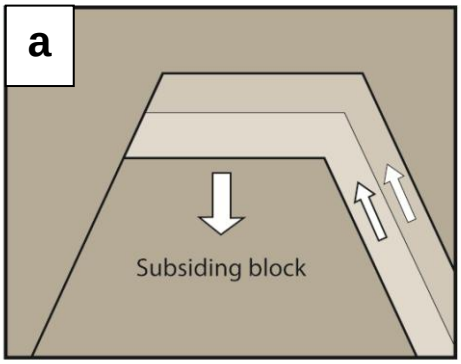

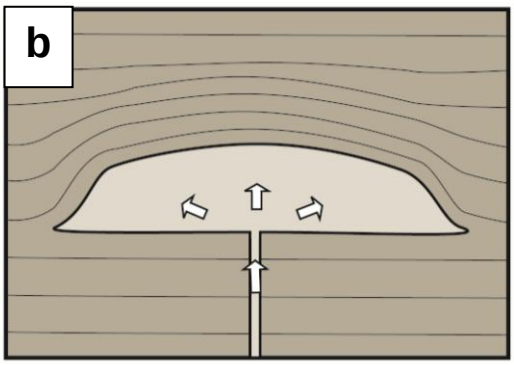

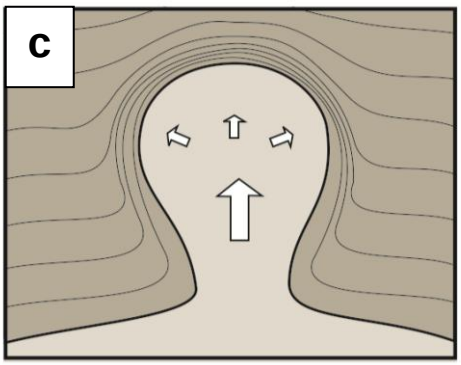

CHAPTER 2: GEOLOGICAL SETTING

This study focuses on the emplacement of the Newry Igneous Complex (NIC), which is predominantly located within Northern Ireland, although a small part straddles the border with Ireland (GSNI, 1997, Cooper and Johnson, 2004) (see section 2.2). The NIC represents one of the late Caledonian *Newer Granites*, which were emplaced as a result of continental collision between Avalonia, Laurentia and a third landmass, Baltica (see Dewey and Strachan, 2003; Soper and Woodcock, 2003). The suite distinguishes these intrusions from other Caledonian granites formed during closure of the Iapetus Ocean prior to this collision (Brown et. al., 2008). The NIC is situated on Laurentian crust although is relatively close to the Iapetus Suture separating this from Avalonian crust (e.g., Bluck, 1985; GSNI, 1997; Cooper and Johnson, 2004) (see fig. 2.1).

2.1: Regional context

2.1.1: Late Caledonian tectonics

Initial convergence between Avalonia and Laurentia is thought to have been largely orthogonal (e.g., Bluck, 1985). By the time the land masses came together, though, there is evidence that the movement between the two was sinistrally transtensional (e.g., Bluck, 1985; Soper and Woodcock, 1990, 2003; Soper et. al., 1992; Dewey and Strachan, 2003; Brown et. al., 2008). Soper and Woodcock (1990) explained this transition by invoking an early stage, anticlockwise 'soft docking' of Avalonia and Laurentia in the Silurian and Early Devonian. This has been referred to as a period of 'sinistral convergence' (Soper and Woodcock, 2003). As final docking occurred the initially 'soft' collision would have become tectonic and

a setting of sinistral transtension developed (Soper and Woodcock, 1990, 2003; Brown et. al., 2008).

The timing of these processes is not precisely known. Deduced rates of sedimentation and magmatisim within the region have been used to suggest that final docking between Avalonia and Laurentia occurred at approximately 420 Ma (Soper and Woodcock, 2003; Brown et. al., 2008), whilst the thermal history of these rocks implies that this took place at around 430 Ma (Stone et. al., 2004). Nevertheless, initial sinistral convergence (or 'soft docking') may have commenced as early as 440 Ma, at least for some parts of the margin (Kemp, 1987; Soper and Woodcock, 1990; Soper and Woodcock, 2003; Brown et. al., 2008).

Intrusion of the NIC, as well as a number of other granites in the area took place during the period of sinistral transtension following final docking of Avalonia and Laurentia (see Brown et. al., 2008; Miles et. al., 2013). These therefore represent *post-subduction* intrusions and part of the later Caledonian Newer Granite Suite (see above).

2.1.2: The Newer Granite and Trans-Suture Suites

The Newer Granite suite comprises many Silurian-Devonian calc-alkaline plutons, together with a number of associated volcanic complexes (see Soper, 1986; Brown, 2008). These have been shown to be of predominantly *I-type* origin (Brown, 1979), although $^{87}Sr/^{86}Sr$ isotope ratios imply significant input from a sedimentary source within some of the intrusions close to the Iapetus Suture (e.g., Brown et. al., 2008; Miles et. al., 2013). Hence the magma is considered to have been mainly

derived from lithospheric mantle and/or lower crustal protoliths (e.g., Stephens and Halliday, 1984; Halliday et. al., 1985; Tarney and Jones, 1994; Fowler et. al., 2001), along with a lesser amount of sedimentary crustal material (e.g., Brown et. al., 2008; Miles et. al., 2013) (see below).

Many models have been put forward to account for the origin of this magmatism (see Miles et. al. (2013) for full discussion). These range from volatile loss within an underlying oceanic slab (e.g., Thirlwall, 1981), to the now more accepted idea of crustal underplating with lamprophyric material during lithospheric thinning (Atherton and Ghani, 2002; Oliver et. al., 2008; Neilson et. al., 2009; Cooper et. al., 2013; Miles et. al., 2013). The lamprophyres may have both directly supplied the Newer Granite Suite, as well as causing partial melting of crustal material which itself supplied the suite (e.g., Miles et. al., 2013).

The emplacement sites of the Newer Granites can be accounted for through tectonic processes. As discussed previously (see Chapter 1), a number of these plutons can be linked to deep-seated pre-Caledonian lineaments (e.g., Hutton, 1992; Hutton and Reavy, 1992; Jacques and Reavy, 1994; Hutton and Alsop, 1996; Dehls et. al., 1998; Stevenson et. al., 2006; Chew and Stillman, 2009; Cooper et. al., 2013). Such lineaments may have been reactivated during sinistral transtension, allowing the ascent of magma within themselves and several intersecting Caledonian shear zones (e.g., Stevenson et. al., 2006). Hence, the shear zones would ultimately determine emplacement sites, although much of the ascent and possibly even melt generation (in the case of S-type magmas) would have been facilitated by deeper crustal structures (e.g., Jacques and Reavy, 1994).

Subdivisions of the Newer Granite Suite

Volumetrically granodiorite represents the most common component of the Newer Granite Suite (e.g., Brown et. al., 2008). However, systematic chemical, isotopic and age variations have been recorded across the intrusions, leading some authors to distinguish several subgroups. These have been categorised (from north to south) as the Argyll and Highlands Suite; the Cairngorms Suite; the South of Scotland Suite and the Trans-Suture Suite (see Brown et. al., 2008; Miles et. al., 2013) (fig 2.2).

The Trans-Suture Suite: The Trans-Suture Suite incorporates intrusions from the Lakes-Leinster Terrane and the Southern Uplands-Down-Longford Terrane, which exist on either side of the Iapetus Suture (see fig. 2.2). This includes the NIC; the Shap and Cheviot plutons in northern England as well as the Criffel-Dalbeatie and Cairnsmore of Fleet plutons in Scotland.

The suite has traditionally been distinguished by its S-type isotopic characteristics (e.g., Stephens and Halliday, 1984; Stone and Evans, 1997). For example, the Cairnsmoor of Fleet and Cheviot intrusions yield εNd values of -3.0 to -3.4; and -4.2 respectively, which are indicative of significant crustal contamination (Halliday, 1984). On the other hand εNd values obtained for the Criffel-Dalbeattie pluton vary between -0.6 and -3.1 (Halliday, 1984). This has been used to suggest that the latter exhibits an I-type marginal area along with an S-type core (Stephens et. al., 1985; Stephens, 1992).

The NIC differs from these along-strike correlatives in that all the isotopic evidence for this intrusion supports an I-type source. Firstly, Dempsey et. al., (1990) obtained an εNd value of -0.5 from the northeast pluton of the complex. Halliday et. al. (1979) also derived 16 initial $^{87}Sr/^{86}Sr$ ratios from across the NIC, which ranged from 0.7051 to 0.7059. In comparison a typical mantle value of this ratio is 0.704, whilst continental crust often shows values of around 0.720 (e.g., Yang et. al., 2005). These were consistently lower than those obtained by the same authors from other Trans-Suture Suite granites, excluding the partly I-type Criffel-Dalbeattie pluton. This indicates a predominantly I-type origin for the NIC, making the intrusion anomalous amongst its correlatives (e.g., Halliday et. al., 1979; Meighan and Neeson, 1979).

The S-type nature of the Trans-Suture Suite has been further supported by the recent work of Miles et. al. (2013), who used both zircon oxygen isotope ($\delta^{18}O$) compositions and zircon Hf model ages to imply a significant input of older crustal material to the Criffel-Dalbeattie, Shap and Cairnsmore of Fleet plutons. The authors linked intrusion of these to the presence of deep crustal *hot zones* (e.g., Annen et. al., 2006), which may have originated due to underplating lamprophyres. The apparent I-type nature of the NIC is inconsistent with a large contribution from such hot zones, but does not preclude a more direct influence from the lamprophyres (i.e., through differentiation of these).

Despite its anomalous isotopic composition, the NIC exhibits much closer age relationships with other intrusions within the Trans-Suture Suite. This has been dated through the U-Pb zircon technique at 423 ± 7 Ma (Meighan et al., 2003);

whereas the Criffel and Shap intrusions are dated at 410 ± 6 Ma and 416 ± 5 Ma respectively from this technique (Miles et al., 2013). The current study provides a new set of ages for the NIC, which places it closer in age to the Criffel and Shap intrusions than previous work suggests (see Chapter 4). As a result, the NIC can be grouped with the other Trans-Suture Suite granites in terms of its contemporaneity with late Caledonian sinistral transtension (see Soper and Woodcock, 2003; Stone et. al., 2004; Brown et al., 2008).

2.1.3: The Southern Uplands- Down-Longford Terrane

The NIC is part of the *Southern Uplands-Down-Longford Terrane*, which extends across Northern Britain and Ireland (see Anderson, 2004). This terrane reflects deposition and deformation associated with final closure of the Iapetus Ocean and subsequent tectonics. It represents the southernmost edge of Laurentia, separated from the Avalonia Leinster-Lakes Terrane by the Iapetus Suture (see fig. 2.2) (Bluck, 1985; GSNI, 1997; Cooper and Johnson, 2004).

The terrane consists of Ordovician and Silurian greywackes, overlying deep-water shales, cherts and basalts (e.g., Leggett et. al., 1979; Barnes et. al., 1987; Cooper and Johnson, 2004). These units are steeply dipping and are sometimes overturned (Barnes et. al., 1987). They are also repeated numerous times throughout the terrane, being separated by oblique-slip reverse faults (Leggett et. al., 1979; Leggett, 1987). The majority of these fault-bounded tracts young to the north, whereas the entire sequence is younger in the south, leading many authors to deduce that the terrane represents an accretionary prism (e.g., Leggett et. al., 1979;

Oliver and Leggett, 1980; Bluck, 1985; Leggett, 1987; Needham and Knipe, 1986; Anderson, 2004).

However, there are other authors who argue that these rocks have a different origin. For example, Murphy and Hutton (1986) suggested that they represent turbidites produced from deposition within a post-subduction basin. These authors explain the presence of separate tracts within the terrane through the sinistral faulting associated with the tectonic setting at this time. This debate has become known as the *Southern Uplands Controversy*.

Subdivisions of the Southern Uplands-Down-Longford Terrane

The terrane is divided into three smaller-scale tracts, termed the Northern, Central and Southern belts (see Barnes et. al., 1987; GSNI, 1997; Cooper and Johnson, 2004). The NIC was intruded into the Central belt, which constitutes the Gala and Hawick Group turbidites (see fig. 2.3 and fig. 2.4). Both of these groups are dominated by greywackes, but the northern Gala Group contains a greater proportion of the underlying Moffat Shale, which only occurs very sparsely in the Hawick Group (GSNI, 1997; Cooper and Johnson, 2004). For this reason it is more difficult to distinguish individual tracts within the latter. The Gala Group is the predominant host rock surrounding the NIC (GSNI, 1997; Cooper and Johnson 2004) (see fig 2.3).

The Cloghy Fault marks the boundary between Gala Group and Hawick Group turbidites in this vicinity (see GSNI, 1997; Cooper and Johnson, 2004; Anderson, 2004). The Hawick Group occurring directly to the south of this fault is thought to be

in contact with the NIC along much the body's southern margin (fig. 2.3). This appears to differ from those within the Gala Group here in that it generally contains a larger diversity of lithologies, which include carbonate-rich siltstones, shales and pebbly greywackes (Barnes et. al., 1987). Thus the Cloghy Fault seems to mark a significant compositional change.

However, Barnes et. al., (1987) investigated parts of the Southern Uplands-Down-Longford-Terrane that were not directly adjacent to the NIC. One of these: the Ards Peninsula on the east coast of Northern Ireland, is approximately 30 km from the intrusion; whereas the others are significantly further away and on the opposite side of the Irish Sea. Furthermore, Barnes et. al., (1987) showed that a large amount of along-strike variation occurs between these sampled areas. Additional variation may therefore occur between these and the NIC.

Structure of the terrane

Much of the detailed structural work on the Southern Uplands-Down-Longford Terrane has been undertaken in Scotland. Here Holdsworth et al. (2002) demonstrates that significantly differing bulk strain patterns are apparent between the constituent Gala and Hawick Groups. These authors show that the Gala Group records a single phase of approximately NW-SE contraction, whereas the adjacent Hawick Group yields deformation patterns that are more consistent with sinistral transpression. This might suggest that the older Gala Group does not record the later transpressional phase in Caledonian history, whereas the younger Gala Group does. However, as has been shown by Barnes et. al. (1987) the Southern-Uplands-Down-Longford Terrane exhibits a large amount of along-strike variation. Therefore,

it is difficult to determine whether these structural characteristics extend to the more poorly-studied ‘Down’ section of the terrane.

It has formerly been thought that the Southern Uplands-Down-Longford Terrane exhibits a consistent ENE-WSW strike (e.g., GSNI, 1997; Anderson, 2004). However, the results from a recent airbourne conductivity survey by Beamish et. al. (2010) suggests that constituent tracts undergo a strike swing from ENE-WSW to NW-SW in the vicinity of the NIC (see fig 2.4). These authors used this evidence to suggest that late Caledonian sinistral tectonism may have resulted in the opening of a pull-apart basin within the area of strike-swing, which in turn could have facilitated emplacement of the NIC (see section 2.2).

2.1.4: Summary and implications for the NIC

This section has showed firstly that the NIC is anomalous amongst other Trans-Suture Suite intrusions in terms of its isotopic characteristics. These imply a predominantly I-type source for the complex, in comparison to the S-type source apparent for most other intrusions within the suite (see Halliday et. al., 1979; Meighan and Neeson, 1979; Halliday, 1984; Dempsey et. al., 1990). This suggests that the NIC was not sourced from a deep crustal hot zone, as has been suggested for its correlatives by Miles et. al. (2013), but instead may consist of upper mantle-derived material.

However, ages obtained for the NIC (Meighan et. al., 2003; current study) are more consistent with those of other Trans-Suture Suite plutons. This suggests that the complex was intruded during a period of sinistral transtension (see Soper and

Woodcock, 2003; Stone et. al., 2004; Brown et al., 2008). Beamish et. al. (2010) in turn proposed that these tectonics may have facilitated emplacement of the NIC, through development of a pull-apart basin within an area of regional strike swing. Therefore, the NIC may reflect space creation within a sinistral tectonic setting (e.g., Hutton, 1982; Stevenson et. al., 2006).

2.2: Geology of the Newry Igneous Complex

2.2.1: Introduction

The NIC comprises three separate largely granodioritic plutons previously referred to as the *Northeast*, *Central* and *Southwest* plutons, along with an intermediate-ultramafic body at its northeast margin (e.g., Reynolds, 1934; Meighan and Neeson, 1979; Neeson, 1984). For ease of reference the former are renamed here as the *Rathfriland*, *Newry* and *Cloghoge* plutons respectively; whilst the more mafic body is named the *Seeconnell Complex* (see fig. 2.5). These names reflect local areas in which representative facies for each of the divisions can be observed.

Neeson (1984) used cross-cutting relationships of the above to determine that the NIC broadly youngs from NE to SW; thus the Seeconnell Complex is the oldest part and the Cloghoge pluton the youngest. However, individually these areas each show a more complex zonation, as is discussed below (see fig. 2.6) and as part of the findings from the current study (Chapter 4).

The NIC has also been intruded by the much later Palaeogene Slieve Gullion Complex. This comprises a ring-shaped margin and central body occupying much of the aereal extent of the Cloghoge pluton (e.g., Richey, 1932; Gamble, 1979; Gamble et al., 1992; Stevenson et al., 2008) (see fig. 2.5 and 2.6). Two other Palaeogene intrusive bodies; namely the Mournes Centres; are additionally located near to the NIC (see fig. 2.5)

2.2.2: Petrology and field relationships

Aside from the Seeconnell Complex, the NIC largely consists of granodiorite, which becomes generally more felsic to the southwest (Reynolds, 1943; Meighan and Neeson, 1979; Neeson, 1984; Hurley, pers. comm., 1998) (fig. 2.6). Small areas of *sensu stricto* granite also occur within the Cloghoge pluton (e.g., Reynolds, 1943; Neeson, 1984; Hurley, pers. comm., 1998). The following section outlines a more detailed petrology of the NIC based on local scale variations.

The Seeconnell Complex

The predominant composition of the Seeconnell Complex is very different to that of the main parts of the NIC. An early study of this area by Reynolds (1934) distinguished five main facies here, which comprised a *biotite pyroxenite*; a *hypersthene monzonite*; '*hybrid'* rock (ranging from augite monzonite to augite biotite diorite), a *granodiorite* and a *peridotite*. The latter two are rare within the Seeconnell Complex and are not further considered here. The biotite pyroxenite and 'hybrid' rock have in turn been shown to have inconsistent relationships with each other, appearing to grade within some areas whilst being interlayered in others (Reynolds, 1934; Meighan and Neeson, 1979)

Meighan and Neeson (1979) infer a further division of the Reynold's 'hybrid' facies in the vicinity of Seeconnell (J326421 – see fig 2.6b), where this is interlayered with the biotite pyroxenite. This was termed *meladiorite*, reflecting the more mafic nature of the facies than the intermediate rocks further to the east (see fig. 2.6b). Meighan and Neeson (1979) also suggest that this, and the biotite pyroxenite, represent cumulates formed by sidewall crystallisation (or near-horizontal cumulates that were

later tilted during emplacement of the main NIC). The authors deduced that the Seeconnell Complex was originally a fractionally crystallising magma chamber, from which the more differentiated components may have been removed to supply a Caledonian volcano. In this scenario the interlayering between the meladiorite and biotite pyroxenite could be the result of several magma pulses passing through the "open system" (Meighan and Neeson, 1979, p. 720).

Fig. 2.6b is constructed from more recent mapping of the Seeconnell Complex completed by Neeson (1984). This is largely consistent with the original work of Reynolds (1934), although shows a more extensive area of interlayered meladiorite and biotite pyroxenite (see fig. 2.6b).

The Seeconnell Complex exhibits a relatively sharp boundary with the main part of the Rathfriland pluton. The granodiorite within the latter is coarse grained and strongly foliated up to within one metre from this boundary, at which point it abruptly grades to quartz diorite (Neeson, 1984). Reynolds (1934, 1936) and Neeson (1984) also recorded the presence of cross cutting granodiorite dykes within the Seeconnell Complex, clearly suggesting that this part of the NIC had cooled and somewhat solidified prior to intrusion of the granodiorite.

Other intermediate areas

In addition to the Seeconnell Complex, there are at least four other areas of distinct intermediate composition within the Rathfriland pluton (Reynolds, 1934; Neeson, 1984). Some of these occur close to the Seeconnell Complex, such as at Leganammy Mountain (J315455) and Rough Hill (J278450) (see fig. 2.5 and 2.6a).

Furthermore, the latter areas have been shown to comprise similar monzonitic and dioritic facies respectively to those observed within the Seeconnell Complex, thus implying a connection (Reynolds, 1934). However, no actual contact has been observed between the Seeconnell Complex and these intermediate bodies.

The other intermediate areas are located in the vicinity of Kilcoo (J278331), at the southern margin of the Rathfriland pluton (see fig. 2.5 and 2.6a). This is significantly further from the Seeconnell Complex and within an area surrounded by granodiorite of the Rathfriland pluton (see below) (Reynolds, 1934; Neeson, 1982). The intermediate rocks here are also more felsic than those within the Seeconnell Complex, containing 7 - 16 volume % quartz (compared to 0 %) and less hornblende (Neeson, 1984). These are thus distinguished as *quartz diorites*. This, together with their location, led Neeson (1984) to suggest that the compositions at Kilcoo are more closely linked to the adjacent Rathfriland pluton granodiorite than to the Seeconnell Complex. Neeson (1984) also observed xenoliths of quartz diorite within the adjacent granodiorite, implying that the intermediate body is older than the main Rathfriland pluton.

The main NIC

The Rathfriland pluton: This is relatively the most mafic pluton of the NIC, comprising a large amount of hornblende granodiorite towards its northeast end (Meighan and Neeson, 1979; Neeson, 1984). The pluton is less mafic in its inner part, which has been suggested to grade into biotite granodiorite (Neeson, 1984) (see fig. 2.6a). Rare diorite has also been inferred at the Rathfriland pluton margin, being distinguished by a quartz content of less than 20 % (Meighan and Neeson,

1979). This is considered different to the diorites discussed previously as it does not appear to represent separate bodies from the main granodiorite mass. In fact, no contacts are observed throughout the entire main Rathfriland pluton, which has led authors to deduce gradational normal zoning, possibly resulting from fractional crystallisation of originally intermediate material at depth (Meighan and Neeson, 1979; Neeson, 1984).

A further variation is represented by the presence of a felsic fine grained granodiorite at Shannaghan Hill (J217407 – see fig 2.5 and appendix 1), along the northern boundary of the Rathfriland pluton (see fig. 2.5 and fig 2.6a) (Neeson, 1984). The facies change between this felsic granodiorite and the marginal hornblende granodiorite in this area occurs abruptly, leading Neeson (1984) to suggest that the former may represent a separately intruded magma pulse. However, no contacts between the two facies have been observed.

The Newry pluton: This pluton contains three much more clearly distinct facies (Reynolds, 1943; Neeson, 1984). These have been named as an outer *biotite granodiorite*; an inner *hornblende granodiorite* and an intervening 'ring' of *porphyritic granodiorite* (see fig. 2.6a) (Neeson, 1984). The outer and inner of these facies are relatively extensive, although the porphyritic 'ring' seems to vary in thickness, as well as being absent in the southernmost part of the pluton (Reynolds, 1943; Neeson, 1984).

Neeson (1984) suggest that these three facies are clearly distinct, without any grading or intermediate compositions. Evidence for this was provided through

petrological sampling, as well as from Goraghwood Quarry (J065321 – see fig 2.5b), where the inner and outer contacts of the porphyritic granodiorite were seen to be "razor sharp" (Neeson, 1984, p.66). The porphyritic granodiorite is also seen to truncate the foliation in the outer biotite granodiorite at this site, indicating that the former is younger (Neeson, 1984). However, no such relationships are apparent at the inner boundary of the porphyritic granodiorite and thus the relative ages of this and the inner hornblende granodiorite cannot be resolved from previous work.

The Cloghoge pluton: Former work suggests that the Cloghoge pluton can be divided into two compositional zones. These comprise an outer *hornblende granodiorite* and an off-centre predominantly *biotite granodiorite* 'core' (see fig 2.6a) (Reynolds, 1943, 1951; Neeson, 1984). The latter area also represents the only part of the NIC that contains *sensu stricto* granite, which hosts occasional muscovite (Neeson, 1984).

The contact between the outer pluton and the off-centre core is not exposed, but its location can be established to within approximately 0.5 km in the east of this pluton. Over this area Neeson (1984) observed a complete transition from one facies to the other without any evidence of gradation. The latter study therefore concluded that the contact between the two was sharp, although could not prove which facies was intruded first.

Satellite bodies

There is also evidence for a further set of igneous bodies occurring outside of the main NIC (see fig. 2.6a). These are apparent from several sites to the north of

the Rathfriland pluton from the most recent geological map of this area (GSNI, 1997), as well as to the southwest of this pluton from early mapping by the GSNI (Egan, 1873) (see fig. 2.6). The bodies have been identified as granodiorites (GSNI, 1997), although their relation to the main NIC has not previously been studied. Due to their location, these intrusions will henceforth be termed the *satellite bodies* (see fig. 2.5).

2.2.3: Contacts with the host rocks

The host greywackes and shales within 2.5 - 3 km of the NIC can be seen to have been predominantly metamorphosed to biotite cordierite hornfels (Neeson, 1984). Field evidence suggests that the contact with these is predominantly sharp and concordant, with little evidence of chilling in the granodiorites (Neeson, 1984). However, this inference has largely been based on extrapolation of visible outcrops and there are relatviely few areas where the contact itself is exposed.

The contact is seen at the well-preserved Newry pluton margin at Aughnagon Quarry (J144251 – see fig. 2.5 and appendix 1). Neeson (1984, p.27) describes it here as being “razor sharp” from field observations, with the adjacent granodiorite being relatively coarse. The contact at Shannaghan Hill (see above) is equally sharp, although here the granodiorite shows evidence of chilling and contains a number of sedimentary xenoliths (see fig. 2.6a) (Neeson, 1984). This led to Neeson’s (1984) deduction (see above) that the fine granodiorite here might represent an earlier-intruded pulse of magma from those making up the other parts of the outer pluton.

Further contact variation can be seen along the northeastern edge of the Rathfriland pluton and some parts of the Cloghoge pluton boundary, where the host rocks appear to be more highly altered. These rocks have been described as *fused sediment* (Reynolds, 1934) and later *mobilised sediment* (Reynolds, 1936). The latter term is preferred as through reasoning outlined by Reynolds herself (1936, p.348) this decribes a “mechanical fact”, whereas the former introduces a less reliable “thermal hypothesis”.

The mobilised sediment comprises irregular to lens-shaped hornfels inclusions within slightly coarser, predominantly streaky hornfels (Reynolds, 1936; Neeson, 1984). Reynolds (1936) interpreted these to represent host sediments that had been extensively altered by the NIC (although those adjacent to the Cloghoge pluton may be related to the Palaeogene Slieve Gullion Complex – see Stevenson et. al., 2008), with the streaks and lens-shaped inclusions corresponding to areas of layered biotite concentration. Reynolds (1936) also noted that the boundary between the mobilised sediment and the NIC was gradational in a well exposed region close to Rough Hill (see above). This shows that the intrusion exhibits diffuse as well as sharp contacts in some areas.

All of the previous examples represent sites where the orientation of the contact and adjacent host rocks are very similar (see Neeson, 1984). On the other hand, Beamish et. al.’s (2010) conductivity survey suggests that structures in the host rocks have been cross-cut by the NIC (see fig. 2.4 in previous section). Explanation for this apparent contradiction is provided by the current study (see Chapter 5).

2.2.4: Structure

Neeson (1984) determined that mineral foliations recorded within the NIC showed largely concentric strikes and outward-directed dips (see fig 2.7). These in turn appear to parallel both the outer contacts of the complex and those between plutons (Reynolds, 1934; Neeson, 1984). Neeson (1984) also suggested that foliation strength varied internally within the Rathfriland and Cloghoge plutons, being generally strongest at their margins. Conversely, the Newry pluton appears to exhibit a consistently weak foliation (Neeson, 1984). Foliations within the Seeconnell Complex have been studied much less extensively and hence their relationship to other parts of the NIC is at present unclear.

Internal boundaries within the NIC also appear to exhibit consistently steep, concentric orientations. This is particularly true within the Seeconnell Complex, where the numerous contacts are almost exclusively steep and strike similarly to the outer pluton boundary (Reynolds, 1934; Neeson, 1984). Where observed the rarer contacts throughout the rest of the NIC seem to show the same characteristics. For example, the outer contact of the porphyritic granodiorite within the Newry pluton is steep and parallel to the adjacent pluton margin (Neeson, 1984). Neeson (1984) also inferred a steep boundary between the outer hornblende granodiorite and off-centre biotite granodiorite 'core' in the Cloghoge pluton, although this was based on inferrence from outcrop patterns.

The outer boundaries of the NIC additionally appear to be steep. Cook and Murphy (1952) suggest from gravity data that these extended approximately vertically downwards, although this study was only based on a small section in the south of

the Rathfriland pluton. Reynolds (1934) and Neeson (1984) also inferred steep boundaries, but suggested that these may extend outwards. Neeson (1984) further proposed that the NIC might be connected in the subsurface to the small but petrologically similar Crossdoney intrusion in County Cavan to the west (see fig 2.1 in previous section).

2.2.5: Isotopic characteristics and radiometric dating

As discussed in section 2.1, the isotopic characteristics of the NIC imply an I-type source. However, Meighan and Neeson (1979) also showed that initial $^{87}Sr/^{86}Sr$ ratios are slightly higher within the main Rathfriland pluton than the Seeconnell Complex. Although the former still implies significant upper-mantle input (see Halliday et. al., 1979), Meighan and Neeson (1979) suggest that this might indicate a small amount of crustal contamination within the Rathfriland pluton.

As has also been mentioned within section 2.1, Meighan et. al. (2003) obtained a U-Pb zircon age of 423 ± 7 Ma for the NIC. This is obtained from the central Newry pluton. However, these authors also present a U-Pb titanite age of 410 ± 1.3 Ma for the Rathfriland pluton, which has been shown to be geologically older. Meighan et. al., (2003) resolved the apparent disparity by interpreting the former date as an emplacement age and the latter as a cooling age. The current study provides 9 new U-Pb zircon dates from various parts of the NIC, which help to constrain a more accurate and precise intrusion history (see Chapter 4).

2.2.6: Previous emplacement models

Early theories

Richey and Thomas (1932) observed that some of the host rock bedding adjacent to the NIC was deflected towards parallelism with the margin of the intrusion. This is one of the key features of an expanding pluton, forming the basis of the *ballooning* emplacement model (e.g., Ramsey, 1989; Brun et. al., 1990; Molyneux and Hutton, 2000; Stevenson et. al., 2007a). However, Richey and Thomas (1932, p. 788) conclude that the observed structures are likely in part due to the NIC's expansion, but may also relate to "regional crustal movements" that could have facilitated emplacement. Hence the authors did not infer a specific emplacement mechanism.

Reynolds (1942, 1943) proposed an entirely different, non-magmatic origin for the NIC. This study used evidence such as the presence of parallel schlieren and host rock xenoliths within the central (now *Newry*) pluton to suggest that the NIC represented a former area of Silurian greywackes that had been transformed in situ to the observed 'igneous' material (i.e., the process of *granitisation*). In this model the ultramafic-intermediate Seeconnell Complex represented an area to which "unwanted" elements migrated and would accumulate (this was termed a *basic front* (e.g., Reynolds, 1942)). As discussed previously, granitisation is now considered to be an unfeasible process within the vast majority of crustal settings due to the very large energy requirements (e.g., Pitcher, 1997).

Tectonically influenced emplacement

It is now widely recognised that the emplacement of many late Caledonian granites was influenced by regional tectonics (e.g., Hutton, 1982, 1988; Hutton and McErlean, 1991; Hutton and Reavy, 1992; McCaffrey, 1992; Jacques and Reavy, 1994; Stewart et. al., 2001; Stevenson et. al., 2006, 2007b; Cooper et. al., 2013). Beamish et. al. (2010) suggest that this was also the case for the NIC, due to an apparent strike-swing within the Southern Uplands-Down-Longford Terrane (see section 2.1). During Late Caledonian sinistral transtension (e.g., Soper and Woodcock, 2003; Brown et. al., 2008) this would have led to tectonic space creation within one or more pull-apart basins (see fig. 2.8). However, prior to the current study the work of Beamish et. al. (2010) represented the only evidence for this process, with no direct investigation of the NIC's emplacement having been published.

2.2.7: Summary in terms of petrogenesis and emplacement

This section has showed that the NIC displays a variety of facies, ranging from ultramafic biotite pyroxenites to true granites. Most significantly for petrogenesis these facies often show abrupt boundaries, such as within the Newry pluton. As a result it can be suggested that the observed compositions may not reflect in situ fractionation, but instead separate magma pulses (e.g., Meighan and Neeson, 1979; Pitcher, 1997). On the other hand, the Seeconnell Complex has been proposed to contain cumulates produced by fractionation within an intermediate magma chamber (Meighan and Neeson, 1979). The current investigation of petrogenesis focuses on the main part of the NIC, using geophysics,

petrology, geochemistry and geochronology to investigate the relationship between various facies.

Previous work on initial $^{87}Sr/^{86}Sr$ ratios suggests an I-type origin for the NIC (e.g., Halliday et. al., 1979; Meighan and Neeson, 1979). However, Meighan and Neeson (1979) also showed that these ratios were slightly higher within the Rathfriland pluton than the Seeconnell Complex, suggesting that the former may contain a minor proportion of crustal material. The current study helps to further understand magma source by investigating compositions within the NIC in terms of magma suites, which can be related to mantle characteristics.

The timing of the NIC's intrusion appears to coincide with a phase of sinistral transtension within the British Caledonides (see Meighan et. al., 2003; Soper and Woodcock, 2003; Brown et. al., 2008). Beamish et. al. (2010) suggest that this tectonic regime led to emplacement of the NIC, through creation of accommodation space along an extensional 'jog' within the Southern Uplands-Down-Longford Terrane.

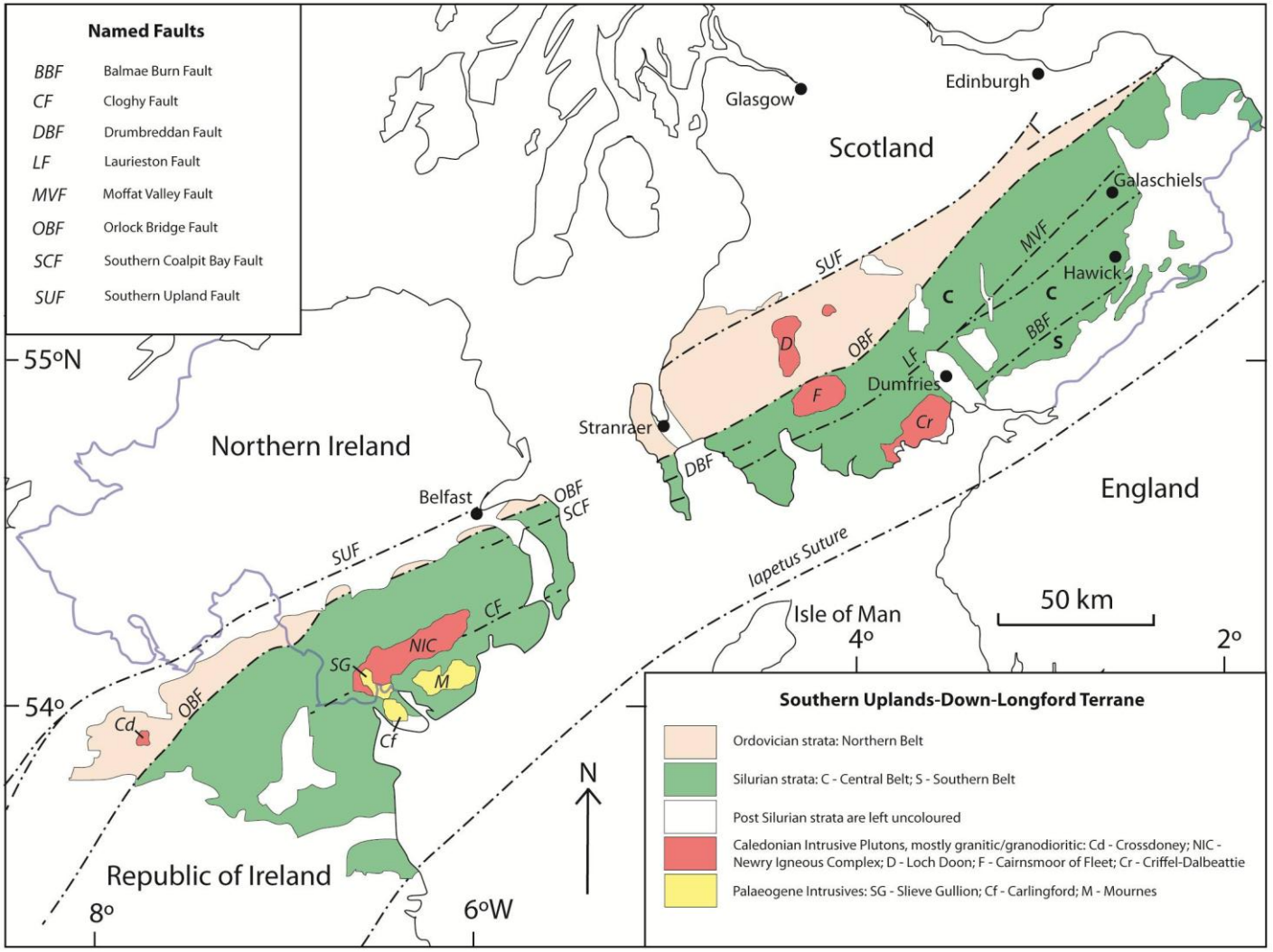

Fig 2.1: UK and Ireland outline highlighting significant faults and Caledonian/post-Caledonian intrusions within the western part of the Southern Uplands-Down-Longford terrane (modified from Beamish et. al., 2010)

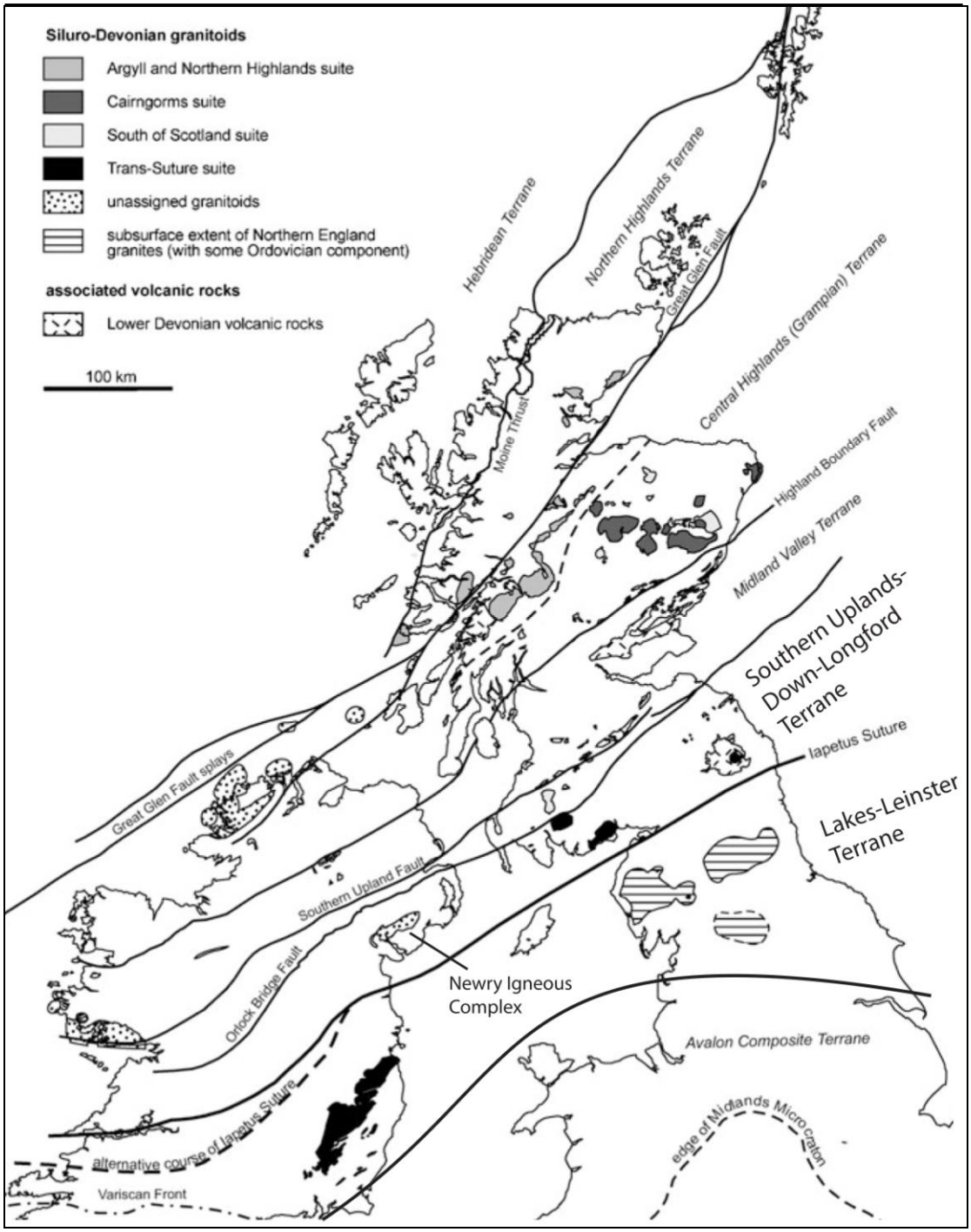

Fig 2.2: Subdivisions of the 'Newer Granites' within the UK and Ireland (modified from Brown et. al., 2010)

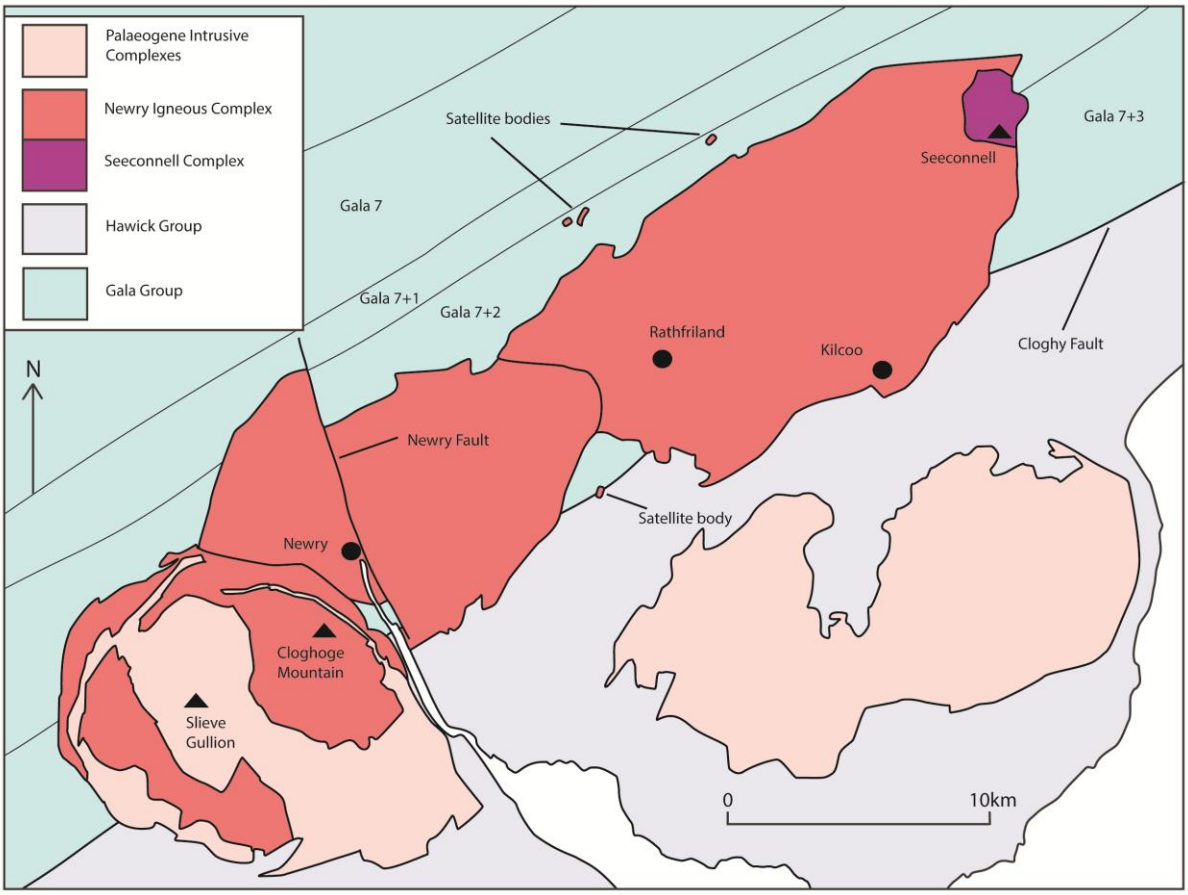

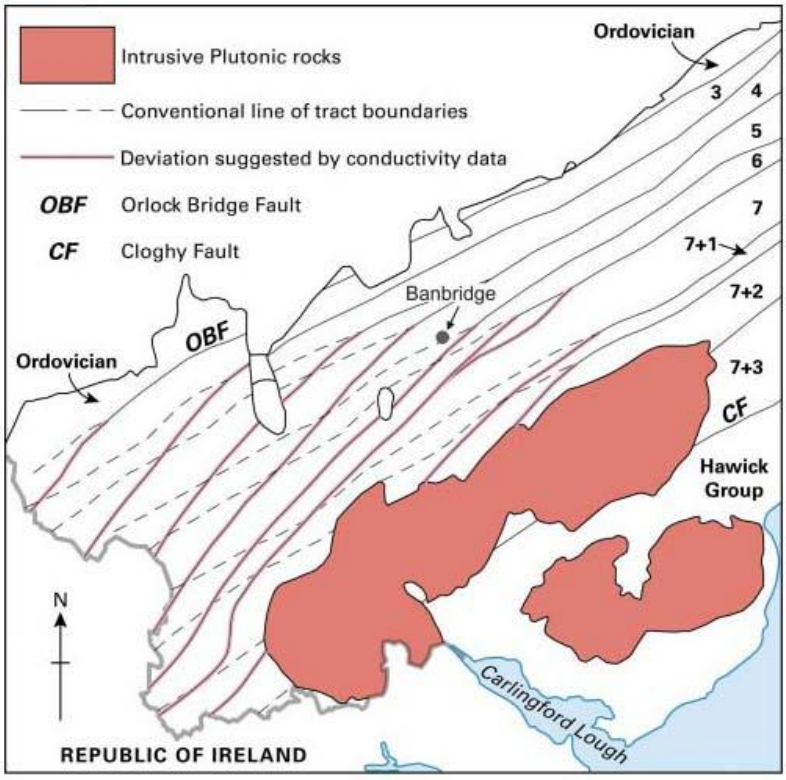

Fig 2.3 (above): Central belt of the Southern Uplands-Down-Longford Terrane, showing approximate locations of tract boundaries and highlighting formations thought to be in contact with the Newry Igneous Complex (constructed from Barnes et. al., 1987; GSNI, 1997; Cooper and Johnson, 2004)

Fig 2.4 (left): Simplified map of the Southern Uplands-Down-Longford Terrane, highlighting the strike-swing of tract-bounding faults suggested by conductivity data (taken from Beamish et. al., 2010)

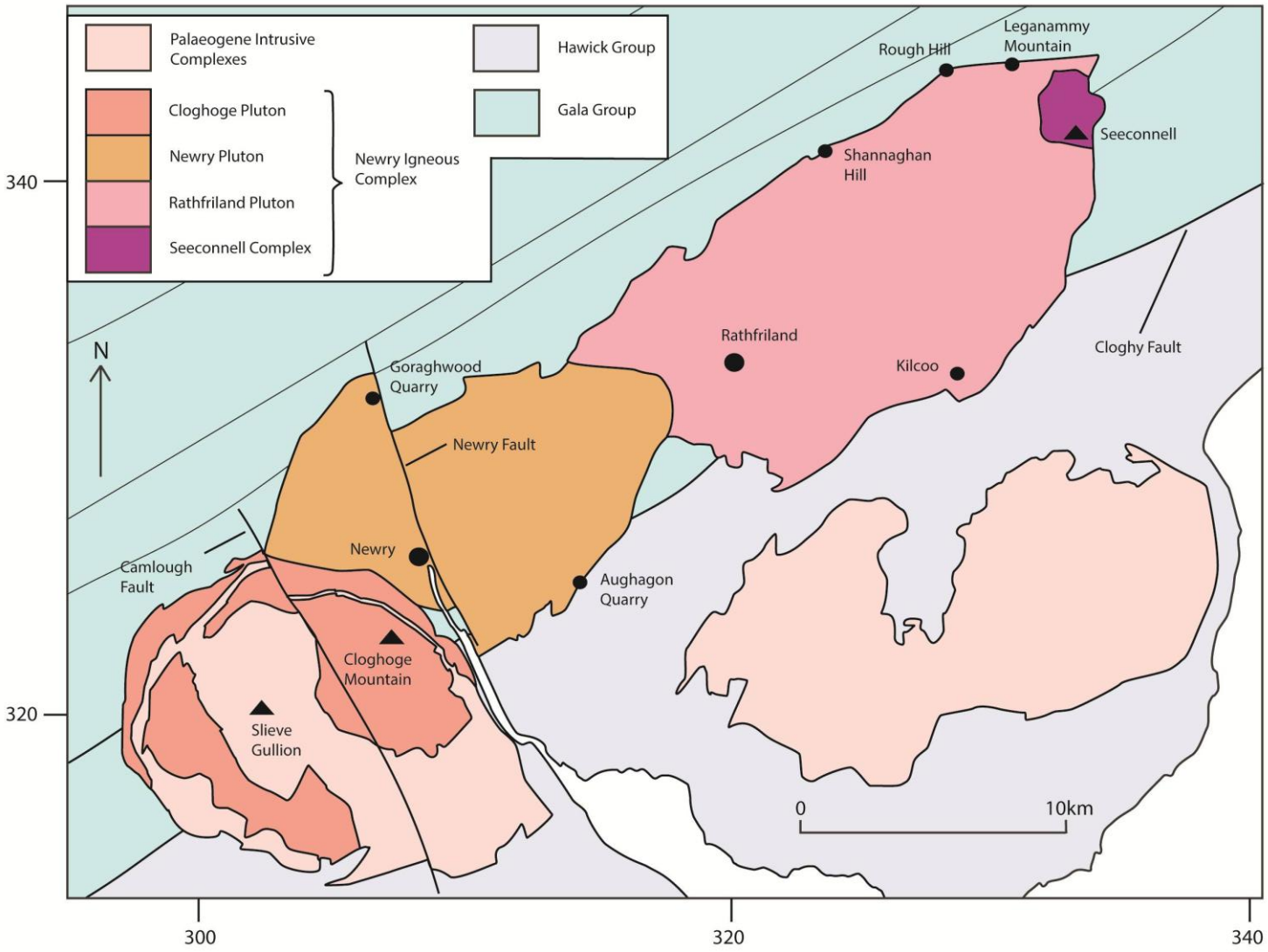

Fig 2.5: Map showing the location and main divisions of the Newry Igneous Complex. Key sites discussed in Chapter 3.2 are also labelled (modified from Cooper and Johnson, 2004)

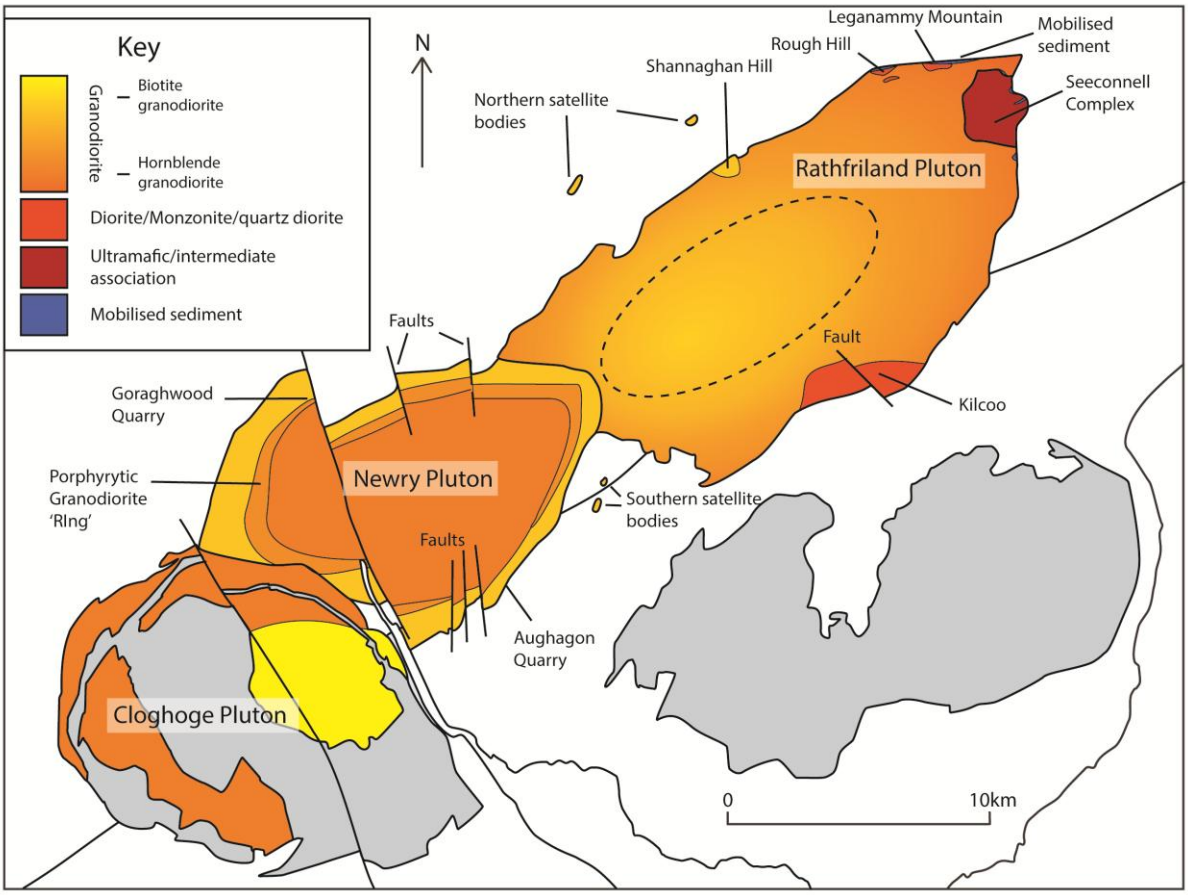

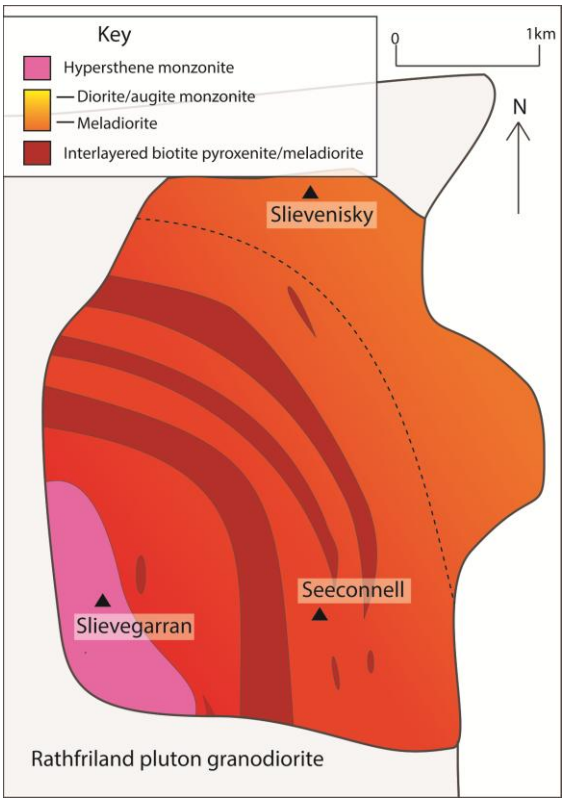

Fig 2.6a (above): Summarised geology of the Newry Igneous Complex from previous work, highlighting key sites discussed in Chapter 3.2 (constructed from work of Egan, 1973; Neeson, 1984; GSNI, 1997)

Fig 2.6b (left): Summarised geology of the Seeconnell Complex from previous work (constructed from work of Reynolds, 1934; Neeson, 1984; GSNI, 1997)

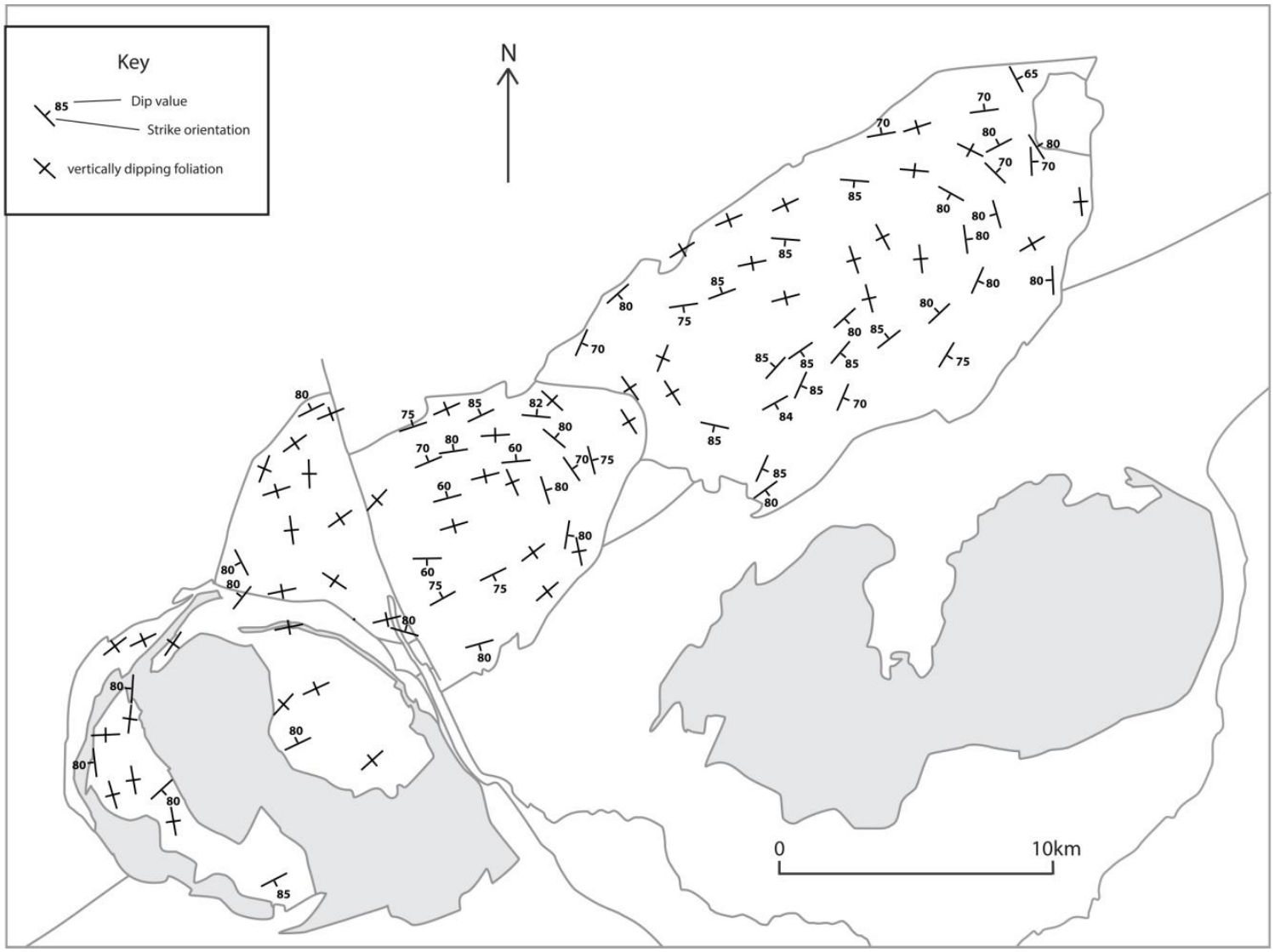

Fig 2.7: Mineral foliations throughout the Newry Igneous Complex (taken from Neeson, 1984)

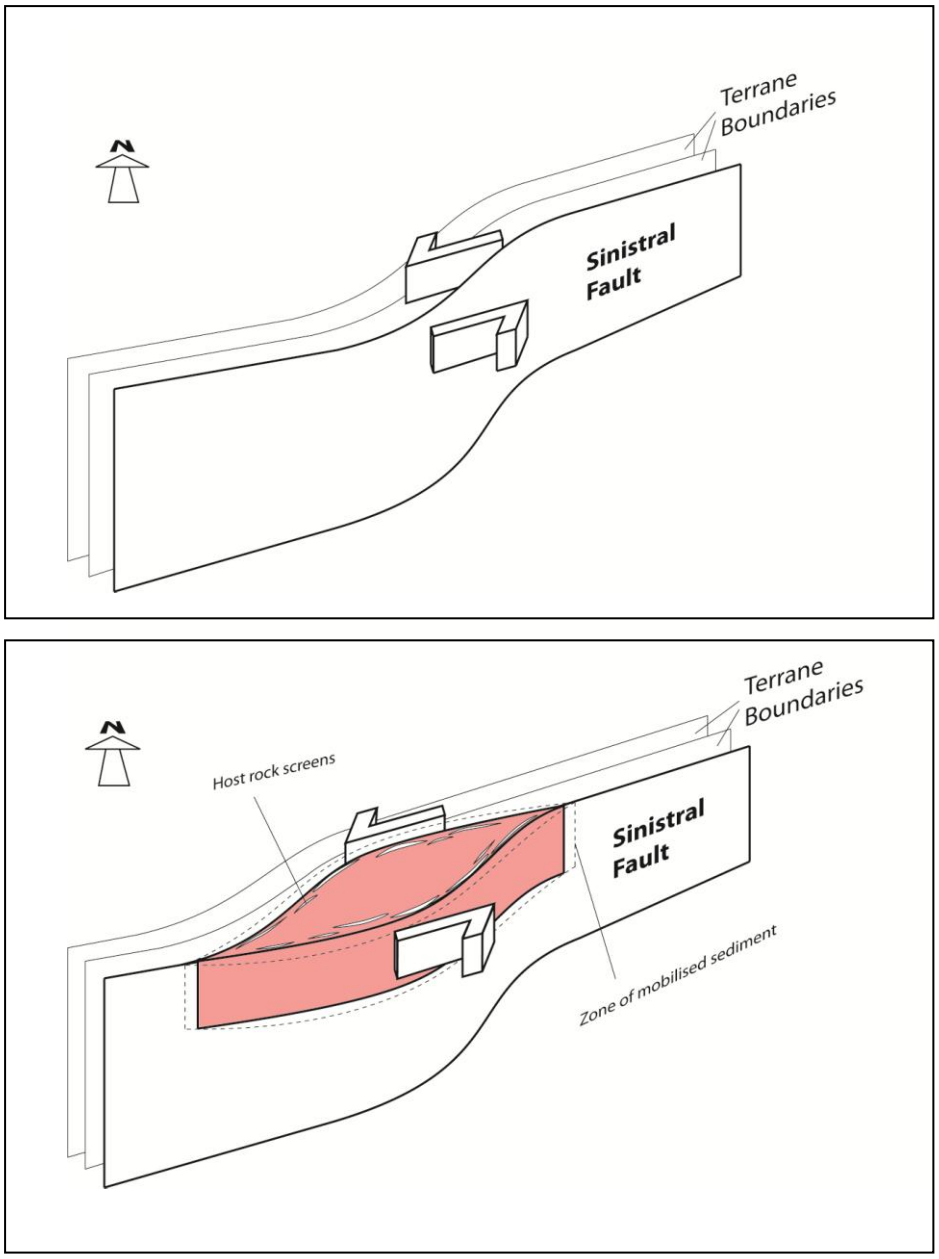

Fig 2.8: Emplacement of a magma pulse of the Newry Igneous Complex due to space creation via a pull-apart basin; a: prior to emplacement b: following emplacement (constructed from work of Beamish et. al., 2010)

CHAPTER 3: APPLIED THEORY

3.1 Zonation in plutons

Plutons were originally assumed to represent single-source, fractionally crystallising magma chambers (e.g., Bowen, 1919; Walker, 1924; Grantham, 1928). Thus, all of the compositional variation displayed would be a result of differentiating processes operating in situ. However, this does not explain the observation that many plutons are composed of relatively homogeneous units, separated by sharp boundaries (e.g., Richey, 1928; Harry and Richey, 1963; Cook and Weir, 1980; Pitcher, 1997; Hecht et. al., 1999; Kryza et. al., 2014). The following section outlines the nature of such divisions, together with explanations that have been provided for these.

3.1.1 Introduction to zonation

Richey (1928) first recognised that the Palaeogene Mournes granites in Northern Ireland could be divided according to the occurrence of several distinct mineral facies. Richey (1928) assigned sequential codes to these facies, according to the assumption that they represented magma pulses that were separately intruded during cauldron subsidence. These codes consisted of a letter pertaining to the overall lithology (i.e., *G* representing granite), together with a suffix number, based on the proposed order of emplacement. Hence a new nomenclature for distinguishing igneous facies was conceived.

Despite contesting the emplacement mechanism (see section 1.3), the work of Stevenson et. al. (2007a) largely supports the original facies divisions of

Richey (1928), again suggesting that intrusion was pulse-like. However, in many plutons such divisions are not as obvious. This has resulted in much debate over how the compositional variation observed in felsic plutons arose (see Pitcher, 1997).

For example, Pitcher and Berger (1972) suggested that marginal assimilation of host rocks surrounding the Thorr pluton in Donegal was a major process contributing to its zonation. However, this interpretation has later been retracted (Pitcher, 1997), whilst other models proposed at a similar time inferred the importance of in situ fractional crystallisation (e.g., Vance, 1961; Taubeneck, 1967). The latter was suggested to have been facilitated by diffusion of melt between a central, largely molten part of the pluton and the interstitial spaces at its outer margin. On the other hand, more recent fractional crystallisation models imply that magma chamber convection plays a larger part in separating solids and melt, hence facilitating the process (see Sawka et. al., 1990; McBirney, 2007).

Such studies suggest that in situ fractional crystallisation may play a role in the compositional development of some felsic plutons (see Pitcher, 1997). Nevertheless, many others consist of relatively homogeneous zones, separated by sharp internal boundaries (Richey, 1928; Stevenson, 2007a). These characteristics are difficult to reconcile alongside the idea of in situ differentiation (see Pitcher, 1997). Therefore, much recent work has suggested that plutons are constructed incrementally via discrete magma

pulses (e.g., Pitcher, 1997; Coleman et. al., 2004; Lipman, 2007; Miller, 2008; Farina et. al., 2012).

3.1.2 Zonation from geophysics

Although zonation has traditionally been determined compositionally, many studies have demonstrated the success of dividing igneous intrusions using geophysics (e.g., Vigneresse, 1990; Petford, 1996; Petford et. al., 2000; Schetselaar et. al., 2000, 2007; Mishra, 2011). Airborne aeromagnetic and radiometric surveying are particularly relevant techniques (see below), as these provide relatively shallow-penetrating signatures which can thus be related to surface geology (see Schetselaar et. al., 2000). On the other hand, gravity data is deeper-penetrating and hence less easily correlated (see Mishra, 2011). Furthermore, 3D interpretations from gravity data are inherently ambiguous and non-unique, thus structural techiques are preferred when considering deep subsurface geometry in the current study.

Aeromagnetic data

Aeromagnetic data is obtained through a magnetometer onboard or being towed by an aircraft. This is flown at low (<100 m) altitudes and at closely spaced intervals over the area being surveyed (e.g., GSNI, 2007). The resulting dataset is *reduced to pole*, meaning that raw, dipolar anomalies are converted to monopolar anomalies that are centred over the features to which they relate (see Baranov and Naudy, 1964; Stavrev and Garovska, 2000; Reynolds, 2011).

Many authors have shown that aeromagnetic data can aid the mapping of igneous intrusions (e.g., Spector and Grant, 1970; Gunn et. al., 1997; Ferris et. al., 1998; Schetselaar et. al., 2000; Anderson et. al., 2013). For example, Schetselaar et. al. (2000) used the technique to identify a previously undetected unit boundary within the Western Slave Granitoid in northeast Alberta (the reliability of this boundary was confirmed through other geophysical data). Schetselaar et. al. (2000) also observed aeromagnetic anomalies within the granitoids of this area that were not consistent with known unit boundaries, suggesting that these represent deformational rather than compositional characteristics. However, these authors also acknowledge that the success of the technique here was largely due to the fact that unit boundaries were sub-vertical. It has been shown elsewhere that shallowly dipping boundaries do not provide such accurate aeromagnetic information (e.g., Spector and Grant, 1970; Gunn et. al., 1997).

Spector and Grant (1970) summarised the relationship between aeromagnetic data and subsurface bodies (e.g., intrusions), suggesting that the depth, width, thickness and magnetisation of these all contributed to the signal produced. From this it can be deduced that a more prominent signature at depth may overide the surface signature within an area in some circumstances. In fact Schetselaar et. al. (2010) suggest that aeromagnetic data could reflect features from depths of some 10 km or more. This can be the case for a shallowly dipping unit boundary within a pluton (see Gunn et. al., 1997). Fig. 3.1 shows how such a boundary could make the surface area

of the unit appear larger or smaller, depending on whether it dips inwardly or outwardly.

Radiometric data

Airbourne radiometric data can be obtained simultaneously with aeromagnetic data, through the use of a gamma-ray spectrometer upon the same aircraft. This detects radiation produced by isotopes of potassium, uranium and thorium (^{40}K, ^{238}U and ^{232}Th) at the ground surface (e.g., Grasty 1975; Cook et. al., 1996; Schetselaar et. al., 2000; Martelet et. al., 2006; Keaney et. al., 2013). Hence, radiometric data will often relate to the content of these three elements within the local topsoil (e.g., Cook et. al., 1996; Martelet et. al., 2006).

This is relevant to the current study because soil contents of the elements have been shown to often correspond to their concentrations within the underlying bedrock (e.g., Broome, 1990; Cook et. al., 1996; Martelet et. al., 2006). Therefore, this technique potentially provides a more reliable indication of surface zonation in an intrusion than aeromagnetic data (see Schetselaar et. al., 2000).

However, Cook et. al. (1996) indicate that where features in the bedrock were small scale (i.e., a dolerite dyke of less than 20 m in width), these may not be identified by the radiometric signature of the overlying soils. Furthermore, Schetselaar et. al. (2000) and Martelet et. al. (2006) show that weathering and mobilisation of the regolith, along with land use and vegetation can result in

large deviations in radiometric data from the composition of the bedrock. This in turn may lead to inaccuracies in the mapping of even pluton-scale features from such data.

Schetselaar et. al. (2000) provide what is considered a reasonable conclusion in relation to the limitations of these geophysical techniques. This was simply that both aeromagnetic and radiometric data could be very useful in the mapping of igneous terranes, but should be regarded carefully and should not replace other more traditional field techniques.

3.1.3 Magma pulses and petrogenesis

Whether evident compositionally or by geophysics, the existence of distinct magma pulses is apparent in terms of both the intrusion (e.g., Meighan and Neeson, 1979; Sawyer, 1996; Schetselaar et. al., 2000; Ruprecht et. al., 2012; Solano et. al., 2012; Morfin et. al., 2014) and eruption (e.g., Huppert and Sparks, 1988; Koyaguchi and Kaneko, 1999; Annen et. al., 2006) of igneous material. However, various explanations have been suggested to account for the origin of these magma pulses.

Many studies show that the variations between upper crustal igneous rocks often result from processes taking place within a deep crustal magma store. Inferred processes include assimilation (e.g., Hildreth and Moorbath, 1988; Solano et. al., 2012); magma mixing (e.g., Douce, 1999); fractional crystallisation (e.g., Meighan and Neeson, 1979; Morfin et. al., 2014) and addition of new material from a mafic source (Annen et. al., 2006, 2009;

Annen, 2011). The significance of each of these can be tested geochemically.

Firstly, assimilation can be simply investigated by considering strontium (Sr) and neodymium (Nd) radiometric isotope compositions (fig. 3.2). Here a mantle-derived magma that has undergone crustal contamination will show initial Sr and Nd ratios that lie on a mixing line with those of the assimilated crust (e.g., Wu et. al., 2000; Yang et. al., 2005) (this will not apply to crustal-derived melts, as these will already exhibit the latter signature). The influence of mixing versus fractional crystallisation can in turn be investigated through compositional variation diagrams, also known as *Harker plots* (e.g., Harker 1909; Hall, 1996; Morfin et. al., 2014 – see fig. 3.3). Where these show curved *liquid lines of descent* this can be indicative of progressive evolution of the melt associated with fractional crystallisation (see Hall, 1996; e.g., Morfin et. al., 2014). On the other hand, pure mixing of two end member components will result in straight line plots on Harker Diagrams (e.g., Douce, 1999). Finally, the idea of successive addition of mafic material to a deep crustal reservoir will essentially display the opposite trend to fractional crystallisaton, whereby the magma becomes less evolved with time (see Annen, 2011).

3.2 Igneous fabrics and recrystallisation textures

Igneous fabrics and recrystallisation textures are the result of numerous factors (e.g., Pitcher, 1997), many of which are discussed at length in the ensuing section. In particular, as has been shown in section 1.3, fabrics can be used to understand the forces operating during emplacement (e.g., Hutton, 1982; Brun et. al., 1990; Stevenson 2007a; Roni et. al., 2014). However, the rheology of a magma also has a large influence on the fabrics and recrystallisation textures recorded (e.g., Vigneresse et. al., 1996; Pitcher, 1997; Picard et. al., 2013). Hence, any deduction of emplacement mechanism from an igneous rock's fabrics and recrystallisation textures first requires a fundamental understanding of the preceding magma's rheology.

3.2.1 *The rheology of granite*

Granitic magma displays a highly dynamic rheology during crystallisation (e.g., Vigneresse et. al., 1996; Pitcher, 1997; Picard et. al., 2013). This is due to a viscosity increase by several orders of magnitude (Miller and Paterson, 1994), leading to a progressive change from Newtonian, to pseudoplastic to ultimately plastic rheological behaviour (e.g., McBirney and Murase, 1994; Fernandez and Gasquet, 1994; Pitcher, 1997). This has largely varied effects on the way the constituent phenocrysts interact; the partitioning of strain and, in turn the final fabrics and recrystallisation textures of the rock (e.g., Pitcher, 1997, Picard et. al., 2013).

For a start, the highest temperature Newtonian stage in a magma's cooling history is characterised by an absence of recorded strain. This is because

any phenocrysts are able to rotate freely in accordance with the forces applied (e.g., Vigneresse et. al., 1996; Petford, 2003) and thus no permanent fabric is produced. The free rotation will also prevent strain-related recrystallisation of the phenocrysts (e.g., McBirney and Murase, 1984; Pitcher, 1997). Vigneresse et al. (1996) proposed that this stage occurred when the melt contained up to 20% particles, defining the latter proportion as the *Liquid Percolation Threshold* (LPT).

Following further crystallisation interaction between phenocrysts begins to occur, meaning the magma behaves as a non-Newtonian pseudoplastic (McBirney and Marouse, 1994; Vigneresse et. al., 1996; Pitcher, 1997; Picard et. al., 2013). Vigneresse et. al. (1996) proposed that a key transition, termed the *Rigid Percolation Threshold* (RTP) takes place when the particle content in the magma is approximately 55%. The authors suggest that at this point the phenocrysts occupy a rigid framework, which can sustain stress and hence plastically deform.

However, more recent work by Picard et. al. (2013) shows that the transitions over this stage cannot be constrained so closely and depend on various factors, such as the shape of the crystals and the stresses applied. Both Vigneresse et. al. (1996) and Picard et. al. (2013, p. 1375) also suggest that this non-Newtonian stage involves progression from a phase of “pervasive” fabric development at higher melt fractions, to later “strain partitioning” fabrics, characterised by localised shear. The latter may be characterised by an

increasing degree of plastic deformation of individual phenocrysts through recrystallisation (e.g., Vernon, 2000).

Finally, the system will become “locked” towards the final stages of crystallisation (Vigneresse et. al., 1996, p. 1579). At this point the magma mush will behave as a solid, within which the phenocrysts will accommodate strain by plastic deformation and recrystallisation (e.g., Gapais and Barbarin, 1986). Vigneresse et. al. (1996) suggested that this occurs when the particle content in the magma is approximately 72 – 75%, defining this as the *Particle Locking Threshold* (PLT). However, other authors have again questioned the certainty of this transition, suggesting that the latter may occur at differing stages according to melt/crystal composition and the stresses applied (e.g., Pitcher et. al., 1997; Burg and Vigneresse, 2002).

3.2.2 *Modelling fabrics and recrystallisation textures*

The fabrics and recrystallisation textures within a cooling granitic body can be classified according to three magma *states*. These are termed the magmatic-, submagmatic- and solid-states respectively (e.g., Vigneresse et. al., 1996; Pitcher, 1997; Vernon, 2000; Picard et. al., 2013). The former is recorded by the alignment of unstrained phenocrysts, whereas in the latter state crystals exhibit significant plastic strain and/or recrystallisation. However, the intermediate submagmatic state can be harder to identify, since this generally corresponds to both recrystallisation and phenocryst rotation (see Vernon, 2000).

The following section outlines the fabric and textural types observed in granitic rocks and the relationship of these to the state of the magma at their time of formation:

Shape-preferred mineral alignments

In an igneous rock *shape-preferred orientation* (SPO) refers to the alignment of inequant mineral grains (see Higgins, 2006). Hence, this develops only when the particles within the magma are able to rotate in response to applied forces. Alignment of such may be linear, planar or a mixture of both, creating the observed fabric in the rock (e.g., Bouchez, 1997).

A linear fabric will display mineral long axes that occur in one consistent orientation, whilst a planar fabric will exhibit orientations that vary within a single plane (e.g., Cloos, 1925; Balk, 1937; Bouchez, 1997) (see fig. 3.3a-b). Fabrics involving non-elongate minerals (e.g., platy minerals such as biotite) are often more difficult to categorise, since these will by definition only show planar alignments clearly. Nevertheless, in such cases a linear component can be deduced from the *zone axis*, which is the axis around which the largest crystal faces in a population are statistically observed to rotate (see Bouchez, 1997) (fig. 3.3c).

In general terms a planar fabric is produced by compression, whilst a linear fabric is produced by constriction (e.g., Bouchez, 1997). However, in most cases igneous fabrics display both planar and linear alignments, suggesting a

combination of influences. The relationship of these components to each other is also likely to vary throughout the cooling of a granite pluton.

As an example, a predominance of ballooning whilst melt is in the magmatic state will result in pure shear fabrics, whereby planar and linear components are parallel (e.g., Caricchi et. al., 2012) (see fig. 3.4a). On the other hand, emplacement into an active shear zone (or other shear during strain partitioning in the submagmatic state – Picard et. al., 2013) may have various effects on fabric development (see fig. 3.4b-c). Arbaret et. al. (1997) used suspensions of biotites within a viscous matrix to model magmatic state deformation during shear. This revealed three principle fabric patterns that depend on the magnitude of the shear applied:

1. For low shear ($\gamma \leq 2$, where $\gamma = \tan \alpha$, with α representing the angle of change of a square element from being right angled due to shear): weak fabrics. In granites these are seen to be poorly-organised, which represent earlier deformation, combined with later shear.
2. For moderate shear ($2 < \gamma < 8$): Clear shear fabrics with lineation orientated at 10° from shear plane (see also Djouadi and Bouchez, 1992) (Fig. 3.6b).
3. For high shear ($\gamma \geq 8$): Clear shear fabrics with lineation orientated approximately parallel to the shear plane. Such would be described as naturally syn-tectonic fabrics (fig. 3.4c).

However, in some cases granite fabrics cannot be accounted for as succinctly as the modelling of Arbaret et. al. (1997) might suggest. Understanding of these may thus require additional geological evidence (e.g., Brun et. al., 1990; Stevenson, 2007b – see below).

Recrystallisation and the submagmatic state

As mentioned above, recrystallisation textures will essentially be absent from fabrics formed in the magmatic state, whilst generally abundant where solid state deformation has taken place (e.g., Vernon, 2000). On the other hand, submagmatic fabrics can be distinguished by localised shear (due to strain partitioning – Picard et. al., 2013) together with recrystallisation of quartz and feldspar phenocrysts (e.g., Gapais and Barbarin, 1986; Vernon, 2000; Sullivan et. al., 2013). As is discussed below, the type of recrystallisation in quartz is key to determining whether deformation occurred in the submagmatic or solid state.

3.2.3 *Fabrics and emplacement*

Various processes have been proposed to account for the fabrics observed in granite plutons, which Paterson et. al. (1989) summarised as follows:

1) Flow during ascent
2) Diapiric emplacement or ballooning
3) Emplacement during regional deformation
4) Regional deformation post-dating emplacement

5) Combinations of the above

The settings inferred by these scenarios are diverse, but can essentially be divided into two categories: those resulting from magma body forces (1 and 2), and those related to tectonic influences (3 and 4) (see previous section; e.g., Hutton, 1982). However, many plutons also show evidence of fabrics formation due to a combination of influences from both magma body and tectonic forces (Brun and Pons, 1981; Brun et. al., 1990; Guineberteau et. al., 1987; Petford et. al., 2000; Miller and Paterson, 2001; Mahan et. al., 2003; Ferré et. al., 2012; Morgan et. al., 2013). For example, Brun et. al., (1990) suggested that the inflation of the Flamanville Granite pluton in northwest France was controlled by lateral opening of tectonic space, so that expansion in other orientations was prevented. This was evidenced by steep, concentric foliations, indicating outward-directed magma pressure, together with shallow, concentric lineations, which the authors ascribed to a perimeter increase due to lateral expansion.

As mentioned above, some fabrics do not fit such general development models and require specific consideration. For example, Stevenson et. al. (2007b) used anisotropy of magnetic susceptibility to identify magma 'flow lobes' from complex fabrics within the Trawenagh Bay Granite in Ireland. These revealed a number of curved magmatic foliation trends, interpretated to represent the lobe shapes; together with shallow, westward-trending lineations, indicating flow direction.

However, other authors have argued that any form of magma flow is very rarely recorded within the final fabric (Benn, 1994; Paterson et. al., 1998). In particular, Paterson et. al. (1998, p. 53) suggest that evidence for all but the very last “increment of strain” will be obliterated from cooling granitic plutons. Nevertheless, the examples presented here and within Chapter 1.3 imply that this is likely an overstatement.

Finally, fabrics can assist in providing estimates of strain intensity during emplacement. Previous studies have attempted this by considering fabric alignment and extents of plastic strain in phenocrysts (e.g., Schulmann et. al., 1996; Wang et. al., 2000). However, as has been shown above, the significance of both fabric alignment and plastic strain in phenocrysts will markedly change throughout cooling of a magma (e.g., Vigneresse et. al., 1996; Pitcher, 1997; Picard et. al., 2013). Hence, the use of these to estimate strain requires understanding of the magma state.

Molyneux and Hutton (2000) preferred the use of mafic enclaves to infer strain, suggesting ballooning within the Ardara pluton in Donegal from the flattening of these close to the pluton margins. The authors argue that since enclave populations are likely to be of similar viscosity to the surrounding magma, these will deform similarly and thus represent reliable strain indicators. However, Paterson et. al. (2004) highlighted several uncertainties regarding the initial shapes, compositions and comparitive rheologies of mafic enclaves in a granitic magma, which represent limitations to this technique.

As a result the latter is considered a semi-quantitative approach to fabric strength analysis (e.g., Paterson et. al., 2004).

3.2.4 Quartz recrystallisation textures

Recrystallisation occurs when simple rotation of grains does not accommodate the applied forces (e.g., Blumenfeld and Bouchez, 1988; Vernon, 2000). This is specifically termed *dynamic recrystallisation*, which is defined as "a solid state process leading to the creation of new (and usually different) grain structure in the course of plastic deformation of crystalline solids" (Guillope and Poirier, 1979, p. 5557). Geologically, this process occurs in a variety of minerals, but is often most clearly observed in quartz.

Gapais and Barbarin (1986) showed that the way quartz recrystallises under strain in a cooling syn-tectonic granite depends on temperature. At high temperatures strained quartz will undergo *grain boundary migration* (see fig. 3.5a), whereby the edges of crystals become lobate in response to the local stress field (see Simpson and Aust, 1972). This has been suggested to occur in both the submagmatic and high temperature solid state, whereas other forms of quartz recrystallisation are restricted to the solid state (Lister and Dornsiepen, 1982; Gapais and Barbarin, 1986). Stipp et al. (2002) inferred from metasediments that this form of recrystallisation usually occurs at temperatures of over 500°C.

At relatively lower temperatures *rotation recrystallisation* occurs, which involves the reorientation of subgrain boundaries within larger grains to

produce a more energetically favourable configuration. The resulting texture is termed *polycrystalline* quartz, within which subgrains reach extinction at varying orientations under cross-polarised light (e.g., Young, 1976) (see fig. 3.5b). Stipp et. al. (2002) suggest that the process of rotation recrystallisation may be transitional with higher temperature grain boundary migration, occurring at temperatures of between approximately 400 and 500°C.

Stipp et. al. (2002) also reported a lower temperature form of grain boundary migration in quartz, termed *grain boundary bulging* (see fig. 3.5c). This involves high angle parts of grain boundaries migrating, producing grain boundary 'bulges', which are again more energetically favourable. The authors suggested that this process occurred predominantly below 400°C. At still cooler temperatures undulose extinction occurs in quartz (Young, 1976).

These forms of recrystallisation represent ways in which accumulated strain in the crystal lattice is allieviated (White, 1976). From metallurgical theory this will ultimately allow the lattice to be further deformed, meaning that a 'snowball effect' develops, whereby each allieviation of strain leads to further recrystallisation and vice versa (Roberts and Ahlblom, 1978). This means that in most examples the extent of recrystallisation strongly correlates with the forces applied to a rock in the high temperature solid state (Bouchez, 1997).

3.2.5 A holistic approach to understanding fabric and textural development

The previous account shows that both igneous fabrics and quartz recrystallisation textures provide much information on the tectonic and magma body forces involved in pluton emplacement. Furthermore, such characteristics have been shown to develop over differing (although potentially overlapping) and widely spread intervals (e.g., Gapais and Barbarin, 1986; Stipp et. al., 2002; Picard et. al., 2013), meaning that they reflect an extensive range of rheologies. This may be particularly relevant to the study of plutons that have been emplaced over protracted time periods, for which magmatic and solid state conditions may occur simultaneously. For example, Zibra (2012) linked solid state recrystallisation within a Neoarchaean granite body to the doming caused by addition and inflation of later magma pulses.

3.3 Anisotropy of Magnetic Susceptibility (AMS)

Igneous fabrics are often measured in the field, based on observed alignments of visible minerals, such as feldspar phenocrysts. Rock fabrics can also be determined by 3D approaches, including CT scanning (e.g., Lynne and Campbell, 2004; Jerram and Higgins, 2007). The AMS technique provides another alternative by recording the magnetic fabric of a rock (e.g., Tarling and Hrouda, 1993; Bouchez, 1997; Dunlop and Özdemir, 2001). This has been shown to relate to both the SPO of the constituent minerals (see previous section) and the magnetic interaction between these (e.g., Hargraves et. al., 1991; Cañón-Tapia, 1996).

3.3.1 Magnetic Susceptibility

Magnetic susceptibility relates to how a material behaves in an applied magnetic field. This parameter is calculated through the following equation, where *H* represents the *applied field*, *M* the *induced field* and K the magnetic susceptibility:

$$M = KH \quad \text{where} \quad K = \frac{M}{H}$$

Since values for *M* and *H* are measured in the same units (Amperes per metre – A/m), K is dimensionless.

All materials will demonstrate a magnetic susceptibility for temperatures above absolute zero, although this can vary by several orders of magnitude. For example, most rock forming minerals show small susceptibilities (K) of

around 1 x 10^{-4} (Borradaile, 1988), whereas ferromagnetic minerals (e.g., magnetite) can yield values of up to 5 (see table 3.1). As a result studies have used this variability to map surface composition (e.g., Gleizes et. al., 1993).

However, it was recognised early in the history of rock magnetism studies that the property of magnetic susceptibility varied depending on the direction of measurement. For example, Ising (1942) showed that clays exhibited greatest susceptibility along their bedding planes, due to the planar alignment of minerals in these orientations. Owens (1974) and Owens and Bamford (1976) elaborated on such ideas by suggesting that all rocks were anisotropic. As a result the study of AMS developed, which involves using magnetic anisotropies to determine rock fabrics (see Thompson and Oldfield, 1986; Tarling and Hrouda, 1993; Bouchez, 1997; Dunlop and Özdemir, 2001).

3.3.2 Representing anisotropy

The AMS technique involves measuring the magnetic susceptibilities of samples in applied magnetic fields (usually low-strength – see Owens, 1974) at varying orientations (see section 5.2). From this six independent quantities can be derived for each sample (see Owens, 1974). These comprise three principal susceptibility magnitudes ($K_1 \geq K_2 \geq K_3$), together with three orthogonal orientations, corresponding to the respective directions of these magnitudes in the field. The results can be illustated as a *susceptibility ellipsoid* (see fig. 3.6), on which the axes lengths represent magnitudes of K_1, K_2 and K_3 respectively (e.g., Nye, 1957).

The susceptibility ellipsoid will therefore vary in shape according to the respective principle magnetic susceptibility magnitudes. For example, a flattened *oblate* shape will imply a planar fabric ($K_1 \sim K_2 > K_3$), whereas an elongated *prolate* shape will imply more of a linear fabric ($K_1 > K_2 \sim K_3$) (see fig. 3.7). On the other hand a *triaxial* shape will show that each susceptibility axis is different and so the fabric exhibits both a significant planar and linear component (see Owens, 1974).

Several parameters can be determined regarding the overall properties of the deduced fabric. These include the mean magnetic susceptibility magnitude, K_{mean}, along with three values representing the degree of alignment (or fabric 'strength'). The latter are referred to as the foliation strength, F (Khan, 1962); lineation strength, L (Khan, 1962) and the overall fabric strength, H (Owens, 1974). The four parameters are calculated as follows:

$$K_{mean} = (K_1 + K_2 + K_3) / 3$$

$$F = (K_2 - K_3) / K_{mean}$$

$$L = (K_1 - K_2) / K_{mean}$$

$$H = L + F \quad \text{or} \quad (K_1 - K_3) / K_{mean}$$

3.3.3 Crystalline and shape anisotropy

The magnetic anisotropy within particular minerals will occur due to either their crystal structure or shape (see Dunlop and Özdemir, 2001). In the former case the preferred orientation of induced magnetism due to the crystal

lattice (see following section) is a dominant factor and hence this is termed *crystalline anisotropy* (e.g., Uyeda et. al., 1963; Besser et. al., 1967). This is relatively common within minerals that acquire weak to moderate induced magnetic fields, such as the feldspars, biotite and haematite (e.g., Thompson and Oldfield, 1986).

However, in minerals exhibiting stronger induced magnetisations (e.g., magnetite) the magnetic anisotropy is often dominantly controlled by particle shape (see fig. 3.8). This is due to the significance of demagnetising fields (which are present although less influential at lower induced magnetisations). These occur through the development of magnetic poles at opposite surfaces of the mineral grain, which configure so as to oppose the induced field (e.g., Lowrie and Fuller, 1971). As shown in fig. 3.8, the development of such surface poles will be minimised when magnetisation occurs parallel to a grain's long axis. Hence, this represents the 'easy axis' of magnetisation and the grain is said to show *shape anisotropy* (see Dunlop and Özdemir, 2001).

3.3.4 AMS fabric carriers

'Carriers' of AMS fabrics can be grouped according to one of three dominant types of magnitisation (e.g., Uyeda et. al., 1963; Owens and Bamford, 1976). These are as follows:

1. Diamagnetism

Diamagnetism is a property shown by all materials. This is caused by the spins of paired electrons precessing to produce a magnetic field in the

opposite direction to an applied field (e.g., Vonsovskii and Hardin, 1974) (fig. 3.9a). Thus, the magnetic susceptibility of diamagnetic material is a negative quantity (see Tarling and Hrouda, 1993). However, the induced field is very weak and will likely be negated if any other type of magnitisation occurs (e.g., Rochette, 1987; Dunlop and Özdemir, 2001). This field also completely disappears when the applied magnetic field is removed and hence a diamagnetic material will exhibit no permanent magnetisation.

Diamagnetic behaviour occurs in minerals that do not contain iron in their crystal structure, such as quartz, calcite and feldspar (see table 3.1; Thompson and Oldfield, 1986). Due to the low strength of the induced field, the associated demagnetising fields are also weak (e.g., Dankers, 1981). The limited effect from the latter means that the anisotropy in such grains will be dominantly controlled by the crystal lattice (i.e., crystalline anisotropy) (e.g., Uyeda et. al., 1963).

2. Paramagnetism

Paramagnetism is a slightly stronger type of magnetisation that occurs in substances with incomplete electron shells (see Tarling and Hrouda, 1993). In this case, the diamagnetic effects are overcome due to the presence of unpaired electrons. The spin of these electrons will not be balanced by others, meaning that each will produce a *net magnetic moment* in an applied field (e.g., Dunlop and Özdemir, 2001) (see fig. 3.9b). The resulting induced magnetic field will be orientated in the same direction as that applied. Thus, the magnetic susceptibility for a paramagnetic material is a positive quantity.

Paramagnetic materials also show no permanent magnitisation, as electron spins do not interact and so become randomised without an applied field.

Paramagnetism occurs in minerals that contain dispersed iron within their crystal lattice (e.g., Thompson and Oldfield, 1986). Common geological examples include biotite, chlorite, hornblende and augite (see table 3.1). As with the diamagnetic minerals, the relatively weak induced magnetic field will again mean that such exhibit dominantly crystalline anisotropy (e.g., Bouchez, 1997).

However, this presents an analytical problem with some minerals. Where crystal axes are not orthogonal, these will not all lie parallel to the deduced principal susceptibility axes (e.g., Borradaile and Henry, 1997; Lagroix and Borradaile, 2000). This will particularly apply to clinopyroxenes and amphiboles. On the other hand, sheet silicates such as biotite show almost exactly orthogonal crystal axes (Martín-Hernández and Hirt, 2003). This means that anisotropies of the latter closely reflect the crystal shape and so will correlate with visible fabrics, whereas the former may not.

3. Ferromagnetism (*sensu lato*)

Ferromagnetism (*s.l.*) can be much stronger than the previous two types (by up to three orders of magnitude) and occurs as a result of "spontaneously coupled" electron spins (e.g., Zener, 1951; Tarling and Hrouda, 1993, p. 4). The behaviour occurs even in the absence of an applied

field, meaning that ferromagnetic (*s.l*) materials also exhibit a *remanent magnetisation* (e.g., Thompson and Oldfield, 1986).

Ferromagnetism (*s.l.*) is largely restricted to elements from the first series of transition metals and compounds containing these elements. This is because such elements possess a number of unpaired electrons within their partially filled *d* and *f* orbitals, between which coupling can take place (e.g., Dunlop and Özdemir, 2001). However, the way in which this occurs can vary and thus there are three fundamentally different types of ferromagnetic (*s.l.*) behaviour (e.g., Tarling and Hrouda, 1993), which are discussed below:

Ferromagnetism (*sensu stricto*): This represents the simplest case, involving only the cations of metallic transition elements, such as iron, nickel and cobalt. Materials exclusively composed of these contain no intervening anions in their chemical structure and so electron spins within adjacent cations will interact and become coupled (e.g., Pauling, 1938; Goodenough, 1968; O'Reilly, 1984). This results in an *exchange force*, whereby the magnetic vectors within the material are consistently orientated, producing a strong induced field that is parallel the applied field (see Tarling and Hrouda, 1993; Dunlop and Özdemir, 2001) (see fig. 3.9c).

Antiferromagnetism: This behaviour occurs when transition metal elements combine with other elements, such as oxygen (e.g., Neel, 1948; Anderson, 1950; O'Reilly, 1984). The latter will exist as anions within the chemical structure of the compound, which share electron spins with their adjacent

cations. This causes a *superexchange force*, whereby the electron spin directions within neighbouring cations oppose one another (e.g., Anderson, 1950). In the ideal case two oppositely magnetised lattices will result, ultimately yielding an induced field with zero net magnetisation (see fig. 3.9d).

However, in some minerals one lattice may be slightly more magnetised than the other, or the lattices may be tilted relative to each other due to imperfections (see Tarling and Hrouda, 1993; Dunlop and Özdemir, 2001). The latter is the case for haematite (Fe_2O_3) (e.g., Morrish, 1994). Such results in a behaviour termed *parasitic magnetism* or *canted antiferromagnetism* (e.g., Dunlop, 1971; Morrish, 1994), whereby a very weak field is induced that does not remain after the applied field is removed. As with the diamagnetic and paramagnetic classes, this behaviour will result in weak demagnetising fields and hence dominantly *crystalline anisotropy* (e.g., Uyeda et. al., 1963).

Ferrimagnetism: This behaviour again involves superexchange forces, although the magnetic lattices producing these are more uneven, typically containing differing numbers of cations (e.g., Neel, 1948). For example, the ferrimagnetic mineral, magnetite (Fe_3O_4), contains 16 cations of iron (eight Fe^{2+} and eight Fe^{3+}) in one lattice, along with just eight (all Fe^{3+}) in the other (e.g., Calhoun, 1954). As a result, both a net magnetic field and a remanent magnisation will occur within the mineral grain (see fig. 3.9e).

The magnetic susceptibility of ferrimagnetic minerals can be very high (see table 3.1). Hence, this will likely dominate the magnetic signature, even where these minerals are present in small amounts (e.g., Thompson and Oldfield, 1986). Ferrimagnetic minerals also generally show a dominant shape anisotropy that develops parallel to the long axis of grains. As is explained above (see section 3.2.3), such is the result of the prominent demagnetising field being minimised in this orientation (e.g., Lowrie and Fuller, 1971).

3.3.5 Solid solution of magnetic minerals in igneous rocks

Iron represents a common component within ferromagnetic (*s.l.*) and paramagnetic igneous minerals, occurring both in its oxidised (Fe^{3+}) and reduced (Fe^{2+}) states. Titanium (Ti^{4+}) can also occur frequently. The three species, represented by oxides Fe_2O_3, FeO and TiO_2 respectively, can combine to form three main solid solutions in magmatic melts. These consist of the ferromagnetic (*s.l.*) *titanomagnetites* and *titanohaematites*, along with the paramagnetic *pseudobrookite* series (e.g., Thompson and Oldfield, 1986; Butler, 1992; Tarling and Hrouda, 1993) (fig. 3.10).

During cooling and crystallisation compositions from each series will often exsolve, resulting in the crystallisation of their respective end members. For example, the titanomagnetite series usually evolves into separate magnetite and ulvospinel (e.g., Butler, 1992). Changes in oxidation state can also have the effect of shifting composition from the titanomagnetites towards the more

oxidised titanohaematite series. The resulting mixtures are termed *maghaemites* (e.g., Thompson and Oldfield, 1986) (see fig. 3.10).

3.3.6 Magnetic domains

Magnetisation of ferromagnetic (*s.l.*) minerals is complex, depending on many factors already discussed, such as mineral composition, grain shape and the nature of the crystal lattice. However, this is also affected by the size of the mineral grain (e.g., Butler and Banerjee, 1975; Butler, 1992; Hubert and Schafer, 1998). This is due to the presence of magnetic domains (see Hubert and Schafer, 1998), which are small (in the range of 1 μm) units in a grain within which magnetisation is uniform. Hence, each magnetic domain possesses a north and south pole, located at opposite points within the unit.

Magnetic domains are separated by *Bloch walls*, which are interfaces separating areas of the grain with opposing magnetic moments (e.g., Hubert and Schafer, 1998). However, these require energy and so there is a limit to the extent to which they can form within a grain (e.g., Kittel, 1946; Hubert and Schafer, 1998). As a result, ferromagnetic grains that are below a certain size range cannot support Bloch wall formation and will only possess a single magnetic domain (i.e., these are *single-domain* (SD) grains). For magnetite and haematite this size limit is approximately 1 μm (e.g., Butler and Banerjee, 1975; Butler, 1992; Hubert and Schafer, 1998).

Grains possessing a number of magnetic domains are conversely termed *multi-domain* (MD) (e.g., Lowrie and Fuller, 1971; King et. al., 1982). The

distinction between SD and MD grains is important in terms of understanding magnetic susceptibilities, especially where the anisotropy is dominantly shape-controlled. The reasons for such are discussed below.

3.3.7 Anisotropy and hysteresis loops

Hysteresis loops are plotted in order to observe the effect of applied fields on the induced fields within magnetic particles (e.g., Dunlop, 1986; Tarling and Hrouda, 1993). Fig. 3.11a firstly shows that ferrimagnetic SD grains (i.e., magnetite) can exhibit their maximum magnetisation (termed *saturation magnetisation*) even when the applied field is zero (e.g., Kittel, 1946). This is due to the magnetically 'easy' long axis of such grains, which will retain its magnetisation even in the absence of an external field (i.e., these show remanent magnetisation)

The stability of this magnetisation means that a weak field applied in the opposite direction will have no effect on the induced field in a grain (e.g., Dunlop, 1986) (see fig. 3.11a). The induced field will change only when the applied field becomes relatively strong, at which time the magnetisation will be reversed so as to occupy an anti-parallel orientation along the same axis. On the other hand, a weak field applied at an angle to this axis (i.e., not parallel or anti-parallel) will have immediate effect on the strength of the magnetisation within the grain, although its direction will again remain unchanged until the applied field strength becomes relatively strong (e.g., Dunlop, 1986) (see fig. 3.11b).

The effect of a weak applied field also increases with the angle of this field from the long axis of the grain (e.g., Potter and Stephenson, 1988; Rochette et. al., 1992). This means that the low-field magnetic susceptibility of the grain will be zero in the direction of this axis and at a maximum perpendicular to the axis. Therefore, in the absence of any other influences (see *distribution anisotropy* below) the AMS fabrics derived from such ferrimagnetic SD grains (i.e., magnetite) will be perpendicular to the SPOs of these grains (see Tarling and Hrouda, 1993). However, this does not apply to antiferromagnetic SD grains (e.g., haematite) due to their relatively weak crystalline anisotropy, which will be altered by even a low-strength parallel applied field (Uyeda et. al., 1963).

MD grains differ again in that regardless of whether these show dominantly shape or crystalline anisotropy, their magnetisation can change relatively easily. This occurs through the adjustment of Bloch walls separating the magnetic domains (e.g., Hubert and Schafer, 1998). As a result an applied field will have an immediate effect upon the induced magnetisation along the 'easy' axis of the grain through rearrangement of such domains. With increasing applied field strength the latter will then steadily increase until it reaches saturation level (see fig 3.11c). This means that the AMS fabrics derived from MD grains will reflect their SPOs (e.g., Bouchez, 1997).

3.3.8 Application to granites

Derived AMS fabrics have been shown to frequently correspond to visible mineral alignments in granites (e.g., Tarling and Hrouda, 1993;

Bouchez, 1997; Dunlop and Özdemir, 2001). As a result, AMS can be used either together with or in place of visible fabrics to understand the emplacement of these (e.g., Bouchez, 1997; Stevenson et. al., 2006, 2007a, 2007b; Martins et. al., 2011; Roni et. al., 2014). There are several benefits to this approach (e.g., Bouchez, 1997), which can be summarised as follows:

1. AMS records very subtle fabrics that may be undetected in the field
2. AMS records linear fabrics, which can often only be observed in the field within areas of favourable outcrop
3. AMS provides quantitative fabric information (i.e., foliation/lineation strength – see Owens, 1974)

However, many authors have also highlighted potential limitations with using AMS to understand fabrics in igneous rocks. Gaillot et. al. (2006) summarised these as follows:

1. The technique does not resolve the mineral(s) contributing to the anisotropy
2. Multiple separate alignments may contribute to the overall fabric
3. Certain magnetic minerals (e.g., single domain magnetites) may exhibit an ‘inverse’ fabric, making interpretation difficult
4. The technique does not distinguish between fabrics produced from alignment of magnetic mineral and those produced from magnetic interaction between these.

Limitation (2) here relates to both AMS and visible fabrics and has been addressed in the previous section. However, the other three limitations relate exclusively to AMS. Hence, these will represent important initial considerations for any AMS study of igneous fabrics:

Resolving minerals contributing to AMS

The magnetic susceptibilities of mafic to intermediate igneous rocks are often largely determined by ferromagnetic (*s.l.*) minerals such as magnetite (e.g., Rochette, 1987; Hargraves et. al., 1991). However, within some granites it is common for paramagnetic minerals to have the dominant contribution (e.g., Stevenson et. al., 2007a). Since these magnetic behaviours are very different it is clear that any fabric interpretations made from AMS results require knowledge of the contributing mineralogy (termed the *magnetic mineralogy*).

Several methods exist for determining magnetic mineralogy. These include using reflected light petrography to identify distinguishing properties of ferromagnetic minerals in thin section (e.g., Gregoire et. al., 1995; Stevenson et. al., 2007a; Petronis et. al., 2012). However, if these minerals are relatively sparsely distributed (as can often be the case – e.g., Stevenson et. al., 2007a) this method may yield unrepresentative results.

A potentially more robust technique involves heating whole-rock samples and observing the effects this has on magnetic susceptibility (i.e., *thermomagnetic analysis*) (e.g., Stevenson et. al., 2007a; Žák et. al., 2009; Tripathi et. al.,

2012). This relies on the fact that the different types of magnetic minerals discussed above respond differently to changes in temperature (see fig. 3.12).

Diamagnetism is temperature independent (e.g., Lonsdale, 1937) and thus minerals showing this behaviour will maintain a consistent negative magnetic susceptibility throughout heating (fig. 3.12a). Conversely, the magnetic susceptibility of paramagnetic minerals decreases significantly with temperature (e.g., Lonsdale, 1937) (fig. 3.12b). Hence, the presence of these can be determined by a region of negative gradient within the overall temperature-susceptibility curve (e.g., Hrouda et. al., 1997).

Ferromagnetic (*s.l.*) minerals relate differently again to temperature, showing generally consistent magnetic susceptibilities until a specific temperature range is reached. This relates to the *Curie temperature* (T_c), which represents the point during heating at which a mineral typically loses its permanent magnetisation (e.g., Lowrie, 1990; Fabian et. al., 2013). Here the mineral will become paramagnetic, as well as undergoing a major reduction in magnetic susceptibility (see Dunlop and Özdemir, 2001) (fig. 3.12c). This will likely be very apparent from the overall temperature-susceptibility curve (e.g., Hrouda et. al., 1997).

However, the Curie temperature varies for different ferromagnetic (*s.l.*) minerals. For example, magnetite has a T_c of 580°C, whereas that for haematite is 680°C (Dunlop and Ozdemir, 2001). Compositions within the natural solid solution series relating to these end members also show distinct

and widely varying Curie temperatures (Hartstra, 1982). Therefore, ferromagnetic (*s.l.*) minerals can often be individually identified from plotting the results of heating experiments on a temperature-magnetic susceptibility graph (e.g., Hrouda et. al., 1997).

The reduction of magnetic susceptibility associated with Curie temperature also occurs over an interval for each mineral, rather than instantaneously (see fig. 3.12). Therefore, a further step is required to determine the precise value of T_c from a broader range. This involves identifying an inflection point on the temperature-magnetic susceptibility graph, corresponding to where the rate of susceptibility change is greatest (e.g., Petrovský and Kapička, 2006; Fabian et. al., 2013)

Identifying anomalous fabrics

Inverse fabrics, in which the maximum magnetic susceptibility is normal to the long axis of the grain (see limitation (3) above – Gaillot et. al., 2006), can also potentially be resolved through thermomagnetic analysis. This is achieved for SD magnetite (a common cause of inverse fabrics, as explained in section 3.3.7) due to the *Hopkinson effect* (Hopkinson, 1889), which manifests as an increase in susceptibility at temperatures immediately below the steep decline associated with the Curie Temperature. The effect results from ferromagnetic (*s.l.*) materials with remanent magnetism being heating beyond the temperature at which this is lost (termed the *blocking temperature*). This results in behaviour termed *superparamagnetic* and increased magnetic susceptibility (e.g., Pfeiffer and Schüppel, 1994).

The Hopkinson effect occurs in both SD and large MD grains. However, in the latter case the susceptibility peak will be relatively narrow, due to the consistently high blocking temperatures of these grains (Dunlop, 1974). On the other hand, SD grains often have lower blocking temperatures and so the peak associated with these would appear wider (e.g., Radhakrishnamurty and Likhite, 1970; Dunlop, 1974). Hence the occurrence of a Hopkinson effect can help to establish the presence of SD magnetite, thus potentially explaining the occurrence of 'inverse' fabrics.

There are further ways in which anomalous AMS fabrics arise in igneous rocks. These include hydrothermal alteration (Rochette et. al., 1992; Ferré et. al., 1999; Raposo et. al., 2004) and weathering processes (e.g., Ferré et. al., 2002), which can each cause the growth of new magnetic material in unpredictable orientations. This should therefore be considered when selecting samples for AMS investigation (e.g., Tarling and Hrouda, 1993).

Shape and distribution anisotropy

In some cases magnetisation does not relate to the properties of individual grains, but instead to the overall distribution of the grains within a sample. This typically occurs in rocks with relatively abundant ferrimagnetic minerals such as magnetite, in which magnetic interaction between these results in an induced field. This field can interfere with and override the shape anisotropy of individual grains (e.g., Morrish and Yu, 1955; Davis and Evans, 1976; Hargraves et. al., 1991; Gregoire et. al., 1995, 1998; Cañón-Tapia,

1996). If the minerals contributing to the induced field have crystallised interstitially, their distribution will likely reflect the orientation of the silicate "template" in which they occur (Hargraves et. al., 1991, p. 2193). The resulting magnetisation will therefore be anisotropic and is referred to as *distribution anisotropy*.

Gaillot et. al. (2006) regarded the uncertainty relating to whether AMS fabrics are the result of distribution or shape anisotropy as a limitation of the technique (see limitation (4) above). Furthermore, authors such as Canon-Tapia (1996) have shown that the relative influences of the two are complex and difficult to predict. However, the generally close relationship of both types of anisotropy to the visible rock fabrics (excluding the inverse fabrics from SD grains) means that each will usually yield very similar AMS orientations and thus their separation may not be necessary (e.g., Hargraves et. al., 1991; Canon-Tapia, 1996).

3.3.9 Use of AMS in the current study

The availability of a large amount of field structural data meant that AMS orientations could be compared to visible foliations, both in terms of general patterns and at a number of specific outcrops. This provided a clear and simple way to determine the relationship of AMS to visible fabrics, which was undertaken in addition to the resolution of magnetic minerologies through the methods described above.

Understanding the causes of the observed AMS fabrics in turn allowed these to be used in a similar way to visible fabrics in deducing emplacement-related processes. As mentioned in section 3.2, this was achieved by Stevenson et. al. (2007b) for the Trawenagh Bay pluton in Donegal. These authors used subtle AMS foliations and lineations within the weakly deformed granite to identify a number of 'flow lobes' associated with its emplacement. There are numerous other examples of studies that have used AMS to either support or replace visible fabric data (i.e., where this is absent) in determining granite emplacement (e.g., Cogne and Perroud, 1988; Bouillin et. al., 1993; Archanjo et. al., 2002; Aranguren et. al., 2003; Žák et. al., 2009; Martins et. al., 2011; Roni et. al., 2014)

The deduced fabric strengths from AMS (see Owens, 1974) also formed a large part of the current study in terms of providing indications of emplacement-related strain. In this sense a parallel can be drawn between these and the enclave populations investigated by Hutton and Molyneux (2000) (see section 3.2). Both potentially relate to the extent of strain, although it is important to note that due to the highly dynamic rheology of granitic magma (e.g., Picard et. al., 2013 – see section 3.2) this will not be a quantitative relationship (see Paterson et. al., 2004). Nevertheless, the numerical AMS fabric strength parameters have been used alongside deductions of the magma rheology to provide useful semi-quantitative information on the extent of strain.

3.4 Study outline

The current study focuses on the zonation and emplacement of the Newry Igneous Complex (NIC). This intrusion has not been extensively studied in approximately 30 years (see Meighan and Neeson, 1979; Neeson, 1984).

3.4.1 Reasons for undertaking the study

The study was motivated by results from the Tellus Project, managed by the Geological Survey of Northern Ireland (GSNI) in 2005-2006 (see GSNI, 2007). These revealed striking concentric aeromagnetic anomalies within two of the three plutons of the NIC, which were unrelated to any recognised feature. The results also implied a number of other aeromagnetic divisions of the intrusion, as well as several radiometric anomalies. The GSNI obtained a set of 9 U-Pb radiometric dates from locations of varying geophysical signature. This provided a foundation upon which to develop a new investigation into the petrogenesis and emplacement of the NIC.

3.4.2 Structure of the study

The study comprised two broad aims, which were as follows:

1. To determine a new zonation for the NIC
2. To establish an emplacement model for the NIC

The initial aim was achieved through use of existing Tellus geophysical data and U-Pb geochronological data, as well as collection of samples for petrological data and geochemistry. These assisted in constraining a number of zones, through which the NIC is mapped in new detail.

Secondly, emplacement was investigated through structural field data (from the current study, the former study of Neeson (1984) and collation of an existing dataset (Hurley, pers. comm., 2010); an investigation of quartz recrystallisation and an AMS (Anisotropy of Magnetic Susceptibility) study. This allowed the theory of tectonic facilitation of the NIC (Beamish et. al., 2010) to be tested, whilst also providing a large amount of new fabric information from which processes taking place within the NIC during emplacement could be derived.

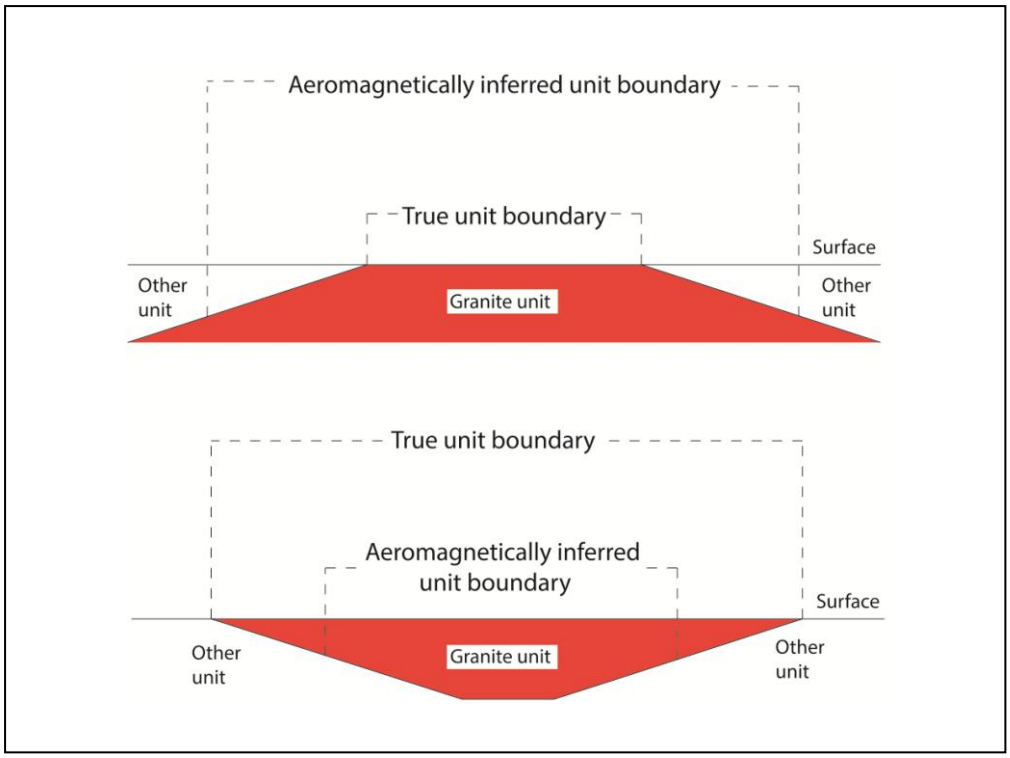

Fig 3.1 (above): Cross sectional view through a pluton showing the effect that dipping boundaries may have on aeromagnetic signature (based on studies by Spector and Grant (1970); Schetselaar et. al. (2000) and Martelet et. al. (2006))

Fig 3.2 (below): Initial $^{87}Sr/^{86}Sr$ versus ε_{Nd} plot, showing distinctions between mantle, lower crustal and upper crustal signatures (modified from Yang et. al., 2005)

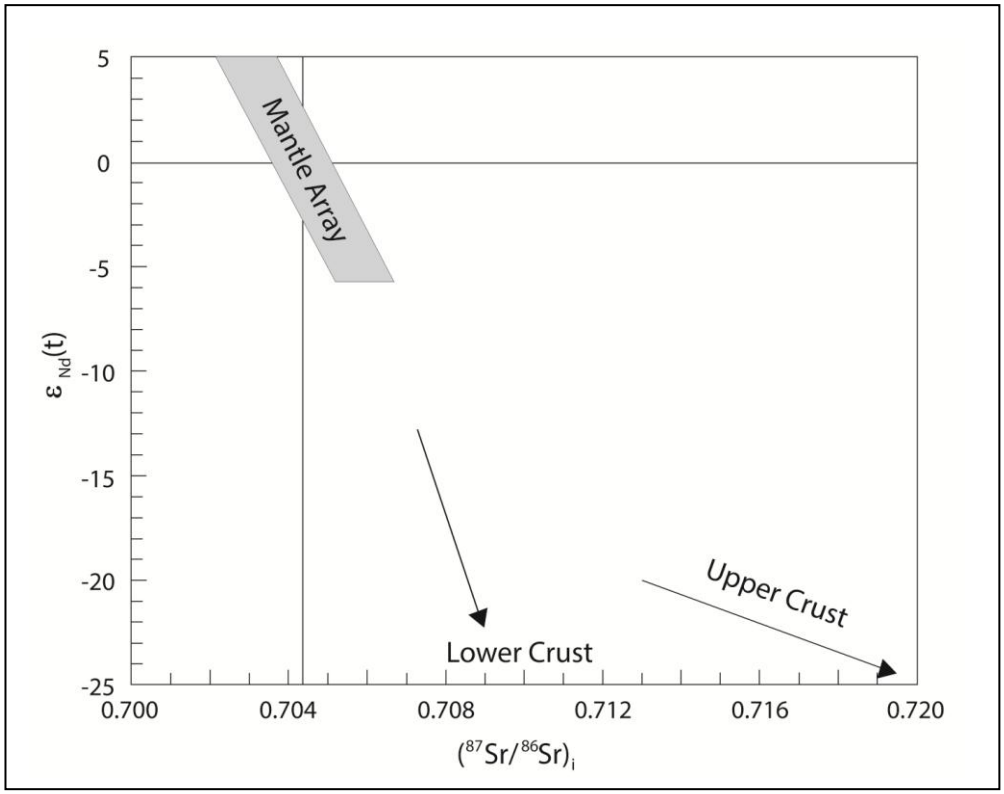

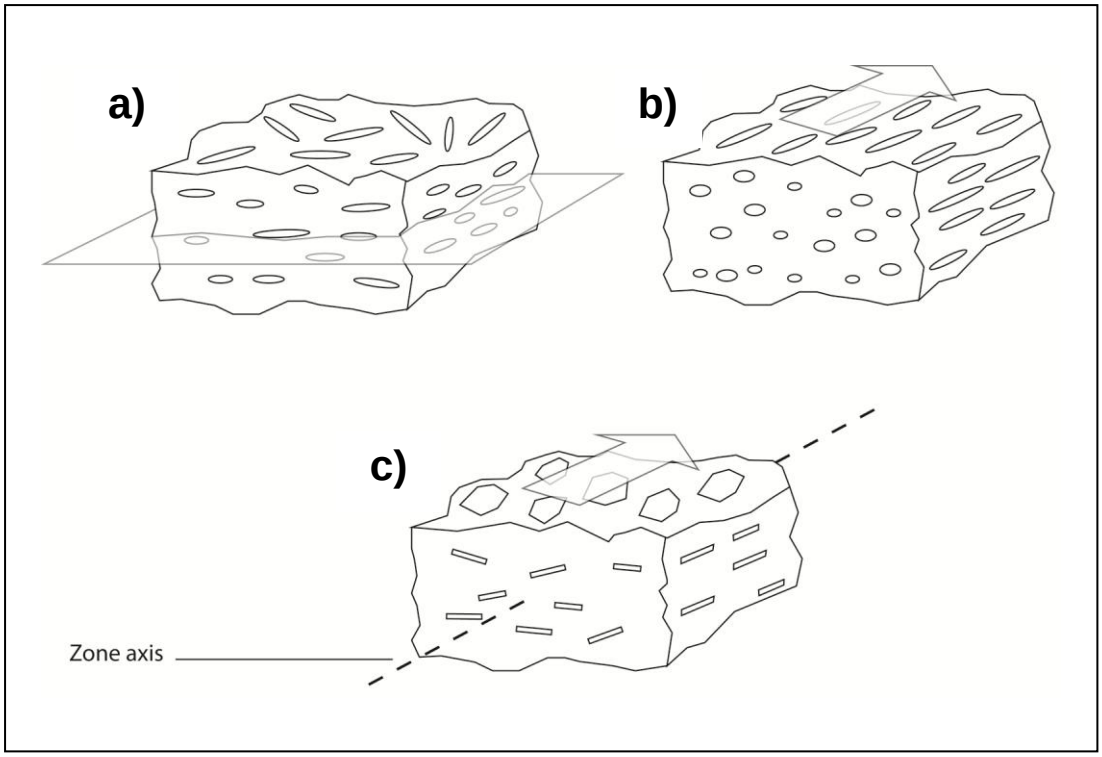

Fig 3.3 (above): Types of basic fabric; **a**: planar fabric; **b**: linear fabric; **c**: linear fabric defined by a non-elongate mineral (after Bouchez, 1997)

Fig 3.4 (below): Response of linear minerals to shear; **a**: pure shear; **b**: moderate shear ($2 < \gamma < 8$); **c**: high shear ($\gamma \geq 8$) (constructed based on findings of Arbaret et. al., 1997)

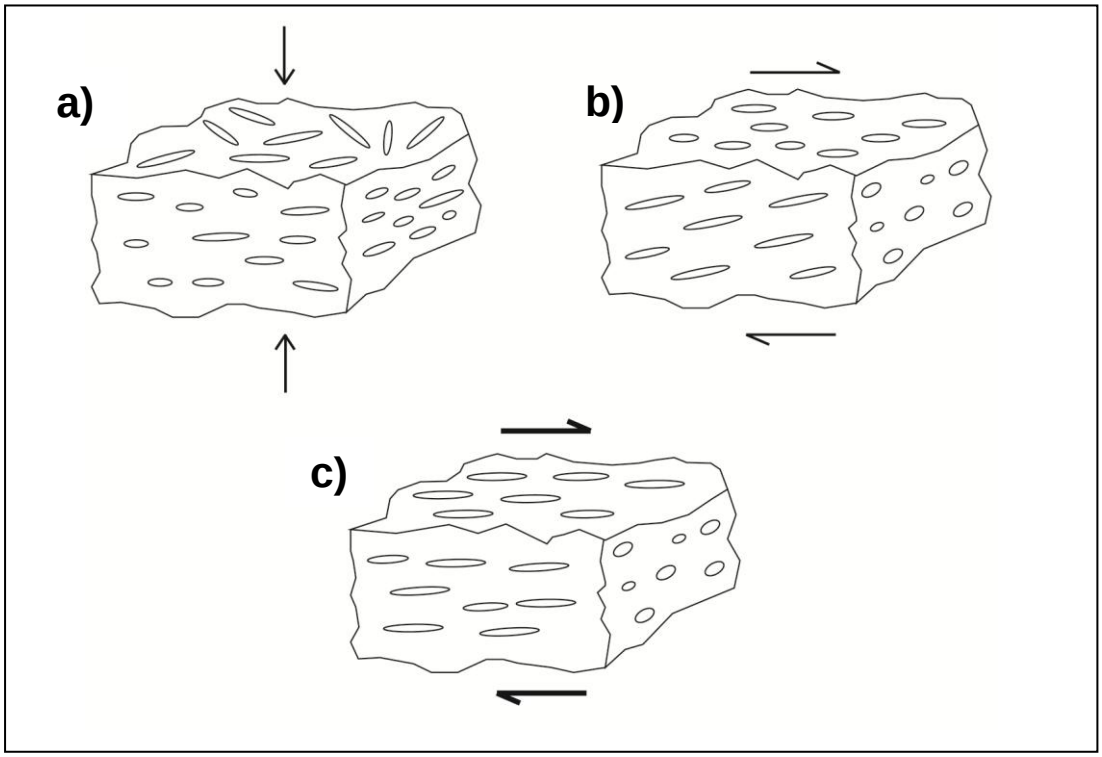

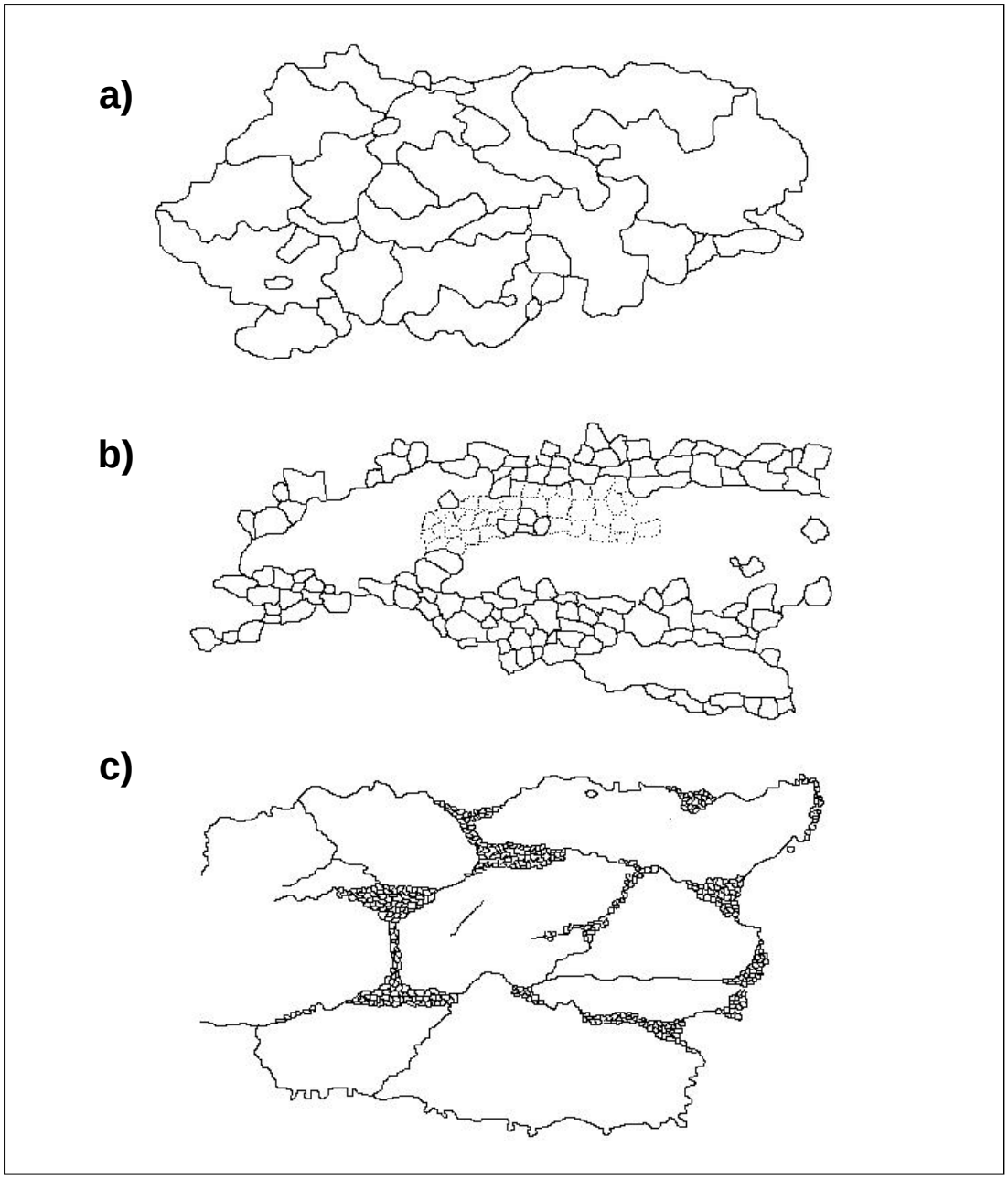

Fig 3.5: Textures displayed by the dynamic recrystallisation of quartz; **a**: Grain boundary migration (T ≥ 500°); **b**: Rotation recrystallisation – polycrystalline quartz (400 ≤ T ≤ 500°); **c**: Grain boundary bulging (T ≤ 400°) (modified from Stipp et. al., 2002)

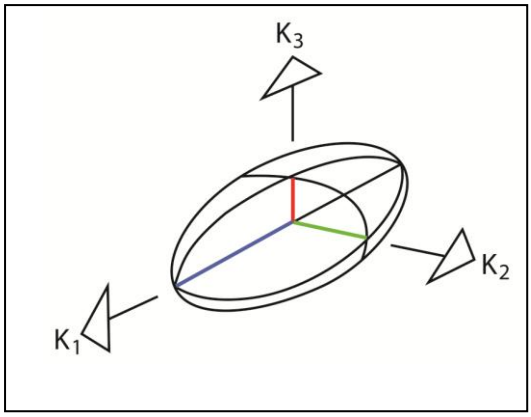

Fig 3.6 (left): Example *Magnetic susceptibility ellipsoid* (after Owens, 1974)

Fig 3.7 (below): Basic fabrics defined by shape anisotropy of magnetic minerals; **a**: planar fabric; **b**: linear fabric (after Owens, 1974)

Fig 3.8 (lower): External demagnetising fields affecting an elongate mineral; where n and s represent north and south magnetic poles respectively; **a**: large field produced by an induced magnetisation (M) along the short axis; **b**: smaller field produced by an induced magnetisation (M) along the long axis (after Dunlop and Özdemir, 2001)

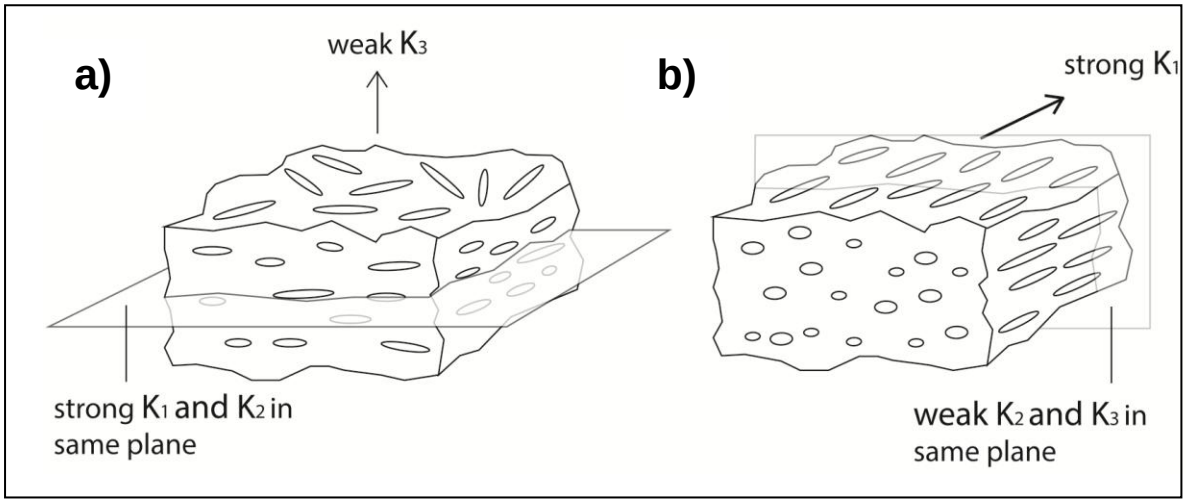

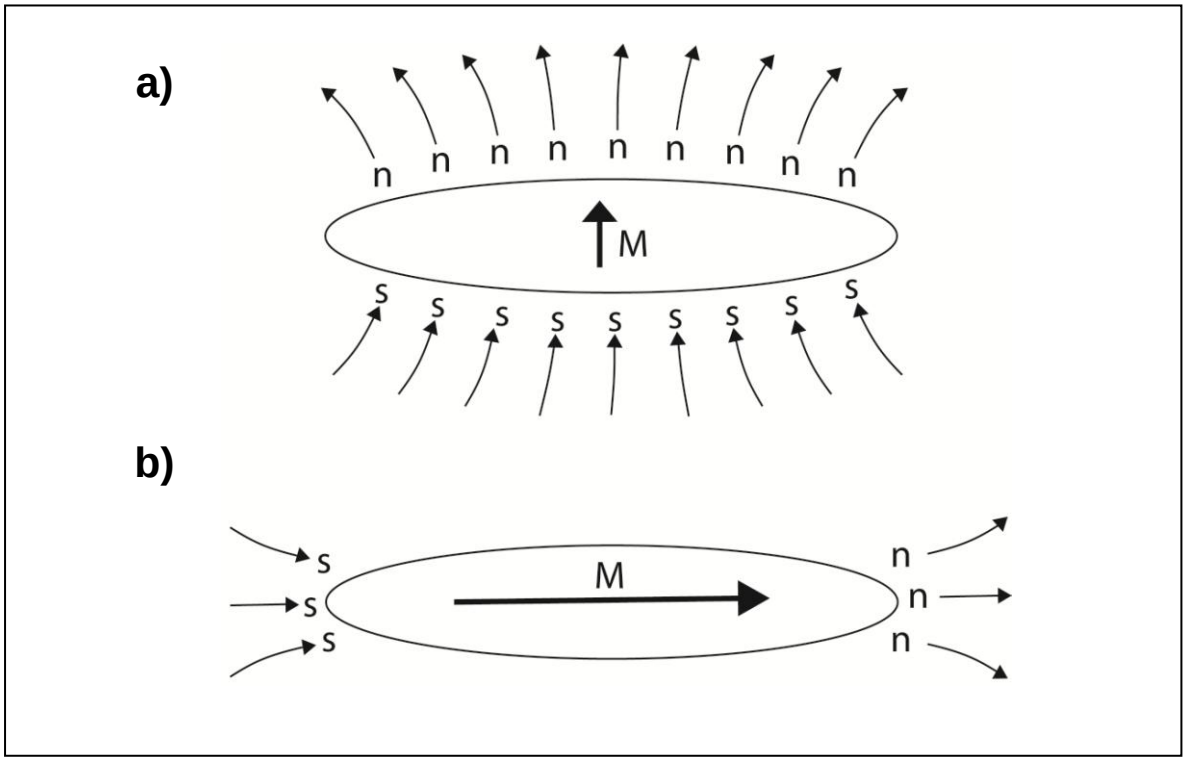

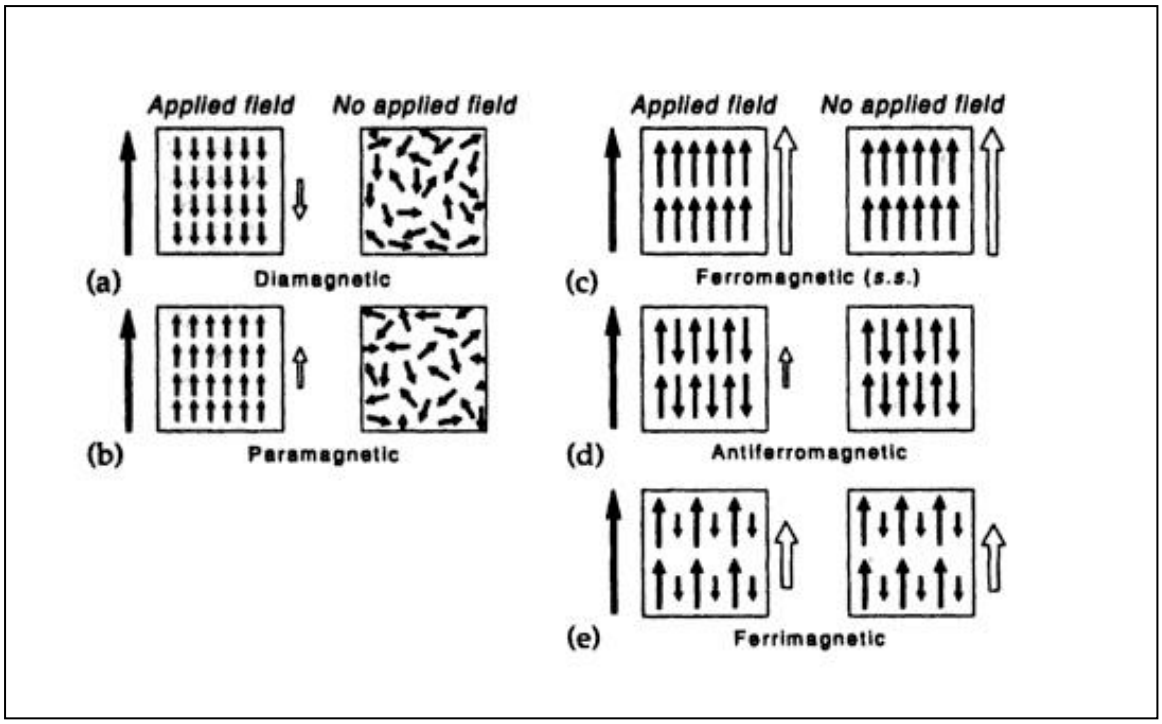

Fig 3.9 (above): Different forms of magnetisation. For each behaviour the left-hand diagram shows the effect of an applied field and the right-hand diagram shows the effect of removing this field (taken from Tarling and Hrouda, 1993)

Table 2.1 (below): Magnetic properties of a selection of common minerals. Modified from Stevenson (2004). Sourced from Deer et. al. (1966); Beausoleil et. al. (1983); Rochette et. al. (1992); Borradaile and Henry (1997); Martin-Hernandez and Hirt (2003)

Mineral	**Composition**	**Magnetic behaviour**	**Magnetic susceptibility (K) (S. I. x 10^{-6})**	**Curie temperature (Tc)**
Quartz	SiO_2	Diamagnetic	-14	-
Feldspar	$(K,Al,Ca)(Al)_{1-2}\ (Si)_{2-3}(O)_8$	Diamagnetic	-14	-
Calcite	$CaCO_3$	Diamagnetic	-14	-
Biotite	$K_3(Mg,Fe^{2+})_{6-4}(Fe^{3+},Al,Ti)_{0-2}$ $[Si_{6-5}Al_{2-3}O_{20}](OH,F)_4$	Paramagnetic	Ca. 1000	-4/44°K
Muscovite	$K_2Al_4[Si_6Al_2O_{20}](OH,F)_4$	Paramagnetic	Ca. 120	-
Hornblende	$(Na,K)_{0-1}Ca_2(Mg,Fe^{2+},Fe^{3+},Al)_5$ $[Si_{6-7}Al_{2-1}O_{22}](OH,F)_2$	Paramagnetic	500 – 5000	-
Magnetite	α-Fe_3O_4	Ferrimagnetic	2-2.8 x 10^6	580°C
Maghaematite	γ-Fe_2O_3	Ferrimagnetic	2-2.8 x 10^6	Ca. 350°C
Haematite	α-Fe_2O_3	Antiferromagnetic	1 x 10^5	680°C

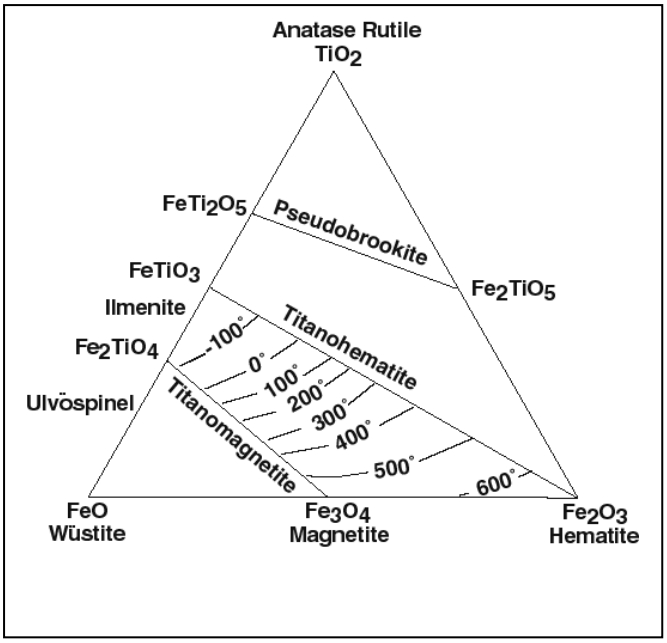

Fig 3.10 (left): Ternary diagram showing solid solution between magnetic minerals that occur in igneous rocks (taken from Saltus et. al., 1999)

Fig 3.11 (below): Hysteresis loops showing the effect of changing applied field (H) on the induced field (M); **a**: for field applied along 'easy' axis of an SD grain; **b**: for a field applied at an angle to the 'easy' axis in an SD grain; **c**: for a multidomain grain. Here H_C = coercivity of the grain; M_{sat} = saturation magnetisation; H_{sat} = saturation field and M_{IRM} = remanent magnetisation (Modified from Tarling and Hrouda, 1993)

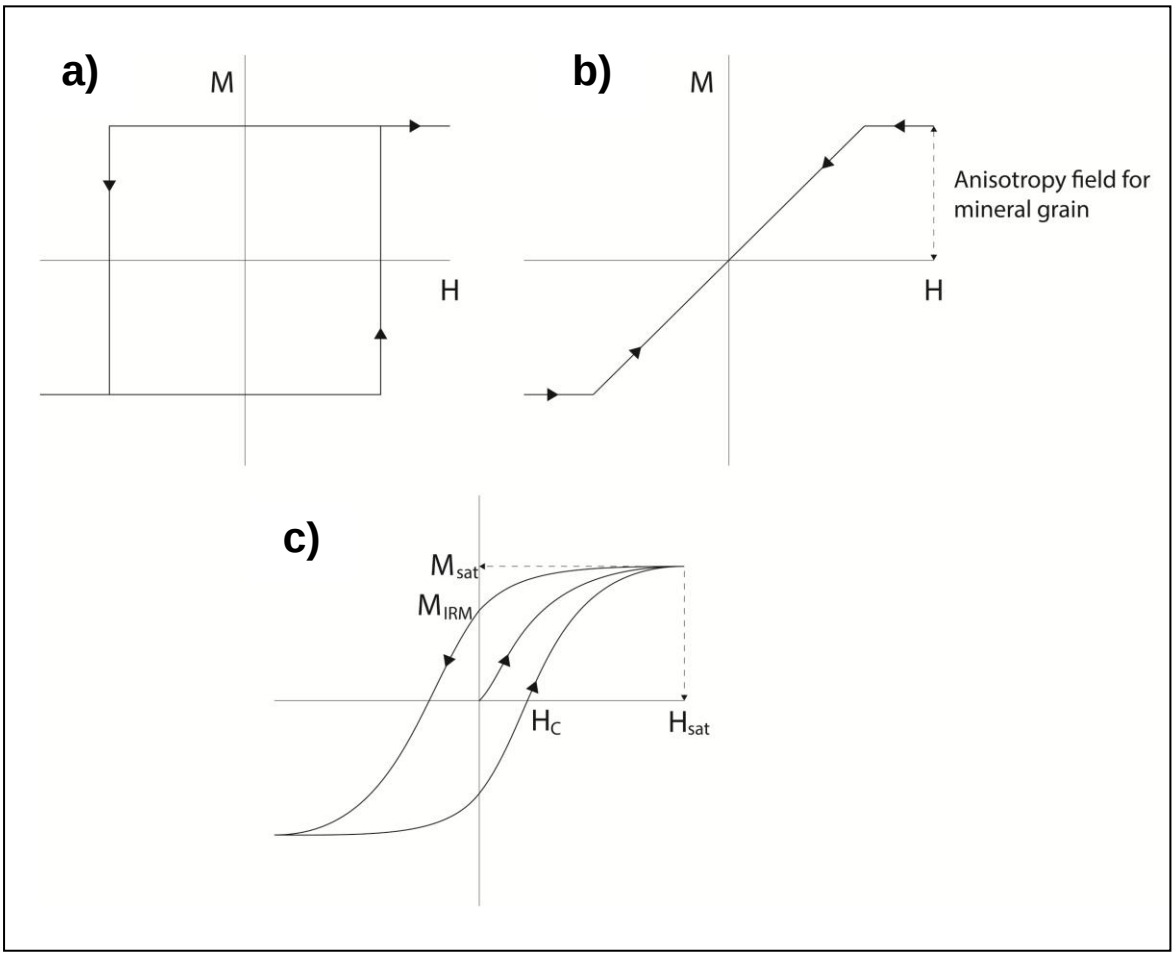

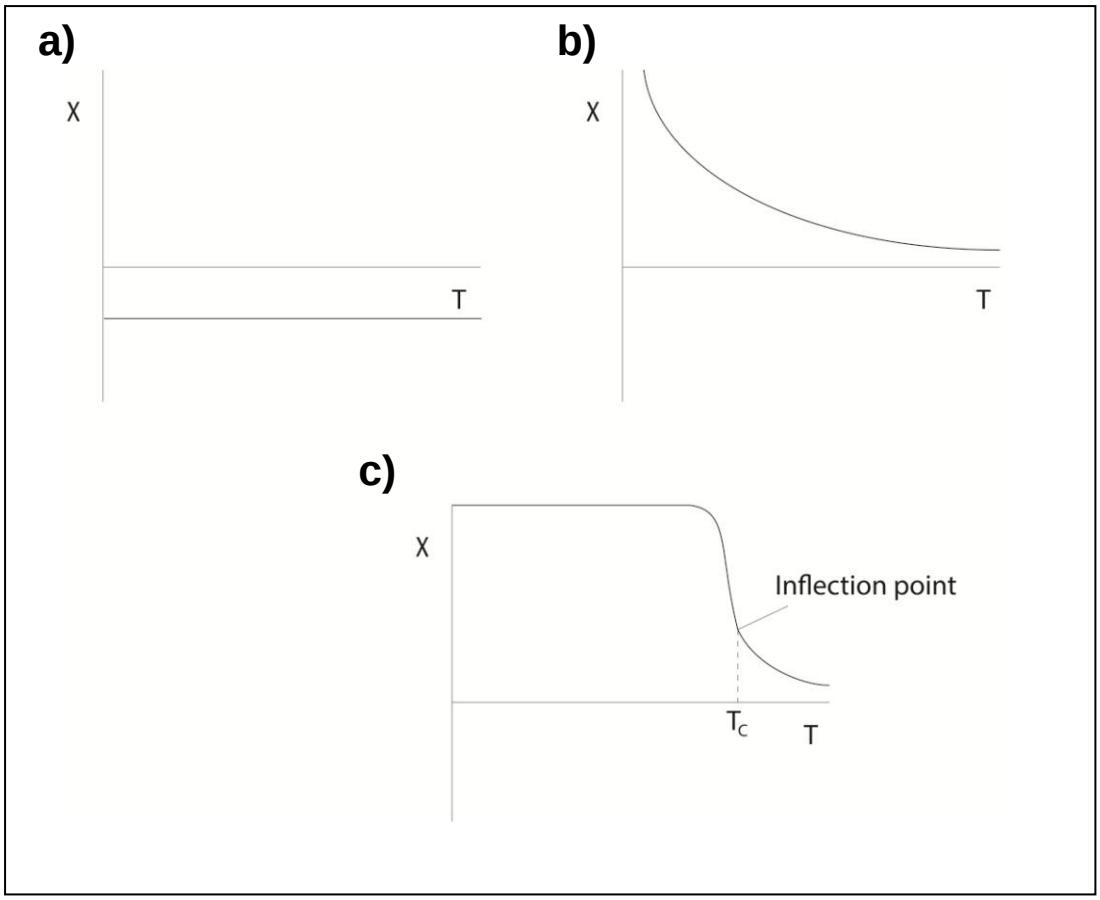

Fig 3.12: Generalised plots showing the relationship of normalised susceptibility (X) with temperature for: **a**: Diamagnetic materials; **b**: Paramagnetic materials; **c**: Ferromagnetic (*s.l.*) materials. For the latter the *Curie Temperature* (T_c) is represented by the inflection point on the decreasing normalised susceptibility curve (after Dunlop and Özdemir, 2001)

CHAPTER 4: ZONATION OF THE NEWRY IGNEOUS COMPLEX

4.1 Introduction

During the current study the Newry Igneous Complex (NIC) was mapped through geophysics, petrology and geochemistry. This defined 17 distinct zones, many of which have not been previously recognised, including several that are only apparent from their aeromagnetic signature. Others were identified in previous work (e.g., Reynolds, 1934; Reynolds, 1943; Meighan and Neeson, 1979; Neeson, 1984) but have been refined in the current study.

Zones have been assigned to a continuous sequence spanning the entire NIC, due to the generally clear age relationships and seemingly continuous nature of some compositions across pluton boundaries. On this basis 15 areas within the NIC have been defined as Zones A to O, whilst the two sets of satellite bodies are defined as Zones X and Y respectively. Each of the zones has also been classified as an igneous unit, following standard nomenclature (e.g., GSNI, 1997).

This division has further relevance in that it distinguishes a number of potential magma pulses. Locations and compositions of these have provided the basis for understanding both the petrogenesis and emplacement of the NIC (see Chapter 4B and 5).

4.2 Methods

4.2.1 Tellus Geophysics

Geophysical data was provided from the Tellus Project, managed by the Geological Survey of Northern Ireland (GSNI) in 2005-2006. This dataset consists of aeromagnetic and radiometric maps constructed from airbourne surveying. The aircraft involved contained two magnetometer sensors for collecting aeromagnetic data, together with a gamma-ray spectrometer for collecting radiometric data. A total distance of 86,000 km was flown at a height of 56 m over all of Northern Ireland (GSNI, 2007).

Prior to use in the current study aeromagnetic data were initially converted to a *reduced-to-pole* (RTP) format. This is a standard way of producing monopolar (rather than dipolar) magnetic anomalies that are centred over their "causative bodies" (e.g., Baranov and Naudy, 1964; Stavrev and Garovska, 2000, p. 317) and are hence easier to interpret. Reduced-to-pole (RTP) aeromagnetic signatures were colour coded in terms of their values in nanoteslas (nT) and plotted on a map of Northern Ireland (GSNI, 2007). This map was subsequently refined during the current study to include only the area in the vicinity of the NIC (see fig. 4.1).

Radiometric results recorded gamma radiation from the spectral windows of Potassium-40 (^{40}K), Uranium-238 (^{238}U) and Thorium-232 (^{232}Th) (GSNI, 2007). The data were again colour coded and plotted on a map of Northern Ireland prior to use in the current study. Here colours were assigned to represent the relative proportions of the three isotopes detected (e.g., Grasty and Charbonneau, 1974). This map was once again refined to include only the vicinity of the NIC (see fig. 4.2).

4.2.2 Petrology

Petrological investigation was conducted mostly for selected samples from the larger geochemistry/AMS sample suite (collection methods discussed below). These were obtained from three areas: the boundary of the quartz diorite within the Rathfriland pluton; throughout the Newry pluton and the northeastern margin of the Cloghoge pluton.

Two samples were obtained from the boundary of the quartz diorite, as these occupied key locations for determining characteristics of this feature (see fig. 4.3). 46 samples were also collected from throughout the Newry pluton, which were all utilised for petrology (see fig. 4.4). Finally, petrological data for the northeast margin of the Cloghoge pluton were derived from two sources. These comprised five samples collected from the area, as well as a number of field observations from a nearby site (fig. 4.5)

For each area the relative proportions of minerals in the samples or observed outcrops were recorded by eye. These were in turn compared to previous work (Neeson, 1984) and findings from current Tellus data (see section 4.4).

4.2.3 Geochemistry

Data acquisition

142 block samples from throughout the NIC were collected for geochemical analysis (this suite also provided petrology and AMS samples; the latter of which are discussed in Chapter 5) (see fig. 4.6). These were generally obtained from areas of good exposure, where fresh rock material was abundant (e.g., the Seeconnell

Complex and eastern boundary of the Rathfriland pluton). Previous studies (i.e., Reynolds, 1934; Reynolds, 1943; Neeson, 1984) provided information on the locations of such areas.

Many samples were also obtained from poorly exposed and previously unstudied areas. Most of these were located through use of the Virtalis *GeoVisionary* suite at the GSNI headquarters in Belfast. This software provides high-resolution topographical and geological visualisation over all of Northern Ireland, allowing areas of obvious outcrop to be observed. Several locations of satellite body exposure were also determined from early geological mapping of the area (Cruise et. al., 1873).

Samples were collected as relatively large blocks (averaging ~ 15 x 15 x 15 cm). After a selection of these were petrologically examined (see previous section) the majority of the overall suite was prepared for AMS. The latter process involved removal of some rock material by coring, as is discussed in Chapter 5. The remaining parts of the blocks (or the full block in the case of those samples not also used for AMS) were then packaged and delivered to the BGS headquarters in Keyworth. Here samples were crushed and their whole rock compositions analysed for a full suite of the 10 major elements and 63 trace elements, using the inductively coupled mass spectrometry (ICP-MS) technique. A full table of the results, together with detection limits, is provided in Appendix 2.

Data processing

Geochemistry results were processed in three ways prior to analysis. These were as follows:

1. Selection of elements for analysis
2. Calculation of mean concentrations
3. Mapping of concentration data for selected elements

The following account describes how this processing was conducted.

(1) Selection of elements for analysis: From the full set of results provided (see Appendix 2), concentrations of 8 major elements were analysed in this study. These comprise silicon (SiO_2), aluminium (Al_2O_3), titanium (TiO_2), iron (Fe_2O_3/FeO – or 'total iron', $Fe_2O_{3(t)}$), magnesium (MgO), calcium (CaO), sodium (Na_2O), potassium (K_2O) (e.g., Harker, 1909).

Five trace elements were in turn selected for detailed analysis. These comprise thorium (Th), uranium (U), rubidium (Rb), strontium (Sr) and zirconium (Zr). Of these, Th and U were selected because of their potential correlation with Tellus radiometric data (this is also the case with the major element, K). Conversely, Rb and Sr were analysed because each of these relate to a mineral that is common in the NIC: rubidium often occurs in biotite and strontium in plagioclase (Best, 2003). Finally, Zr was selected as an example of a generally immobile element (Pearce and Cann, 1973; Floyd and Winchester, 1975).

This is particularly the case during hydrothermal alteration (Finlow-Bates and Stumpfl, 1981). As a result, Zr may provide a more reliable primary trace element signature for parts of the complex like the Cloghoge pluton, where later Palaeogene

intrusion has caused such alteration (Reynolds, 1952; Gamble et. al., 1992). Zr is also relatively abundant within the NIC, due to the high proportion of zircon throughout (Meighan and Neeson, 1979; Neeson, 1984).

(3) Calculation of mean concentrations: Mean concentrations of the majority of selected elements were calculated for the main parts of the NIC. These comprised five of the eight major elements which were considered representative of overall evolution (SiO_2, TiO_2, $Fe_2O_{3(t)}$, MgO and K_2O), along with all five selected trace elements (Rb, Sr, Th, U, Zr), as these exhibit more variable relationships (see table 4.2).

More localised mean concentrations were calculated for the radiometric elements K_2O, Th and U. These were obtained for each compositionally distinct area of the NIC (see fig. 4.9), allowing comparison between airborne radiometric data and actual geochemical concentrations within these.

(4) Mapping of concentration data: Concentration data were mapped for 117 samples throughout the NIC (see fig. 4.6a for locations). This suite excludes the Seeconnell Complex as the latter contains its own varied set of geochemical subdivisions (e.g., Meighan and Neeson, 1979), which would require further study to understand.

Data were mapped for the major elements SiO_2 and $Fe_2O_{3(t)}$, along with the trace elements Sr and Zr. The former were chosen because they are major components within minerals and are indicators of felsic and mafic composition respectively (e.g.,

Harker, 1909). The trace element Sr was also chosen due to its abundance, as well as its presence in plagioclase, which is almost ubiquitous throughout the NIC (Meighan and Neeson, 1979; Neeson, 1984). Finally, Zr was selected due to its general immobility (Pearce and Cann, 1973; Floyd and Winchester, 1975; Finlow-Bates and Stumpfl, 1981). As previously discussed, this may compensate for areas of the Cloghoge pluton where other trace elements (i.e., Sr) might be remobilised by later events (see Reynolds, 1952; Gamble et. al., 1992).

The concentration values were mapped by representing samples as variably grey shaded symbols (see fig. 4.7 and 4.8). This was achieved by assigning each value a percentage representing its comparative magnitude in relation to the maximum and minimum concentrations for the element in question (see appendix 1). These percentages were in turn applied to mapped symbols by setting them as the *k* ('grey shade') parameter in the Adobe Illustrator colour palette. Hence, the minimum concentration (0) would be displayed as a white symbol, the maximum concentration (100) as a black symbol, with intermediate values being shown as varying grey tones.

4.2.4 U-Pb Geochronology

Prior to the current study 9 samples for geochronology were collected from across the NIC. These were obtained from each area of geophysical anomaly, excluding the outermost Newry pluton and outer Cloghoge pluton. Locations of these samples relative to these anomalies are shown in fig. 4.10.

The samples were dated through U-Pb zircon geochronology at the NERC Isotope Geoscience Laboratory (NIGL). This involved standard Isotope Dilution Thermal Ionisation Mass Spectrometry (ID-TIMS) methodologies (see Tilton et. al., 1955; Krogh, 1973). Zircons were also subject to a modified chemical abrasion pre-treatment for the effective elimination of Pb-loss (Mattinson, 2005). Finally, the accuracy of the final dates were controlled by the gravimetric calibration of the EARTHTIME U-Pb tracer (ET535) and the determination of the ^{238}U decay constant (Condon et. al., 2007; Jaffey et. al., 1971).

The results obtained from this process, together with further details of sampling and errors are illustrated within table 4.3.

4.3 Tellus geophysics

4.3.1 Aeromagnetic data

The Rathfriland (NE) and Newry (central) plutons display the most prominent aeromagnetic anomalies (fig. 4.1). These include strongly positive signatures in the northeast and south of the Rathfriland pluton (Ca. 50nT). The former appear to correspond to the Seeconnell Complex and adjacent intermediate (monzonite and diorite) bodies, whilst the latter closely match locations of quartz diorite outcrop (Reynolds, 1934; Neeson, 1984) (see fig 2.6a).

Other prominent signatures include two concentric (ring-like) weaker (Ca. 20nT) positive anomalies within the Rathfriland and Newry plutons. However, only one of these appears to relate to an area which is known to be lithologically distinct. This is the anomaly from the Newry pluton, which can be closely correlated with outcrop of the ring-like porphyritic granodiorite (Neeson, 1984) (see fig. 2.6a).

The other parts of these two plutons show generally negative aeromagnetic signatures (fig. 4.1), although some of these are equally prominent. This is the case in the Newry pluton, where both a central and outer negative aeromagnetic zone display very strong signals (Ca. -100nT). On the other hand, the negative aeromagnetic signature within the southeast of the Rathfriland pluton is almost indistinguishable from the majority of host rocks in the region. This appears to transition into a more prominent negative signature (Ca. -50nT) that occupies much of the outer Rathfriland pluton as well as the centre of this pluton.

These results suggest that both the strength and polarity of the observed aeromagnetic signature bear little relation to the composition of the NIC. For example, the outer and inner parts of the Newry pluton display almost identical strong negative signatures, despite the known reverse zoning of this intrusion. However, many of the shifts in aeromagnetic signature do appear to occur at facies boundaries, suggesting that these may have a key influence on aeromagnetic signature.

Further negative aeromagnetic anomalies occur in areas outside of the main NIC (see fig. 4.1). These comprise a large region to the north of the Newry and Cloghoge plutons, as well as a smaller area to the north of the Seeconnell Complex. There is abundant evidence that both locations consist almost entirely of sedimentary rocks (e.g., GSNI, 1997; Beamish et. al., 2010).

However, a third area of negative aeromagnetic anomaly outside of the main NIC may relate to igneous rocks at the surface. This consists of a narrow arc to the north of the Rathfriland pluton and within the marginal part of this pluton (fig. 4.1), which closely relates to at least two small granodiorite bodies (GSNI, 1997). These represent the satellite bodies discussed in section 2.2, which may therefore be more extensive in the subsurface.

In contrast to other areas of the complex, the Cloghoge (SW) pluton exhibits a consistently strong positive magnetic signature. However, this extends across both the Caledonian and Palaeogene parts of the composite intrusion. The signal may therefore reflect a single dominant magnetisation from one of these areas, which

overprints the effects of the other. Such a scenario could occur if the results relate to a magnetic signature from a depth at which the pluton is more uniform (see Gunn et. al., 1997; Schetselaar et. al., 2000). The fact that this distinct aeromagnetic signature only occurs in the vicinity of Palaeogene rocks suggests that these might be the contributing factor.

The Cloghoge pluton therefore reveals a limitation of the aeromagnetic results, in showing that these cannot consistently be linked to surface features. Consideration of the most recent geological map (GSNI, 1997) provides further evidence for this. The map shows that the extent of the Seeconnell Complex is in fact notably smaller than its aeromagnetic signature suggests. Hence, aeromagnetic data is clearly useful as a guide to surface composition, although this correlation cannot be assumed to be precise (e.g., Spector and Grant, 1970; Gunn et. al., 1997; Schetselaar et. al., 2000).

In two locations aeromagnetic anomalies can be seen to continue beyond the surface boundaries of facies. This is observed for the Seeconnell Complex and the southwest margin of the Rathfriland pluton (fig. 4.1). The latter is most apparent due to the prominent aeromagnetic ring in this area, which can be traced within the adjacent Newry pluton (fig. 4.1). These results may imply that the zones in question are present in the subsurface beneath other parts of the NIC (e.g., Schetselaar et. al., 2000).

4.3.2 Radiometric data

Radiometric data divides the NIC into three broad areas (fig. 4.2). These comprise a crescent-shaped region of apparent thorium enrichment in the northeast of the complex; a potassium-enriched region that occurs throughout the Newry and much of the Rathfriland plutons and an area of mixed thorium and potassium signature (with a smaller amount of uranium) within the Cloghoge pluton. The boundaries between these areas appear to be abrupt, whereas the three divisions themselves each show a relatively consistent signature.

Radiometric data also reveals two more localised divisions of the NIC. The first of these closely correlates with the known outcrop of the Seeconnell Complex (GSNI, 1997). Here the radiometric signature implies higher potassium content than the surrounding thorium-elevated area (fig. 4.2). The other localised radiometric distinction occurs in the Cloghoge pluton. Here areas of Caledonian outcrop (see fig. 3.6a; GSNI, 1997) can be seen to show apparent potassium enrichment in comparison to areas shown to be Palaeogene.

However, a single area of exception exists in the north of the Cloghoge pluton. Here a radiometric signature that is more consistent with the Newry pluton occurs adjacent to the latter (fig. 4.2b). The original mapping of the NIC by Neeson (1984) in fact included this area as part of the Newry pluton. Hence, the current results support Neeson and imply that adjustment of the pluton's most recently mapped boundary (GSNI, 1997) is required.

4.4 Petrology

4.4.1 The extent of the Rathfriland pluton quartz diorite

Petrological investigation reveals that samples R5A and R5B both represented quartz diorites. However, these were obtained from outside the aeromagnetic anomaly corresponding to this facies (see fig. 4.3). Therefore, this further suggests that aeromagnetic data does not reliably relate to boundaries observed at the surface.

4.4.2 Facies divisions within the Newry pluton

Table 4.1 shows the identified mineralogies of samples within the Newry pluton based on areas of the pluton derived from the work of Neeson (1984) and current Tellus data. This implies that samples obtained from the inner part of the Newry pluton are generally more mafic (higher hornblende proportions) than those from closer to its margins. These results supports the work of Neeson (1984), which inferred an inner hornblende granodiorite and an outer biotite granodiorite. Furthermore, the current study identified distinctive fine and porphyritic granodiorites (samples N22A and N22C in fig. 4.4) in the same area as the porphyritc granodiorite 'ring' mapped by Neeson (see fig 3.6a). These are considered to represent part of the 'porphyritic ring facies' identified by Neeson (1984).

However, the current study also reveals some exceptions to Neeson's (1984) straightforward three-zone division of the pluton. Samples N5A to N10 from Neeson's (1984) central hornblende granodiorite in fact yield abundant biotite together with little or no hornblende, thus matching the outer pluton facies much more closely (see table 4.1). On the other hand, two samples (N2 and N3) which

should clearly locate within Neeson's (1984) outer biotite granodiorite facies (see fig. 3.6a) yield large amounts of hornblende (see table 4.1 and fig. 4.4). Nevertheless, the majority of samples investigated in the current study closely match the mineralogies predicted by Neeson (1984) (see table 4.1).

Aeromagnetic data also supports the separation of the Newry pluton into three distinct areas (see fig 4.1). Furthermore, the prominent positive aeromagnetic 'ring' appears to occupy a similar relatively narrow region of the outer pluton as the porphyritic granodiorite (see fig 3.6a). However, this correlation is not precise, as samples N22B and N21B located within the eastern part of the aeromagnetic 'ring' are respectively coarse and very felsic (see table 4.1 and fig. 4.4). The same is observed in the south of the pluton, where differing facies have been deduced from numerous samples that plot within the area of positive aeromagnetic anomaly (see fig. 4.4). Therefore, the porphyritic granodiorite only appears to correspond to the inner margin of the positive aeromagnetic 'ring'.

However, these observations can be accounted for if the porphyritic granodiorite is outward dipping. This is considered to be likely, since many of the structures within the NIC have been recorded as such (Neeson, 1984; current study). The result would be that the facies yields an aeromagnetic signature not only for its area of surface outcrop, but also for where this is present in the subsurface closer to the margin of the Newry pluton (e.g., Gunn et. al., 1997; Schetselaar et. al., 2000). With this considered the current results largely support the three-way division of the Newry pluton proposed by Neeson (1984).

Fig. 4.4 hence resolves the zonation of the Newry pluton based on these three dominant areas. Due to the internal variation highlighted in the inner and outer facies, this was achieved mainly by considering the relationship of samples to the distinctive porphyritic granodiorite 'ring'. Several samples exhibited clear porphyritc textures and so were assigned to this zone (see table 4.1). Those that plotted more centrally or more marginally were in turn considered as inner or outer zone facies respectively, even though some of these varied from the distinct compositions implied by Neeson (1984).

However, within the eastern Newry pluton outcrop of the porphyritic granodiorite is sparse. Hence, the location of the facies boundaries here are determined using a combination of data from rare observed outcrops (see fig. 4.4) and aeromagnetic results (which was considered appropriate due to the correlation discussed above) (see fig 4.1). The resolved zonation in this area indicates that the porphyritic granodiorite lies further from the eastern margin of the pluton than has been inferred by Neeson (1984) (compare fig. 3.6a with fig. 4.1 and 4.4). Hence, the original mapping of the Newry pluton by Neeson (1984) can be refined, with the porphyritic granodiorite ring exhibiting a smaller radius (see derived locations in fig. 4.4).

4.4.3 The northeast margin of the Cloghoge pluton

The Cloghoge pluton is in contact with the Newry pluton at its northeast margin (fig. 4.5; see appendix 1 for site locations). However, this margin alone appears to exhibit a greater variety of facies than throughout each of the adjacent plutons. These have exclusively been observed in steeply orientated sheets that display a range of contact relationships with one another.

A number of the observed facies do resemble those seen in the adjacent plutons. These comprise a coarse mafic granodiorite, a fine hornblende granodiorite, a felsic granodiorite, a more typical medium-grained granodiorite and a granite (see appendix 1). Whereas the first two of these are similar to the composition of both the outer Cloghoge pluton and the inner Newry pluton, the last clearly shows a closer affinity with the felsic 'core' of the former (see Neeson, 1984). On the other hand, the felsic and more typical granodiorites could equally relate to the outer Newry pluton or the non-granitic parts of the Cloghoge pluton 'core' according to petrographic observations from these areas (see Neeson, 1984).

The remaining two facies recorded in this boundary zone are more mafic than any part of the adjacent plutons, comprising a porphyritic diorite and dolerite. Nevertheless, the former porphyritic diorite shows an obvious textural similarity with the porphyritic granodiorite within the Newry pluton (see Neeson, 1984). This suggests that although the area is currently mapped within the Cloghoge pluton, it may also have a close relationship to parts of the Newry pluton.

A number of the above facies observed at site 132 shown in fig. 4.5 (J 079 239 – see appendix 1) display variable contact relationships. These include straightforward cross cutting, whereby one facies has intruded the other in a dyke-like form, but also extensive mingling and even potential of mixing of the same facies (see photo 4.1 – 4.3). This variability is demonstrated by all the facies at this site, suggesting that none consistently post date any of the others and thus the facies are likely to have been intruded near-contemporaneously.

4.5 Geochemistry

4.5.1 General geochemical trends

Evolution towards the southwest

Consideration of the mean concentrations of elements within the main parts of the NIC reveals several broad trends (table 4.2a). Firstly, an increase in silica (SiO_2) occurs towards the southwest of the complex, together with a decrease in total iron ($Fe_2O_{3(t)}$), titanium (TiO_2) and magnesium (MgO) in the same direction. On the other hand, the abundance of potassium (K_2O) does not have such a clear trend. Nevertheless, these results largely suggest an evolution from more mafic to felsic facies towards the southwest of the NIC, supporting the previous work of Reynolds (1943), Meighan and Neeson (1979) and Neeson (1984).

Strontium (Sr), shows a similar southwest-directed trend to most of the major elements (table 4.2b). The concentration of Sr is clearly elevated within the Seeconnell Complex, and consistently decreases towards the southwest of the NIC. However, the other analysed trace elements do not seem to exhibit consistent NE-SW directed trends on this scale (table 4.2b).

Zoning of individual plutons

Mapping of the recorded geochemical concentrations supports previously inferred zoning of individual plutons (see Meighan and Neeson, 1979; Neeson, 1984) (fig. 4.7 and 4.8). For example, SiO_2 is significantly lower in concentration in the outer parts of the Rathfriland pluton than in its centre, with the opposite occurring within the Newry pluton (fig. 4.7a). Similar but reversed patterns are observed for

the other major elements. This indicates normal and reverse zoning within the respective plutons.

Major elements also strongly support the idea of an off-centre, felsic 'core' to the Cloghoge pluton (see Neeson, 1984). Within the area where this has been inferred (Neeson, 1984, see fig. 3.6a) silica is consistently high and recalculated Fe_2O_3 is consistently low (fig. 4.7). The opposite applies for most of the pluton outside of the core, again implying a clear normal zoning pattern.

The trace elements Sr and Zr also show an inward change within each of the plutons (see fig. 4.8a-b). However, unlike the major elements, these both display highly variable concentrations within the inferred core of the Cloghoge pluton. Such large and unique changes in composition may reflect secondary processes.

4.5.2 Localised geochemical trends

Geochemical data also helps to reveal a number of more localised variations. Some of these reflect the zonation apparent from Tellus geophysics, petrology and former work on the NIC, whereas others represent formerly unknown or uncertain divisions. The following section explains how geochemistry aids the division of such areas for specific parts of the NIC.

The Seeconnell Complex

Although the Seeconnell Complex has not been geochemically mapped within the current study, the available results suggest that it is clearly unique. Firstly, raw geochemical data shows that there is virtually no overlap in the concentrations of

SiO_2, TiO_2, $Fe_2O_{3(t)}$, MgO and Sr between here and any other part of the NIC (see appendix 2). In addition, the mean concentrations of these elements are shown to be obviously distinct within the Seeconnell Complex area in table 4.2. The current geochemical data therefore supports former work (Meighan and Neeson, 1979; Neeson, 1984) and other parts of this study (see Chapters 4.3 and 4.4), which consistently separate the Seeconnell Complex.

The northeast 'mafic' rim of the main Rathfriland pluton

Mapped trends in both major and trace element abundance (fig. 4.7 and 4.8) reveal another distinct area of the Rathfriland pluton. This constitutes a crescent-shaped region in the northeast of the intrusion (see the same shape defined by radiometric data in fig. 4.2 and section 4.3). Here SiO_2 is relatively low (approximately 53 – 65 wt%) and $Fe_2O_{3(t)}$ is high (approximately 4 – 8 wt%), implying an overall relatively more mafic composition than inner parts of the pluton (fig. 4.7, appendix 2A). Zr is also notably high in this area (approximately 250 – 350 mg/kg), although Sr concentrations are more variable (approximately 400 to 1400 mg/kg) (fig. 4.8, appendix 2B). These results largely support Neeson's (1984) inference that the area is the most mafic part of the main pluton (i.e., excluding the Seeconnell Complex) and predominantly consists of hornblende granodiorite.

However, the data also implies a relatively abrupt geochemical boundary to this area (fig. 4.7 and 4.8), which has not been reported in previous work. The radiometric data from the current study defines the same boundary (see fig. 4.2). This corresponds to a shift from Th-elevation in the outer pluton rim to lower radiometric element concentrations in its interior. The fact that major elements also show a

variation here suggests that this boundary may represent a significant compositional division.

Some samples within the northeast rim of the Rathfriland pluton additionally display even more mafic geochemistries that resemble those obtained from the Seeconnell Complex (see appendix 2). This is primarily apparent from the low SiO_2 and high $Fe_2O_{3(t)}$ contents of such samples, although the Sr concentrations of these are also typically higher (i.e., Seeconnell-like) (fig. 4.7 and 4.8). Excluding samples R5A and MRC364 (see fig. 4.6), which are part of the quartz diorite (see appendix 1) these all locate within what has previously been distinguished as an outer hornblende granodiorite (Neeson, 1984) (see fig 3.6a). Within this the samples are relatively widely spread but consistently occur close to the Seeconnell Complex and intermediate bodies (see fig. 3.6a).

These results may therefore imply the existence of a further major facies within this part of the Rathfriland pluton. This would occur peripheral to the intermediate bodies, separating these from the main outer hornblende granodiorite (see fig 3.6a). The new facies is referred to as *mafic granodiorite* and is considered a further subdivision of the pluton.

The inner Rathfriland pluton

The inner (including the southwest) part of the Rathfriland pluton clearly represents another distinct compositional zone. The concentrations of SiO_2 and recalculated Fe_2O_3 remain at largely consistent levels throughout this area, but differ significantly from those within the northeast rim of the pluton (fig. 4.7). This is

inconsistent with the work of Neeson (1984), which alluded to a gradual transition between an outer hornblende granodiorite and an inner biotite granodiorite within the pluton (see fig. 3.6a). Instead the current work suggests that a single major boundary at the edge of the northeast pluton rim (see above) separates these facies.

The major element proportions within the inner Rathfriland pluton (particularly recalculated Fe_2O_3) are also closely comparable with the outer Newry pluton. The immobile trace element, Zr, shows a similar pattern. Hence, the overall composition of the NIC appears to change more notably at the boundary of the Rathfriland pluton northeast rim than throughout the remainder of the Rathfriland and outer Newry plutons.

Nevertheless, Tellus data implies two significant aeromagnetic boundaries within the inner Rathfriland pluton (see Chapter 4.3). These comprise an outer and central negative anomaly, together with an intervening positive aeromagnetic ring (fig. 4.1). As has been previously discussed, the lack of geochemical variation corresponding to these changes suggests that aeromagnetic anomalies may not reflect composition.

The main Newry pluton

Geochemistry of the Newry pluton shows a single abrupt shift corresponding to the area in which the narrow porphyritic granodiorite 'ring' has been inferred (fig. 4.8). Hence these results do not distinguish all three distinct compositions discussed in section 4.4 (also see Neeson, 1984).

The precise location of the geochemical division is uncertain. $Fe_2O_{3(t)}$ implies a boundary at the inner margin of the porphyritic ring facies, separating an outer felsic area of the pluton (low recalculated Fe_2O_3) from an inner mafic area (high recalculated Fe_2O_3) (see fig. 4.8b). On the other hand, SiO_2 implies that the porphyritic granodiorite itself is separated into an outer felsic (high SiO_2) part and inner more mafic (low SiO_2) part (fig. 4.8a). These are each more similar to the concentrations in adjacent zones than to each other, suggesting that the main division of the pluton passes through the 'ring' facies.

Fig. 4.8 also reveals clear anomalous concentrations within the other facies of the pluton. These occur within two samples (NTS1 and N31) from the outer facies, along with one (N30B) from the central facies. However, since petrology (see section 4.2) indicates a reasonable degree of variation within each of these areas, the anomalies are not considered significant. Therefore, these results are not considered to be inconsistent with generally distinct outer and inner facies of the Newry pluton.

Nevertheless, the results suggest that the zonation of the Newry pluton is likely to be more complex than previous work (Reynolds, 1943; Neeson, 1984) implies. The former divisions are still appropriate, although the three facies should not be considered as homogeneous or consistently distinct from one another.

Anomalous area within the central Newry pluton

Zr concentrations are anomalously low within part of the central Newry pluton. This is apparent from 6 samples close to the Newry Fault, which have almost

exclusively lower Zr concentrations than anywhere else in the NIC (fig. 4.8b). The only area where Zr proportions appear to resemble this is the off-centre 'core' to the Cloghoge pluton, although concentrations here are mixed. However, the Newry pluton samples are not anomalous in terms of any other analysed trace or major element. This could imply the presence of zircon or the involvement of secondary processes.

The 'mafic' outer Cloghoge pluton

The outer Cloghoge pluton can be clearly distinguished from the off-centre 'core' of this intrusion by its more mafic major element geochemistry (fig. 4.7a-b). Concentrations of both SiO_2 and Zr here also closely match those within areas of hornblende granodiorite throughout the NIC (i.e., the northeast rim of the Rathfriland pluton and the central Newry pluton – see fig. 4.7a, fig. 4.8b). Therefore, the outer 'mafic' Cloghoge pluton appears to show more geochemical similarity with parts of other plutons than it does to its own 'core'.

However, the geochemistry of the outer Cloghoge pluton does not appear to be completely consistent throughout. In particular, an area of frequent and varied sheeting close to the northeast margin of the pluton (see photo 4.1 – 4.3 and appendix 1) corresponds to equally variable concentrations of both major and trace elements (fig. 4.7). As has been outlined in section 4.5, this area appears to show relationships to various other parts of the Cloghoge and Newry plutons, which geochemistry results seem to support. On the other hand, the west of the pluton displays much less geochemical variation (see fig. 4.7 and 4.8).

The off-centre felsic 'core' of the Cloghoge pluton

Geochemistry reveals a distinct felsic area to the Cloghoge pluton that closely corresponds to Neeson's (1984) proposed off-centre 'core' (see fig. 3.6a). Evidence for this is provided most clearly from SiO_2 (fig. 4.7a), which shows very high concentrations. Hence, the geochemical shift between the felsic 'core' and the 'mafic' outer part of the Cloghoge pluton is very large, resembling that recorded between the northeast rim and inner part of the Rathfriland pluton.

However, the sample in the west of the proposed core (C2D in fig. 4.6) does not appear to match the composition of others from this zone. Instead this exhibits a more mafic geochemical signature in terms of SiO_2 (65.30 wt%) and $Fe_2O_{3(t)}$ (4.07 wt%) (fig. 4.7a-b). Petrology shows, though, that the site in question does in fact host felsic biotite granodiorite (see locality 8 in appendix 1), and so this sample may represent an anomaly rather than an exception to Neeson's (1984) zonation.

Concentrations of the trace elements Sr and Zr appear to be very variable throughout this area (fig. 4.8a-b). Each of these elements also exhibits several significantly lower concentrations here than they do across the majority of the NIC. However, as mentioned above, the fact that such characteristics are not displayed by the major elements suggests that these may be the result of secondary processes.

At first glance geochemistry suggests that the Cloghoge pluton also exhibits a second clearly felsic area, which is apparent from a number of high SiO_2 concentrations further to the north of the intrusion (fig. 4.7a). Yet as has been formerly discussed (see Chapter 4.3), both radiometric data and mapping by Neeson

(1984) suggest that this zone in fact represents part of the adjacent Newry pluton. Geochemistry also reveals very similar major element concentrations within both of these areas (fig. 4.7a-b). Hence, the boundary between the Newry and Cloghoge pluton shown on the most recent geological map of the area (GSNI, 1997) appears to be incorrect.

The satellite bodies

Major element concentrations of the satellite bodies consistently resemble those within the inner Rathfriland and outer Newry plutons (fig. 4.7). Conversely, concentrations of the trace elements Sr and Zr appear to link more closely with the hornblende granodiorite from the northeast Rathfriland and central Newry plutons. Hence the precise relationship of these bodies to the main NIC is unclear from these results.

4.5.3: Relationships of the radiometric elements

Mean concentrations of the radiometric elements (thorium (Th), uranium (U) and potassium (K_2O)) appear to vary somewhat systematically when plotted for localised parts of the NIC (see fig. 4.9). Firstly, these results illustrate that the concentrations of K_2O in the Seeconnell Complex are significantly higher than those in any proximal part of the main NIC (fig. 4.9a). This matches the findings from Tellus airborne radiometric data.

However, elevated K_2O is also apparent within the off-centre 'core' of the Cloghoge pluton, which cannot be observed from the Tellus data. This is likely to be the result of the additionally elevated Th concentration (fig. 4.9b), which will override the effect

of changes in K_2O due to its higher overall concentration. Therefore, this shows that the Tellus radiometric data should be considered with caution, as this only reveals relative proportions of the three detected elements.

On the other hand, the northeast rim of the main Rathfriland pluton (particularly areas R1 and R2 in fig. 4.9b) shows a clear Th-enrichment from both geochemical and airborne radiometric data. This area also shows an enrichment in U, which is not revealed by the airborne data. This lack of correlation may be the result of the mean U concentration being lower than that of Th, meaning that the latter dominates the radiometric signature, as is suggested above for the 'core' of the Cloghoge pluton.

It has also been important to acquire radiometric element data from the satellite bodies, since these show no obvious signature from airborne radiometric data (see fig. 4.2). Samples from here yield radiometric concentrations of such elements that are in fact similar to those within the main part of the NIC, particularly the inner Rathfriland and Newry plutons (i.e., low Th, relatively low K_2O) (see fig. 4.9). This supports major element geochemistry (see table 4.2) and also suggests that the lack of radiometric anomaly associated with the satellite bodies may simply reflect their limited aerial extent (see Cook et. al., 1996; Schetselaar et. al., 2000; Martelet et. al., 2006).

4.6 U-Pb geochronology

4.6.1 General trends

U-Pb zircon ages were obtained from 9 samples representing areas of various geophysical signature throughout the NIC (see Chapter 1.4). These indicate that the NIC generally becomes younger to the southwest. This is apparent from the position of the oldest (414.02 ± 0.18 Ma) and youngest (407.23 ± 0.35 Ma) samples in Seeconnell Complex and the Cloghoge pluton 'core' respectively. However, samples from other parts of the NIC also support this relationship, suggesting that younging occurs consistently towards the southwest (see table 4.3 and fig. 4.10 and 4.11).

The results also imply that individual plutons young towards their centres. This is clearest from the Rathfriland pluton, from which 6 samples were obtained that support this relationship (see fig 4.11). The Newry pluton also shows evidence for inward younging, although this is only based on two samples, which show slightly overlapping error margins (see fig 4.11). Age relationships within the Cloghoge pluton are uncertain from this data, since only one sample was obtained from here.

4.6.2 Localised relationships

U-Pb dates have also been applied to further understanding several recognised divisions of the NIC (see section 4.3-4.6). Firstly, the dates appear to show conclusively that the Seeconnell Complex is a separate, older part of the NIC. The derived age for this area is more than 0.5 Ma older than any other, and remains older even when error margins are considered (see fig. 4.11). Hence these results confirm former work, Tellus geophysics and geochemistry.

However, the dates for two areas in the south of the Rathfriland pluton are clearly unexpected considering other data. These represent the quartz diorite body and outer hornblende granodiorite labelled in fig 4.11. Neeson (1984) showed that xenoliths of the quartz diorite occur in adjacent granodiorites, implying that the former is older. Yet the current geochronology suggests that the quartz diorite is in fact younger than the nearby hornblende granodiorite. The most likely explanation for this is that Neeson (1984) observed quartz diorite xenoliths within the undated *mafic* granodiorite. Therefore, the quartz diorite body would pre-date the adjacent mafic granodiorite but post-date the nearby hornblende granodiorite.

The close relationship of the intermediate facies in the north of the Rathfriland pluton with the Seeconnell Complex (Meighan and Neeson, 1979; Neeson, 1984; current study) provides greater constraint on the age of the former. As a result this intermediate facies is thought to be older than the other northeast rim facies.

Based on these considerations, the sequence of intrusion within the northeast Rathfriland pluton (see fig. 4.11) would be as follows:

Seeconnell Complex > Diorite bodies > Mafic granodiorite (1) > Hornblende granodiorite > Quartz diorite > Mafic granodiorite (2)

Such age relationships can be seen to be very consistent with the general southwest younging of the NIC discussed above.

The U-Pb ages from the more homogeneous inner Rathfriland pluton suggest that this may young with consecutive aeromagnetic zones. The ages for the outer two zones are within error of each other, whereas the central negatively magnetic zone yields a distinctly younger date (see fig. 4.11). These suggest that the three divisions of the pluton here may have been intruded sequentially.

U-Pb ages from the two locations within the Newry pluton correspond to the area of central negatively aeromagnetic signature and that of the positive aeromagnetic 'ring' (see fig. 4.11). However, the latter does not represent the porphyritic granodiorite relating to this anomaly as petrology clearly shows that this is an area of the outer pluton facies (see section 4.4 for explanation). Radiometric dates from the two samples are again indicative of inward younging, although these display slightly overlapping error margins in their ages, meaning this relationship cannot be conclusively confirmed (see table 4.3 and fig. 4.10 and 4.11).

The final age, relating to the off-centre 'core' area of the Cloghoge pluton, is significantly younger than any other (see table 4.3 and fig. 4.10 and 4.11). However, this area is also surrounded by the outer part to the pluton, which would be expected to be older in accordance with the pattern observed in the other two plutons. If this were the case the overall intrusion history of the NIC would appear to be relatively continuous.

4.7 A new detailed zonation

Tellus geophysics, petrology, geochemistry, geochronology and former mapping provide a number of clear and time-constrained divisions within the NIC. The following account explains how these results have been combined to provide a new detailed zonation for the intrusion, which comprises a total of 17 distinct zones within the NIC and satellite bodies (see fig 4.12). Zones have been assigned to a continuous age-related sequence spanning the entire NIC, attesting to the apparently continuous nature of compositions across pluton boundaries. Each of the zones has also been classified as an igneous unit, following a standard nomenclature (e.g., GSNI, 1997).

For ease of reference this account separates the zones into those occurring within each of the main parts of the NIC (i.e., the three plutons and the satellite bodies). However, as has been illustrated there are very close links between some of these areas, regardless of pluton boundaries.

4.7.1 Zonation of the Rathfriland pluton

Former mapping of the Rathfriland pluton by Neeson (1984) implied that this area consisted of several distinct marginal bodies, but otherwise exhibited smooth compositional transitions. The current study supports the presence and distinctive nature of the marginal facies. However, the study also reveals a number of significant boundaries within the main part of the pluton, with some of these corresponding to major compositional shifts. The characteristics of the facies in between these boundaries are in turn shown to be relatively homogeneous. Therefore, the zonation of the Rathfriland pluton appears to be much more

punctuated than has been previously thought, allowing the entire area to be divided into the distinct zones A to I (see fig 4.12).

Zone A – the Seeconnell Complex

The Seeconnell Complex represents one of the clearly distinct marginal parts of the NIC. This is already a separately mapped area (GSNI, 1997) and is known to exhibit characteristic ultramafic to intermediate compositions (Reynolds, 1934; Neeson, 1984) (see fig 4.12). Both current geochronology together with field relationships (see Meighan and Neeson, 1979; Neeson, 1984) also suggest that the Seeconnell Complex is the oldest part of the overall intrusion. Therefore, this is defined as **Zone A**.

This zone had essentially already been defined by previous work (i.e., Reynolds, 1934; Meighan and Neeson, 1979; Neeson, 1984; GSNI, 1997), thus the current study focused on providing further ways to characterise the area. This was achieved through geochemistry and Tellus geophysics results. Geochemistry confirms a compositional distinction of the Seeconnell Complex by showing that the mean concentrations of major elements here are significantly more mafic than within any other part of the NIC and its satellite bodies.

Tellus geophysical data also reveals aeromagnetic and radiometric anomalies associated with the Seeconnell Complex. These comprise a strong positive magnetic signature and an implied enrichment in potassium respectively. The latter is supported by geochemistry, which reveals a clearly elevated mean K_2O concentration within the Seeconnell Complex (3.95 wt% – see table 4.3a). This is

particularly prominent in relation to other parts of the Rathfriland pluton, which all appear to yield relatively low amounts of K_2O (mean value of 3.27 wt%).

However, the aeromagnetic anomaly is larger in area than the surface extent of the Seeconnell Complex. This is explained through the fact that these data have been shown to relate to features from depth (e.g., Spector and Grant, 1970; Gunn et. al., 1997; Schetselaar et al., 2000). This is supported by the work of Reynolds (1934) and Neeson (1984), which suggests that the boundaries of the Seeconnell Complex extend outwardly beneath the Rathfriland pluton.

Former work has also establishes numerous subdivisions within the Seeconnell Complex itself (e.g., Reynolds, 1934; Meighan and Neeson, 1979; Neeson, 1984 – see Chapter 3.2). These relate to abrupt and locally frequent alterations between the dominant intermediate and ultramafic compositions, as well as larger scale gradational variations (see fig 3.6b). It has been beyond the scope of the current study to subdivide the Seeconnell Complex in terms of zones.

Zone B-F – The northeast margin (excluding the Seeconnell Complex)

This area of the Rathfriland pluton is distinguished as a whole through both its geochemisty and radiometric signature (see fig. 4.12). Geochemically it is consistently more mafic relative to the inner parts of the intrusion, whilst radiometric data for the area shows obvious thorium enrichment. The latter is additionally supported by mean trace element concentration data. This suggests a refinement to the previous mapping of the Rathfriland pluton (e.g., Reynolds, 1934; Meighan and Neeson, 1979; Neeson, 1984) whereby this is divided by a major compositional

boundary, rather than being gradationally zoned (see fig. 4.12). The current study has also helped to constrain several further subdivisions of the northeast Rathfriland pluton margin, which are discussed below.

Firstly, the presence of several intermediate bodies in the very north of the Rathfriland pluton appears to correlate with strong positive aeromagnetic anomalies. This provides another characteristic through which these bodies can be distinguished. Former work has linked the bodies to the intermediate part of the Seeconnell Complex, as these display similar dioritic to monzonitic compositions (Reynolds, 1934; Meighan and Neeson, 1979; Neeson, 1984). As a result, the intermediate bodies are likely to be as old or slightly younger than the Seeconnell Complex, thus these are defined as **Zone B** (see fig. 4.12).

Current data also indicates the presence of a previously unrecognised facies adjacent to Zones A and B. This is more felsic than the intermediate compositions within each of these areas, but clearly more mafic than most of the remaining Rathfriland pluton. Hence the facies is referred to as a *mafic granodiorite* (specifically the *mafic granodiorite (1)*). Due to its close proximity and compositional similarity to Zones A and B, this facies is inferred to be the next oldest in the NIC and is defined as **Zone C** (see fig. 4.12).

Within fig. 4.12 the areas of Zone C exposure are shown to be connected between Zones A and B. This is due to the consistency of mafic compositions recorded in these areas, even for samples that are more distal from the bodies. However, there

is also a clear sampling gap in this region, meaning it is also plausible that a different composition (e.g, a more typical granodiorite) exists here.

Three distinct facies are apparent in the east of the Rathfriland pluton. These comprise a hornblende granodiorite; a quartz diorite and another previously unrecognised mafic granodiorite (which is named here as the mafic granodiorite (2)). Current geochronology shows that the hornblende granodiorite predates the quartz diorite. Xenoliths of the quartz diorite have in turn been observed within the facies now referred to as the mafic granodiorite (2), implying that the former is older (see Neeson, 1984). Therefore, the age relationships in this part of the NIC are clear. Furthermore, geochronology implies that these facies predate the inner part of the pluton. Thus the hornblende granodiorite is defined as **Zone D**; the quartz diorite as **Zone E** and the mafic granodiorite (2) as **Zone F**.

The quartz diorite is further distinguished by a strong positive aeromagnetic anomaly, similar to that observed for Zones A and B. However, much of the area covered by the surrounding Zones D and F (along with part of G) exhibits an aeromagnetic signature that is almost indistinguishable from the surrounding host rocks. This is not observed within any other part of the main NIC. A possible explanation is that these areas yield a negative aeromagnetic signature (as is observed for other parts of Zone G) that is effectively cancelled by the presence of the positively aeromagnetic quartz diorite at depth (see Spector and Grant, 1970; Gunn et. al., 1997; Schetselaar et. al., 2000).

Zones G, H, I – *magnetically variable inner biotite granodiorite*

As has been discussed above, an abrupt compositional and radiometric shift occurs at the boundary of the northeast Rathfriland pluton margin, which is inconsistent with Neeson's (1984) inferred gradational facies changes. Geochemistry from the internal part of the pluton further supports non-gradation by revealing virtually homogeneous major element compositions throughout this area. Samples from here are relatively felsic, suggesting that the central biotite granodiorite described by Neeson (1984) may extend over a much wider area than has previously been thought.

Due to the lack of compositional variation this part of the pluton is separated into zones according to only aeromagnetic data (see fig. 4.12). Firstly, the outermost area displays a mixed aeromagnetic signature. Part of this in the south is continuous with the 'neutral' signature of Zones D and F (see above), although the majority displays a negative magnetic anomaly that appears similar to that of the older mafic granodiorite in the north of the pluton (Zone C). However, geochronological data suggests that the area in question is younger than the adjacent northeast pluton rim, hence this is defined as **Zone G** (see fig. 4.12).

Towards the interior of the pluton the aeromagnetic signature abruptly shifts to being positive, although retaining a similar intensity. Overall this area defines a relatively extensive, approximately ring-shaped anomaly. Due to the consistent inward younging pattern observed throughout the NIC, the area is considered likely to postdate the adjacent Zone G, although the error margins of the respective radiometric dates are significantly overlapping. It is thus defined as **Zone H** (see fig. 4.12).

A third division of the inner pluton is apparent by a further area of negative magnetic anomaly in the centre of the previous. The signature here is again of similar intensity to the former two, although it covers a significantly smaller area. Geochronological data clearly suggests that this central area is the youngest part of the Rathfriland pluton and hence it is defined as **Zone I** (see fig. 4.12).

The clarity of each of the aeromagnetic zones described allows these to be easily mapped (fig. 4.12). However, as has been discussed previously, these anomalies may not accurately reflect surface characteristics (see Spector and Grant, 1970; Gunn et. al., 1997; Schetselaar et. al., 2000). In particular, if the anomalies relate to outwardly-dipping features (as is typical throughout the NIC – see Neeson (1984)) they would be expected to record a shift in this direction.

A single part of the inner Rathfriland pluton does appear to exhibit a distinct composition. This occurs at Shannaghan Hill (J 217 407), at the very northern margin of the pluton. The granodiorite facies here is anomalously felsic, leading Neeson (1984) to deduce that it may represent a separately intruded pulse. Nevertheless, the boundaries between this and the adjacent granodiorites are not observed, and so their relationship is unconfirmed. The facies also exhibits no distinctive aeromagnetic or radiometric signature. As a result of the uncertainties in terms of its extent and relationships to other facies, the felsic granodiorite at Shannaghan is therefore not currently considered as a distinct zone of the NIC, instead being included within Zone G.

4.7.2 Zonation of the Newry pluton

Former work has suggested that the Newry pluton is reversely zoned (Meighan and Neeson, 1979; Neeson, 1984). Current geochemistry supports this by showing that major element concentrations become relatively more mafic towards the centre of the pluton.

Both current geochemistry and petrology also broadly support the three facies of the Newry pluton proposed by Neeson (1984). These represent an outer biotite granodiorite; a porphrytic granodiorite 'ring' and an inner hornblende granodiorite. Current geochronology suggests that the outer of these facies predates the inner, whilst the foliation in the outer facies has also been shown to be cross cut by the porphyritic granodiorite 'ring' (Neeson, 1984). Hence the outer biotite granodiorite is the oldest of the three facies, although the relative ages of the other two are unclear from this evidence.

The outer biotite granodiorite can additionally be seen to cross cut the western boundary of the Rathfriland pluton (Neeson, 1984; GSNI, 1997). As a result this is considered to post date the zones within the latter and is thus defined as **Zone J** (see fig. 4.12). The other two facies are in turn considered to likely follow the inward younging pattern confirmed elsewhere in the NIC. Therefore, the porphyritic granodiorite 'ring' in defined as **Zone K** and the inner hornblende granodiorite as **Zone L** (see fig. 4.12).

However, the current results also show that some characteritics of the three facies are inconsistent with Neeson's (1984) original zonation. Firstly petrology suggests

that none of these are as homogenous as might be expected, with overlap occurring particularly between the outer and inner facies. The granodiorite 'ring' (Zone K) is more distinctive, showing a dominantly porphyritic texture and a consistently fine grain size. This ring also exhibits a positive aeromagnetic anomaly, in contrast to the consistent strong negative signature throughout the rest of the pluton. On the other hand, geochemistry (specifically recalculated Fe_2O_3 concentrations) implies some overlap between the composition of the porphyritic granodiorite and the other pluton facies, although this is only evident close to the margins of 'ring'.

Due to the generally distinctive nature of the porphyritic granodiorite 'ring' (Zone K) this has been used in the current study to investigate Neeson's (1984) proposed facies boundaries. These are shown to be accurate throughout much of the Newry pluton. However, in the east of the pluton, both petrology and aeromagnetic data suggest that the porphyritic granodiorite occurs more centrally than has previously been thought. Therefore, fig. 4.12 represents a refinement to the original zonation illustrated in fig 3.6a.

Current results also show that part of the central hornblende granodiorite (Zone L) exhibits an anomaly in terms very low Zr concentrations. The cause of this is currently unknown.

4.7.3 Zonation of the Cloghoge pluton

Determining the zonation of the Cloghoge pluton is potentially more difficult due to the presence of the Palaeogene Slieve Gullion Complex. Nevertheless, former work has distinguished two main divisions (Neeson, 1984; see also Reynolds,

1934). These consist of an off-centre felsic 'core', occurring to the east of the main Slieve Gullion Complex, together with an outer mafic part occupying the remaining Caledonian areas of the pluton. The current study confirms these divisions through geochemistry, as well as identifying a third, previously unrecognised division at the eastern margin of the intrusion (see fig. 4.12). This is discussed below.

Zone M – Mixed facies marginal sheets

Numerous steeply orientated sheets occur within part of the Cloghoge pluton that is immediately adjacent to the Newry pluton. These show a wide range of compositions (from doleritic to granitic), which appear to display very variable contact relationships with one another. This is considered to reflect intrusion of the respective facies over a short timescale.

Some of these sheet facies, such as the dolerites, show unique compositions within the NIC. However, many more exhibit close petrological similarities with either the Newry pluton or other parts of the Cloghoge pluton. The clearest examples of such are a set of felsic sheets that can be matched to the Cloghoge pluton 'core' and a set of porphyritic diorites that shows textural resemblance to the Newry pluton 'ring' facies (Zone K). This relationship of the sheeted area to both plutons suggests that it might be intervening in age. Furthermore, Neeson (1984) observed that the Cloghoge pluton cross cuts the Newry pluton (see GSNI, 1997) and hence post dates the latter. Therefore, the sheeted area is considered to be the earliest-intruded part of a younger pluton and is thus defined as **Zone M** (see fig 4.12).

Due to its limited outcrop the exact extent of this zone is uncertain. This is partly constrained by the presence of the adjacent off-centre 'core' to the Cloghoge pluton (see below) and the other outer facies of the Newry pluton. However, the lateral continuation of the zone along the pluton margin is less constrained due to poor outcrop over this area. Hence the boundaries of Zone M illustrated in fig. 4.12 are estimated.

Zone N-O – Outer and 'core' areas of the pluton

Current geochronology shows that the off-centre 'core' area of the Cloghoge pluton is notably younger than any other dated part of the NIC. Although no other radiometric dates are available from the Cloghoge pluton, the off-centre 'core' is therefore considered to likely represent the youngest part of this. This is supported by the consistency of the inward younging relationship observed in other plutons. Hence the outer pluton facies is defined as **Zone N** and the pluton 'core' as **Zone O**.

The only clear inconsistency of the current results to the zonation of the Cloghoge pluton proposed by Neeson (1984) is observed in the presence of Zone M (see above). Since this was previously unrecognised, the area covered by the zone formed part of the originally mapped outer hornblende granodiorite facies. Excluding the latter, fig 4.12 maps the divisions of the Cloghoge pluton in the same locations as Neeson (1984) inferred.

This includes a deviation from the boundary between the Cloghoge and Newry pluton illustrated in the most recent geological map of the area (GSNI, 1997). Neeson (1984) originally mapped the western part of this boundary as extending

further to the south (see dashed trend in fig. 4.12). Current results support this, revealing that the facies immediately to the north of Neeson's (1984) boundary display much clearer geochemical and radiometric resemblance to the Newry pluton than to the outer Cloghoge pluton. Hence fig. 4.12 disregards recent mapping and re-establishes the pluton boundary inferred by Neeson (1984).

The current study also highlights that the abundance of Sr and Zr is very variable within the 'core' facies (Zone O). As it the case for the low Zr concentrations within the central Newry pluton (Zone L) the cause of this is currently unknown.

The Cloghoge pluton is additionally separated as a whole from the other plutons through its geophysical signature. However, the strong positive aeromagnetic anomaly here is considered to most likely reflect the presence of the Palaeogene Slieve Gullion Complex at depth throughout (see Spector and Grant, 1970; Gunn et. al., 1997; Schetselaar et. al., 2000). This is due to the uniqueness of the signature in comparison to that from the other plutons, which the distinct characteristics of the Slieve Gullion facies can account for. Hence, aeromagnetic properties have not been used to characterise the Cloghoge pluton.

On the other hand, Tellus radiometric data separates the Caledonian and Palaegene parts of the Cloghoge pluton. Geochemistry confirms that the signature within the former corresponds to a significant enrichment in both K_2O and Th compared to other parts of the NIC. Therefore, this is characterising as an area of *mixed* radiometric signature (see fig. 4.12).

4.7.4 Other divisions of the NIC

Zone X, Y – The satellite bodies

Both early and more recent geological mapping of the area (Cruise et. al., 1873; GSNI, 1997) reveal a number of satellite granodiorite bodies outside the main NIC. Current petrology shows that these are consistently fine grained, whilst geochemistry suggests that the bodies are compositionally similar to the Rathfriland and Newry plutons. The satellite bodies to the north of the Rathfriland pluton also appear to display a negative aeromagnetic signature that can be traced in a concentric arc, which parallels the trend of Zone G of the Rathfriland pluton and ultimately cross cuts Zone C to the east (see fig. 4.12). Hence these bodies are thought to be more extensive than their scattered surface exposure suggests. The satellite bodies to the southeast of the Newry pluton do not display an obvious geophysical trace, but appear to occupy a similarly concentric trend, which in this case parallels Zone J of the Newry pluton (see fig. 4.12).

Due to the dominantly external locations of the satellite bodies their age relationships with specific zones of the NIC are unresolved. However, the association of the bodies with the older Rathfriland and younger Newry plutons respectively provides an indication of their ages relative to one another. Therefore, the satellite bodies to the north of the Rathfriland pluton are defined as **Zone X**, whilst those to the southeast of the Newry pluton are defined as **Zone Y** (see fig. 4.12).

Neither set of satellite zones exhibits a radiometric signature that is distinctive from that of the surrounding host rocks. However, like the other geochemistry results, measured concentrations of radiometric elements in the bodies imply a link with

parts of the Rathfriland and Newry plutons. Therefore, it is likely that the lack of airborne radiometric signal from the satellite bodies is a result of their relatively limited aerial extent (see Cook et. al., 1996; Schetselaar et. al., 2000; Martelet et. al., 2006).

4.7.5 Potential subsurface continuation of the NIC

The areas of negative aeromagnetic anomaly immediately outside much of the NIC margin may reflect continuation of the intrusion in the subsurface (see Spector and Grant, 1970; Gunn et. al., 1997; Schetselaar et. al., 2000). This is consistent with the work of Reynolds (1934) and Neeson (1984), which suggested that the boundaries of the NIC are outward-dipping.

A much more extensive negative aeromagnetic anomaly can also be seen to the north of the Cloghoge pluton. This is clearly distinct from the predominant host rock signature and most closely resembles that from parts of the Newry pluton. Therefore, it is suggested that the anomaly here may represent another pluton, which is only present within the subsurface. This would support Neeson's (1984) proposal that the NIC continues laterally at a deeper level. However, this proposal centred on a link between the NIC and the Crossdoney intrusion to the southwest in County Cavan, which remains unconfirmed.

4.7.6 Classification of igneous units

Each of the zones within the NIC has been classified as an igneous unit (see table 4.4 and fig. 4.13). These have been assigned the prefix *G* representing granodiorites and *H* representing monzonites and diorites (e.g., GSNI, 1997). The

rarer biotite pyroxenites within the Seeconnell Complex have in turn been assigned the prefix *P* (e.g., Boudreau et. al., 1997). Suffix numbers have also been added to signify the relative ages of each of these broad divisions (e.g., Richey, 1928). Each of the three plutons (along with the Seeconnell Complex) are divided independently, so that for example the oldest granodiorite within the Rathfriland pluton is termed the *Rathfriland G1* unit; whilst that within the Newry pluton is termed the *Newry G1* unit. This nomenclature could be used for future geological mapping of the NIC.

Units derived by this approach are exclusively lithologically based. This means that they are very similar to the derived zones, but differ within the inner Rathfriland pluton, where zones have only been distinguished by aeromagnetic signature. Hence zones G, H and I here have been currently classified as a single unit (*Rathfriland G4* – see table 4.4 and fig. 4.13), although there is a possibility that future work will reveal petrological distinctions between these. Derived igneous units also differ from zonation in terms of the Seeconnell Complex, which has been petrologically subdivided according to former work (Reynolds, 1934; Meighan and Neeson, 1979; Neeson, 1984 – see Chapter 3.2). This was beyond the scope of the zone distinctions made from current data.

For the purposes of considering emplacement (Chapter 5) the classified ‘zone’ distinctions are used over igneous units. This is because plutons are petrologically non-discrete, with compositions appearing to span their boundaries. As a result it has been more useful to consider the emplacement of the NIC as a whole, which is facilitated through use of the sequential zonation.

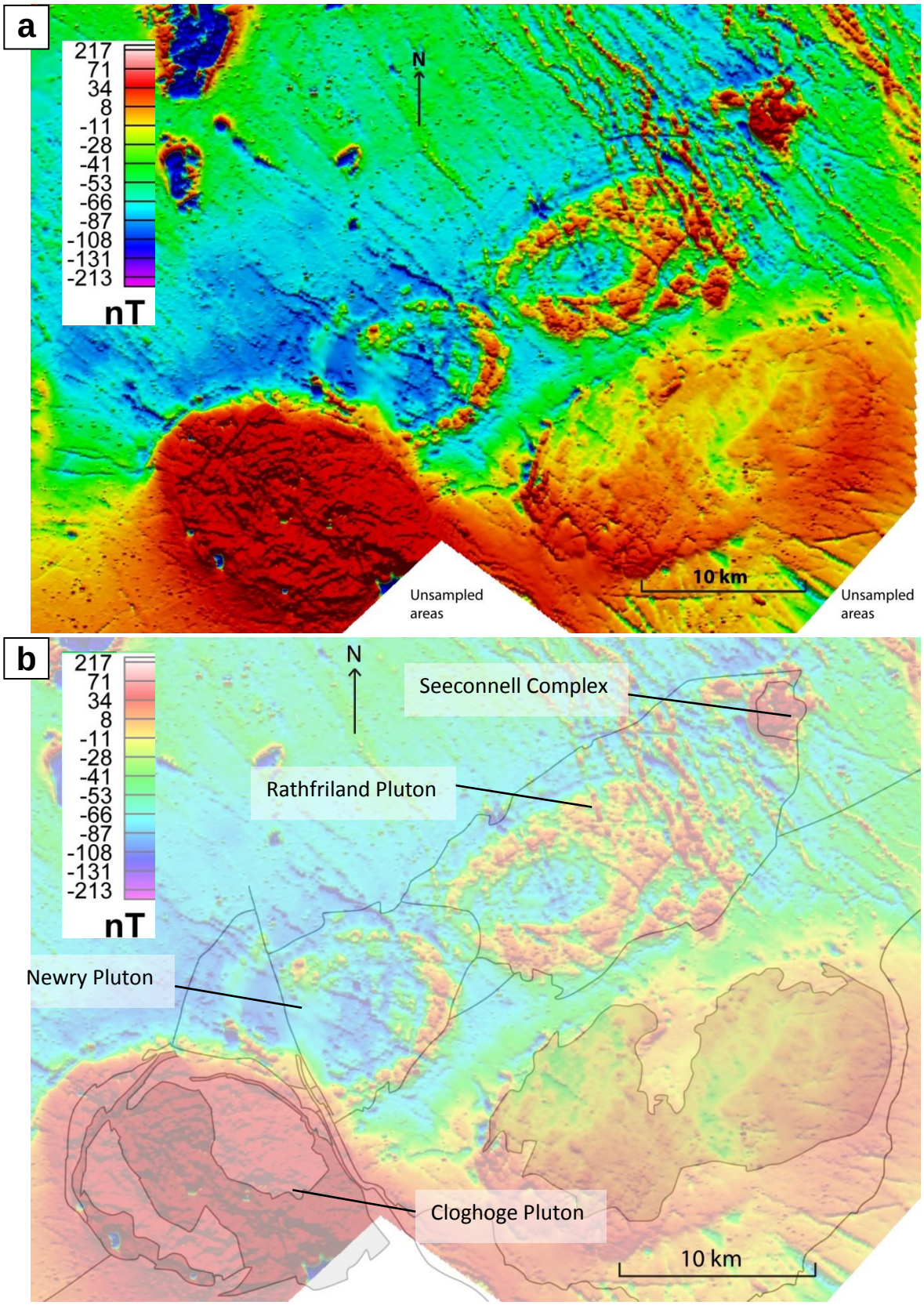

Fig 4.1: Tellus Survey aeromagnetic data: **a**: RTP data **b**: RTP data with overlaid NIC outline

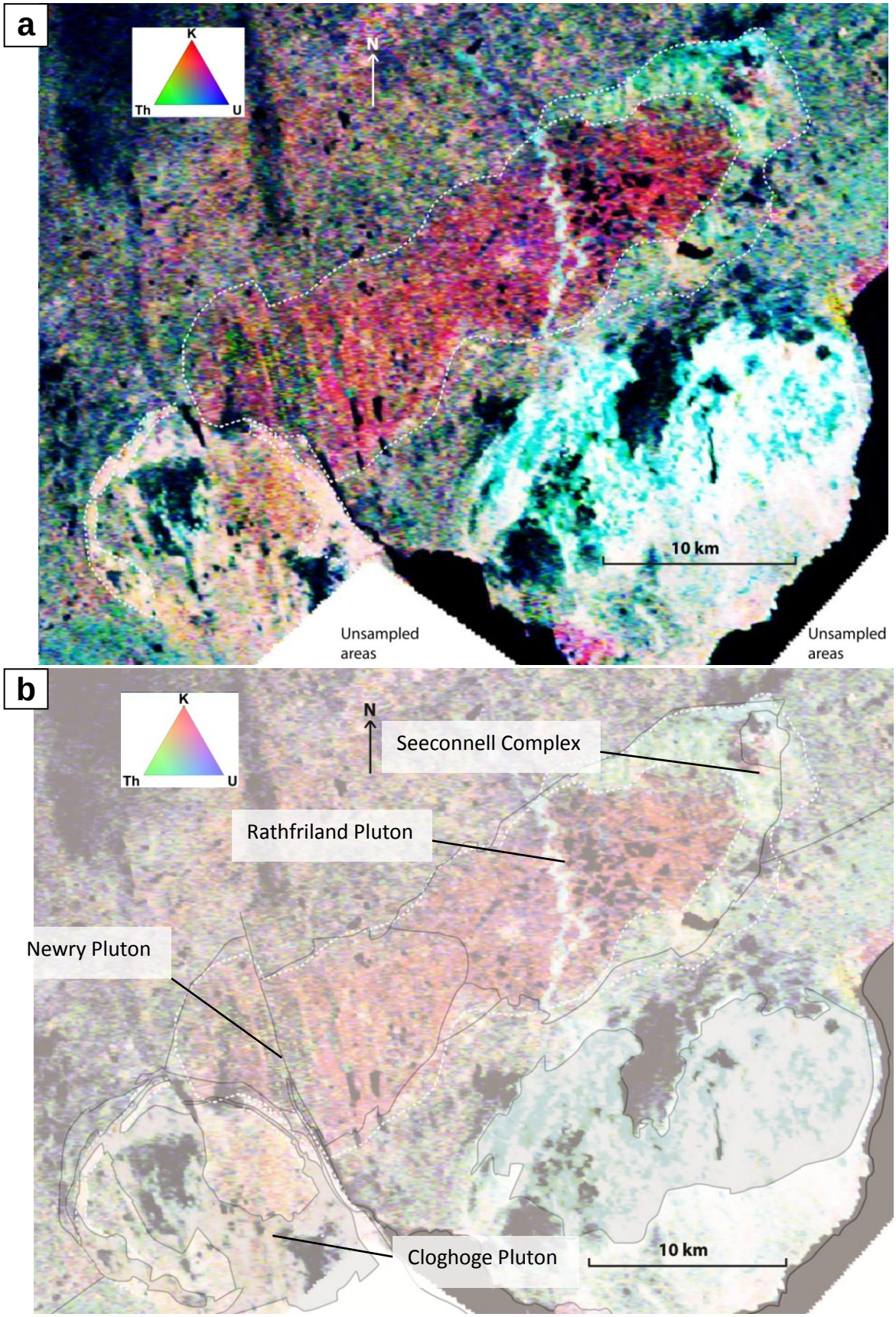

Fig 4.2: Tellus radiometric data: **a**: Raw data **b**: Data with overlaid NIC outline

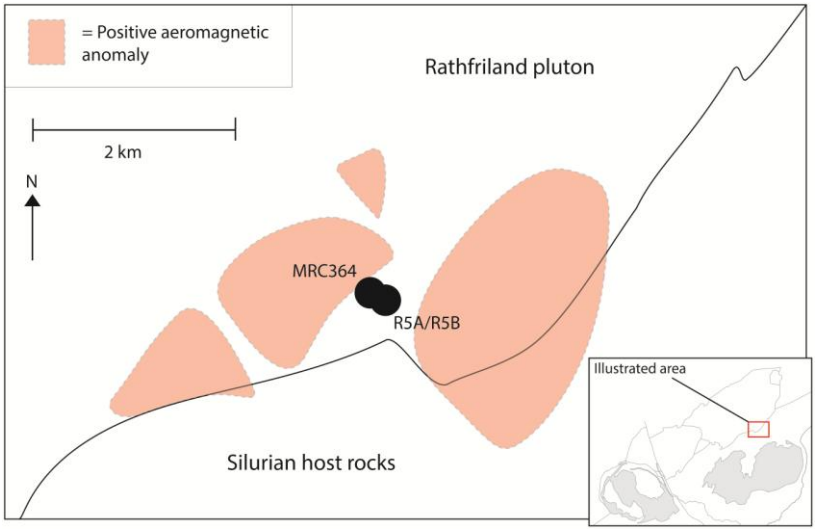

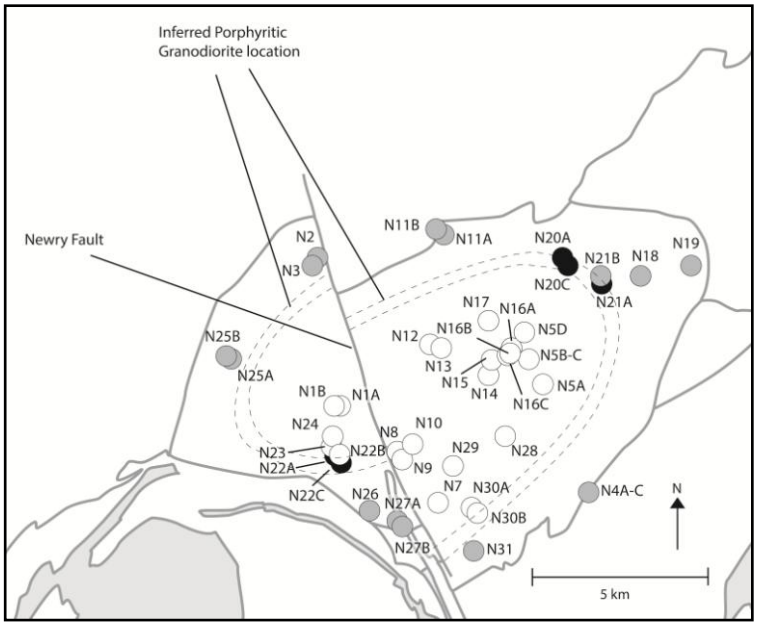

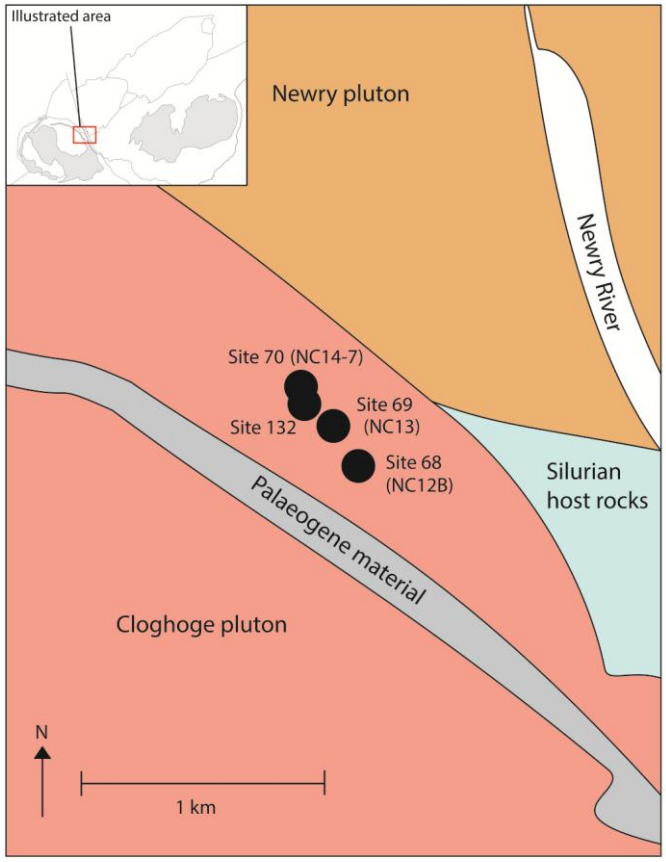

Fig 4.3 (above left): Quartz diorite sample locations in relation to positive aeromagnetic anomalies

Fig 4.4 (left): Derived facies within the Newry pluton: outer biotite granodiorite (grey); porphyritic granodiorite (black); inner hornblende granodiorite (white)

Fig 4.5 (above): Sites for petrographic investigation (and sample numbers) within the sheeted marginal Cloghoge pluton

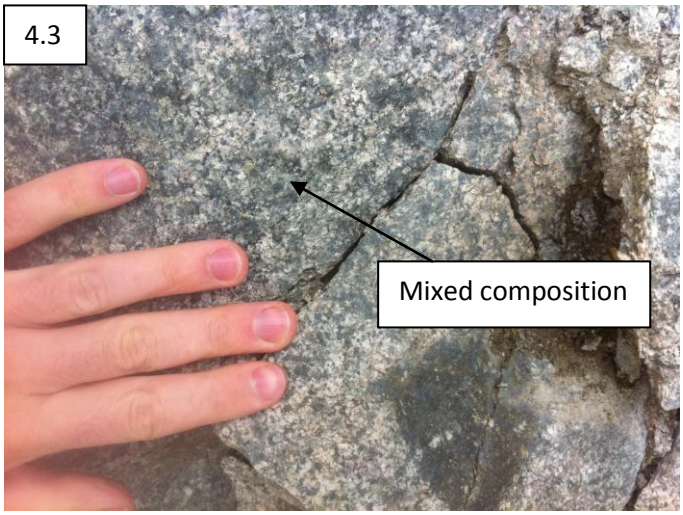

Photos 4.1 – 4.3: Evidence for cross cutting (photo 4.1), mingling (photo 4.2) and mixing (photo 4.3) observed at site 132 at the northeast edge of the Cloghoge pluton (see fig. 4.5 for location)

Sample	Grid Reference			Observed lithology	Part of pluton from Neeson (1984)	Derived part of pluton
N1A	J	07273	27746	Hornblende Granodiorite	Inner	Inner
N1B	J	07193	27777	Hornblende Granodiorite	Inner	Inner
N2	J	06517	32120	Hornblende Biotite Granodiorite	Outer	Outer
N3	J	06463	32019	Hornblende Biotite Granodiorite	Outer	Outer
N4A	J	14423	25146	Very coarse, unfoliated Biotite Granodiorite	Outer	Outer
N4B	J	14423	25146	Very coarse, unfoliated Biotite Granodiorite	Outer	Outer
N4C	J	14423	25146	Very coarse, unfoliated Biotite Granodiorite	Outer	Outer
N5A	J	12565	29160	Coarse, unfoliated Biotite Granodiorite	Inner	Inner
N5B	J	12584	29088	Coarse, unfoliated Biotite Granodiorite	Inner	Inner
N5C	J	12584	29088	Coarse, unfoliated Biotite Granodiorite	Inner	Inner
N5D	J	12960	28503	Coarse, unfoliated Biotite Granodiorite	Inner	Inner
N7	J	10126	24878	Medium-coarse Biotite Granodiorite	Inner	Inner
N8	J	09229	26385	Foliated Biotite Hornblende Granodiorite	Inner	Inner
N9	J	09207	25930	Unfoliated Biotite Granodiorite	Inner	Inner
N10	J	09023	26444	Biotite Hornblende Granodiorite	Inner	Inner
N11A	J	10126	32674	?	Outer	Outer
N11B	J	10103	32713	Hornblende Biotite Diorite	Outer	Outer
N12	J	09972	29393	Unfoliated Biotite Granodiorite	Inner	Inner
N13	J	10064	29275	Biotite Hornblende Granodiorite	Inner	Inner
N14	J	11623	28626	Unfoliated Biotite Granodiorite	Inner	Inner
N15	J	11666	28942	?	Inner	Inner
N16A	J	12208	29260	Biotite Hornblende Granodiorite	Inner	Inner

Table 4.1: Petrological classification of samples from the Newry pluton

Sample	Grid Reference			Observed lithology	Part of pluton from Neeson (unpub)	Derived part of pluton
N16B	J	12202	29204	Coarse unfoliated Hornblende Biotite Granodiorite	Inner	Inner
N16C	J	12172	29181	Coarse Biotite Hornblende Granodiorite	Inner	Inner
N17	J	11519	30136	Coarse Biotite Hornblende Granodiorite	Inner	Inner
N18	J	15873	31380	Unfoliated Biotite Granodiorite	Outer	Outer
N19	J	17357	31656	Coarse unfoliated felsic Biotite Granodiorite	Outer	Outer
N20A	J	13693	31946	Hornblende Biotite Granodiorite	?	Ring
N20C	J	13592	31955	Fine porphyritic Hornblende Biotite Granodiorite	?	Ring
N21A	J	14774	31161	Fine Biotite Hornblende Granodiorite	?	Ring
N21B	J	14702	31325	Unfoliated Biotite Granodiorite	?	Outer
N22A	J	07170	26306	Fine foliated Hornblende Biotite Granodiorite	?	Ring
N22B	J	07170	26306	Coarse Biotite Hornblende Granodiorite	?	Inner
N22C	J	07170	26306	Fine Porphyritic Hornblende Biotite Granodiorite	?	Ring
N23	J	07112	26595	Coarse unfoliated Biotite Hornblende Granodiorite	Inner	Inner
N24	J	07096	26817	Hornblende Biotite Granodiorite	Inner	Inner
N25A	J	04180	29061	Coarse Hornblende Biotite Granodiorite	Outer	Outer
N25B	J	04129	29099	Coarse Biotite Hornblende Granodiorite	Outer	Outer
N26	J	08149	24615	Coarse Biotite Hornblende Granodiorite	Outer	Outer
N27A	J	08960	24250	Biotite Granite	Outer	Outer
N27B	J	08971	24205	Biotite Granite	Outer	Outer
N28	J	12039	26799	Biotite Hornblende Granodiorite	Inner	Inner
N29	J	10517	25924	Coarse Biotite Hornblende Granodiorite	Inner	Inner
N30A	J	11085	24743	Medium-coarse Biotite Hornblende Granodiorite	Inner	Inner
N30B	J	11108	24736	Hornblende Biotite Granodiorite	Inner	Inner
N31	J	11141	23536	Coarse Biotite Granodiorite	Outer	Outer

Table 4.1 (continued): Petrological classification of samples from the Newry pluton

a

Area of the Newry Complex	SiO_2 (wt %)	TiO_2 (wt %)	$Fe_2O_{3(t)}$ (wt %)	MgO (wt %)	K_2O (wt %)
Seeconnell Complex	53.35	1.38	8.29	6.77	3.95
Main Rathfriland pluton	65.41	0.61	3.86	2.62	3.27
Newry pluton	67.60	0.54	3.36	1.77	3.48
Cloghoge pluton	67.90	0.52	3.17	1.68	3.83
Satellite bodies	67.18	0.43	3.02	1.70	3.20
Entire Complex	**64.43**	**0.71**	**4.37**	**2.93**	**3.58**

b

Area of the Newry Complex	Rb (mg/kg)	Sr (mg/kg)	Th (mg/kg)	U (mg/kg)	Zr (mg/kg)
Seeconnell Complex	121	1175	12	4	177
Other Rathfriland pluton	120	521	13	3	184
Newry pluton	114	407	10	3	141
Cloghoge pluton	131	390	12	3	158
Satellite bodies	111	436	9	3	159
Entire Complex	**121**	**578**	**12**	**3**	**164**

Table 4.2: Mean concentrations of selected elements measured within the main parts of the NIC: **a)** Major elements; **b)** Trace elements

Fig 4.6a: Geochemistry sample locations from the main NIC and satellite bodies

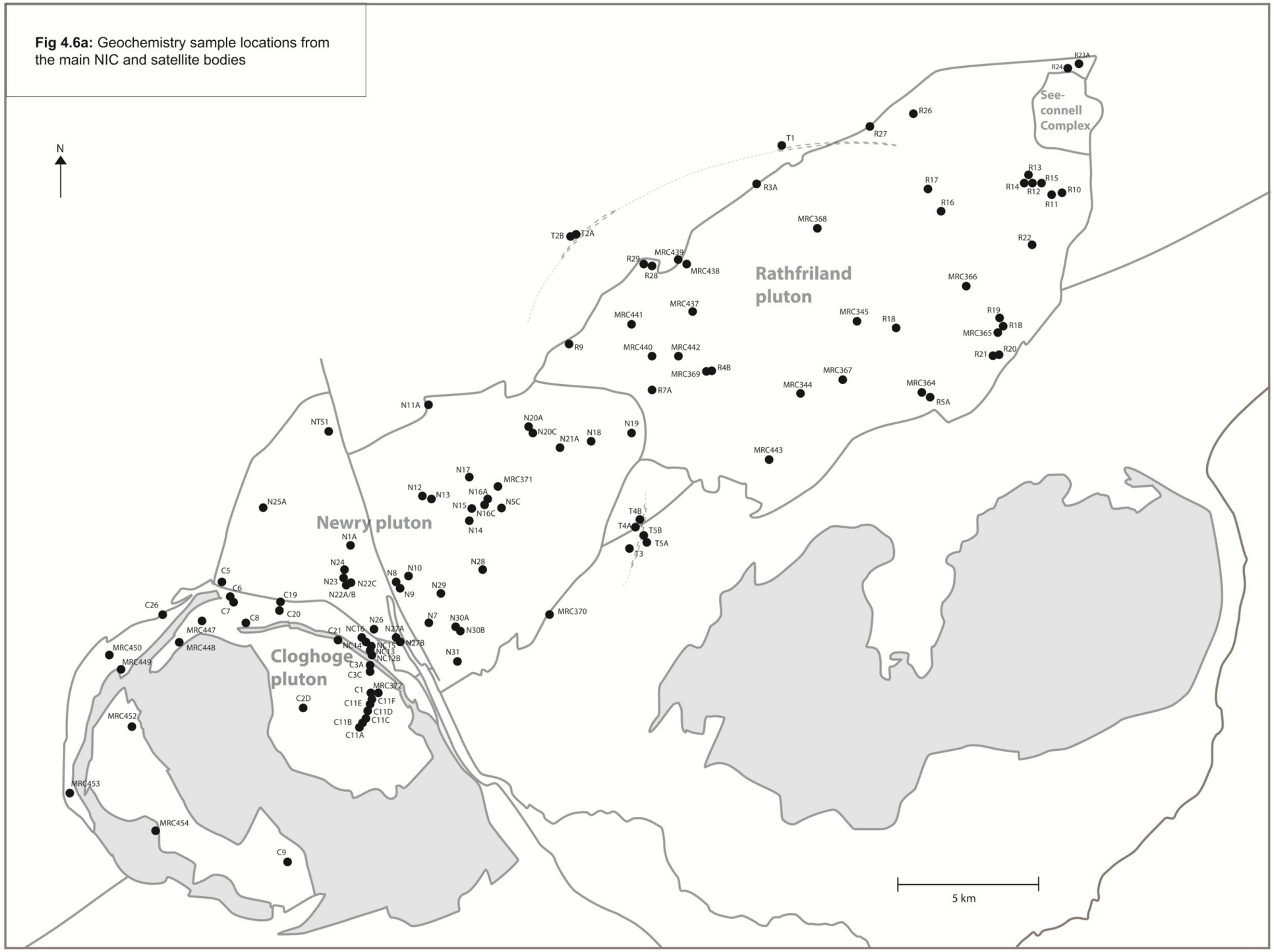

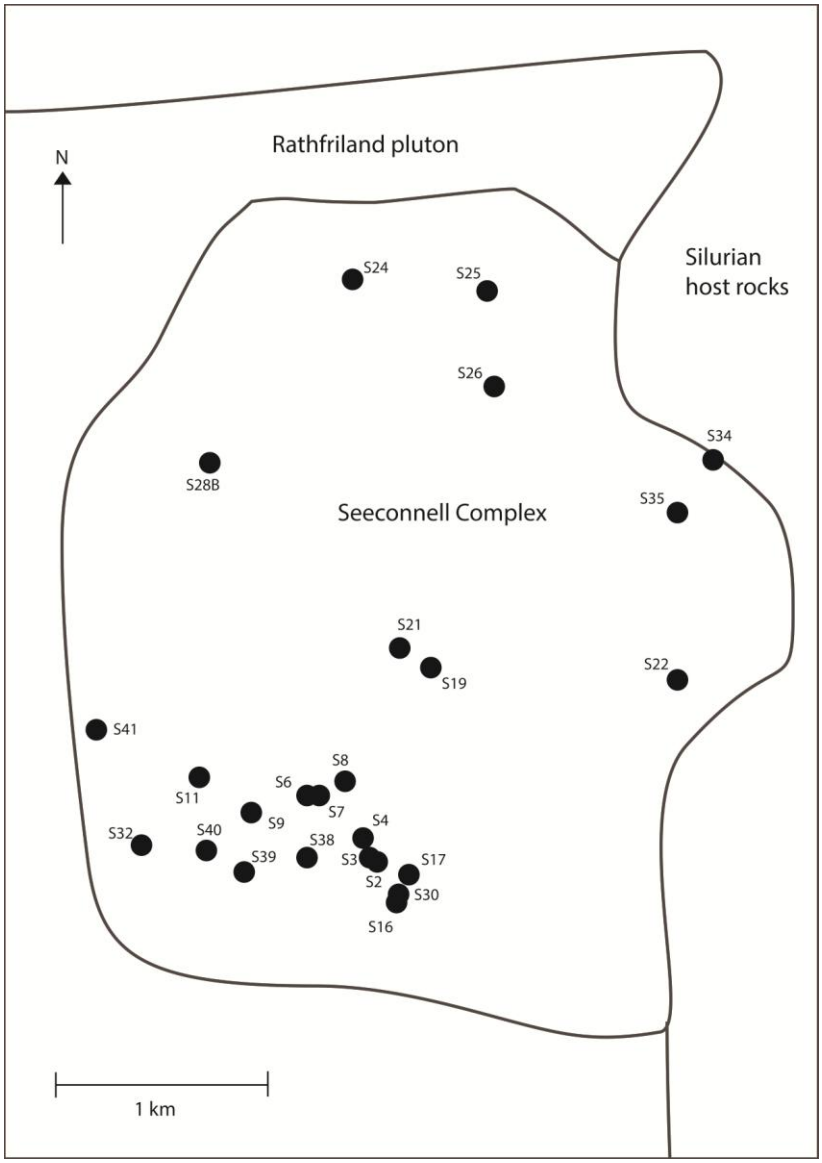

Figure 4.6b: Geochemistry sample locations from the Seeconnell Complex

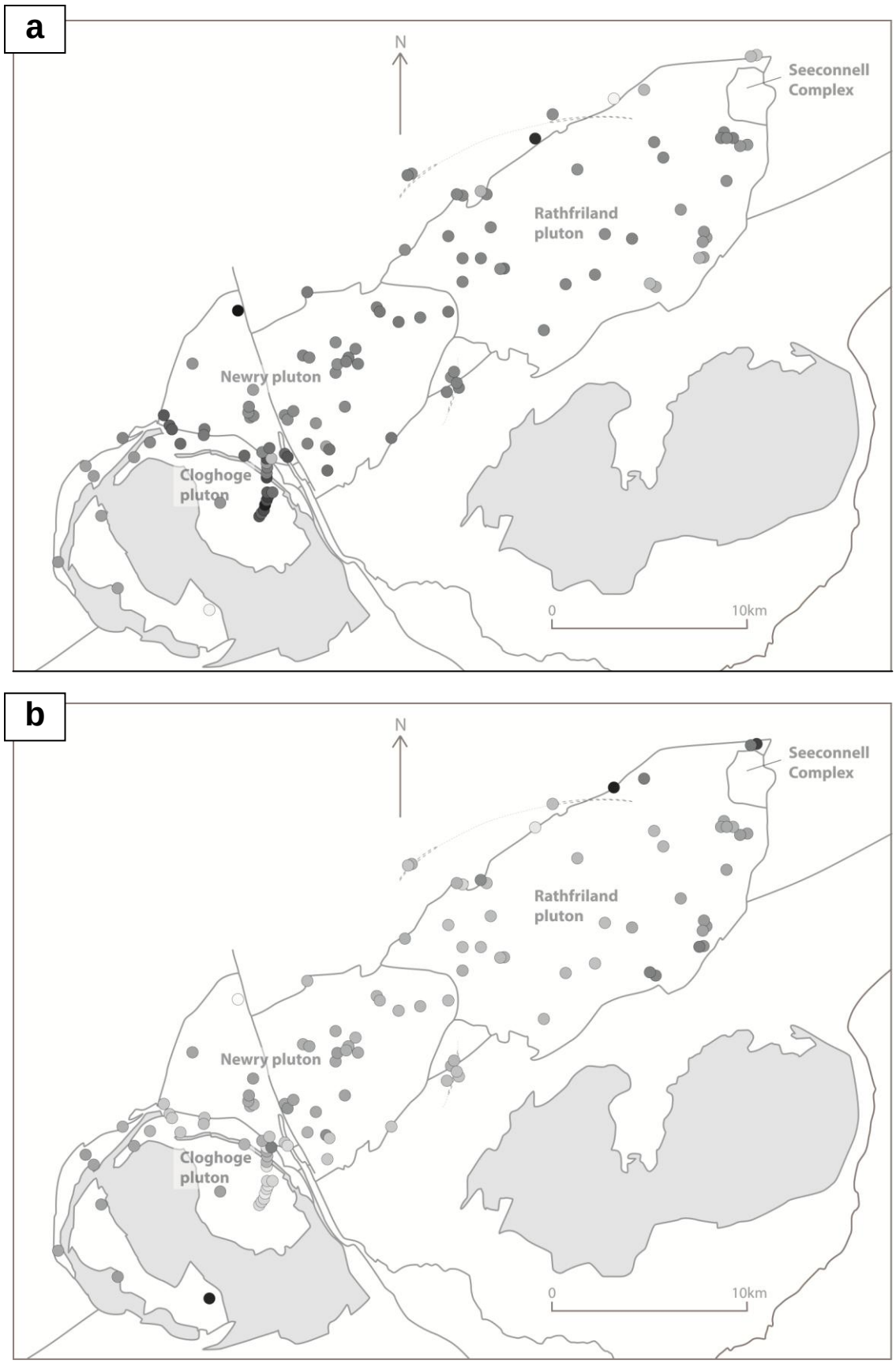

Fig 4.7: Mapped abundance of major elements from samples throughout the main NIC and satellite bodies (black=highest concentration, white=lowest concentration): **a)** SiO_2 **b)** Recalculated Fe_2O_3

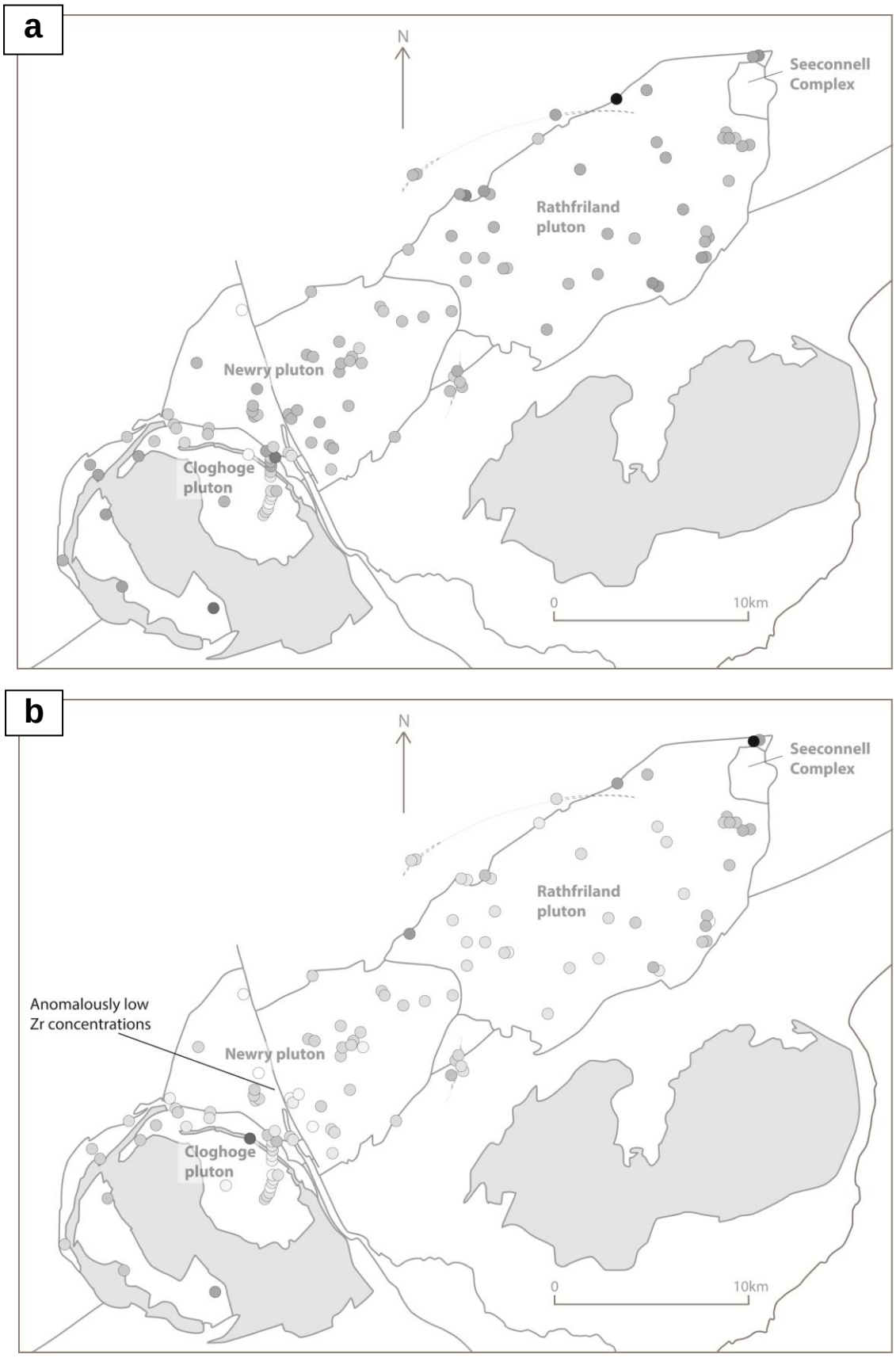

Fig 4.8: Mapped abundance of trace elements from samples throughout the main NIC and satellite bodies (black=highest concentration, white=lowest concentration): **a)** Sr **b)** Zr

Fig 4.9 (below): Means concentrations of radiometric elements from distinguished compositional areas throughout the main NIC and satellite bodies: **a)** K_2O

Abbreviation codes for compositional areas:

(Rathfriland pluton)
- SC = Seeconnell Complex
- R1 = NE Mafic granodiorite (1)
- R2 = NE Hornblende granodiorite
- R3 = NE Quartz diorite
- R4 = NE Mafic granodiorite (2)
- R5 = Inner biotite granodiorite

(Newry pluton)
- N1 = Outer biotite granodiorite
- N2 = Porphyritic granodiorite
- N3 = Inner hornblende granodiorite

(Cloghoge pluton)
- C1 = Marginal sheeted facies
- C2 = Outer hornblende granodiorite
- C3 = Biotite granodiorite 'core'

(Satellite bodies)
- S1 = Northern Satellite bodies
- S2 = Southern Satellite bodies

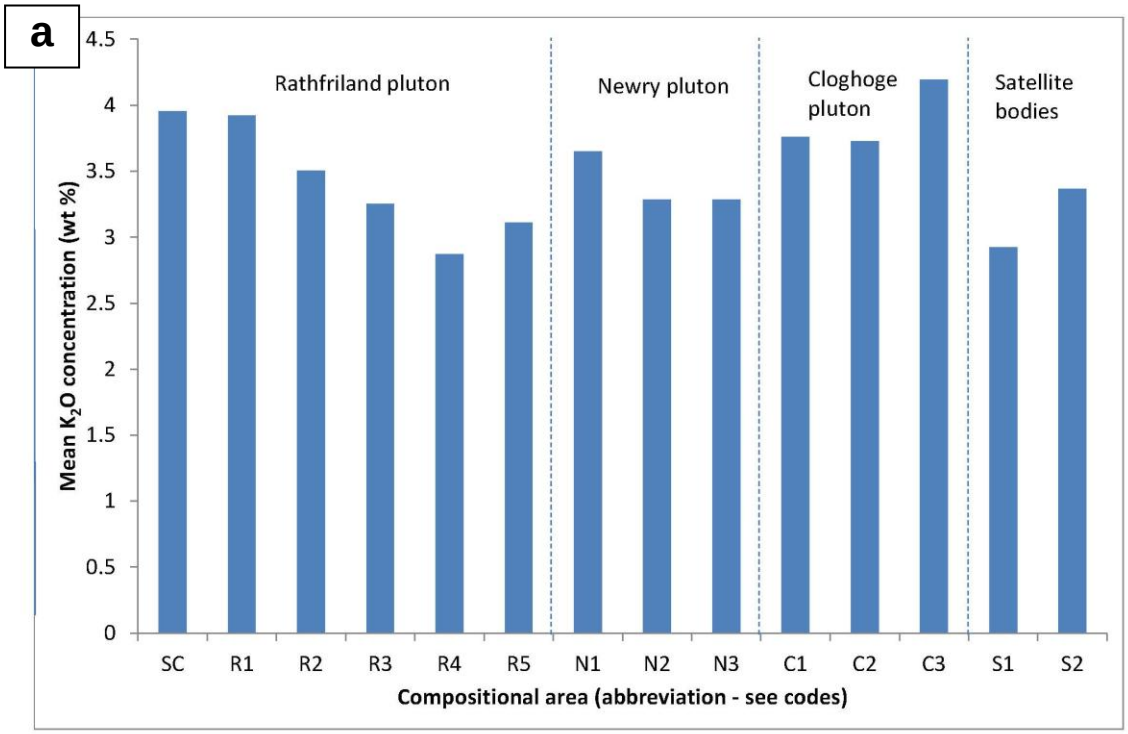

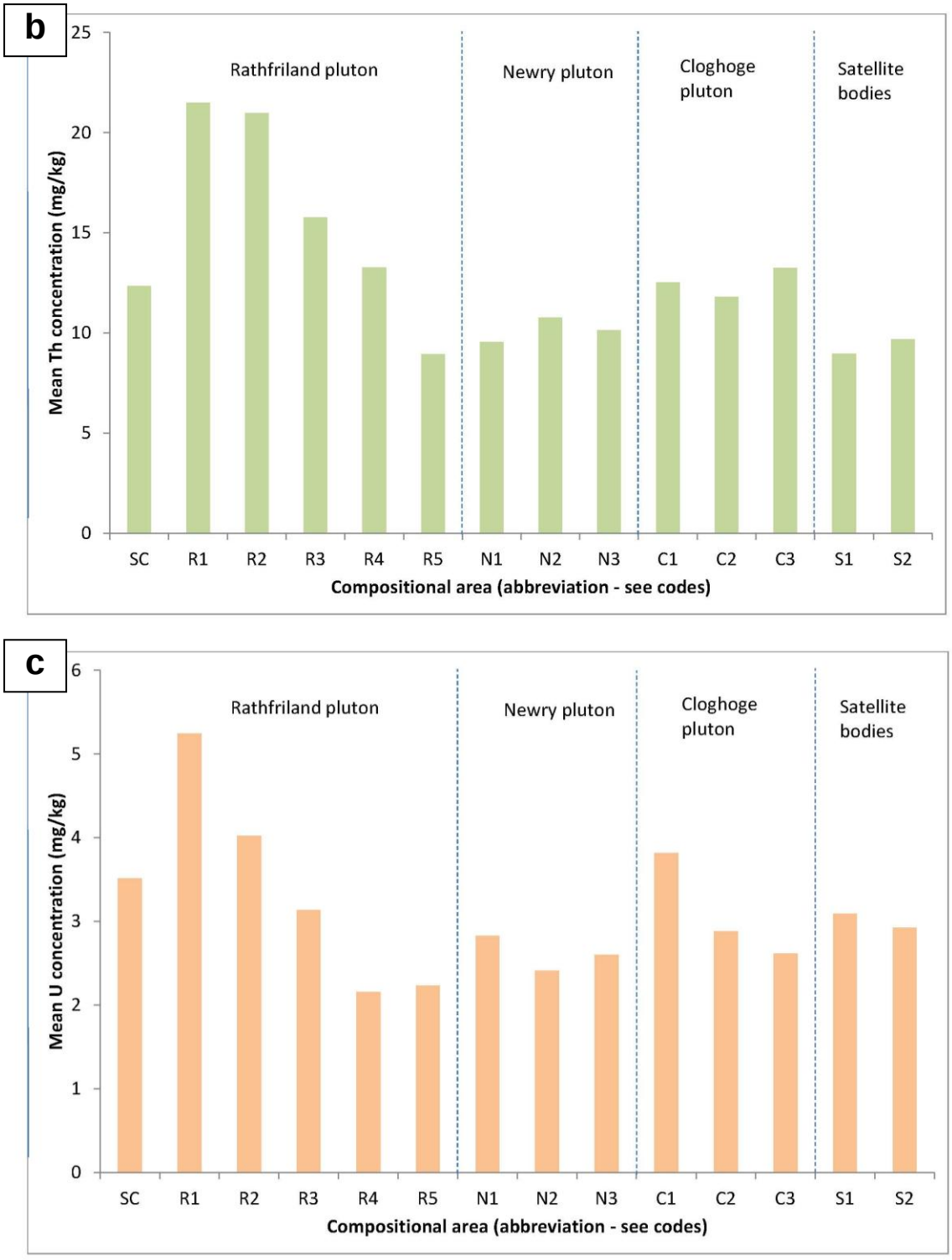

Fig 4.9 (continued): Means concentrations of radiometric elements from distinguished compositional areas throughout the main NIC and satellite bodies: **b)** Th **c)** U
(see previous for abbreviation codes)

	Pluton	$^{206}Pb/^{238}U$ date (Ma)	± (2σ)
MRC 363	Rathfriland	414.02	0.18
MRC 364	Rathfriland	412.53	0.33
MRC 365	Rathfriland	413.44	0.37
MRC 366	Rathfriland	411.94	0.34
MRC 367	Rathfriland	412.09	0.36
MRC 369	Rathfriland	411.09	0.18
MRC 370	Newry	411.00	0.58
MRC 371	Newry	410.29	0.20
MRC 372	Cloghoge	407.23	0.35

Table 4.3 (above): U-Pb ages obtained for 9 samples, with 2σ (95.4%) uncertainty margins shown (see appendix 4 for full results)

Fig 4.10 (below): Timeline plot showing relationship of derived ages and 2σ (95.4%) error margins for each sample

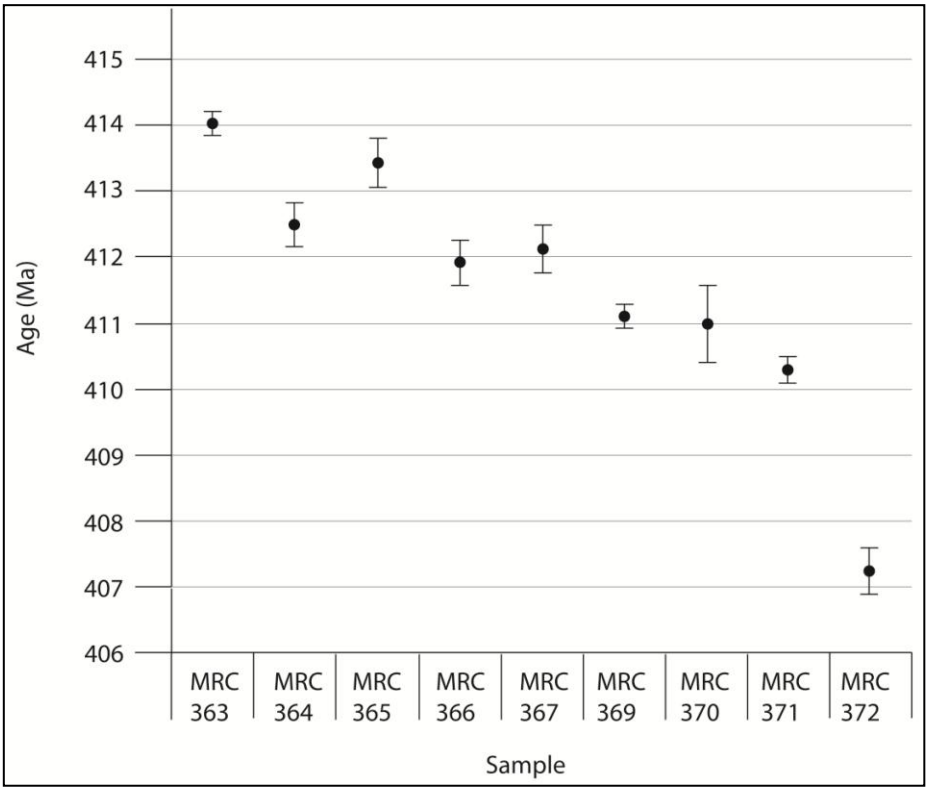

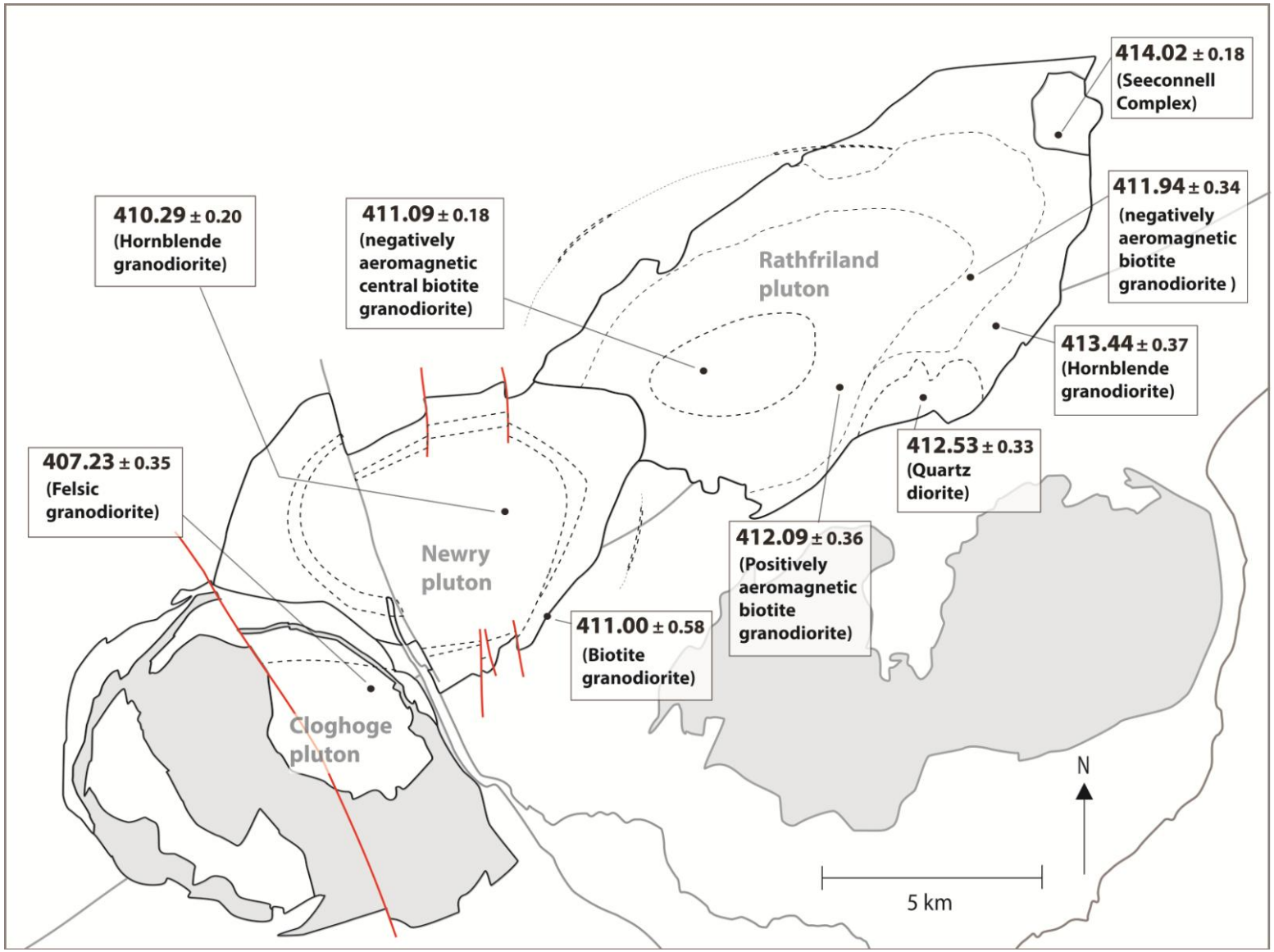

Fig 4.11: U-Pb ages and associated errors for samples across the NIC

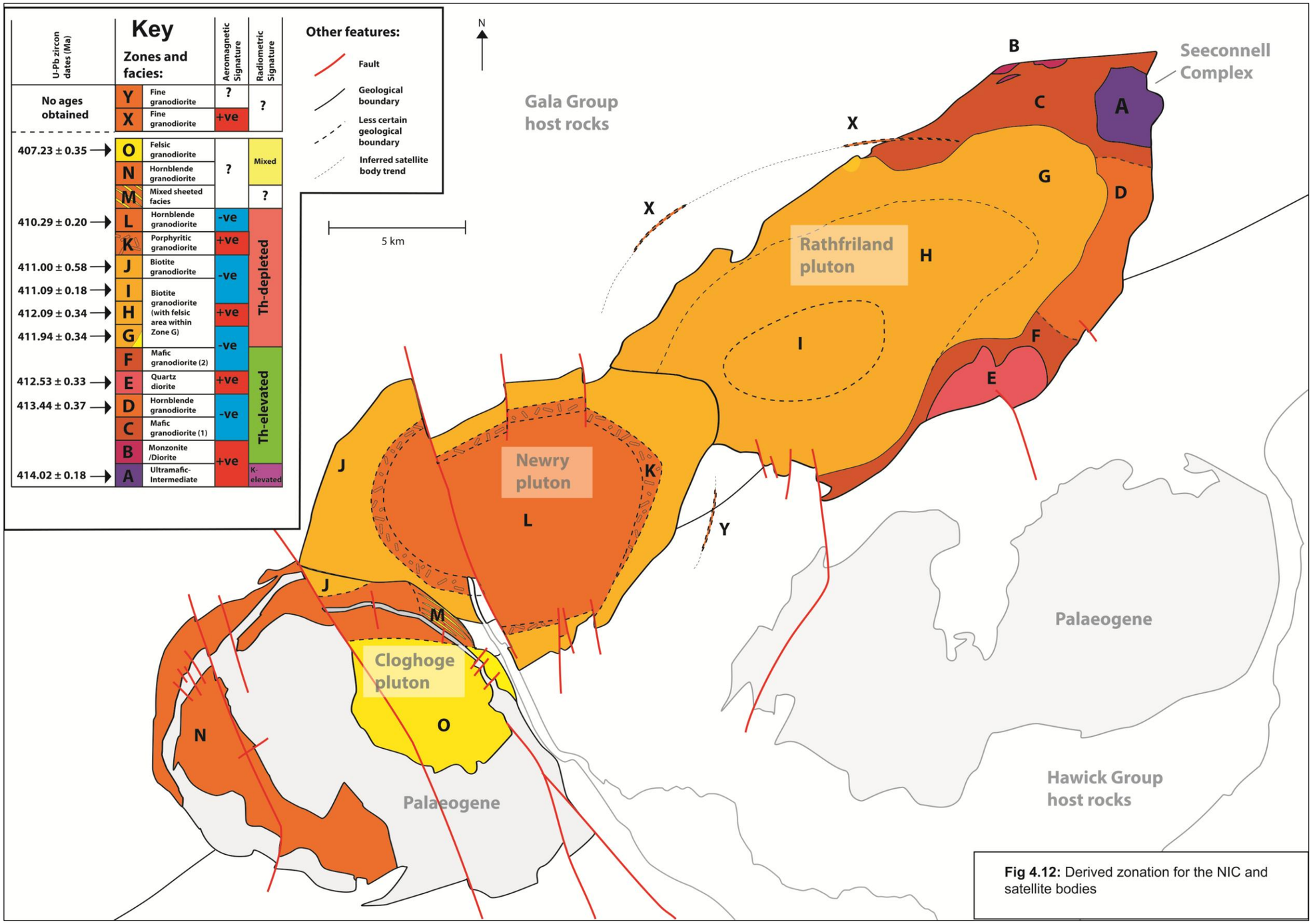

Fig 4.12: Derived zonation for the NIC and satellite bodies

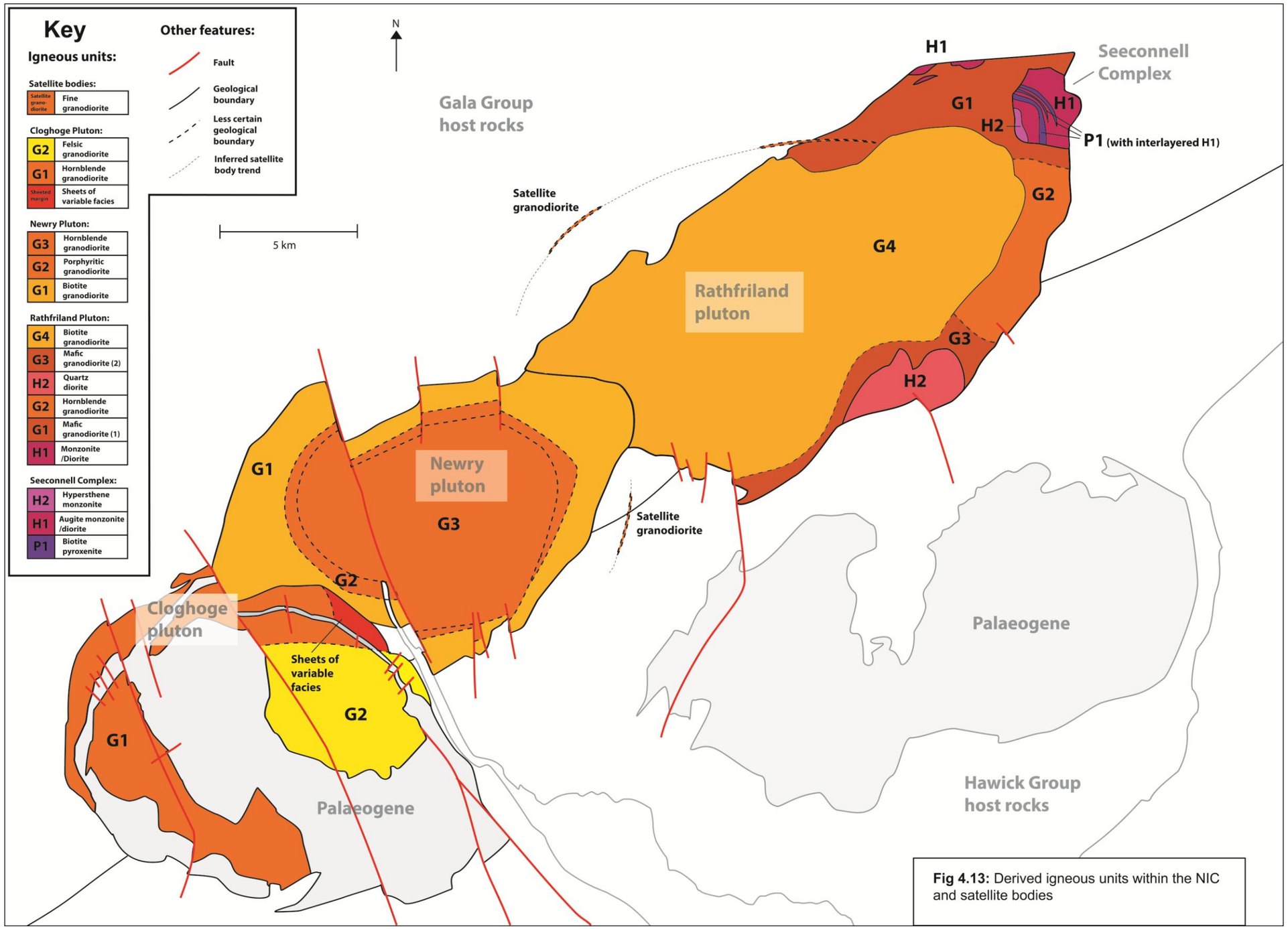

Fig 4.13: Derived igneous units within the NIC and satellite bodies

Zone	Facies	Unit
A	Biotite pyroxenite	Seeconnell P1
	Augite monzonite/Diorite	Seeconnell H1
	Hypersthene monzonite	Seeconnell H2
B	Augite monzonite/Diorite	Rathfriland H1
C	Mafic granodiorite (1)	Rathfriland G1
D	Hornblende granodiorite	Rathfriland G2
E	Quartz diorite	Rathfriland H2
F	Mafic granodiorite (2)	Rathfriland G3
G	Biotite granodiorite	Rathfriland G4
H	Biotite granodiorite	
I	Biotite granodiorite	
J	Biotite granodiorite	Newry G1
K	Porphyritic granodiorite	Newry G2
L	Hornblende granodiorite	Newry G3
M	Sheets of variable facies	Cloghoge sheeted margin
N	Hornblende granodiorite	Cloghoge G1
O	Felsic biotite granodiorite	Cloghoge G2
X	Fine granodiorite	Satellite granodiorite
Y	Fine granodiorite	

Table 4.4: Derived igneous units within the NIC and satellite bodies

CHAPTER 5: EMPLACEMENT OF THE NEWRY IGNEOUS COMPLEX

5.1: Introduction

Emplacement of the Newry Igneous Complex (NIC) has been investigated through structural field data; the extent of quartz recrystallisation and an Anisotropy of Magnetic Susceptibility (AMS) study. This reveals that the NIC is likely to have been tectonically accommodated through tension-releasing bends on two faulted tract boundaries within the Southern Uplands-Down-Longford Terrane. The process is proposed to have been facilitated by reactivation of two deep-seated crustal lineaments, which caused the strike swing within the terrane. Intersection of these with shear zones relating to the tract boundaries at depth allowed magma from deep in the crust to ascend to its emplacement site.

In addition to tectonic accommodation the NIC has also been shown to have laterally inflated, producing concentric foliations, shallow concentric linear fabric components and deflected host rock orientations. Evidence of inflation within individual magma pulses is also provided from the strong fabrics and high degrees of quartz recrystallisation associated with major pluton boundaries. Hence the NIC was incrementally assembled through magma pulses that were initially tectonically accommodated, before laterally expanding. The occurrence of cross cutting of the host rocks along some of the NIC margin further suggests that a small degree of stoping may have taken place, although this is likely to have been volumetrically insignificant.

Finally, magma flow may be evident in areas where the typical inflation-related fabrics are absent or not fully developed. This appears to be more common at the pluton margins, the outer margins of individual zones and within sheets and is proposed to relate to the faster cooling of these areas against the host material. Lineations at the pluton margins are generally steep, possibly indicating the upward ascent of magma into the emplacement site. However, fabrics from the sheeted areas and an individual zone boundary are less abundant and would require work to resolve in terms of magma flow direction.

AMS results have been shown to be largely reliable through close correlation with visible fabrics. Thermomagnetic investigation also suggests that these dominantly reflect the distribution anisotropy of magnetite, although some shape-controlled fabrics provided by single domain magnetite may also occur. A smaller number of fabrics show a correlation between low bulk magnetic susceptibility and fabric obliquity to the general concentric structure of the NIC. Therefore, these alone are considered to be potentially unreliable and have not been included in the AMS investigation of emplacement.

5.2 Methods

Emplacement of the NIC was investigated through the four main approaches outlined below. Results from each were considered alongside the evidence for separate magma pulses (i.e., the deduced zones) provided in Chapter 4. This has been undertaken for all three main plutons and the satellite bodies, although the Seeconnell Complex is not considered in depth, due its characteristics as a separate intrusion (Meighan and Neeson, 1979; Neeson, 1984; current study).

5.2.1 Structural field data

Structural field data from Neeson (1984) and Hurley (pers. comm., 2012) has been reviewed and combined with the data collected during the current study (see appendix 1). The new structural data was collected alongside sampling for geochemical/AMS analysis and so many of the localities coincide (see section 4.2). Other sites were specifically targeted in order to obtain data from close to the margins of the NIC and satellite bodies (see fig. 5.1). Data were also obtained across a wide spread of host rock localities at varying distances from the NIC (see fig. 5.2). As with geochemistry sampling, these data locations were selected through a combination of approaches, including reference to former work (i.e., Egan, 1973; Reynolds, 1934; Reynolds, 1943; Meighan and Neeson, 1979; Neeson, 1984; Hurley, pers. comm., 2010), and use of the GeoVisionary suite at the GSNI headquarters in Belfast (see section 4.2).

Some of the igneous foliation data from the current study and that of Hurley (pers. comm., 2010) showed a coverage that was too dense to be clearly displayed in fig.

5.1. Therefore, in fig. 5.1 these are displayed as representative orientations (see appendix 1 for full data).

5.2.2 Quartz recrystallisation

Data acquisition and preparation

Samples for analysis of quartz recrystallisation comprised 42 thin sections from various parts of the NIC (see fig. 5.4; appendix 4). 19 of these had already been prepared by the GSNI prior to the current study. The 23 additional thin sections were obtained from selected geochemistry/AMS sample blocks (see section 4.2 for details of collection), so as to provide a wide coverage of the NIC. These were prepared using the facilities at the University of Birmingham.

Data analysis: a newly developed technique

A semi-quantitative analysis of the extent of high temperature quartz recrystallisation has been developed within the current study. This is largely derived from the work of Stipp et. al. (2002), which identified possible temperature intervals that relate to variations in the quartz recrystallisation mechanism (see section 2.2).

Of these mechanisms, the current analysis is entirely focused on *subgrain rotation recrystallisation.* This is because the latter links exclusively to strain taking place in the high temperature solid state (e.g., Gapais and Barbarin, 1986; Bouchez, 1997; Stipp et. al., 2002). In this state virtually all deformation is accommodated by plastic strain and related recrystallisation, as opposed to phenocryst rotation, which will occur in the magmatic/submagmatic states (Paterson et. al., 1998; Bouchez, 1997). Furthermore, the majority of strain recorded for an emplaced pluton has been

suggested to take place in the high temperature solid state (see Paterson et. al., 1998). Therefore, subgrain rotation recrystallisation is a good indicator of the overall extent of deformation occurring throughout an important period during a pluton's cooling.

Within the current study the extent of subgrain boundary rotation recrystallisation was inferred by assessing the degree of polycrystalline quartz development (see Gapais and Barbarin, 1986; Stipp et. al., 2002). This was achieved by assigning a score (termed the *high temperature quartz recrystallisation* – or *HTQR* – score) to each thin section (see fig. 5.4). Scores ranged from 0 to 4, with each extreme representing the minimum and maximum degree of polycrystalline quartz development within the sample suite.

Photos 5.4 to 5.8 illustrate typical examples of quartz recrystallisation extents corresponding to each of these scores. Where in rare thin sections individual quartz crystals showed varying degrees of recrystallisation, a judgement was made regarding which score best described the sample as a whole (see appendix 4).

5.2.3 AMS data

Sample collection

113 blocks from throughout the NIC were collected for AMS analysis. As mentioned above, this suite was collected alongside geochemical samples/AMS analysis and so many of the localities coincide (see Chapter 4.2; see fig. 5.6 for specific AMS sampling localities).

Sample preparation

Block samples were orientated in the field prior to their extraction. This involved recording the strike and dip of one particular sample face (or part of a face where its orientation is variable). The block was labelled so as to preserve this original field orientation, which would ultimately provide a reference from which to orient the deduced fabric (see Owens, 1994 – further details also provided in appendix 5).

Following its orientation, a number of sub-samples were then obtained from each block (usually from 8 to 15, depending on the size of the block). These were initially drilled as several continuous cores, before being sawn into appropriately sized cylinders. The size of the latter was determined so that they would fit into the specimen holder of a KLY-3S Kappabridge spinning magnetometer (i.e., a diameter of 25 mm and a length of 22 mm).

A further measurement was also taken at this stage to relate the orientation of the acquired sub-samples to that of the original block in the field (see appendix 5).

Sample analysis and data processing

Sub-samples were analysed within an AGICO KLY-3S Kappabridge spinning magnetometer. This allowed measurement of each specimen's magnetic susceptibility in three different orientations, hence yielding a result on its overall *anisotropy* of magnetic susceptibility. A measurement of bulk susceptibility was also obtained from the specimen.

Following measurement of an entire set of sub-samples (i.e., a single sample block), the Kappabridge produced a data file containing information on the deduced magnetic fabric and its anisotropy. This included the orientation of K_1, K_2 and K_3 (e.g., Owens, 1974) at confidence limits of 95%. The latter were plotted stereographically (see fig. 5.5), as well as being interpreted as planar and/or linear fabrics (e.g., Owens, 1974), which were mapped throughout the NIC (see fig. 5.6). The process of deriving these fabrics is discussed in section 5.5.1, as this first requires an introduction to the AMS data obtained.

Finally, values of the H, F, L and K_{mean} parameters were obtained for each sample (e.g., Khan, 1962; Owens, 1974) (see Chapter 2). These are presented within figs. 5.7 to 5.12, with details of their derivation being provided in appendix 6.

5.2.4 Causes of AMS

Within the current study the causes of the observed AMS results have been investigated through two different approaches. These comprise comparison with existing field structural data, along with acquisition and analysis of thermomagnetic data, which reveals the relationship between magnetic susceptibility and temperature. Each of these is discussed below:

Comparison with field structural data

This comparison involved consideration of the orientations of planar fabrics deduced from AMS block samples. These are compared to other structural trends relating to the NIC; firstly by mapping of the former alongside the measured igneous foliations (see fig. 5.13). Secondly, a table was constructed focusing on specific

sites at which planar AMS fabric orientations are available alongside a wider range of structural field data (see table 5.1). This comprised orientations of visible foliations, internal contacts, shear zones and pluton boundaries.

Thermomagnetic analysis

Thermomagnetic data was obtained for five samples. These were selected from the larger suite of AMS sample blocks so as to represent a wide area of the NIC (see fig 5.16).

Material from the selected blocks was crushed using the facilities at the Scottish Universities Research Centre (SUERC), in East Kilbride, Glasgow. The resulting powder was analysed at the University of Birmingham. This was carried out on a CS-3 furnace apparatus, which functions in cooperation with an AGICO KLY-3S Kappabridge spinning magnetometer (see previous section). Analysis involved samples being heated from room temperature to a maximum of 700°C, before being cooled back to room temperature. This process lasted from three to four hours, during which time magnetic susceptibilities were automatically measured at approximately 15 second intervals. The results are shown graphically in fig. 5.17 and provided in full within appendix 6.

5.3 Structural field data

5.3.1 Igneous foliations

The current data confirms the predominantly steep (mostly 60-90°), outward-dipping nature of the foliations within the NIC reported by Neeson (1984) (fig. 5.1; also see fig. 3.7). However, there are exceptions towards the outer part of the Rathfriland pluton where inward-dipping foliations occur, although these are almost exclusively very steep (80° or more). Other exceptions comprise a number of significantly shallower (less that 30°) foliations within the inner Newry pluton.

These foliations also show the same broad concentric pattern within each pluton as the results obtained by Neeson (1984). However, the current study also highlights a rare oblique foliation trend. Foliations occupying this trend appear to be aligned approximately perpendicular to any adjacent outer pluton contact (fig 5.1).

These are apparent within three sites throughout the NIC, referred to here as the ***Upper Motorway Terrace*** (**J079239**), ***Ballymagreehan Quarry*** (**J304355**) and ***Knockiveagh Hill*** (**J178376**) sites (see fig. 5.1). Both of the former relate to relatively rare sheeted areas of the complex (see appendix 1) and thus a link is proposed between sheeting and oblique fabrics. The possible origin of these fabrics is further discussed within the subsequent AMS section (section 5.5). The Knockiveagh Hill site is located adjacent to a very variably orientated pluton boundary, which is again uncommon amongst the sites from which measurements are obtained (see fig. 5.1). Hence, it is considered that the oblique fabrics here may parallel the adjacent variably orientated boundary, which would be consistent with outward-directed magma pressure (e.g., Hutton, 1988; Paterson and Vernon, 1995).

5.3.2 Bedding and cleavage within host rocks

The current study shows that respective bedding and cleavage measurements in the vicinity of the NIC are consistently subparallel (almost exclusively within 10°) (see fig. 5.2). This observation is largely supported by the work of Barnes et. al., (1987), who showed that bedding and S_1 cleavages display similar orientations throughout much of the Southern Upland-Down-Longford Terrane. As a result, these respective measurements can be used together when making comparisons that involve large obliquities, such as within the current study.

Measured bedding and cleavage orientations appear to closely correspond to the mapped outer contacts of the NIC in terms of both its trend and steepness. This link is most clearly evident to the south of the Newry/Cloghoge pluton contact, at the ***Dublin Road Bridge*** (**J082241**) site (fig. 5.2). Here host rock bedding and cleavage can be seen to curve around concave trend of the NIC margin, hence showing parallism with its adjacent orientation in each location of measurement. This relationship is illustrated in fig 5.3.

On the other hand, some bedding/cleavage measurements relate more closely to the proposed strike-swing of the Southern Uplands-Down-Longford Terrane (Beamish et. al., 2010). This appears to be the case in the vicinity of the ***Slieve Croob*** (**J319454**) site (see fig. 5.2). Here bedding/cleavage is oblique to both the NIC margin and originally mapped tract boundaries of the terrane (GSNI, 1997), yet parallels those predicted by Beamish et. al. (2010). The ***Ballydoo Road*** (**J166292**) site to the south of the NIC exhibits a similar host rock obliquity, although the predicted tract boundaries of Beamish et. al. (2010) did not extend to this area.

However, in the vicinity of the ***Silverbridge*** (**H972185**) site (see fig. 5.2) it can be seen that distance from the NIC margin affects the host rock trend. Here several measurements obtained from 1 – 7 km outside the complex follow the tract boundaries inferred from Beamish et. al. (2010), whereas a number of these from closer to NIC (within 1 km of its margin) instead match the approximately perpendicular pluton boundary trend. Therefore, the relationship of host rock orientation to the NIC may be conditional on the distance of these from the intrusion. Ultimately, this means that areas where host rocks are oblique to the NIC do not necessarily correspond to cross cutting unless this is observed to occur in the field.

The satellite bodies may display a different relationship with the host rocks. Firstly, the inferred trend of these bodies is significantly oblique to the measured host rock orientations towards the east of Zone X and the north of Zone Y (see fig. 5.2). This is also confirmed by field relationships (see appendix 1), which reveal that several cross-cutting relationships can be observed throughout the satellite bodies.

5.3.3 The extent of host rock deformation

It is known that areas of 'mobilised sediment' occur abundantly around the northeast end of the NIC (e.g., Reynolds, 1936) (see fig. 3.5a). Reynolds (1936) interpreted these to have been extensively altered and potentially show a gradational contact with the Newry Complex (see Chapter 3.2). Similarly altered rocks have been observed to occur within ***Camlough Quarry*** (**J037246**) at the Cloghoge pluton margin (see photo 5.3; see fig. 5.2 for location), where they are clearly distinct from the adjacent granite. However, previous work has suggested that intrusion of the

later Slieve Gullion Complex may have caused this mobilisation (Stevenson et. al., 2008).

Conversely, there are areas of the aureole surrounding the complex where alteration of the host rocks does not appear to be extensive. Examples include ***Aughnagon Quarry*** (**J144251**) in the Newry pluton, where host rocks immediately adjacent to granodiorite are hornfelsed but not mobilised (appendix 1; see fig. 5.2 for location); as well as at ***Clade Quarry*** (**J115209**), close to the eastern boundary of the Cloghoge pluton, where sediments are folded but are otherwise apparently undisrupted (photo 5.1; appendix 1). There are also areas where sediments are extensively deformed but not mobilised. For example, photo 5.2 illustrates the host rocks within the ***Belleeks*** (**H999255**) site immediately to the north of the Cloghoge pluton, which display a clear schistosity. However, the latter may again relate to the Palaeogene Slieve Gullion Complex (Stevenson et. al., 2008).

Such variety in host rock deformation adds to the complexity of the NIC margin. As a result, it appears that the latter may relate to its host rocks in a number of different ways, rather than fitting a single model scenario.

5.4 Quartz recrystallisation

5.4.1 General trends

Fig. 5.4 illustrates the *High Temperature Quartz Recrystallisation* (HTQR) *scores* for numerous samples from the NIC. These appear to closely relate to the distance of the samples from the edge of the intrusion. Of the five samples with maximum HTQR Score (4), three locate at the very edge of the Rathfriland and Newry plutons respectively, whilst the other two locate less than 2 km from the edge of the Rathfriland pluton. On the other hand, none of the samples from the large central zone (L) of the Newry pluton or the two innermost zones (H and I) of the Rathfriland pluton show HTQR Score of greater than 2. Samples close to (but not at) the edge of all three plutons additionally show relatively variable scores. This suggests a general outward increase in the extent of high temperature quartz recrystallisation, with particularly high amounts occurring at the very edges of the complex. This in turn implies that high temperature solid state strain was greatest at the margins of the NIC (e.g., see Gapais and Barbarin, 1986; Bouchez, 1997).

5.4.2 Relationship to internal divisions

Within the outer NIC HTQR scores appear to be particularly high close to the inner boundaries of Zones C, D, G and J, whereas these are significantly lower within other marginal locations (see fig. 5.4). In particular Zones E and the part of Zone C adjacent to the Seeconnell Complex (Zone A) exhibit relatively low HTQR scores. The difference between locations of high and low HTQR score in the pluton margin appears to relate to their separation from major concentric pluton boundaries. Zones C, D, G and J all border such boundaries, whereas Zones C and E are separated by distance and the presence of an intervening facies respectively.

Therefore, some of the internal boundaries of the NIC seem to correlate with quartz crystallisation and hence solid state strain. This supports a model whereby the intrusion of new pulses deforms existing ones. Exception exists within the Cloghoge pluton, where extents of quartz recrystallisation appear to be exclusively low.

The HTQR scores for the satellite bodies are very variable. These are low in the bodies to the north of the NIC (Zone X), but higher in the sample obtained from the southern bodies (Zone Y). However, due to the limited data for these bodies, it cannot be determined whether this is a consistent pattern.

5.5 AMS data

5.5.1 Sterographic projection and derivation of AMS fabrics

A selection of AMS fabrics from various parts of the NIC are presented in fig. 5.5. It is clear that the majority of these display *oblate* (dominantly planar) fabrics, as indicated by the fact that the projected 95% confidence limits of K_1 and K_2 extend towards one another and are in some cases overlapping (e.g., Nye, 1957; Owens, 1974). Samples R7B, N24 and C11B in fig. 5.5 demonstrate this feature. It implies that the magnitude of maximum and intermediate magnetic susceptibility values are likely to be similar, as would be expected in a planar fabric (see Owens, 1974). The planes defined by the 95% confidence limits of K_1 and K_2 in turn represent the orientation of such AMS fabrics

Fig. 5.5 also reveals a smaller number of *prolate* (dominantly linear) fabrics. These are apparent from extended/overlapping 95% confidence limits of K_2 and K_3, along with a relatively well-constrained confidence limit for K_1. Examples include the samples R21 and C6 (fig. 5.5). Such results mean that the maximum magnetic susceptibility value is significantly larger than the two other similarly-sized susceptibilities, implying a stronger linear component (e.g., Owens, 1974).

On the other hand, some samples (e.g., R9, N25A and C7) show little evidence for being oblate or prolate (see fig. 5.5). These represent the *triaxial* magnetic alignments defined by Owens (1974). In this case the susceptibility measurements exhibit relatively small, separated 95% confidence limits (i.e., $K_1 > K_2 > K_3$ – see Owens, 1974).

Despite the dominant fabric characteristics apparent from the stereonets, AMS results also show that every sample has at least a small component of both planar and linear alignment (i.e., there are no perfectly oblate or prolate fabrics). Hence all of the derived fabric orientations displayed in fig. 5.6 include both an oblate and prolate component.

The fabrics displayed in fig. 5.6 are distinguished in terms of their strengths of alignment. This is achieved through the use of *F* and *L*, the respective planar and linear strengths of alignment (Khan, 1962; Owens, 1974). The parameters are fully examined subsequently (see fig. 5.8 and 5.9), but for the current purpose they were divided into stronger and weaker sets of values. The cut-off between these was determined as 5% and 3% for F and L respectively, which are the median values for each set of the data (see appendix 6). Fig 5.6 shows higher values of either parameter being represented by bold fabric symbols; whilst lower values are represented by feinter symbols (see below for description of results).

5.5.2 Derived planar AMS fabrics

Planar AMS fabrics show a generally concentric, steeply-dipping trend that is clearly very similar to that displayed by visible foliations in the NIC (see fig. 5.6). There are also two distinct areas of planar AMS fabrics that are oblique to the general structure of the complex. These occur across the ***Cloghoge Roundabout North*** (**J080238**) and ***Cloghoge Railway Track*** (**J077213**) sites, along with the ***Newry Railway Tunnel*** (**J071266**) site (see fig. 5.6). Of these the Cloghoge Roundabout North site represents the off-centre ‘core’ (Zone O) of the Cloghoge pluton; the Cloghoge Railway Track site represents the marginal sheeted facies

(Zone M) of the Cloghoge pluton and the Newry Railway Tunnel site represents the inner boundary area of the Newry pluton porphyritic granodiorite (Zone K). AMS fabrics from the Cloghoge Roundabout North site are also oblique to the visible mineral alignments here, which are approximately parallel to the pluton margin (see appendix 1). However, visible fabric data was unavailable from the other locations and so it is unclear whether this is also the case here.

Fig. 5.6 additionally reveals a relationship between the fabric strength parameters (F and L) and planar fabric obliquity. This shows that the oblique planar alignments are consistently either very weak, or dominated by the linear component. The latter is the case in the Newry Railway Tunnel site, whereas the other locations correspond to low values of both F and L. Hence, none of the oblique planar AMS alignments within these various parts of the NIC relate to a strongly planar fabric. This implies that development of planar fabrics preferentially occurs in concentric orientations.

AMS provides more detailed coverage of the satellite bodies than has been available from visible fabrics. These data suggest that the planar fabrics within the bodies consistently parallel their contact trends (see fig. 5.6). At first glance this does not appear to be the case for the result from the ***Doyles Close*** (**J227418**) site. However, field relationships show that the contact here is locally deflected to an orientation that is very similar to that of the planar AMS fabric (see appendix 1). On the other hand, the minor local contact deflection observed at the ***Leode Road Quarry*** (**J177280**) site does not correspond to a differing AMS alignment. Therefore, it is suggested that the scale of such deflections determines whether these are recorded in the adjacent igneous fabrics.

5.5.3 Derived linear AMS fabrics

Linear AMS fabrics largely show a concentric orientation within each pluton of the NIC (see fig. 5.6). These are also generally shallow to moderately dipping, although they are consistently steeper at the edges of the NIC and in the boundary areas between individual plutons. The steeper marginal fabrics can be seen most clearly in the mafic granodiorites (Zones C and F) at the northeast rim of the Rathfriland pluton and along the Newry-Cloghoge pluton boundary.

There are also a number of examples of linear AMS fabrics that are oblique to the general concentric trend. These occur in a much wider variety of areas than the former anomalous fabrics (see fig 5.6) and can be grouped according to three different fabric strength characteristics:

1. **Fabrics with a more significant linear component (L>F):** occurring within the sheeted Cloghoge pluton margin (Zone M); the inner boundary area of the Newry pluton porphyritic granodiorite (Zone K) and the mafic granodiorite in the south of the Rathfriland pluton (Zone F).
2. **Weakly anisotropic fabrics (low H):** occurring within the quartz diorite (Zone E); the Cloghoge pluton 'core' (Zone O); the southernmost Newry pluton (Zone J) and some of the satellite bodies (Zone Y).
3. **Moderately anisotropic fabrics (moderate H):** occurring in sporadic samples within the eastern Newry pluton (Zone J); the central Newry pluton (Zone L) and some of the satellite bodies (Zones X/Y).

It is clear from these characteristics that the majority of oblique linear AMS fabrics correspond to weak planar alignments. As a result there may be a degree of exclusivity between well developed foliations and oblique lineations.

5.5.4 AMS fabric strength (H, F and L)

Overall fabric strength (H)

The overall AMS fabric strength (H) can be seen to be consistently moderate throughout much of the NIC (see fig. 5.7). However, there are also several areas where particularly strong or weak fabrics are recorded. Firstly, a number of high H values appear to be associated with the boundaries of Zone K in the Newry pluton (the porphyritic 'ring' facies) and the boundary between Zones G and H in the Rathfriland pluton. Examples of these can be seen at the ***A25 Farmland*** (**J136319**), ***Greenan Lough*** (**111235**), ***Newry Railway Tunnel*** (**J071266**) and ***Curley Lane*** (**J150348**) sites in fig. 5.7. These generally represent locations at which high extents of quartz recrystallisation have been observed (see section 5.4) (although the inner boundary of Zone K is uninvestigated in terms of quartz recrystallisation).

Areas of significantly weak AMS fabrics are also apparent from fig. 5.7. Clear examples of such can be seen at the ***Cloghoge Railway Track*** (**J077213**) site in the 'core' of the Cloghoge pluton (Zone O) and the ***Kilcoo*** (**J278330**) site in the southern Rathfriland pluton (Zone E). Weak AMS fabrics also occur within the northern area of mafic granodiorite (Zone C); parts of the outer Newry pluton (Zone J) and some of the satellite bodies (Zone Y). The sites within Zones C and E of the Rathfriland pluton are particularly significant in that they have also been shown to exhibit low

extents of quartz recrystallisation (see Chapter 5.4). Therefore, both the AMS and high temperature solid state textures in these areas are poorly developed.

Many of the sites of high and low AMS fabric strengths discussed above correspond to areas that are respectively proximal to and separated from major concentric internal boundaries (excluding the outer Newry and Cloghoge pluton, which are accounted for below) (see fig. 5.7). The same relationship is apparent from quartz recrystallisation extents across a larger number of zones and is considered to support intrusion of these as separate magma pulses (see section 5.4). Hence the AMS fabric strength results suggest that such magma pulses may not only affect recrystallisation but also fabric development within previously intruded material. The weakly developed AMS fabrics in question (i.e., within the outer Rathfriland pluton) are also anomalously oblique to the general concentric pluton structure (see fig. 5.6; section 5.5.3 above), suggesting that fabric-formation associated with internal pulses may produce concentric alignments.

Planar and linear AMS fabric strength (F and L)

A plot of linear versus planar AMS fabric strength (L vs F) shows that a relatively weak correlation exists between these parameters (see fig. 5.10). The plot also shows that high L values can occur without similarly high F values, whilst the opposite does not apply. This suggests that the fabric-forming process producing the planar fabrics also created linear alignments, but that some linear alignments occurred through a separate process.

These results additionally reveal that the majority of high-H value samples mentioned above comprise both a strong planar and linear component. These samples in particular occur close to the inner boundary of Zone J of the Newry pluton and the boundary between Zones G and H of the Rathfriland pluton (see fig. 5.8). On the other hand a smaller number of high-H value samples are prominent only in terms of their L values. These represent samples N22-N24 close to the inner boundary of Zone K, at the ***Newry Railway Tunnel*** (**J071266**) site (see fig. 5.9). Hence these samples show the relatively rare characteristic of an independently strong linear fabric. Fabrics showing this characteristic have also been shown to be oblique to the pluton structure, in contrast to the clearly concentric fabrics that show high values of both F and L (see fig. 5.8 and 5.9). Therefore, it appears that the fabric-forming process producing both planar and linear fabrics aligns these concentrically, whilst processes that produce weak or exclusively linear fabrics result in more oblique alignments. This supports the results reported in section 5.5.3 above.

A further example of a fabric that displays a notably higher L value is observed at the ***Cloghoge Roundabout North*** (**J080238**), within the sheeted Cloghoge pluton margin (Zone M) (see fig 5.8 and 5.9). Here both planar and linear fabrics have been shown to be oblique to the concentric pluton structure, whilst nearby visible foliations at the ***Upper Motorway Terrace*** (**J079239**) site (see fig. 5.6) have also been shown to be oblique. Oblique visible foliations have been shown to be very rare amongst visible fabrics and thus again supports the idea that alignments without a significant planar component are more likely to be oblique.

5.5.5 Considering bulk magnetic susceptibility (K_{mean})

A plot of the bulk magnetic susceptibility, K_{mean} (see Owens, 1974), versus H reveals little correlation between the parameters at moderate to high K_{mean} values (see fig. 5.10). However, at lower K_{mean} values (i.e., less than around 1000) the magnitude of H is clearly smaller. This has important implications in that a number of the weakly anisotropic fabrics determined by AMS may be so as a result of their low bulk magnetic susceptibility. Hence where samples show weakly magnetic anisotropy the derived AMS fabrics may be less reliable.

This could therefore account for the oblique linear fabrics observed within the some of the weakly anisotropic areas mentioned in section 5.5.4. In particular these include areas of the Cloghoge pluton 'core' (Zone O), the outer Newry pluton (Zone J) and satellite bodies (Zone Y) which display low H values (see fig. 5.11). The latter values and fabric obliquities are thus thought to likely represent artefacts of the samples' low magnetic susceptibilities.

5.6 Cause of AMS fabrics

5.6.1 Correlation of AMS and field structural data

Fig. 5.13 provides a comparison of the orientations of derived AMS and visible foliation measurements. This suggests that the two display the same broad alignment pattern. The close relationship is apparent both in terms of fabrics that follow the general concentric trends throughout the complex and those that do not. For this reason these AMS results can generally be applied to understanding the visible fabrics and vice versa.

The only area in which clear differences are apparent is the 'core' area of the Cloghoge pluton (Zone O), where a number of irregular, oblique fabrics are apparent. Visible foliation data was not available from these particular sites, although foliation data from proximal areas suggests that fabrics are much more regular (Neeson, 1984). However, as has been shown in the previous section, samples in the Cloghoge pluton 'core' show very low levels of bulk susceptibility, which are suggested to result in unreliable fabrics. Therefore, although AMS fabrics generally parallel visible mineral foliations, those with particularly low bulk susceptibilities should be considered with caution. Fortunately, outside Zone O of the Cloghoge pluton these occur very sporadically.

5.6.2 Thermomagnetic analysis

Plotted normalised susceptibility values during the heating and cooling of five samples from various parts of the NIC (see fig. 5.14) reveals four obvious relationships (see fig. 5.15). These are as follows:

1. Abrupt susceptibility decrease

All plots show a consistent, sharp decline from a relatively high susceptibility (0.7-0.8) to zero between approximately 570 and 600°C (fig. 5.15). The abrupt decrease occurs in the form of a slightly curved line, with an inflection point at around 580°C in all cases, reflecting a consistent Curie Temperature (see Petrovský and Kapička, 2006; Fabian et. al., 2013). The general trend is indicative of a ferromagnetic (*s.l.*) mineral, whilst the Curie Temperature represents that for pure magnetite (see Dunlop and Özdemir, 2001). Therefore, these results suggest that magnetite is the main magnetic component in each of the analysed samples.

2. Hopkinson peak

The plot for sample C3B (fig. 5.15b) exhibits a high-temperature rise in susceptibility on the heating curve. This occurs from just over 400°C until immediately before the abrupt susceptibility decline, although due to the data being very scattered it is difficult to interpret the precise characteristics of the trend. Such a feature is consistent with the *Hopkinson effect* (Hopkinson, 1889; Dunlop, 1974), which can be the result of either the presence of single-domain magnetic grains or that of large multidomain grains (e.g., Radhakrishnamurty and Likhite, 1970; Dunlop, 1974). However, in the latter case the *Hopkinson Peak* produced will be relatively narrow, due to the consistent, high blocking temperatures of these large grains (Dunlop, 1974). The observed wide peak therefore suggests that single-domain grains are more common. As has been established above, these are most likely to primarily consist of magnetite.

However, only sample C3B shows any indication of the Hopkinson effect (see fig. 5.15). Hence, for other parts of the complex (represented by the other four plots) single-domain magnetite may be less common. The lack of even a narrow Hopkinson Peak in these plots further suggests that the magnetite in such areas is likely to be multi-domain, but not 'large multi-domain' (Dunlop, 1974).

The evidence for both single- and multi-domain magnetite within the NIC suggests that the factors controlling anisotropy may also vary. Multi-domain grains are more likely to magnetically interact, producing an induced magnetic field referred to as *distribution anisotropy* (e.g., Hargraves et. al., 1991). Conversely, the anisotropy of single-domain magnetite is more likely to be controlled by the shapes of individual grains (i.e., *shape-controlled anisotropy* – e.g., Hargraves et. al., 1991; Galliot et. al., 2006). Yet the two are generally considered to have little difference on the actual orientations of the deduced AMS fabrics (Hargraves et. al., 1991; Canon-Tapia, 2001). Therefore, in the absence of evidence that suggests otherwise (i.e., oblique AMS fabrics), the presence of single-domain magnetite is considered to have little relevance to AMS alignments within the NIC.

3. <u>Mid temperature susceptibility 'hump'</u>

An additional feature of these plots is the repeated presence of a 'hump' (or in fig 5.15d more of a step-like curve) in the heating trend. This generally peaks at around 300°C, although the amplitude and length of the feature can be seen to vary. Its position on the temperature axis is not always consistent either, with sample C3B (fig 5.15b) showing a peak at around 200°C. For these reasons it is difficult to link such a section of the plots to a particular mineral.

The rise leading up to the peak and decline in susceptibility is best explained by the growth of new magnetic minerals during heating (e.g., Boer and Dekkers, 2001). The higher-temperature section of decline might in turn be a result of the presence of a paramagnetic mineral (likely biotite or hornblende due to the mineralogy of the rocks defined in Chapter 4A), which shows susceptibility reduction with increasing temperature (e.g., Tarling and Hrouda, 1993; Hrouda et. al., 1997). However, the fact that this decline occurs over a relatively small temperature range and involves a normalised susceptibility reduction of generally less than 0.2 suggests that this represents a relatively minor magnetic component.

4. Variation between heating and cooling trends

The cooling trends of the five samples also consistently plot lower than their heating trends (fig. 5.15). The plots reveal that this almost exclusively occurs by the same amount as the mid-temperature susceptibility decline (see above). Small exceptions occur in samples C2D and R4B (fig 5.15a/e), though, where the gap between the respective curves is slightly larger than the latter.

Authors such as Böhnel et. al. (2002) have attributed such results to oxidation of minerals during cooling. In the case of the NIC this is likely to occur predominantly in the paramagnetic component (i.e., biotite/hornblende), due to the relationship of the gap to the mid-temperature susceptility decline associated with the latter (see above). Within samples C2D and R4B a small amount of another mineral (possibly magnetite) may have been oxidised, although this is more difficult to determine.

5.6.3 Summary and implications

Investigation into the cause of AMS fabrics within the NIC reveals two major interpretations. These are as follows:

1. The vast majority of planar AMS fabrics parallel visible foliations. Rare exceptions occur, which are most significant within the Cloghoge pluton 'core'. These correspond to low degrees of bulk magnetic susceptibility, which may have led to the development of irregular fabrics.
2. AMS results are considered to correspond predominantly to the distribution anisotropy of multi-domain magnetite. However, within the eastern Cloghoge there is evidence for single-domain magnetite, which may provide a dominantly shape-controlled magnetic anisotropy. Nevertheless, there is little evidence either from the current study or former work that the alteration between these has any effect on AMS fabric orientation. A smaller proportion of a paramagnetic mineral is also thought to consistently contribute to the AMS results. Due to the mineralogy of the rocks this is likely to represent biotite or hornblende.

These interpretations ultimately suggest that AMS represents a reliable and well-constrained proxy for visible mineral alignments. Thus the use of this technique to infer processes that would normally be interpreted from the latter is fully justified.

5.7 Discussion

This section interprets the results from structural field measurements, quartz recrystallisation investigation and AMS in terms of emplacement of the NIC. The emplacement model derived from this analysis is presented in fig. 5.17 and fig. 5.18.

5.7.1 Tectonic influence

General mechanism of accommodation

The results from the current study largely support the tectonic space creation mechanism inferred by Beamish et. al., (2010). This is most clearly evident within two sites located to the northeast and south of the intrusion respectively. The former shows bedding and cleavage orientations that are consistent with the general pattern of strike swing illustrated by Beamish et. al. (2010); whereby host rock tracts curve towards and truncate against the NIC. The other site is located within an area where host rock trends were not extrapolated by Beamish et. al. (2010). However, this area shows similarly oblique host rock trends to both the formerly mapped structure of the terrane and the margins of the NIC (GSNI, 1997). Hence, these results are consistent with the regional strike swing that Beamish et. al. (2010) suggest would lead to tectonic space creation via a releasing bend during Late Caledonian sinistral transtension (see Soper and Woodcock, 1990; 2003; Brown et. al., 2008; Miles et. al., 2013).

On the other hand, many bedding/cleavage measurements are parallel to the edges of the NIC. These are mostly restricted to sites that are proximal to the intrusion. As a result, it appears that the tract boundary predictions made by Beamish et. al. (2010) may occur at distance from the NIC, but not adjacent to its margins. This is

accounted for by the evidence for inflation of the NIC discussed in the following sub-section.

Involvement of crustal structures

Upper crustal structures: The releasing bend model requires both a regional strike swing, together with a fault across which opening can occur during transcurrent movement (e.g., Guineberteau and Bouchez, 1987; Beamish et. al., 2010). It is proposed that two of the tract boundaries within the Gala Group of the Southern Uplands-Down-Longford Terrane represent such faults. These are the boundaries between Gala Group Tracts 7+2 and 7+3 together with 7+1 and 7+2 (see fig. 5.16).

Each of the former can be seen to show the required strike swing (Beamish et. al., 2010). Furthermore, when extrapolated through the NIC these tract boundaries also intersect the centres of the three plutons and in one case (the Tract 7+2/7+3 boundary) additionally the Seeconnell Complex (fig. 5.16). The pluton centres represent sites at which intrusion of magma would necessarily occur during the growth of concentric bodies during tectonic opening. Hence, the two boundaries show a strong potential link to intrusion of the concentric Newry, Cloghoge and inner Rathfriland plutons. The inferred predominant occurrence of tectonic opening at these pluton centres also explains the general circular shapes of the NIC intrusions (see fig. 5.16 and fig. 5.17c-d).

The Seeconnell Complex is additionally important, as it represents the oldest part of the northeast Rathfriland pluton rim. However, the non-concentric distribution of facies within this area suggests that tectonic facilitation may not have occurred at a single site. Instead this is proposed to have initiated in the area of the Seeconnell Complex along the Gala Group Tract 7+2/7+3 boundary, before migrating to the southwest to facilitate intrusion of the subsequent outer pluton zones.

Further migration of tectonic opening to the SW would have ultimately enabled intrusion of the inner Rathfriland pluton (see fig. 5.17b). This process is considered to have split and spread the earlier intruded zones to form the observed crescent-shaped pluton rim. It is proposed that this did not occur for the Seeconnell Complex earlier in the migration of tectonic opening due to its more mafic nature, which may have provided the area with a greater degree of rigidity (e.g., Blake and Fink, 2000; McBirney, 2007) (see fig. 5.17b).

The satellite bodies may also relate to the tectonic space creation process. These are concentric about the centres of the Rathfriland and Newry plutons respectively and are compositionally similar to each (see Chapter 4). However, the presence of host rock separating the bodies from the rest of the NIC precludes the idea that they are intruded at any of the sites discussed above. Therefore, it is inferred that these are produced by intrusion of magma within concentric fractures, created by the same tectonic extension that facilitated intrusion.

The development of such concentric sheeting has traditionally been linked to the cauldron subsidence model introduced in Chapter 1 (e.g., Richey, 1932; Anderson,

1936). However, sub-circular fractures are also an observed characteristic of strike-slip pull-apart tectonics (Mann et. al., 1983; Smith, 2004). Thus in the absence of any clear evidence for the traditional cauldron subsidence process it is considered that the satellite bodies most likely to represent dykes emplaced into sub-circular fractures associated with the local strike-slip pull-apart regime.

The idea of tectonically accommodated intrusion within a strike-slip terrane has been inferred for a number of other areas (e.g., Hutton, 1982; Guineberteau et. al., 1987; Brun et. al., 1990; Petford et. al., 2000; Rabillard et. al., 2014 – see Chapter 1). In most cases such models involve relatively steep contacts. This is because classical pull-apart tectonics will result in horizontal extension (e.g., Aydin and Nur, 1982) and hence opening of more vertically extensive space. Results from the NIC confirm that this appears to be the case. This is evident firstly from the fact that observed contacts are consistently steep (predominantly 60-80°), but also because the surrounding host rocks show little evidence of tilting. This means that the currently steep contacts were originally intruded steeply, rather than being tilted, for example by laccolithic doming.

The tracts implied by Beamish et. al. (2010) also clearly suggest that a large amount of host rock material is missing in the vicinity of the NIC (see fig. 2.4). For example, the entire of tract 7 + 2 is absent across the extent of the Newry and Cloghoge plutons. It is clear that this cannot be accounted for by mobilisation or compression of the host rocks. Furthermore, assimilation has been suggested to be minor and so is not likely to explain the missing host rock material either. Instead it is suggested that the NIC initially intruded as relatively thin sheets that cross cut the steep host

rock structure. Subsequent laccolithic inflation of these sheets (see below) would have resulted in the observed missing host rock. This idea is supported by the fact that aeromagnetic data appears to detect of signatures of zones in the subsurface, thus implying that the NIC is composed of relatively tabular bodies.

Lower crustal structures: The location of the NIC may also relate to a set of deep-seated crustal lineaments. The importance of these in terms of Caledonian magmatism has been inferred by numerous authors (e.g., Hutton, 1992; Hutton and Reavy, 1992; Jacques and Reavy, 1994; Hutton and Alsop, 1996; Dehls et. al., 1998; Chernicoff et. al., 2002; Weinberg et. al., 2004; Chew and Stillman, 2009; Cooper et. al., 2013 – see Chapter 1). Cooper et. al. (2013) summarised a set of such lineaments extending throughout Ireland and Northern Ireland, in particular linking intrusion of the Sperrin Mountains suite to one of these termed the Omagh Lineament. This work also showed that two other deep-seated lineaments intersect the NIC (see fig. 5.16).

Intersection of the *Argyll* and *Newry Lineaments* occurs close to three of the sites within the NIC from which tectonic opening is proposed (fig. 5.16). Firstly, the trend of the Argyll Lineament meets the edge of the Seeconnell Complex. The more westerly Newry Lineament in turn appears to intersect both the centre of the Newry pluton and the off-centre ‘core’ of the Cloghoge pluton. The only proposed opening site that does not correlate with a deep-seated lineament is the central Rathfriland pluton.

The interaction of deep-seated lineaments with Caledonian shear zones has previously been interpreted as the cause of plutonism within the British Caledonides (e.g., Jacques and Reavy, 1994; Stevenson et. al., 2006). These authors suggest that the lineaments may represent earlier shear zones in the Pre-Caledonian basement, which were reactivated during the Caledonian. They propose that "transtensional voids" occurring at the intersection sites between these and the Caledonian shear zones may have facilitated a range of magmatic processes; from melting to ascent and ultimately emplacement higher in the crust (Jacques and Reavy, 1994, p. 968).

Therefore, it is suggested that the faulted tract boundaries within the Southern Uplands-Down-Longford Terrane could be upper crustal expressions of ductile shear zones that intersect with these lineaments at a deeper level. By this model it is feasible that creation of space at depth by relative movement along Caledonian and Pre-Caledonian structures could be linked to emplacement of the NIC (e.g., Jacques and Reavy, 1994; Stevenson et. al., 2006). Such connectivity throughout the crust may also allow magma to ascend relatively quickly.

Adaptation of this model to the NIC implies that intrusion initiated due to space creation directly above the intersection of the 7+2/7+3 tract boundary and the Argyll Lineament (see fig. 5.17a). Intrusion of the central Rathfriland pluton in turn occurred due to southwestward migration of magma ascent along the 7+2/7+3 tract boundary, following filling of the initial space created directly above its intersection with the Argyll Lineament (see fig. 5.17b). Both the Newry and Cloghoge plutons

were then intruded at two sites approximately above the intersection of the.subparallel 7+1/7+2 tract boundary and the Newry Lineament (see fig. 5.17c-d).

It is further suggested that the two deep-seated crustal lineaments may have caused the regional strike swing within the terrane in the first place. The orientation of the strike swing is consistent with surface manifestation of sinistral movement along the approximately north-south trend of the lineaments (see fig. 5.19). Such movements would be feasible as a result of reactivation of these features during Late Caledonian sinistral transtension. Hence the deep-seated lineaments may be significant not only in terms of facilitating magma ascent through the crust, but also by determining the site at the surface where tectonic accommodation occurred.

The process of magma ascent is considered to have occurred through dyking. This is firstly due to the theoretical problems with the diapiric ascent model (e.g., Marsh, 1982; Schwerdtner, 1990; Clemens and Mawer, 1992; Petford, 1996; Clemens, 1998). However, even the modified nested diapir model (e.g., Paterson and Vernon, 1995; Paterson et. al., 1998) would require relatively large conduits for magma flow within the upper crust. Considering the fact that ascent of magma to produce the NIC appears to have been facilitated by faults and shear zones (see above), it is thought more likely that transport within these would occur within narrower dykes (e.g., Hutton, 1992; Petford et. al., 2000).

5.7.2 Laccolithic intrusion and inflation

Evidence for inflation in general

The NIC also shows evidence for forceful emplacement, which is inferred to have occurred due to the addition of a greater volume of magma than the accommodated space provided for (see fig 5.17). This would have led to expansion of each pluton in a similar way to that outlined in the ballooning model (e.g., Ramsay, 1989; Clemens, 1998; Molyneux and Hutton, 2000; Shan et. al., 2004). However, the term *inflation* is preferred to ballooning here, since the latter implies a spherical shape. Due to the proposed facilitation model, host rock relationships discussed above and linear AMS fabrics (see below), plutons within the NIC appear instead to have dominantly expanded laterally. This is similar to the proposed inflation model proposed for the Flamanville pluton in northwest France (Brun et. al., 1990) (see section 1.3.3).

Inflation within the NIC can be deduced from a variety of techniques. Firstly, investigation of quartz textures within each pluton shows that there is clearly an outward increase in the extent of high temperature solid state recrystallisation. As a result, it can be inferred that the margins of the NIC have been subjected to the greatest extent of plastic strain (e.g., Bouchez, 1997). This would be consistent with intrusion from a central source causing outward directed inflation, which has been shown to result in increasing plastic deformation toward the outer margins of a pluton (e.g., Hutton, 1988; Paterson et. al., 2004). This is proposed to be the result of solid state conditions within the outer magma during continued inflation within inner parts of a pluton.

Support for this idea is provided by the explicability of two areas of anomalous High Temperature Quartz Recrystallisation (HTQR) scores. These represent the extreme northeast part of the Rathfriland pluton (i.e., to the north of the Seeconnell Complex) and the quartz diorite in the south of this pluton (see fig. 5.17). The anomalously low HTQR score within the very northeast of the Rathfriland pluton can be accounted for by the fact that the area locates on the opposite side of the Seeconnell Complex to the central pluton. Hence deformation through later stage inflation may essentially be buffered by the older, solidified Seeconnell Complex. The equally low HTQR score for the quartz diorite can in turn correlate with the fact that the facies is separated from a major concentric pluton boundary by an area of mafic granodiorite. As a result, a similar buffering effect from the inflation of the inner Rathfriland pluton is suggested.

Further evidence for inflation is provided from host rock structural data. In close proximity to the NIC bedding and cleavage measurements within these consistently parallel the margin of the intrusion. This is a common feature of the host rocks surrounding ballooning plutons (e.g., Pitcher, 1997; Molyneux and Hutton, 2000; Stevenson et. al., 2007).

The igneous fabrics within the main NIC additionally provide strong evidence for inflation. Firstly, measured field foliations are generally steep and concentric, which are again consistent with the outward-directed magma pressures that necessarily accompany this process (see Molyneux and Hutton, 2000). In particular, at the Shannaghan Hill site these foliations are shown to cross-cut a compositional boundary, implying that they formed later. This precludes the idea that such

alignments are developed contemporaneously with intrusion of the magma; for example through the process of sidewall crystallisation. Nevertheless, sidewall crystallisation is considered a strong possibility within the Seeconnell Complex, where crystal cumulates are evident (Meighan and Neeson, 1979).

The linear components of the recorded AMS fabrics generally display similar concentric orientations, which are mostly shallowly-dipping. This pattern has been observed within the Flamanville granite in northwest France (Brun et. al., 1990). The linear fabric components within the Flamanville granite have been linked to lateral expansion of the pluton, which results in a concentric, horizontally-orientated field of extension (see Chapter 1). Therefore, these results support the idea that inflation of the NIC occurred essentially outwardly, without significant doming of the host rocks. The shallowly-dipping linear fabric components also preclude the traditional emplacement models of diapirism or cauldron subsidence (see Cruden, 1990; Emeleus et. al., 2012).

The relationship between inflation of plutons and individual magma pulses

As has been shown in Chapter 4, the NIC consists of a number of separately intruded pulses. Current results provide possible evidence for inflation occurring within these individually, as well as for the NIC as a whole (see fig. 5.17). This is most clearly apparent from the inner margins of several zones throughout the NIC, which appear to show high extents of quartz recrystallisation and hence solid state deformation. This supports the idea of an internal, younger pulse deforming previously intruded material.

In particular, the inner margins of Zones G and J of the Rathfriland and Newry plutons exhibit high extents of quartz recrystallisation as well as strong AMS fabrics. These imply that the magma was subjected to deformation by internal pulses (Zones H and K) at both higher and lower temperatures, resulting in respective fabric alignment and solid state recrystallisation. It has been shown that highly crystalline magma mushes will behave similarly to “plastically deforming solids” under stress (Nicolas and Ildefonse, 1996, p. 2013). The results suggest that the inner parts of Zones G and J had cooled to this state prior to the intrusion of the respective inner Zones H and K, leading to the development of strong AMS alignments. The areas would subsequently have cooled further under conditions of continued outward-directed pressure, resulting in the development of the observed recrystallisation textures.

The AMS fabrics within Zones G and J are hence interpreted to be submagmatic (e.g., Bouillin et. al., 1993; Bouchez, 1997; Paterson et. al., 1998). Conversely, those throughout other parts of the NIC show no evidence of the fabric-forming process discussed above. As a result these are interpreted to represent magmatic fabrics, produced from simple phenocryst rotation in a largely liquid magma (Paterson et. al., 1989). The observed solid state fabrics and textures are in turn considered to represent an overprint to the original magmatic or submagmatic alignment (e.g., Gapais and Barbarin, 1986).

Therefore, the NIC exhibits evidence of strain occurring over a wide cooling interval. This can be broadly divided into the following three strain-producing events: (1) Inflation from early in the cooling history of each pulse produces a ubiquitous

concentric magmatic mineral alignment; (2) Inflation of newly intruded pulses causes recrystallisation and a strong, submagmatic mineral alignment at the inner edges of adjacent, previously intruded pulses; and (3) Continued inflation within the central parts of a pluton produces a solid state overprint within the cooled, crystallised outer areas.

This contradicts the work of Paterson et. al. (1998, p. 53), which suggests that only the final “increment of strain” will be recorded within a felsic pluton. A study on the Ross of Mull Granite in northwest Scotland (see Petronis et. al., 2012) also contradicts the work of Paterson et. al. (2012). Here an older magmatic emplacement fabric is apparent, along with a later partial overprint from a tectonic fabric.

The low extents of fabric development and quartz recrystallisation within parts of the northeast Rathfriland pluton rim that are separated from major concentric pluton boundaries (see above) suggests that intrusion of this area may not have had a significant forceful component here. This idea is supported by the fact that the area displays concentric fabrics, its boundaries are clearly more irregular. Hence, the concentric fabrics here are proposed to result from inflation of inner magma pulses, whilst the areas of weak fabrics and low recrystallisation represent sites where this influence was absent (for reasons explained above). As a result, it can be deduced that the early intrusion history of the NIC was likely to have been dominated by tectonic accommodation, rather than forceful emplacement (see Hutton, 1982; Stevenson et. al., 2006).

Laccolithic stacking within the NIC

From the evidence for overlapping relations discussed above the NIC is interpreted to consist of at least five separate tabular bodies. These are illustrated in figure 5.18 as a series of stacked laccoliths, which were likely to have been supplied by a southwestward-migrating source. An approximate northeast-southwest traverse (fig. 5.18) would reveal the Seeconnell Complex as the oldest and deepest part of the NIC, followed by at least one distinct body comprising much of the northeast Rathfriland pluton rim. The inner Rathfriland pluton (and possibly the mafic granodiorite (2)) would in turn comprise a distinct body, followed by each of the remaining plutons. Hence, the Cloghoge pluton is inferred to have been emplaced at the shallowest crustal level.

Schetselaar et. al. (2000) show that aeromagnetic data can reveal features at depths of 10 km or more. However, the general clarity of the resolved subsurface signatures within the NIC suggests that these occur at significantly shallower depths. Hence, the bodies comprising the NIC are estimated to be in the range of 1 to several km in vertical extent.

Stacking of successive laccolithic bodies has been observed within the Henry Mountains in Utah (Morgan et. al., 2005; Horsman et. al., 2009) and on the Italian island of Elba, where the arrangement of granite porphyries is described as *Christmas tree* laccolithic stacking (Rocchi et. al., 2002; Westerman et. al., 2015). This term is applied due to the significant (km-scale) differences in emplacement depth between the Elba intrusions (Rocchi et. al., 2002). In contrast the bodies

comprising the NIC appear to show a large amount of vertical overlap, with much of the spatial variation between these being horizontal.

5.7.3 The margins of the NIC: competing influences

The results show that both tectonic accommodation and inflation have affected the boundary areas of the NIC. This has led to the occurrence of a variety of relationships in these boundary areas. Most obviously the host rocks immediately adjacent to the NIC boundaries can be seen to consistently follow the trend of these boundaries, which has been interpreted to result from lateral expansion (e.g., Brun et. al., 1990). This relationship occurs within host rocks showing a wide range of characteristics, including mobilisation, ductile deformation and contact metamorphism. The observed parallelism provides evidence for not only inflation but also general concordance of the original contact with host rock structure.

However, recent remapping of the host rock tracts (Beamish et. al., 2010) implies cross cutting of these by the NIC (see fig. 5.16). It is therefore suggested that host rocks only follow the trend inferred by Beamish et. al. (2010) at distance from the NIC, whereas in close proximity (less than 1 km) to the intrusion these have been realigned through the process of lateral inflation. This is thought to have been facilitated partly by the observed mobilisation (see Reynolds, 1934; Meighan and Neeson, 1979; Neeson, 1984) and deformation (i.e., development of a schistosity) in the host rocks, which could have led to narrowing of tracts in the vicinity of the NIC (e.g., Marsh, 1982).

Yet as discussed above the evidence for missing host rocks in the area implies that some of these were additionally removed. It is suggested that combined stoping (and possibly subsequent assimilation), together with laccolithic inflation following cross cutting of the host rocks (fig. 5.18), provide the most likely explanations for this (e.g., Marsh, 1982; Fowler and Paterson, 1997). The former is supported by the presence of sedimentary enclaves within some of the pluton boundary areas, as well as the work of Meighan and Neeson (1979), which showed that initial $^{87}Sr/^{86}Sr$ ratios within the main NIC were slightly higher than might be expected for an exclusively I-type source.

Nevertheless, it is thought that stoping would have represented a relatively minor process in comparison to both sinistral pull-apart opening and inflation of the NIC. This is due to the theoretical problems with the stoping process as a primary emplacement mechanism highlighted by Glazner and Bartley (2006). Furthermore, the relatively low proportions of enclaves within the NIC (~1-3%) have been shown to be insufficient for this process to be volumetrically significant. For example, Glazner and Bartley (2008) suggested that for 30% of accommodation space to have been created by stoping, the resulting pluton would be required to contain ~30-50% magmatic breccia. Due to these limitations it is thought that the particular inferred process of laccolithic inflation may have dominantly contributed to the observed cross cutting (see section 5.7.1).

The satellite bodies also appear to show obvious local-scale cross-cutting of the host rocks. This is due to the areas where the inferred trend of these is clearly significantly oblique to the predicted tract boundaries (see fig. 5.17). This is

supported by the available field evidence, although this also reveals some local variation in the boundaries of the satellite bodies.

A final observation that has been made regarding the NIC boundary is that in some cases fabrics appear to parallel local contact variations, whereas in others these show more of a general concentric trend. The former is most clearly observed within the Knockiveagh Hill site. Changes in contact orientation here occur over a relatively wide area and so it is interpreted that the scale of this variation is influential in determining whether fabrics will parallel the contacts. This may attest to the operation of magma pressures that are sufficient to compress intruded material against the wall rocks, rather than simply producing a concentric alignment (e.g., Hutton, 1988; Paterson and Vernon, 1995).

5.7.4 Evidence for magma flow

The majority of relatively strong planar AMS fabrics are shown to be concentric, as well as relating to parallel, shallow-dipping, relatively strong linear AMS fabrics. These have been interpreted above to represent largely magmatic alignments, produced by inflation from a central source. Even some relatively weak planar AMS fabrics show the same relationship, suggesting that little magma pressure is required to cause these alignments. This interpretation supports the work of Paterson et. al. (1998, p. 53) in that although such fabrics do not represent the “final increment” of strain, they appear to have overprinted any evidence of magmatic processes prior to inflation.

However, in rarer cases predominantly linear AMS fabrics occur that are oblique to the general trend, either in terms of their azimuth or plunge. This is frequently observed at the edges of plutons, in particular the northeast Rathfriland pluton, where these fabrics have been shown to be consistently steeply plunging and often obliquely trending. The anomalous nature of the fabrics here is proposed to reflect an earlier phase of fabric development. This may have been preserved due to the faster cooling of the magma against relatively cold host rock at pluton boundaries, which would have prevented the development of a significant inflation-related fabric (e.g., McBirney, 2007) (see fig. 5.17).

Magma flow is considered to represent the best explanation for the earlier fabric-development phase (e.g., Stevenson et. al., 2007a). From the AMS data alone, shear would be an equally plausible cause, although field evidence for this occurring in the observed predominantly steep orientation is lacking (Neeson, 1984; Hurley, pers. comm., 2010). Hence, on the basis that the anomalous linear fabrics do reflect magma flow, it is inferred that this flow occurred steeply within the areas in question. This supports the idea that ascent of magma supplying the NIC was controlled by the intersections of an upper crustal shear zone with two deep-seated lineaments directly beneath the emplacement site (see above).

The sheeted Cloghoge pluton margin and the outer boundary of the central Newry pluton hornblende granodiorite also show a number of fabrics that have strong linear components and are oblique to the typical inflation-related trends described earlier. It is suggested that these magmas also cooled quickly, due to their intrusion alongside

older, more crystallised facies. Hence the observed fabrics may again represent an earlier phase of magma flow.

However, it has been demonstrated that AMS fabrics within sheets can be complex, with K_1 often being oblique to the direction of magma flow (e.g., Callot et. al., 2001; Aubourg et. al., 2002; Geoffroy et. al., 2002). Therefore, although the fabrics within the sheeted Cloghoge pluton margin may represent magma flow, it is beyond the scope of the current study to resolve the orientation of this. The AMS fabrics from the outer part of the Newry pluton hornblende granodiorite are in turn very variable. Some of these are steep although others show plunges that are typical of the other material throughout the pluton. Hence, no confident deductions of magma flow can be made from either of the locations.

5.7.5 The obliquity of weak fabrics

Low AMS fabric strength (H) within the NIC has been shown to frequently correspond to low bulk magnetic susceptibility (K_{mean}) values. This is demonstrated within the Cloghoge pluton 'core', the southwest Newry pluton and the southern satellite bodies. AMS fabrics within these areas have also been shown to be frequently obliquely orientated in relation to visible fabrics. These results have been interpreted to suggest that for the NIC AMS samples with low K_{mean} values are unreliable as visible fabric indicators. Hence AMS data from the areas in question has been disregarded during consideration of emplacement.

Fig 5.1: Mineral foliation measurements from the main NIC and satellite bodies

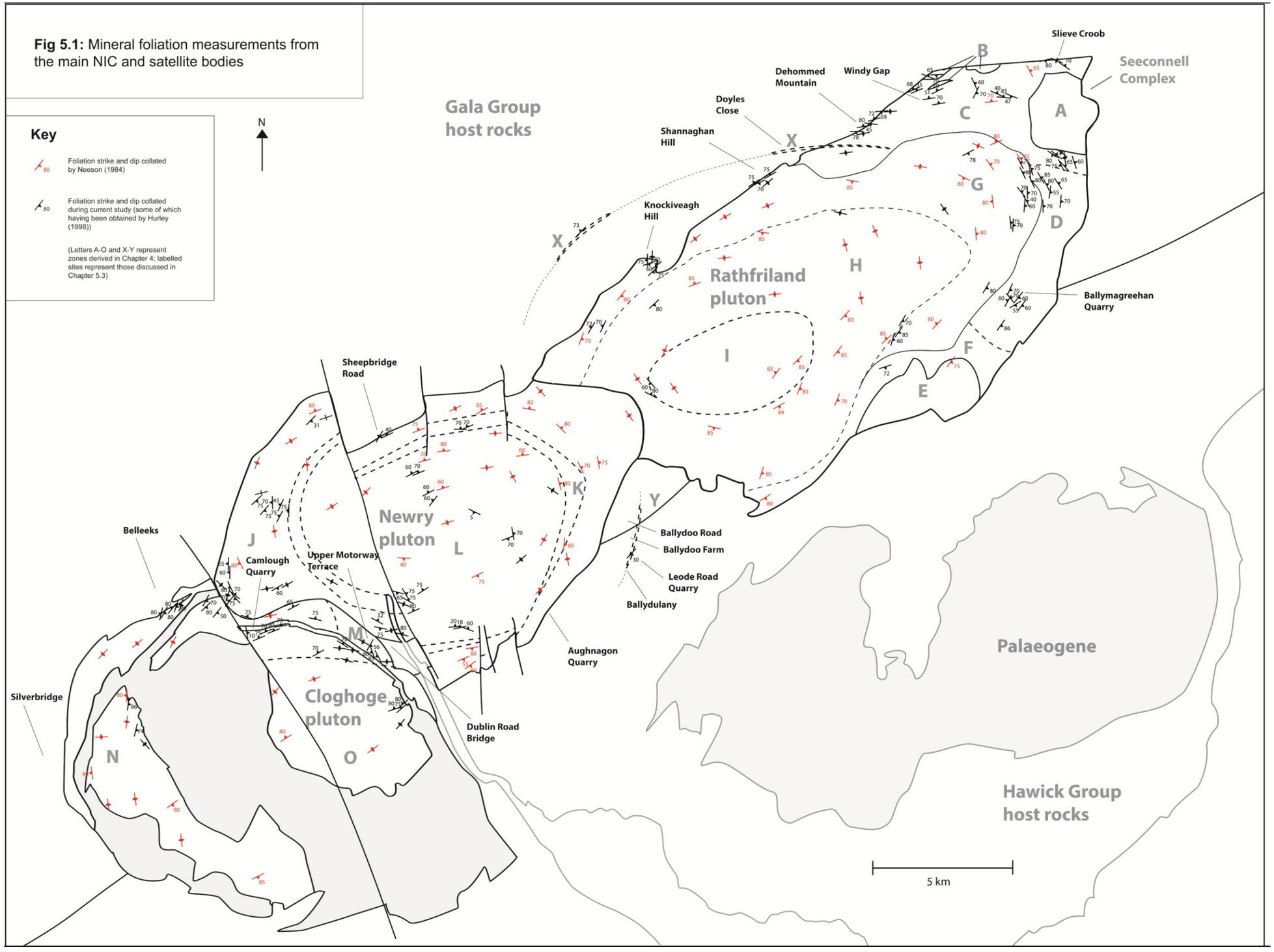

Fig 5.2: Host rock bedding and cleavage measurements in the vicinity of the NIC

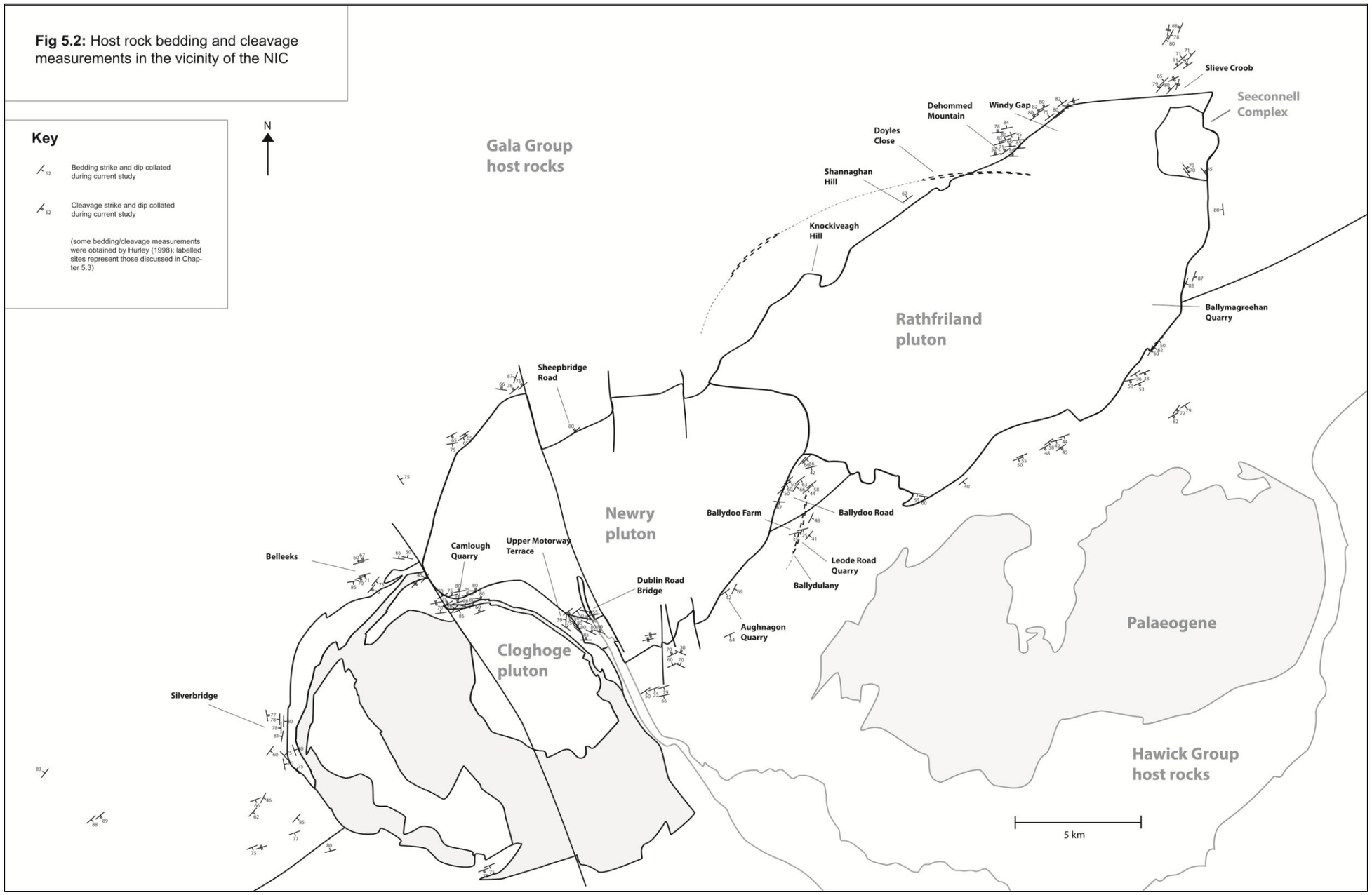

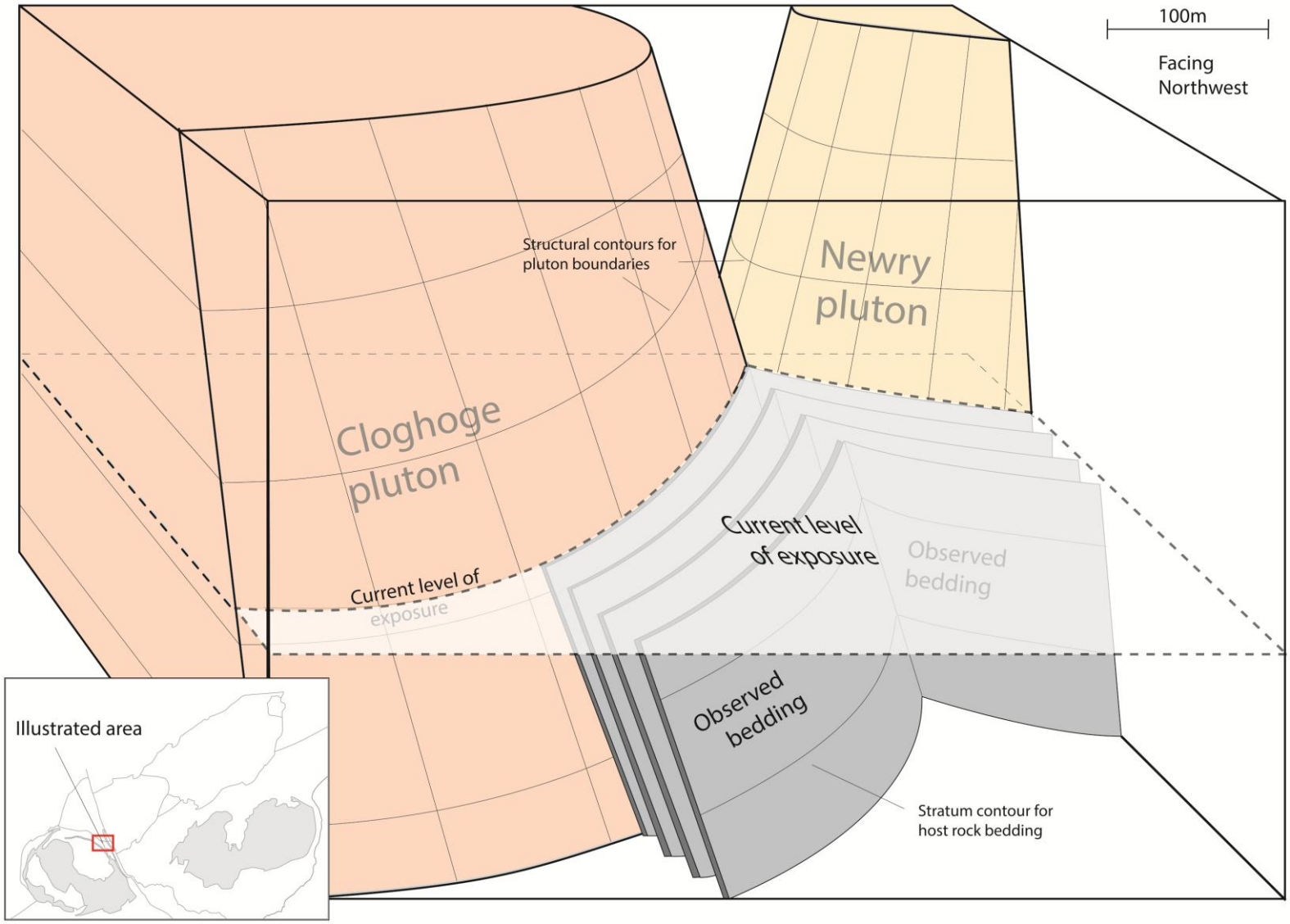

Fig 5.3: Illustration of the relationship between host rocks and the outer contacts of the Newry and Cloghoge pluton at the ***Dublin Road Bridge*** site

Photo 5.1 (left): Unmobilised sediment at ***Clade Quarry***, adjacent to the eastern Cloghoge pluton

Photo 5.2 (below): Ductile deformation at ***Belleeks***, adjacent to the northern margin of the Cloghoge pluton

Photo 5.3 (above): Intrusion into mobilised sediment at ***Camlough Quarry***

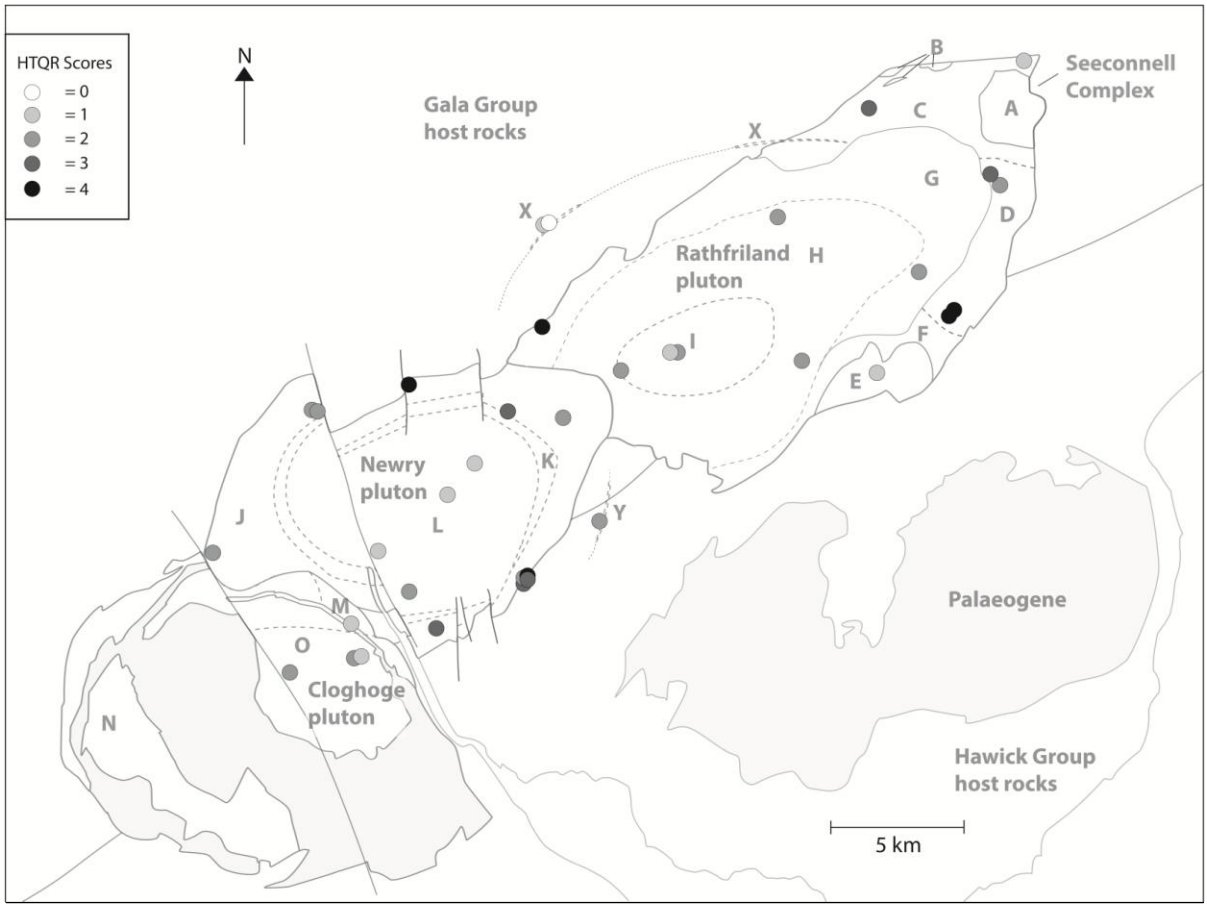

Fig 5.4: Assessment of the extent of quartz recrystallisation throughout the NIC and satellite bodies, through HTQR (High Temperature Quartz Recrystallisation) Scores

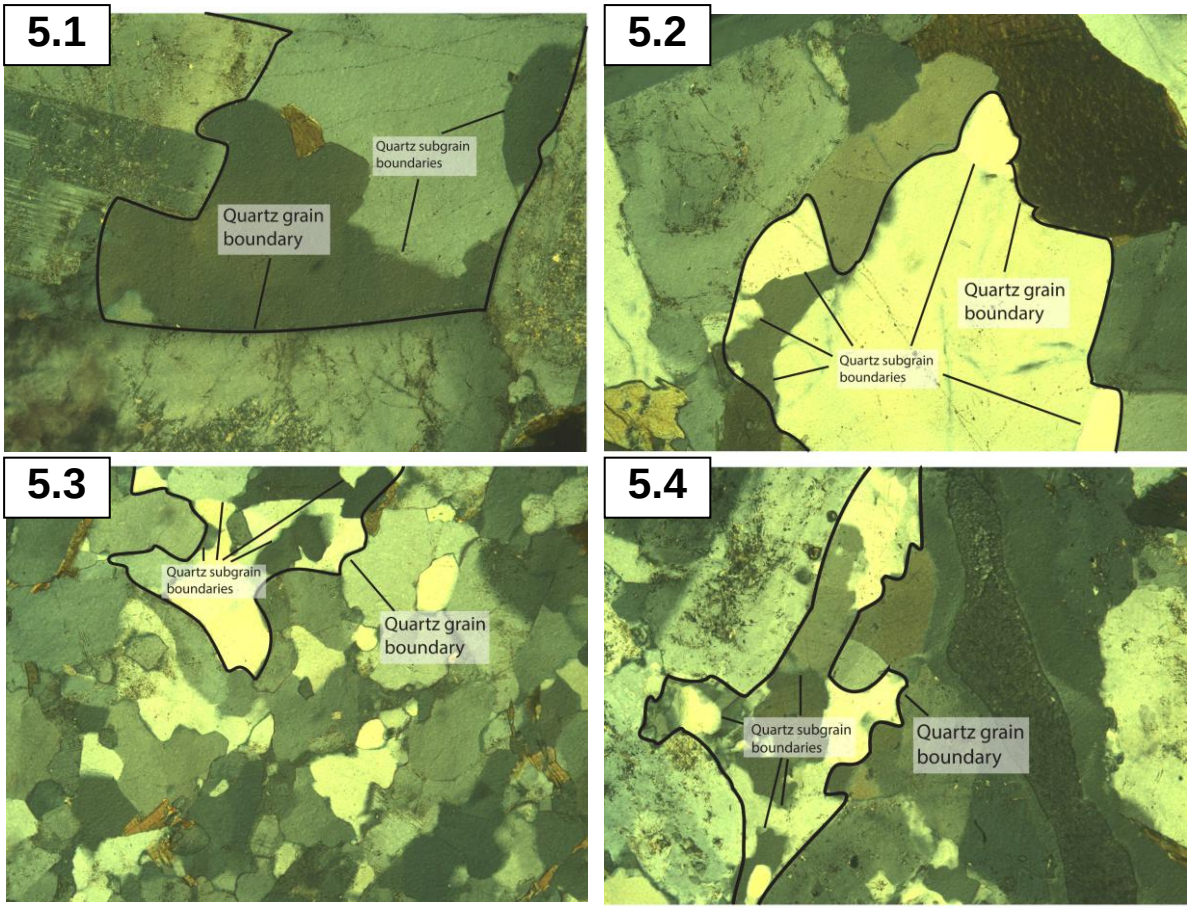

Photos 5.1-5.4: Examples of quartz recrystallisation for which differing HTQR scores have been derived in the current study: **5.1)** HTQR score = 1 (sample MRC369); **5.2)** HTQR score = 2 (sample mrc366); **5.3)** HTQR score = 3 (sample mrc63); **5.4)** HTQR score = 4 (sample mrc365) (see appendix 1 for sample locations)

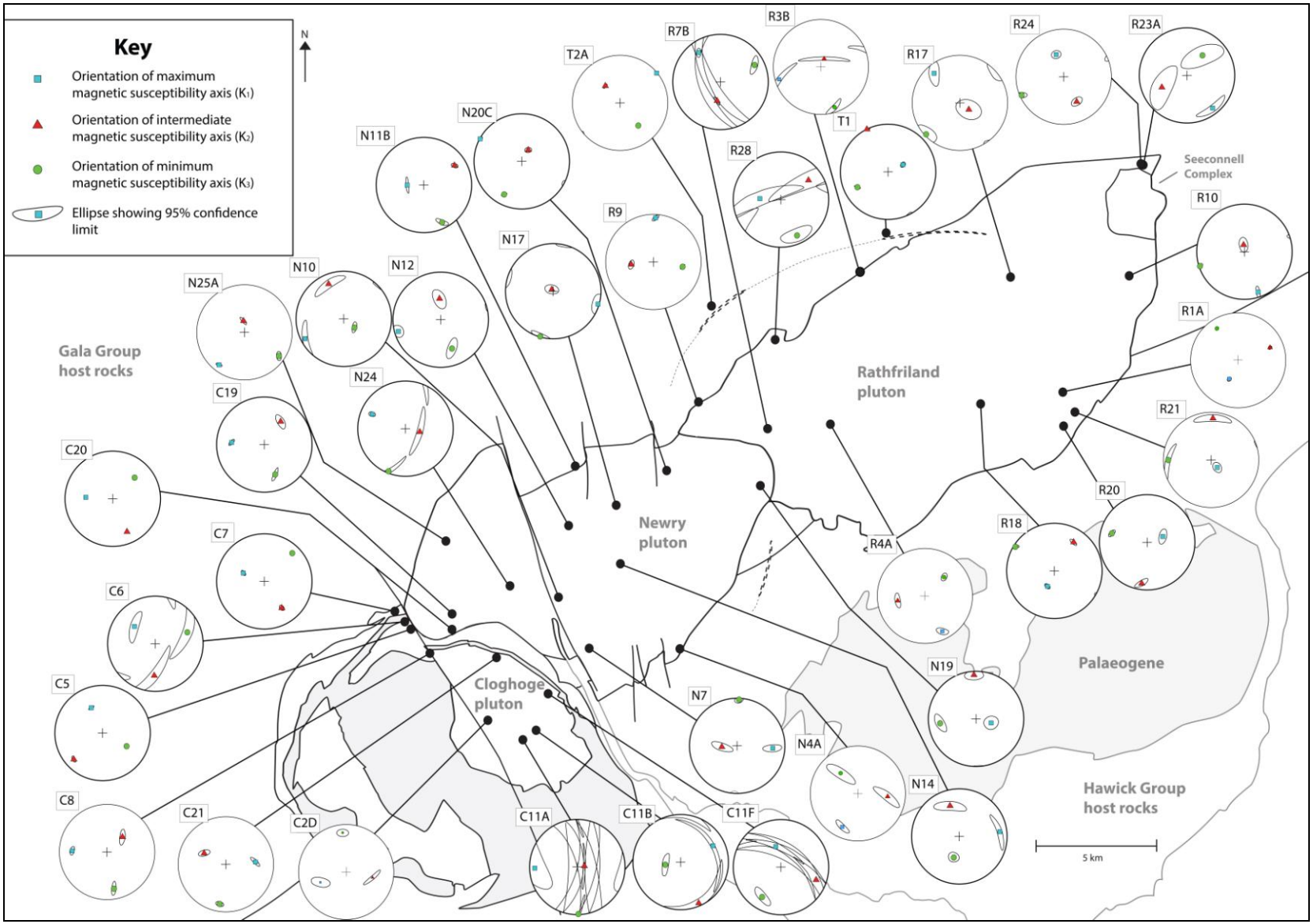

Fig 5.5: A selection of AMS results from the main NIC and satellite bodies (see fig 5.11 for deduced fabrics)

Fig 5.6: Derived AMS fabrics throughout the main NIC and satellite bodies

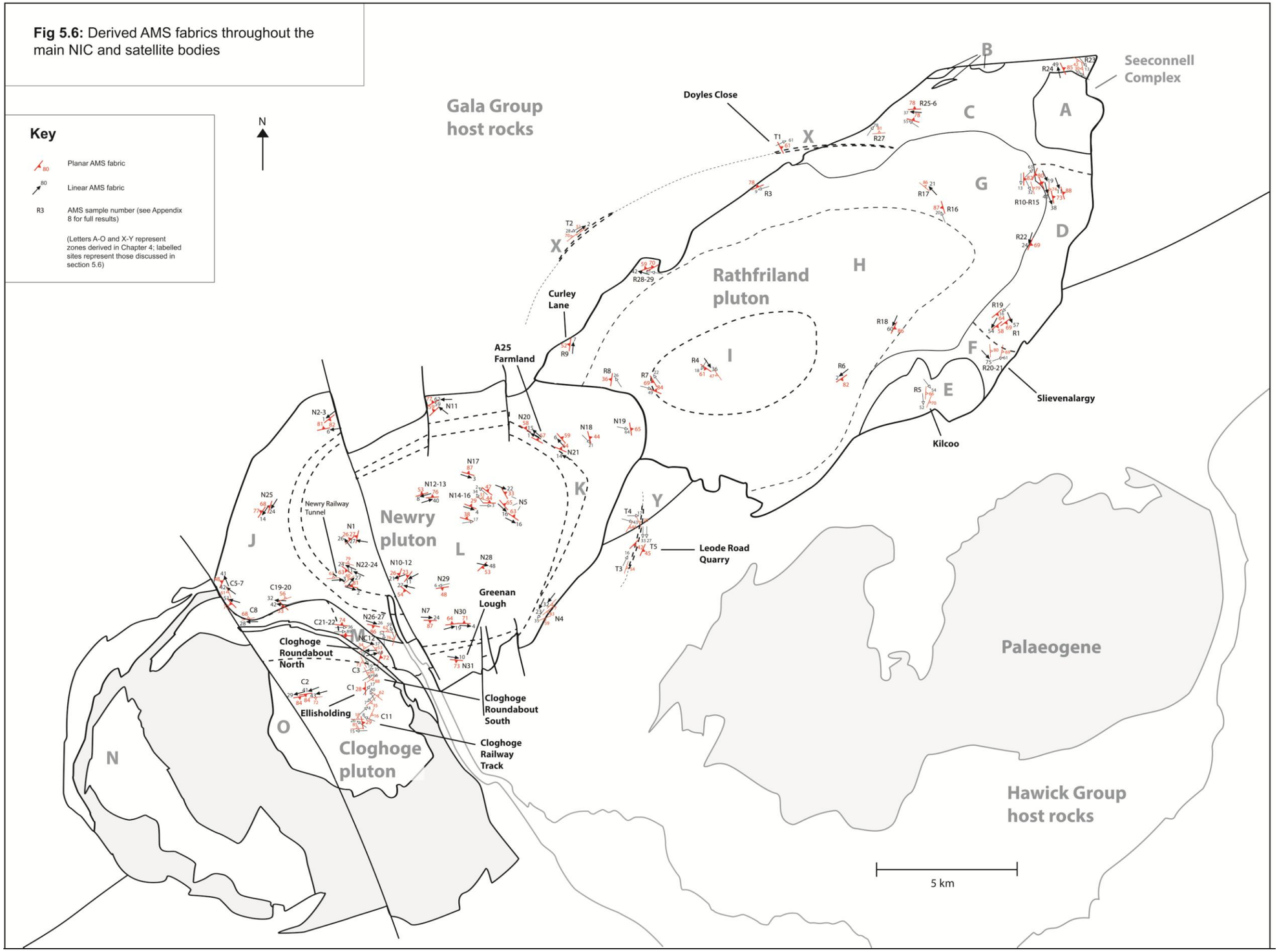

Fig 5.7: Overall fabric strength (H) throughout the main NIC and satellite bodies

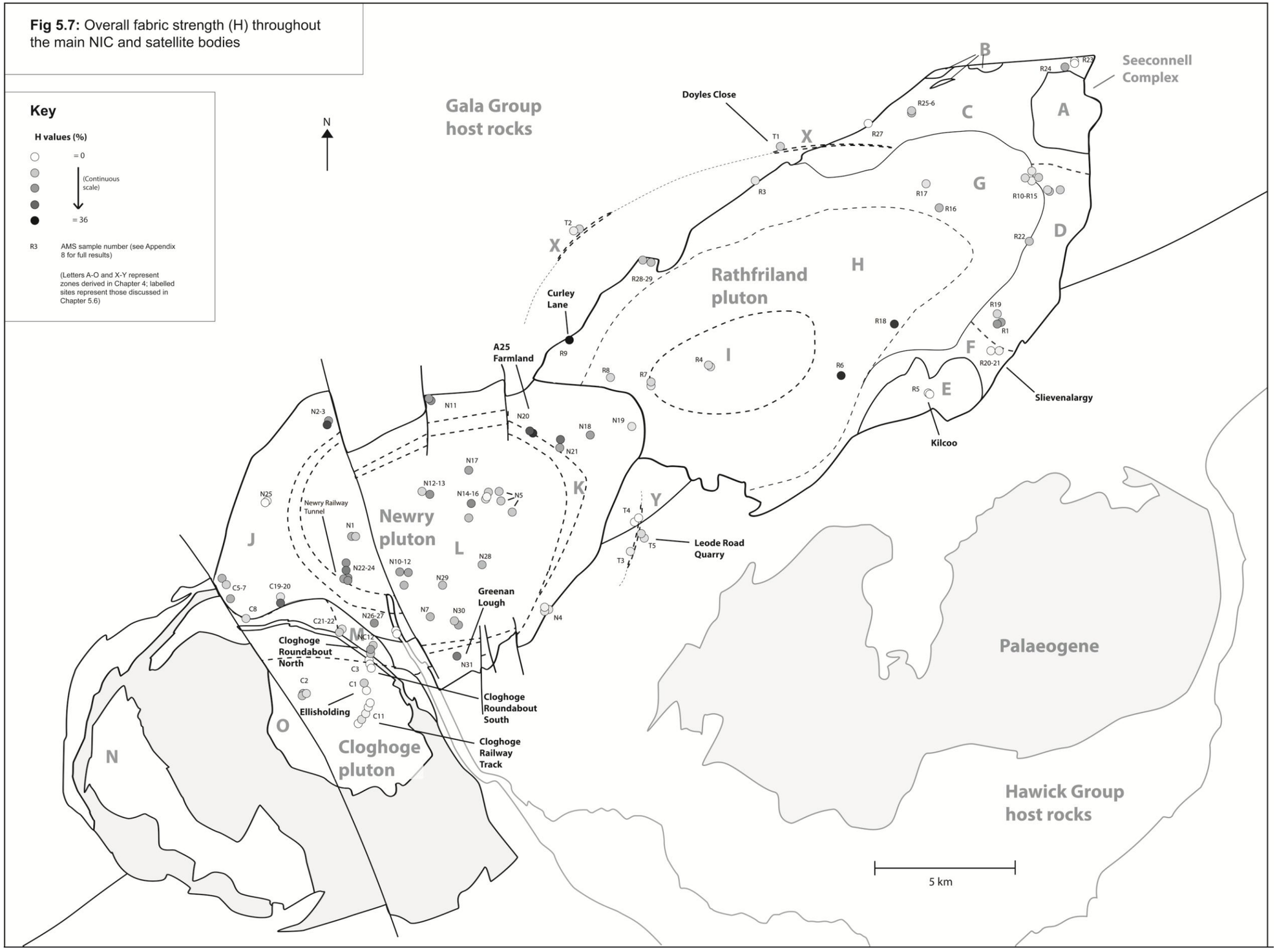

Fig 5.8: Planar fabric strength (F) throughout the main NIC and satellite bodies

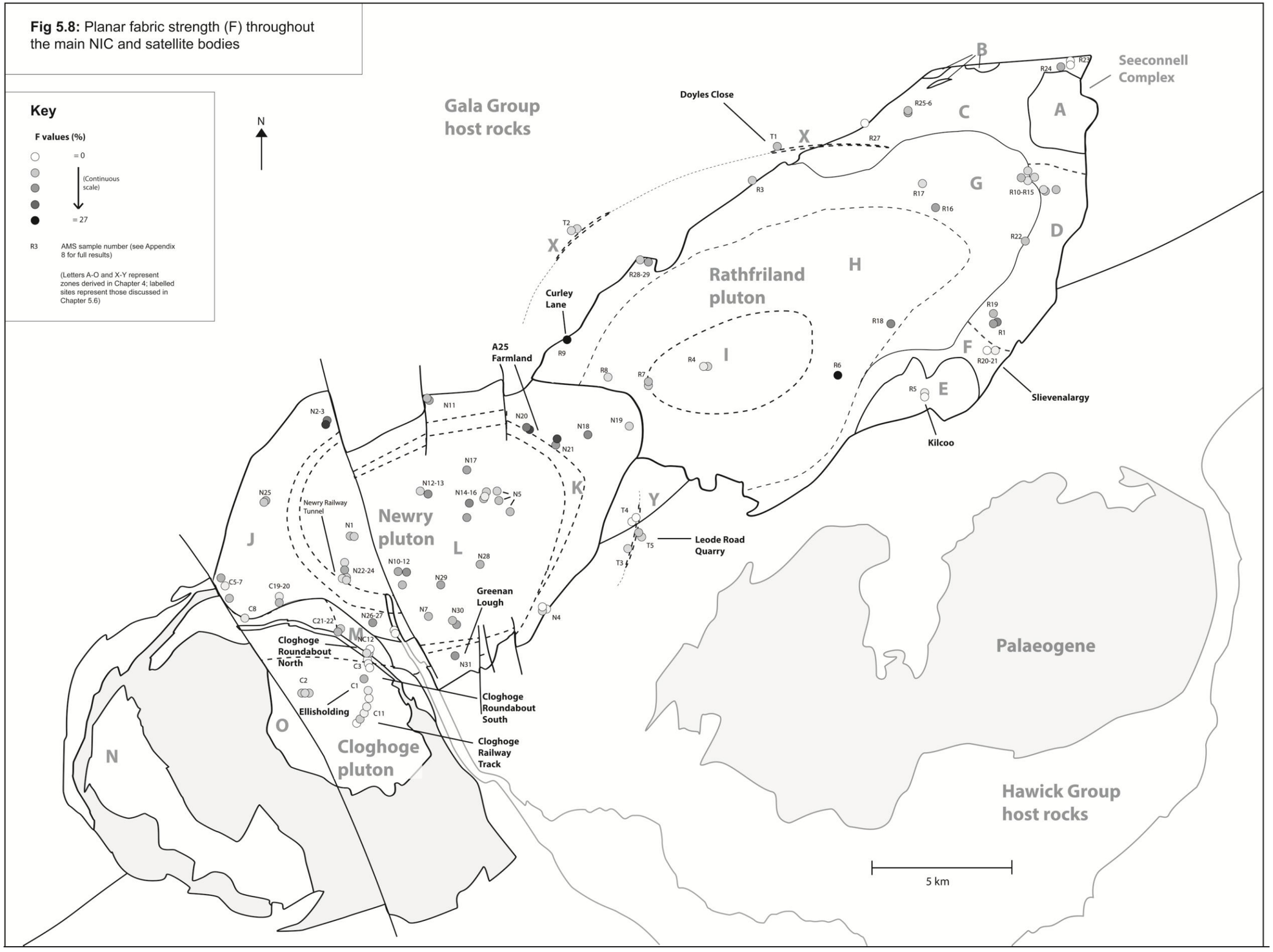

Fig 5.9: Linear fabric strength (L) throughout the main NIC and satellite bodies

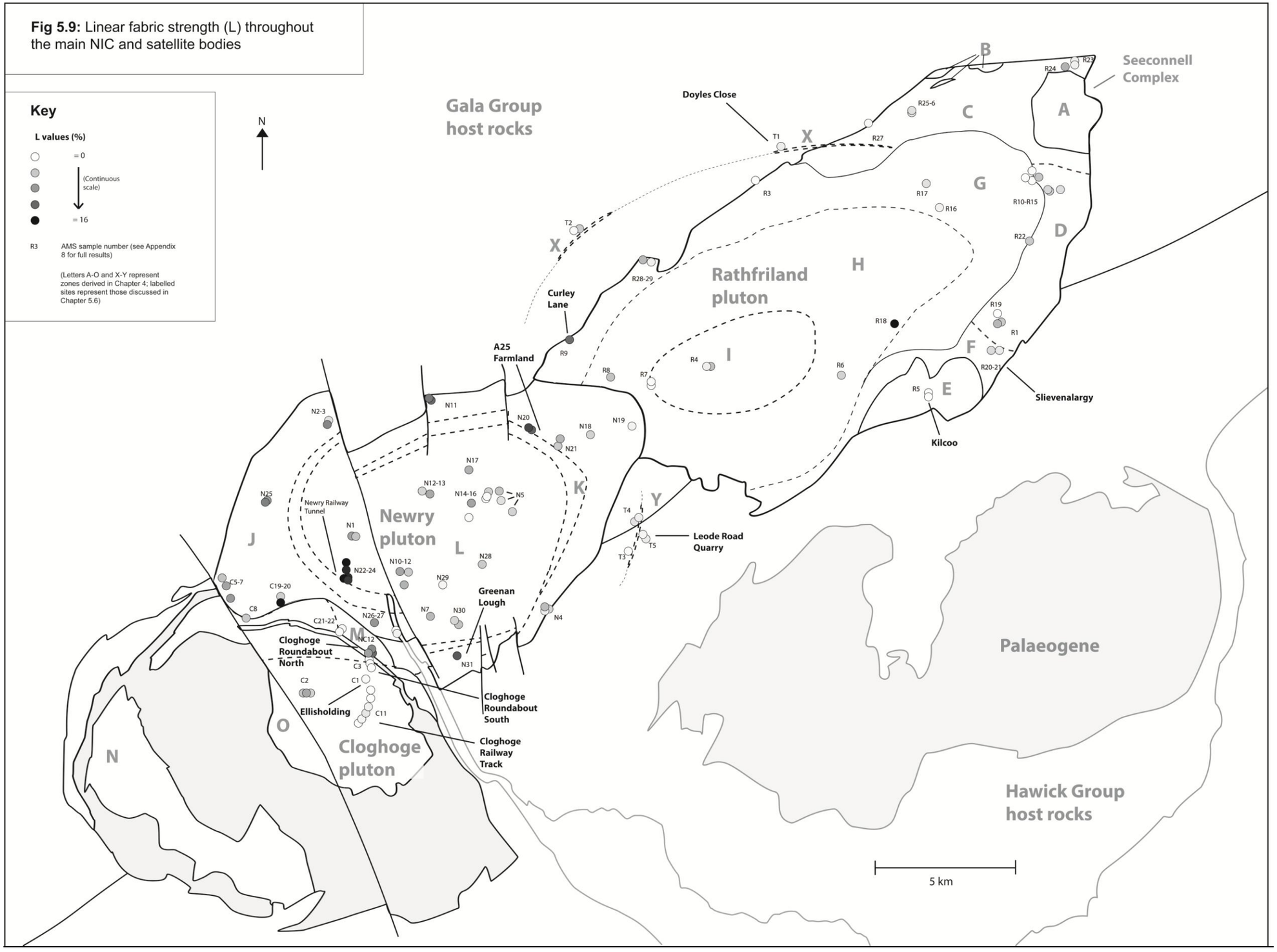

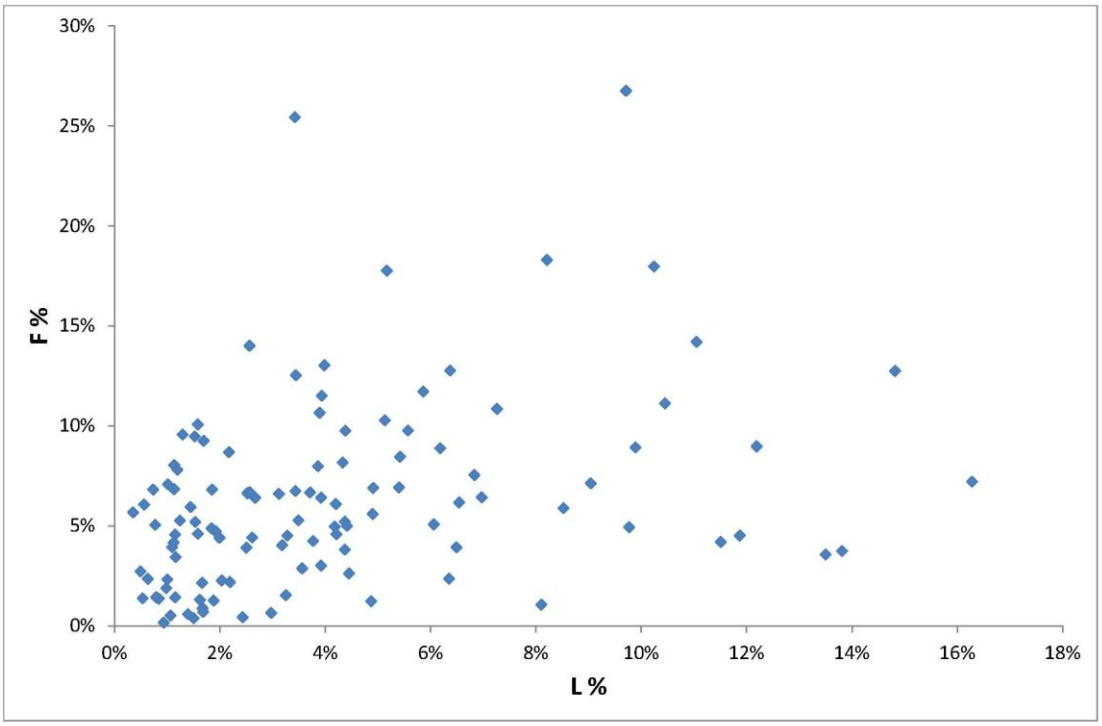

Fig 5.10 (above): Plot of linear fabric versus planar fabric strength (L vs F)

Fig 5.11 (below): Plot of bulk magnetic susceptibility (Kmean) versus overall fabric strength (H)

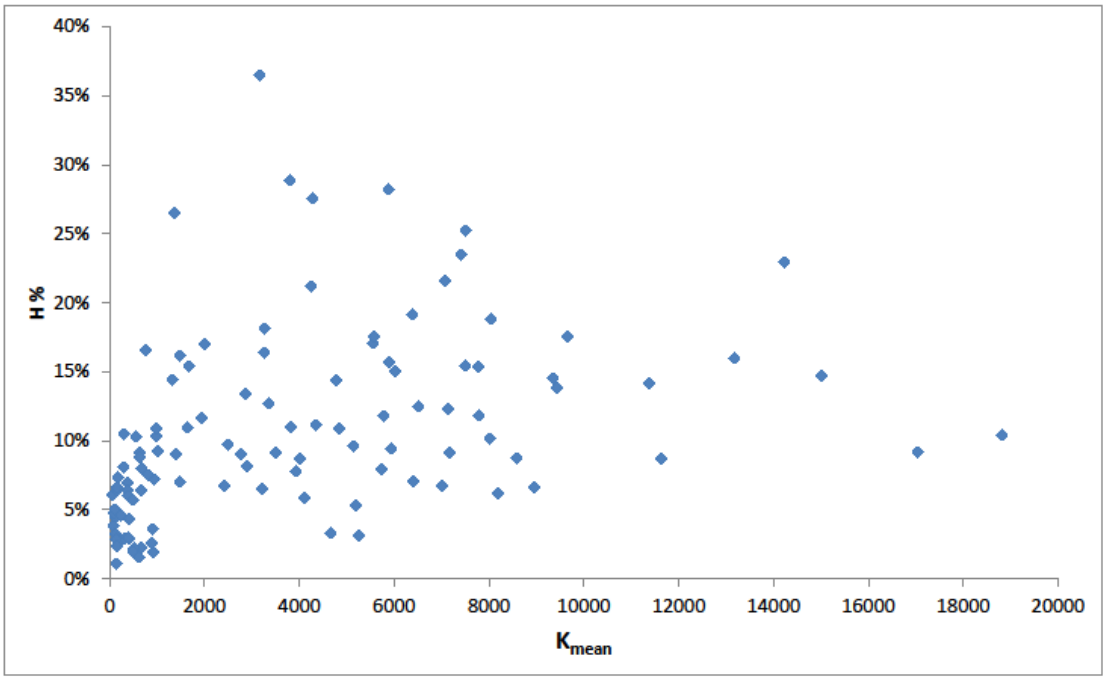

Fig 5.12: Values of bulk magnetic susceptibility (K_{mean}) throughout the main NIC and satellite bodies

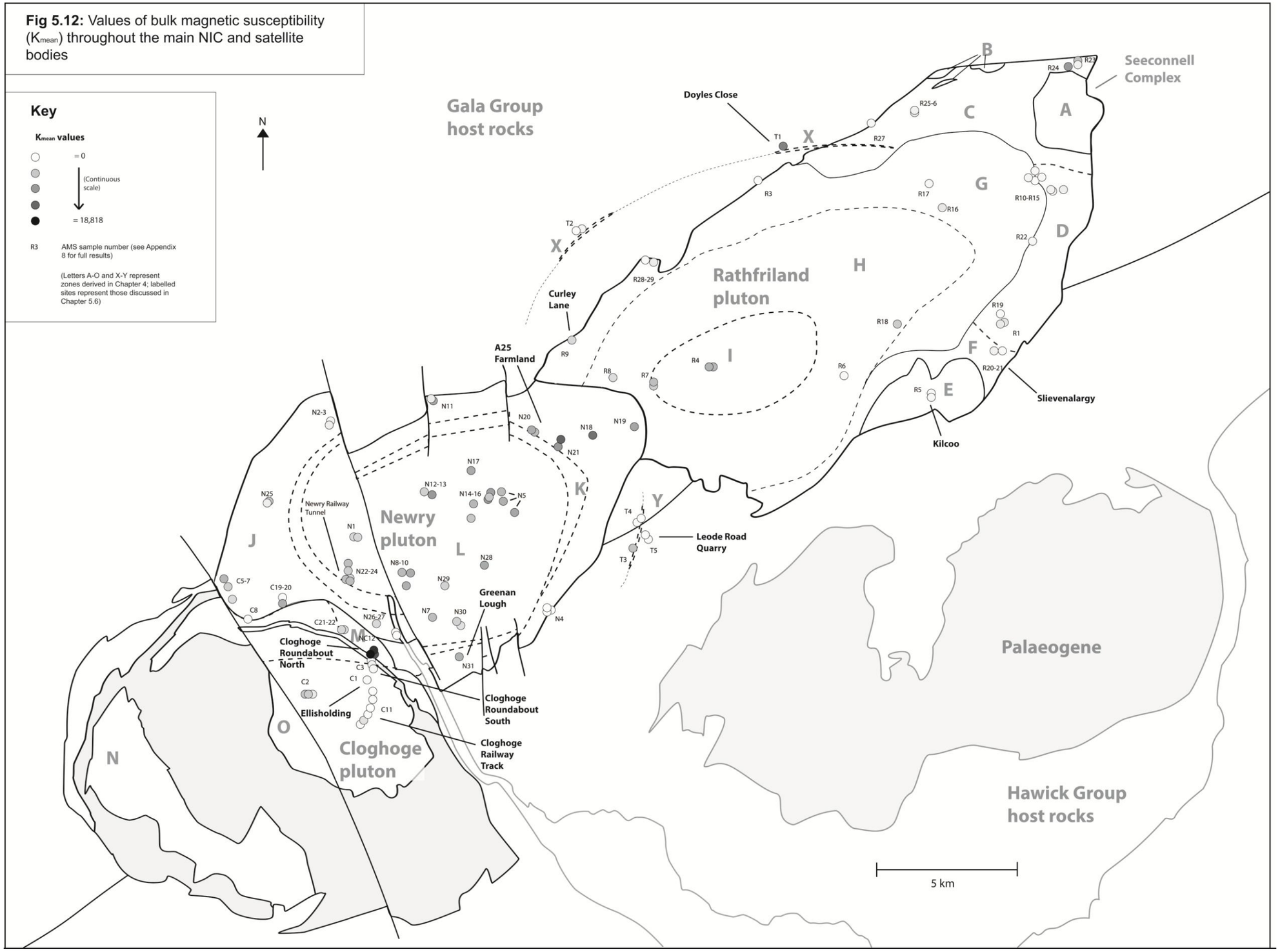

Fig 5.13: Comparison of mineral foliation and planar AMS fabric data throughout the main NIC and satellite bodies

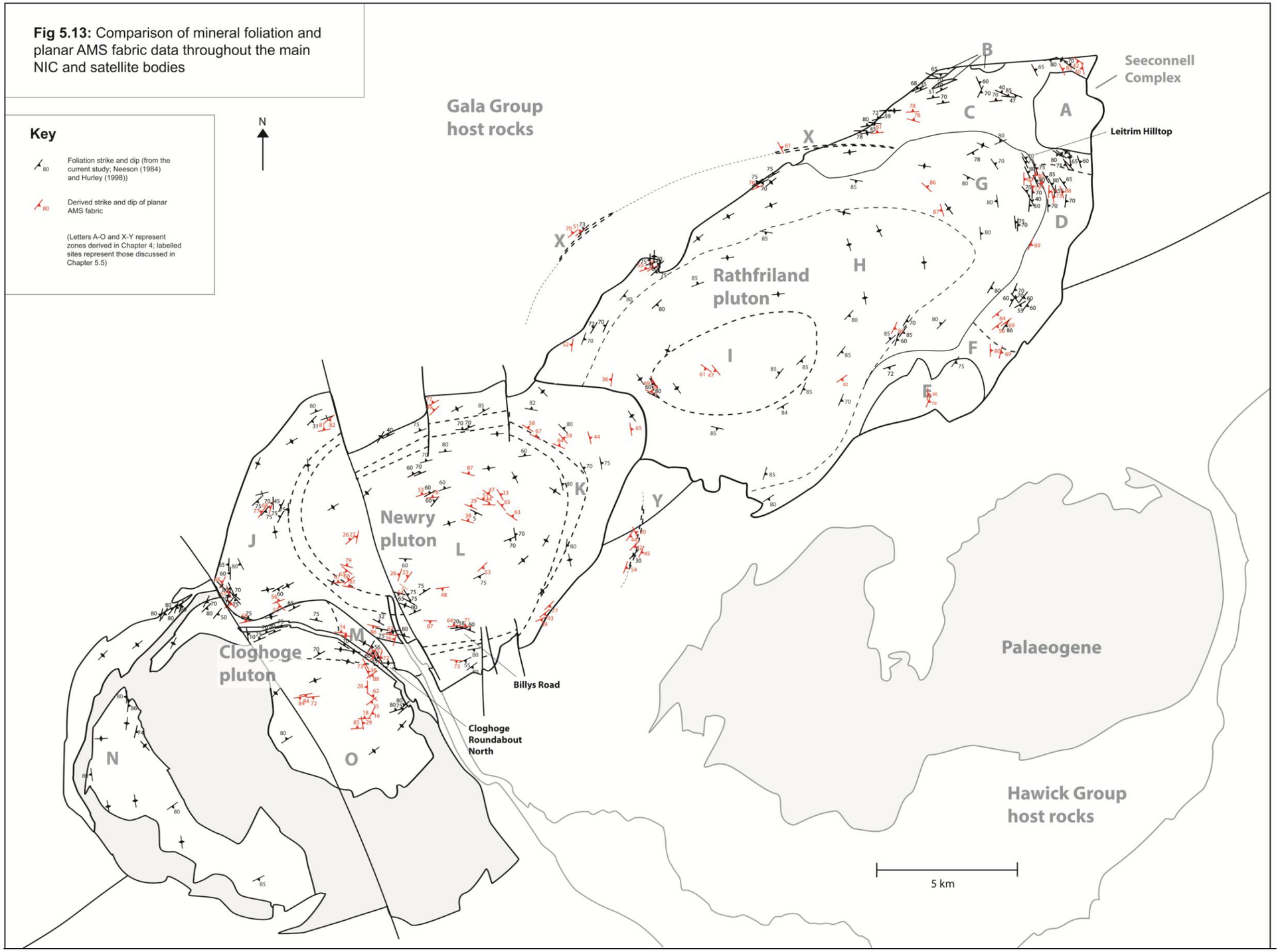

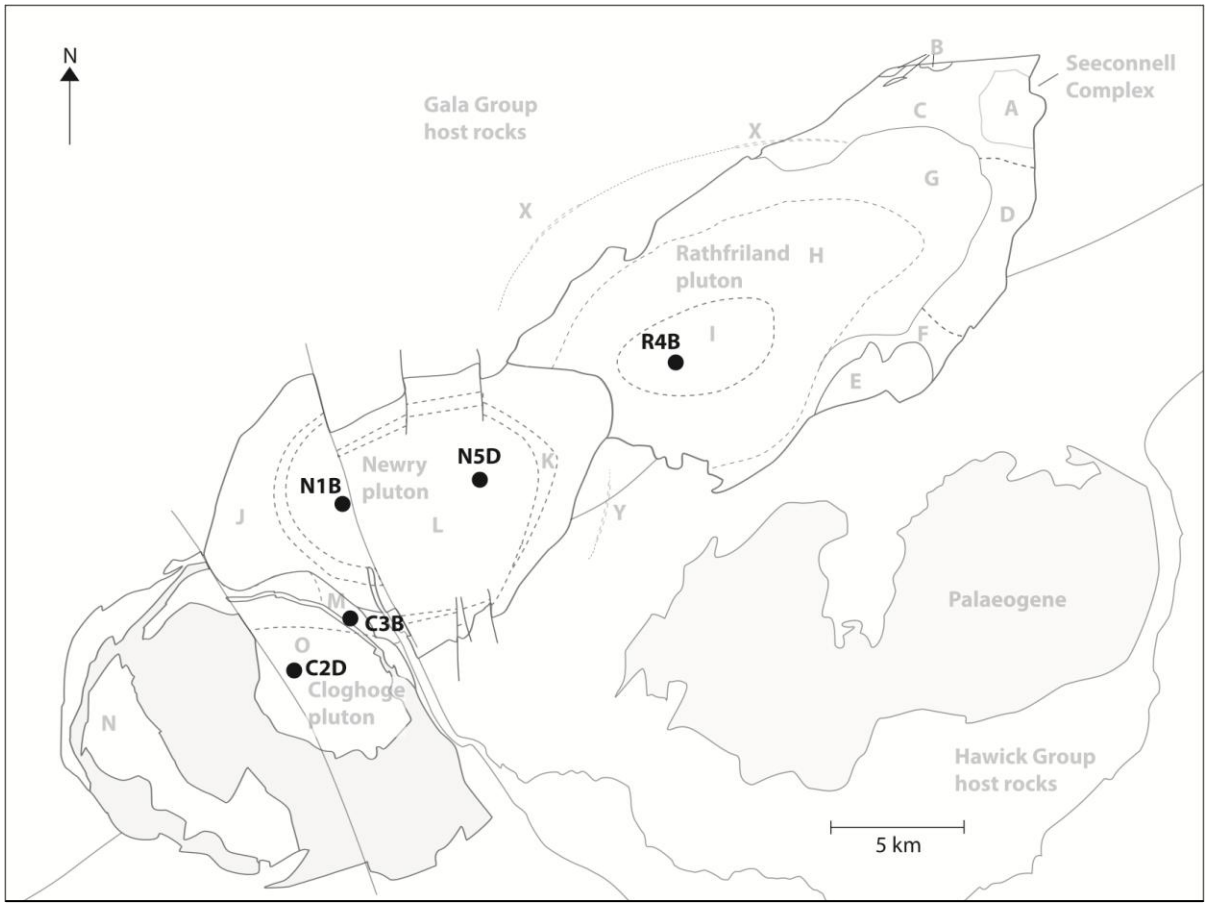

Fig 5.14: Locations of samples for which thermomagnetic analysis results were obtained

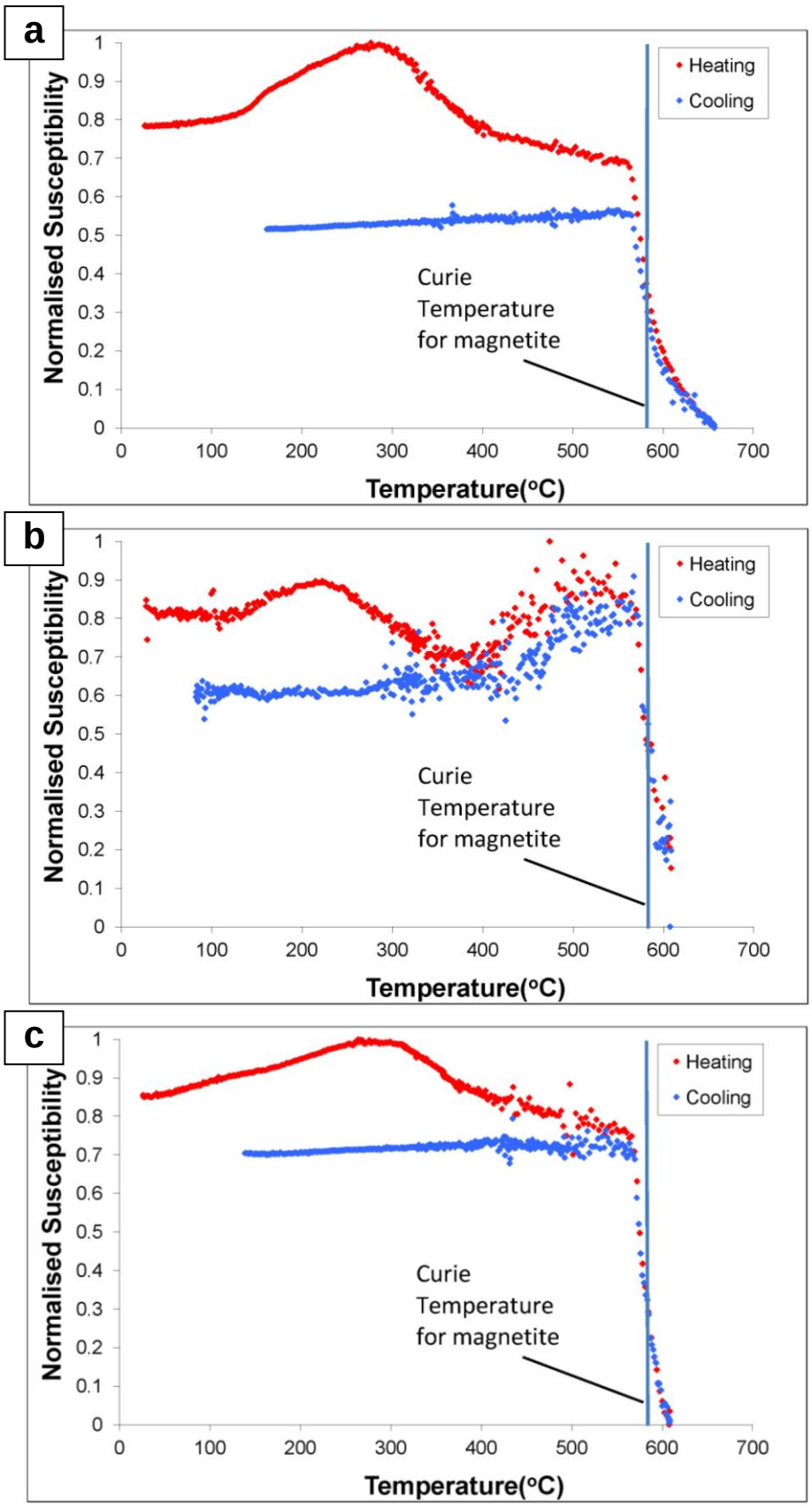

Fig 5.15: Variation of normalised magnetic susceptibility during heating and subsequent cooling: **a:** C2D **b:** C3B **c:** N1B

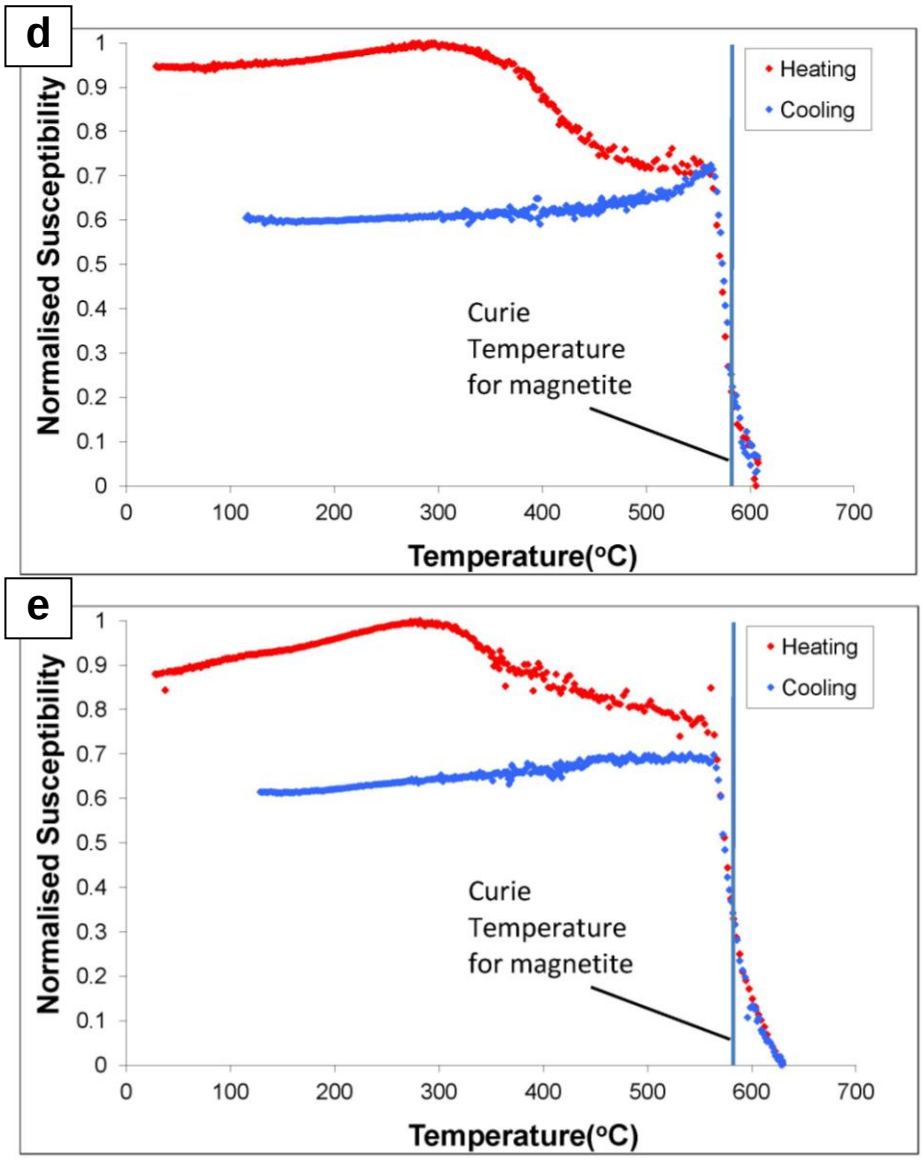

Fig 5.15 (continued): Variation of normalised magnetic susceptibility during heating and subsequent cooling: **d:** N5D **e:** R4B

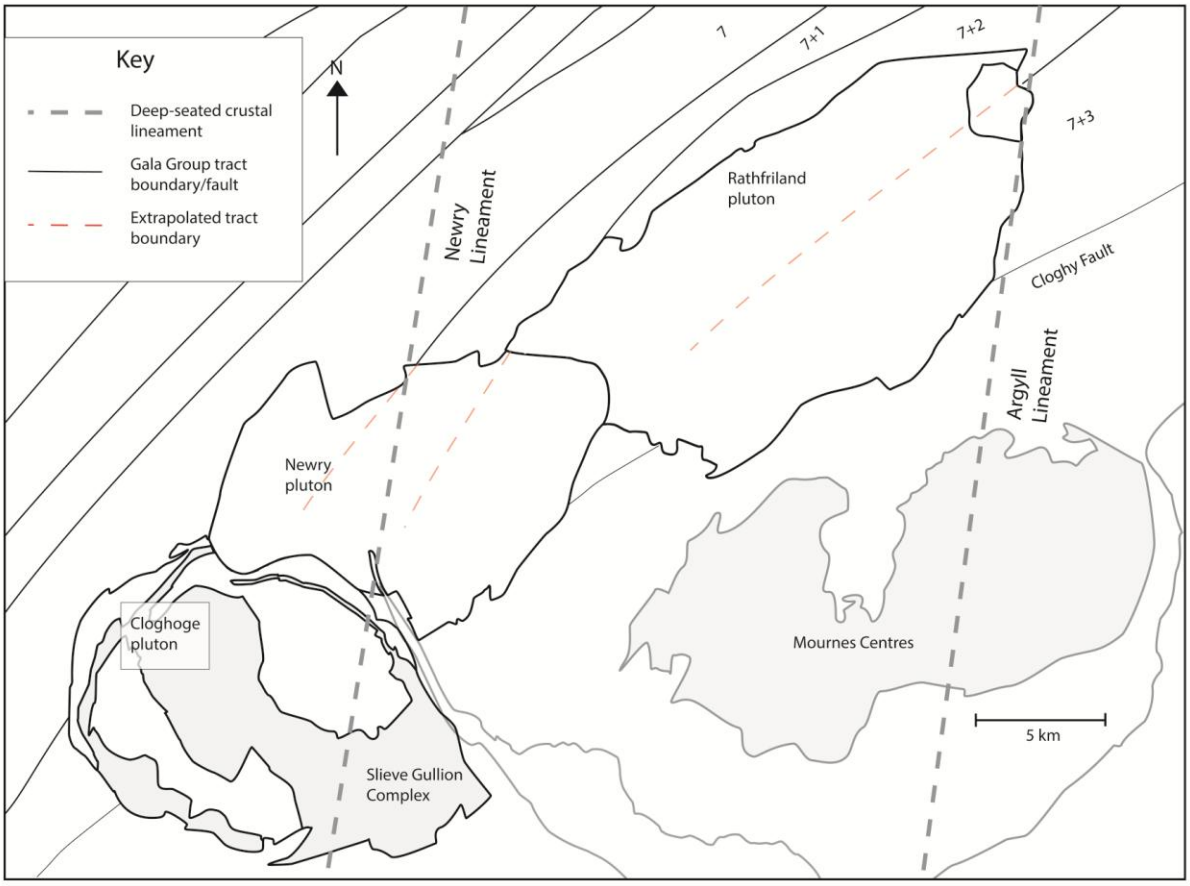

Fig 5.16: Map showing Gala Group tract boundaries and deep-seated crustal lineaments in the vicinity of the NIC (modified from Beamish et. al., 2010; tract boundaries from Cooper et. al., 2013)

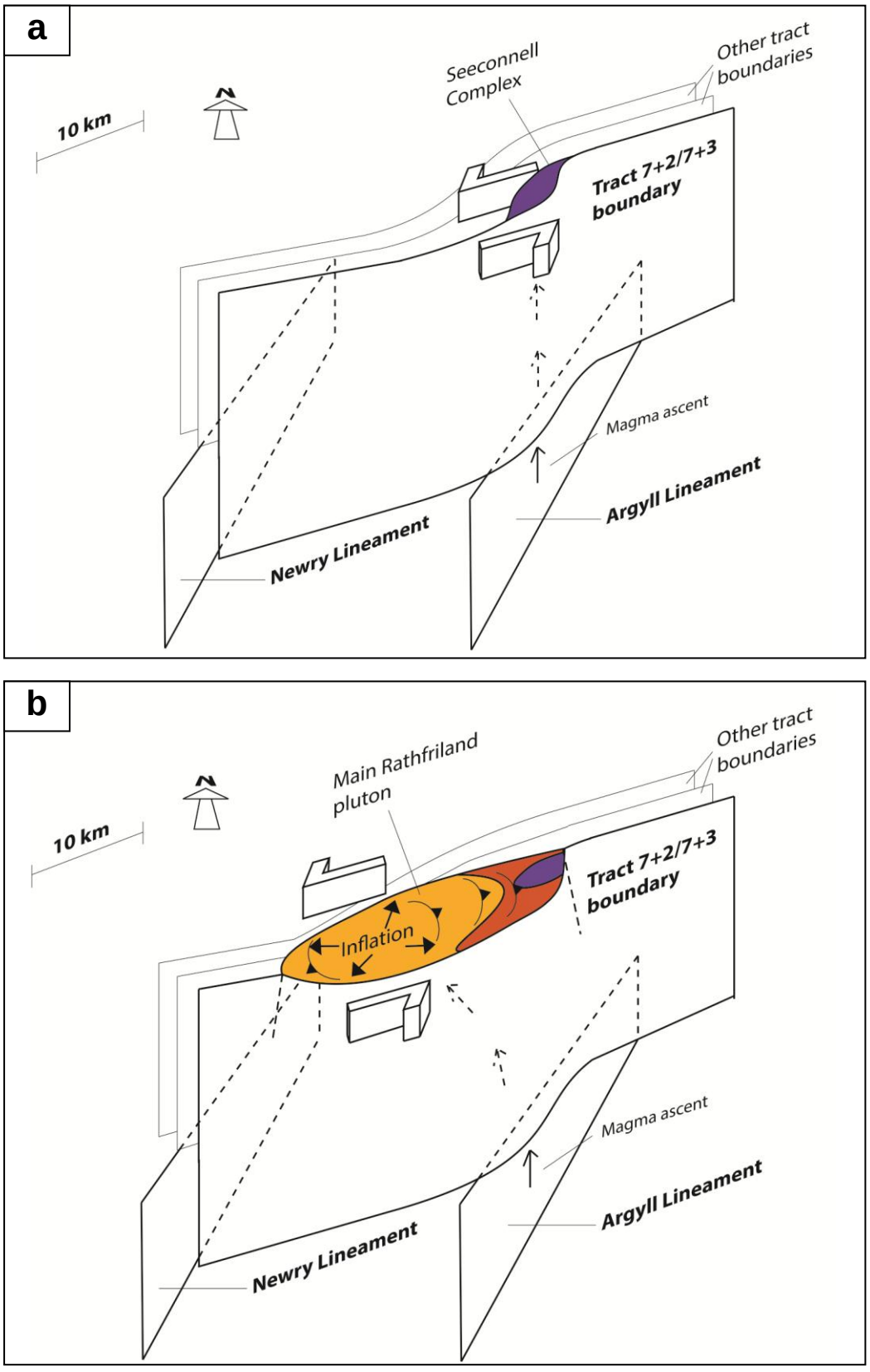

Fig 5.17: Intrusion history of the NIC, showing influence of deep-seated lineaments and tract-bounding faults: **a)** (upper) Seeconnell Complex (Ca. 414 Ma); **b)** (lower) Main Rathfriland pluton (Ca. 413-412 Ma) (deduced from findings of current study)

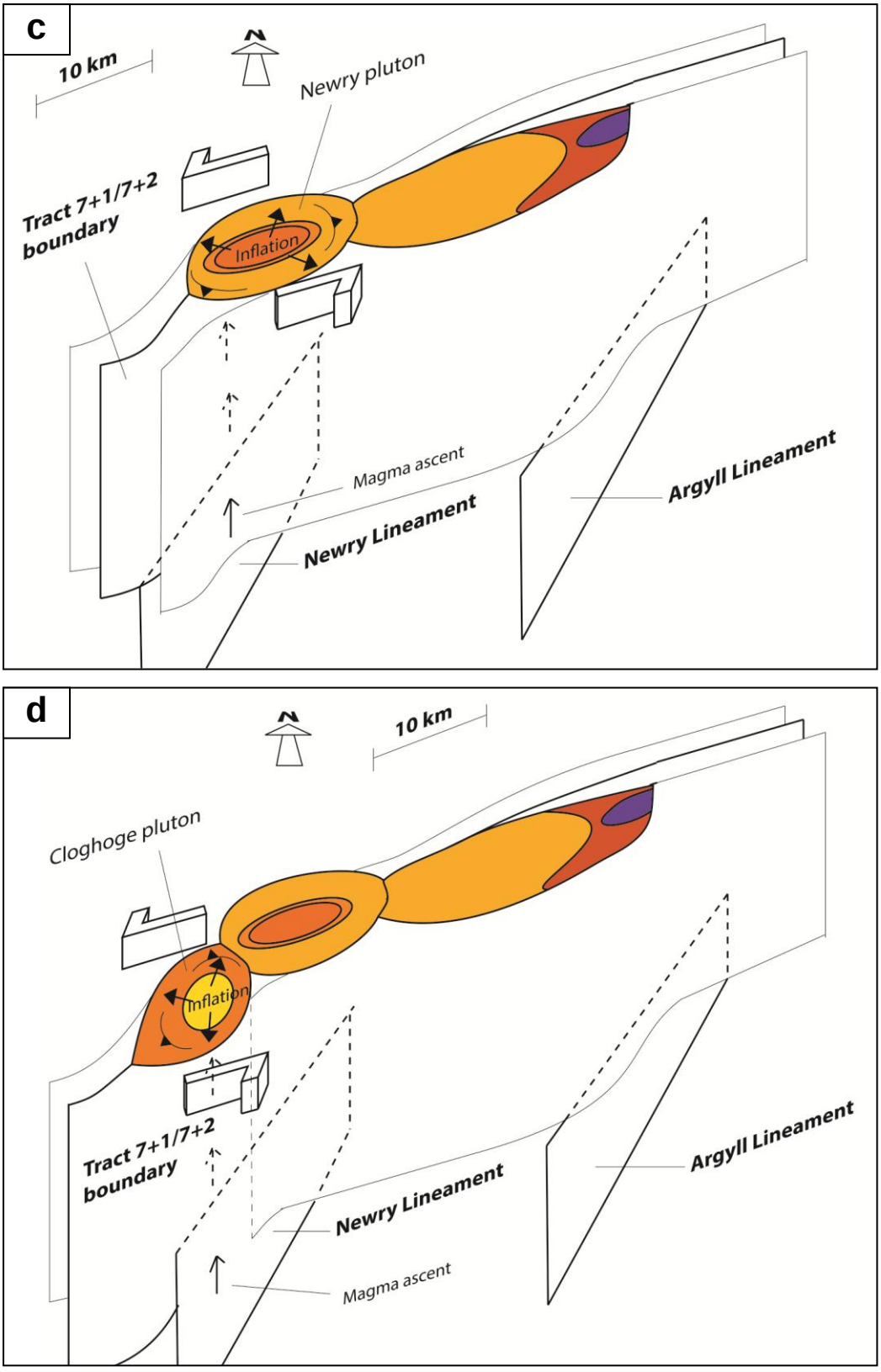

Fig 5.17 (continued): Intrusion history of the NIC, showing influence of deep-seated lineaments and tract-bounding faults: **a)** (upper) Newry pluton (Ca. 411-410 Ma); **b)** (lower) Cloghoge pluton (Ca. 410-407 Ma) (deduced from findings of current study)

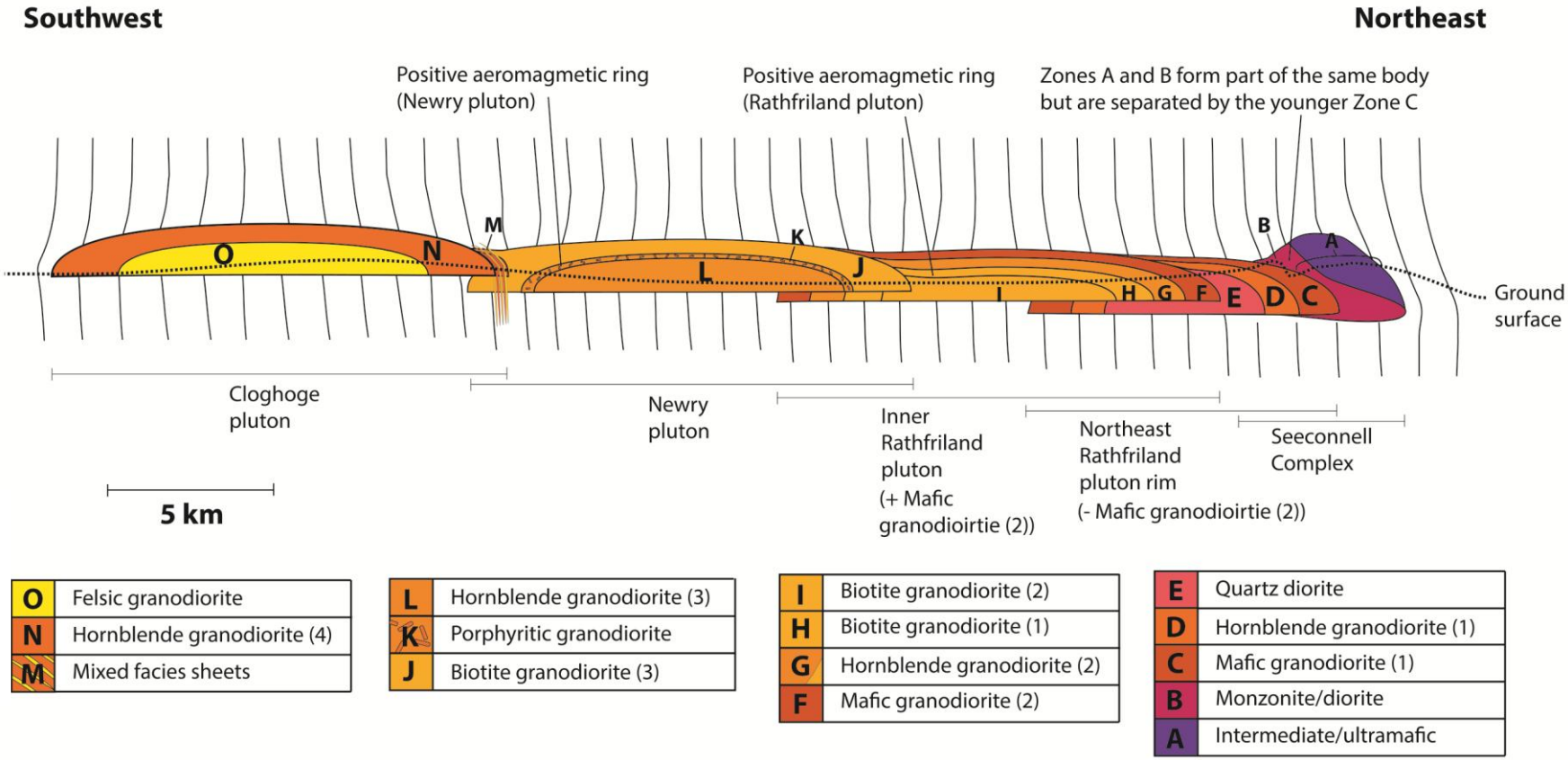

Fig 5.18: Laccolithic stacking of the NIC, illustrating successively higher crustal levels of emplacement

CHAPTER 6: CONCLUSIONS AND FUTURE WORK

6.1 Summary of new zonation

Results from Tellus geophysics, petrology, geochemistry and U-Pb geochronology help to determine a number of distinct zones within the Newry Igneous Complex (NIC). Several of these have been recognised in previous work (i.e., Egan, 1973; Reynolds, 1934; Reynolds, 1943; Meighan and Neeson, 1979; Neeson, 1984; GSNI, 1997). The zones comprise the intermediate-ultramafic Seeconnell Complex; the intermediate bodies within the main Rathfriland pluton; the discrete facies within much of the Newry and Cloghoge plutons and the satellite bodies.

The current study provides refinement and further characterisation for these zones. This has largely been aided by Tellus Survey aeromagnetic data, which reveals anomalies relating to several previously mapped facies. However, these anomalies do not precisely correspond to surface extents of the facies, as has been shown for other intrusions (Spector and Grant, 1970; Gunn et. al., 1997; Schetselaar et. al., 2000). It is inferred that deviations within the NIC predominantly result from the outward dip of the constituent units. Exception exists in the Cloghoge pluton, within which the consistently strong positive aeromagnetic signature is interpreted to reflect underlying material from the Palaegene Slieve Gullion Complex. Tellus Survey radiometric data provides further characterisation of parts of the NIC, including more accurate distinction of the Cloghoge pluton.

A number of zones identified from the current data have not previously been recognised as discrete divisions of the NIC. These are as follows:

1. Two geochemically-determined areas of *mafic granodiorite* within the outer Rathfriland pluton.
2. A significant compositional boundary between the northeast margin and inner part of the Rathfriland pluton, revealed by geochemistry and radiometric data
3. Three aeromagnetic divisions within the central Rathfriland pluton, including a prominent ring-shaped anomaly. These variations have been shown to be independent of composition.
4. An extensively sheeted marginal area of the Cloghoge pluton, within which individual sheets appear to show characteristics of facies from both the Cloghoge and Newry plutons.

U-Pb geochronology and field relationships have been used to determine age relationships between the distinguished areas of the NIC. Through this the areas have been labelled sequentially as Zones A to O in the main NIC, along with Zones X and Y representing the northern and southern satellite bodies respectively (see fig. 4.11). This reflects the continuous nature of some compositions across pluton boundaries. Each zone has also been classified in terms of an igneous unit name, following a standard nomenclature (e.g., GSNI, 1997) (see fig. 4.12).

6.2: Emplacement

Host rock data supports the strike-swing in the Southern Uplands-Down-Longford Terrane inferred by Beamish et. al. (2010) from conductivity data. As these authors suggested, this could have resulted in the opening of one or more pull-apart basins, creating tectonic space for intrusion of the NIC. The steep orientations of host rocks in the vicinity of the NIC and the sub-circular trends of the satellite bodies (see Mann et. al., 1983; Smith, 2004) are consistent with this model.

When extrapolated through the NIC, two respective tract boundaries (see Beamish et. al., 2010) intersect the deep-seated Argyll and Newry Lineaments (see Cooper et. al., 2013) beneath key areas of each pluton. It is proposed that the tract boundaries represent shear zones at depth, which were connected to the deep crustal lineaments, facilitating magma ascent throughout the crust (e.g., Jacques and Reavy, 1994; Stevenson et. al., 2006; Cooper et. al., 2013). It is further suggested that reactivation of the Argyll and Newry Lineaments during Late Caledonian sinistral transtension may have both caused the strike swing of the Southern Uplands-Down-Longford Terrane in the first place.

However, there is also evidence for significant areas of missing host rock in the vicinity of the NIC. It is suggested that although a small degree of stoping would have contributed to this, the main cause is initial cross cutting of the host rocks prior to laccolithic inflation of the constituent parts of the NIC. Evidence for inflation of the NIC includes deflected host rock bedding and cleavage in the vicinity of the complex. Concentric foliations and high degrees of recrystallisation within outer, initially intruded facies also support inflation from a near-central source.

Aeromagnetic evidence supports tabular pluton geometries, but also indicates that the NIC can be divided into several bodies that were emplaced at successively higher crustal levels. These comprise the Seeconnell Complex and at least two other divisions of the Rathfriland pluton, along with the Newry and Cloghoge plutons. Thus the NIC represents a set of stacked laccoliths, likely supplied by a southwestward migrating source.

The current study additionally suggests that individual magma pulses within the NIC underwent inflation. This is evident from high levels of recrystallisation and submagmatic AMS fabric development within facies that are adjacent to younger pulse boundaries, implying that the facies were deformed by the latter. Such processes are not apparent within the northeast part of the Rathfriland pluton, which is proposed to reflect a phase of predominantly tectonically accommodated intrusion during the early history of the NIC.

These results reveal several phases of fabric and textural development, contradicting the argument of Paterson et. al. (1998, p. 53) that only the final “increment of strain” will be recorded within a felsic pluton (see also Petronis et. al., 2012). The phases can be summarised as follows:

1. Inflation from early in the cooling history of each pulse produces a ubiquitous concentric magmatic mineral alignment.

2. Inflation of newly intruded pulses causes recrystallisation and a strong, submagmatic mineral alignment at the inner edges of adjacent, previously intruded pulses.
3. Continued inflation within the central parts of a pluton produces a solid state overprint within the cooled, crystallised outer facies.

However, the current study also provides evidence for rarer fabrics possibly relating to magma flow (e.g., Stevenson et. al., 2007a). These occur within the margin of the NIC; at the margin of an individual zone and within a sheeted area of a pluton. It is proposed that flow is preserved here due to fast cooling and crystallisation of the respective magmas against relatively cold host material, which would limit development of the ubiquitous, inflation-related concentric alignment. This is evidenced by generally weak planar AMS fabric strengths in such areas. The inferred flow is steep at the pluton margins and has been proposed to reflect magma ascent into the emplacement site (see Petford et. al., 2000). On the other hand, fabrics from the sheeted areas and the individual zone boundary are less abundant and would require further work to resolve in terms of magma flow direction.

AMS has been shown to be a largely reliable proxy for visible fabrics through close correlation with measured foliations. Thermomagnetic investigation also suggests that AMS fabrics dominantly reflect the distribution anisotropy of magnetite, although some shape-controlled fabrics provided by single domain magnetite may also occur. However, the weak anisotropy (low H value) within a number of samples appears to directly relate to their low bulk magnetic susceptibilities (K_{mean}). Hence, the derived

AMS fabrics within such samples are thought to be less reliable and have not been implemented in the current investigation of emplacement.

6.3 Future work

Future work suggestions arising from the current study are as follows:

1. ***Investigation of the cause of aeromagnetic anomalies***. The hypothesis that differing polarities of aeromagnetic data reflect changes in the orientation of the Earth's magnetic field (see Chapter 4.11) could be tested through thermoremanent magnetisation (TRM) data. Cogné (1988) used such data to show that the Flamanville granite in northwest France exhibited a magnetisation reflecting the Earth's field, but that this was also influenced by strain within the pluton. Since this granite represents a similar laterally expanded pluton to those within the NIC (see Brun et. al., 1990), acquisition of TRM data would represent a viable method for testing the proposed hypothesis. This would be most useful when applied to numerous respective areas of positive and negative aeromagnetic anomaly.
2. ***Investigation of shear within the NIC***. A focused study on the orientation of shear throughout the NIC could potentially confirm its syn-tectonic nature (e.g., Hutton, 1982; Stevenson et. al., 2006). However, the work of Arbaret et al. (1997) shows that in conditions of weak shear ($\gamma \leq 2$), the relating fabrics will be poorly developed. Since previous studies of the NIC (e.g., Reynolds, 1934; Neeson, 1984) have not established a consistent sense of shear, this might be the case for the intrusion.

Appendix 1: locality information and field data

Key to abbreviations: Gd = granodiorite; Di = diorite; Qtz = quartz; Lampro = lamprophyre; Bt = biotite; Peg = pegmatite; H.rock = host rock; Hb = hornblende; Mobil = mobilised

Locality							Sample			Structural data			
Loc. No.	Hurley Loc. No.	GSNI site	Irish Grid reference			Locality Name (if applicable)	Sample number	GSNI sample no.	Lithology	Measurement type	Strike	Dip	Direction of dip
			Grid	Easting	Northing								
1			J	32634	42114				Bt pyroxenite				
			J	32495	42297				melodiorite				
2			J	30431	35453	Ballymagreehan Quarry	R1A						
			J	30444	35453		R1B		Gd				
		GSNI	J	3045	3545			MRC 365	Gd				
		GSNI	J	304	354			MRC 60	Di enclave				
			J	306	364				Gd	Fabric	10	65	SE
			J	306	364				Gd	Fabric	20	70	SE
			J	306	364				Gd	Fabric	178	8	E
			J	306	364				Lampro dyke	Dyke Contact	79	90	N
	190		J	307	366				Coarse Gd	Fabric	26	70	S
			J	307	366				Coarse Gd-Fine Gd	Internal Contact	26	60	S
			J	307	366				Coarse Gd-Fine Gd	Internal Contact	25	40	S
3						Magheramayo			Gd				
		MRC 366	J	2927	3694			MRC 366					
	213		J	296	439				Lampro dyke	Dyke Contact	120	-	
			J	296	439				Gd	Fabric	40	60	E
			J	296	439				Gd	Fabric	25	70	E
			J	296	439				Gd	Fabric	160	60	E
5			J	20062	33973	Rathfriland Centre Quarry	R4A		Coarse gd				
							R4B						
		MRC 369	J	2006	3395			MRC 369					
		MRC 67	J	187	344			MRC 67	Gd				
		MRC 68	J	204	354			MRC 68	Gd				
6			J	07273	27746	Newry Train Station	N1A						
			J	07193	27777		N1B						
7			J	07860	22504	Cloghoge Mountain Road Cutti	C1						
		MRC 372	J	0786	2251			MRC 372					
8			J	05557	22080	Carn Hill	CTS1		Bt (felsic) gd				
			J	05557	22080				Enclave				
			J	05545	22111		C2B		Enclave				
			J	05545	22111		C2C		Enclave				
			J	05545	22111		C2D		Enclave				
10			J	06517	32120	Goragh Wood Quarry	N2		Hb bt gd				
			J	06464	32083								
			J	06463	32019		N3						
		MRC 65	J	066	319			MRC 65	Granitic pod				
		MRC 66	J	066	319			MRC 66	Hornfels & peg				
11			J	08014	23657	Dublin Road Bridge	C3A						
			J	08009	23629		C3B						
			J	08004	23587		C3C						
			J	08077	23550		C3D						
12			J	21671	40681	Shannaghan Hill	R3A		Gd				
			J	21671	40681		R3B						
	229		J	217	407				Gd	Fabric	56	75	N
			J	218	407				Gd	Fabric	48	70	N
			J	218	407				H.rock	Xenolith cleavage	28	90	
			J	218	407				Gd	Fabric	60	90	
			J	218	407				H.rock	Xenolith orientation	55	75	N
			J	218	408				Gd dyke	Dyke Contact	120	90	
			J	218	408				Gd dyke	Fabric	58	75	N
14			J	27834	33094	Kilcoo	R5A		Quartz di				
			J	27806	33134		R5B		Quartz di				
		MRC 364	J	2782	3315			MRC 364	Quartz di				
15			J	24837	33582	St Mary's Church	R6						
		MRC 367	J	2483	3360			MRC 367	Gd				
16			J	16626	29174	Ballydoo Road							
			J	16630	29171				H.rock	Bedding	32	66	E
			J	16630	29171				H.rock	Cleavage	95	67	S
			J	16630	29171				H.rock	Bedding	50	44	SE
			J	16630	29171				H.rock	Bedding	53	58	SE
			J	16630	29171				H.rock	Bedding	55	63	SE
17			J	14423	25146	Aughnagon Quarry	N4A		Gd				
			J	14423	25146		N4B		Gd				
			J	14423	25146		N4C		Gd				
		MRC 370	J	1439	2515			MRC 370	Gd				
		MRC 62	J	145	251			MRC 62	Gd				
		MRC 63	J	145	251			MRC 63	Gd				
		MRC 64	J	145	251			MRC 64	Hornfels				
18			J	12565	29160	Benagh Road	N5A						
			J	12584	29088		N5B						
			J	12584	29088		N5C						
			J	12960	28503		N5D						
		MRC 371	J	1242	2982			MRC 371	Gd				
	266		J	129	286				Bt Gd	Fabric	130	Uncertain	NW?
19			J	10126	24878	Road Stud Installations	N7						
	351		J	094	255				Medium-Coarse Gd	Fabric	65	80	N
20			J	09229	26385	Concrete Football Pitch	N8						
21			J	09207	25930	Newry Junction	N9						
22			J	09023	26444		N10						
23			J	02755	26310		C5						
24			J	02908	25932	Camlough Lake	C6						
25			J	02939	25811		C7						
	341		J	029	258				Granite	Fabric	138	75	W

Locality							Sample			Structural data			
Loc. No.	Hurley Loc. No.	GSNI site	Irish Grid reference			Locality Name (if applicable)	Sample number	GSNI sample no.	Lithology	Measurement type	Strike	Dip	Direction of dip
			Grid	Easting	Northing								
			J	029	258				Granite	Fabric	38	70	N
	337		J	0295	2600				Medium granite	Fabric	18	90	
			J	0295	2600				Medium granite	Fabric	15	90	
			J	0295	2600				Medium granite	Fabric	130	70	NE
	338		J	029	261				Medium granite	Fabric	150	90	
	339		J	0285	2610				Granite	Fabric	135	80	W
			J	0285	2610				Granite	Fabric	130	80	W
	340		J	0295	2590				Granite	Fabric	138	75	W
26			J	03568	24829		C8						
		MRC 61	J	037	246			MRC 61	Mobil hornfels and gd				
	359		J	035	251				Felsite-Gd	Internal Contact	120	Uncertain	
			J	035	251				Medium-Coarse Gd	Fabric	110	75	N
			J	035	251				Felsite-Gd	Sheet Contact	80	80	N
	325		J	0410	2375				Medium-fine Granite	Fabric	60	Not specified	
	326		J	034	247				Granitic sheet	Sheet Contact	75	75	N
			J	034	247				Granitic sheet-h. Rock	Sheet Contact	70	90	
			J	034	247				Felsite intrusion	Sheet Contact	115	50	N
			J	034	247				Granitic sheet-h. rock	Sheet Contact	60	65	N
	329		J	025	252				Granite	Fabric	40	50	S
	331		J	028	268				Coarse Gd	Fabric	180	65	W
			J	028	268				Coarse Gd	Fabric	180	60	W
27			J	10126	32674	Corcrechy Road	N11A						
			J	10103	32713		N11B						
28			J	09972	29393		N12						
	270		J	101	293				Bt gd	Fabric	40	60	W
29			J	10064	29275		N13						
	271		J	100	295				Bt gd	Fabric	62	60	NW
30			J	11623	28626		N14						
	268		J	115	287				Bt gd	Fabric	118	5	S
31			J	11666	28942		N15						
32			J	12208	29260	Shanlieven Stone Quarry	N16A						
			J	12202	29204		N16B						
			J	12172	29181		N16C						
33			J	11519	30136		N17						
34			J	18069	33162		R7A						
			J	18128	33437		R7B						
	259		J	179	333				Bt gd	Fabric	150	60	W
			J	179	333				Bt gd	Fabric	142	70	W
	260		J	179	331				Gd	Fabric	119	80	N
			J	179	331				Gd	Fabric	130	70	N
35			J	15873	31380		N18						
36			J	17357	31656		N19						
37			J	16559	33427		R8						
	258		J	166	331				Bt gd	Fabric	160	?	E
			J	166	331				Lampro-gd	Dyke contact	68	90	N
38			J	15097	34837	Curley Lane	R9						
39			J	13693	31946	A25 Farmland	N20A		Gd				
			J	13592	31955		N20C		Porphy gd				
40			J	14774	31161		N21A		Fine gd				
			J	14702	31325		N21B						
41			J	05178	16385	Moore's Bridge	C9						
42			J	05194	16288		C10						
43			J	07786	21341	Cloghoge Railway Track	C11(A)						
			J	07871	21379		C11B						
			J	08055	21477		C11C						
			J	08197	21534		C11D						
			J	08492	21812		C11E						
			J	08610	22299		C11F						
44			J	32567	40175		R10		Coarse bt gd				
	435		J	326	399				Gd	Fabric	5	75	E
	436		J	326	398				Gd	Fabric	6	65	E
45			J	32407	40199		R11		Bt gd				
			J	32404	40149		R11B		Bt gd	Fabric	8	55	E
	437		J	325	405				Gd	Fabric	150	65	E
46			J	31820	40634		R12			Fabric	330	85	NE
47			J	31667	40641		R13		Fine hb bt gd	Fabric	335	80	NE
48			J	31511	40671	Leitrim Hilltop	R14		Fine hb bt gd				
	438		J	312	412				Fine Gd	Fabric	158	70	E
			J	312	412				Fine Gd	Fabric	140	70	E
			J	312	412				Aplite vein	Vein Orientation	80	50	S
			J	312	412				Aplite vein	Vein Orientation	70	65	S
	439		J	312	411				Fine Gd	Fabric	150	75	E
	440		J	313	410				Fine Gd	Fabric	155	80	E
			J	313	410				Aplite vein	Vein Orientation	120	90	
			J	313	410				Aplite vein	Vein Orientation	95	90	
	441		J	314	410				Lampro dyke	Dyke Contact	85	90	
			J	314	410				Fine Gd	Fabric	160	75	E
49			J	31672	40808		R15						
50			J	28375	39567		R16			Fabric	142	90	
	187		J	313	400				Gd	Fabric	140	70	E
			J	314	399				Gd	Fabric	160	50	E
			J	314	399				Gd	Fabric	160	30	E
			J	314	399				Aplite vein	Vein orientation	91	75	N
			J	314	400				Gd	Fabric	175	60	E
			J	314	400				Gd	Fabric	8	70	S

Locality							Sample			Structural data			
Loc. No.	Hurley Loc. No.	GSNI site	Irish Grid reference			Locality Name (if applicable)	Sample number	GSNI sample no.	Lithology	Measurement type	Strike	Dip	Direction of dip
			Grid	Easting	Northing								
			J	314	398				Fine Gd	Fabric	9	65	E
			J	314	398				Coarse Gd	Vein orientation	100	55	E
			J	314	398				Vein of Coarse Gd	Fabric	150	40	E
			J	314	398				Gd	Fabric	180	70	E
			J	314	398				Gd	Fabric	9	50	E
			J	314	399				Lampro Dyke	Dyke Contact	49	85	S
			J	314	399				Gd	Fabric	160	70	E
	188		J	308	391				Bt Gd	Fabric	4	75	E
			J	308	391				Bt Gd	Fabric	173	70	E
51			J	27888	40407		R17						
52			J	26797	35287		R18			Fabric	35	85	SE
	277		J	267	352				Coarse Gd	Fabric	20	90	
			J	267	352				Fine Gd	Fabric	24	70	SE
			J	267	352				Fine Gd	Fabric	20	60	S
			J	267	352				Diorite	Fabric	20	60	S
			J	267	352				Fine Gd vein	Fabric	20	60	S
			J	267	352				Fine Gd vein-diorite	Vein orientation	13	63	S
	276		J	269	355	Poags Bridge			Aplite vein	Fabric	40	90	
			J	269	355				Aplite vein	Fabric	42	79	S
			J	269	355				Lampro dyke-Gd	Dyke contact	98	79	S
			J	269	355				Coarse Gd	Fabric	32	65	S
			J	269	355				Coarse Gd	Fabric	35	70	S
			J	269	355				Coarse Gd	Fabric	34	70	S
			J	269	355				Aplite dyke	Dyke contact	170	70	E
53			J	30446	35749		R19						
54			J	30344	34490		R20		Hb bt gd				
55			J	30251	34416		R21		Hb bt gd				
			J	302	344				Stringers (mainly qtz)	Vein Orientation	25	60	S
			J	302	344				Gd	Mainly Msfabric	60	65	S
			J	302	344				Gd	Shear zone	120	Uncertain	
	210		J	301	346				Gd	Shear zone	170	Uncertain	
	211		J	302	347				Lampro Dyke	Dyke Contact	148	80	NE
			J	302	347				Lampro Dyke	(Dyke) cleavage	175	85	E
			J	302	347				Qtz vein	Vein Orientation	88	50	S
			J	302	347				Gd	Deformation zone	150	Uncertain	
			J	302	347				Lampro Dyke	(Dyke) cleavage	124	54	NE
			J	302	347				Lampro Dyke	(Dyke) cleavage	180	62	E
			J	302	347				Sedimentary xenolith	Xenolith orientation	24	70	E
			J	302	348				Lampro Dyke	?Dyke Contact	150	70	E
			J	302	348				Lampro Dyke	(Dyke) cleavage	15	65	E
			J	302	348				Gd	Fabric	180	60	E
			J	302	348				Gd	Fabric	90	65	S
	212		J	301	348				Gd	Fabric	95	65	E
			J	301	348				Gd	Fabric	55	60	S
			J	301	348				Lampro Dyke	Dyke Contact	145	Uncertain	
			J	301	348				Lampro Dyke	Dyke Contact	120	90	
			J	301	348				Lampro Dyke	(Dyke) cleavage	150	65	NE
56			J	31548	38363	Castlewellan Forest Park	R22		Bt Gd				
57			J	33156	44833		R23(A)		Mafic gd				
			J	33140	44836		R23B						
58			J	32812	44579		R24		Fine hb gd				
	217		J	326	448				Gd	Fabric	126	70	E
			J	326	448				Xenolith	Xenolith orientation	18	Uncertain	
	218		J	324	449				Gd	Fabric	115	90	
			J	324	449				Hornfels	Xenolith orientation	115	90	
	219		J	323	450				Lampro Dyke	Dyke Contact	5	80	E
			J	323	450				Gd	Fabric	110	80	SW
			J	323	450				Lampro Dyke	Fabric	78	90	
59			J	27402	43019	Windy Gap	R25						
60			J	27372	43049		R26		Bt gd				
	221		J	272	444				Qtz vein	Vein Orientation	60	80	N
			J	272	444				Qtz vein	Vein Orientation	80	78	N
	222		J	273	439				Coarse Gd	Fabric	65	68	N
			J	273	439				Coarse Gd	Fabric	68	35	N
	243		J	281	438				Gd	Fabric	85	65	N
			J	281	438				Qtz diorite?	Fabric	60	70	N
			J	281	438					Internal contact	60	Uncertain	NW-SE
			J	281	4348				Gd	Fabric	80	70	N
	245		J	278	444	Rough Hill			?H. rock-Qtz diorite	Contact	50	90	N
			J	278	444				?Qtz diorite	Fabric	85	65	S
			J	278	444				?Qtz diorite	Fabric	110	70	N
61			J	25804	42543	Dehommed Mountain	R27		Mafic granodiorite				
	223		J	256	428				Aplite vein	Vein Orientation	156	20	E
			J	256	428				Aplite vein	Vein Orientation	136	15	W
			J	256	428				Aplite vein	Fabric	75	72	N
			J	256	428				Fold in aplite vein	Fold axial plane	79	72	N
			J	255	426				Host rock-Gd	Contact	100	Uncertain	
			J	255	426				Gd	Dyke Contact	18	38	E
			J	255	426				(Dyke) Gd	Fabric	82	80	N
			J	255	426				(Dyke) Gd	Fabric	100	45	
			J	255	426				Country rock-Gd	Contact	90	Uncertain	
	224		J	253	424				Gd	Msfabric	88	90	
			J	253	424				Coarse Gd	Msfabric	80	78	N
			J	253	424				Lampro Dyke	Dyke Contact	175	90	
	225		J	262	432				Gd	Fabric	85	59	N
			J	262	432				Gd	Fabric	86	90	
			J	262	432				Lampro Dyke	Dyke Contact	162	90	
62			J	17804	37634	Knockiveagh Hill	R28		Hb gd				

Locality							Sample			Structural data			
Loc. No.	Hurley Loc. No.	GSNI site	Irish Grid reference			Locality Name (if applicable)	Sample number	GSNI sample no.	Lithology	Measurement type	Strike	Dip	Direction of dip
			Grid	Easting	Northing								
63			J	17759	37687		R29		?Qtz diorite				
	233		J	178	377				Gd	Fabric	180	75	W
									Gd	Fabric	15	80	W
	234		J	182	378					Fabric	48	75	S
										Fabric	30	90	W
	235		J	183	377				Lampro dyke	Dyke contact	60	70	S
									Gd	Fabric	60	70	S
	236		J	181	378				Lampro dyke	Fabric	46	70	N
	238		J	180	378				Gd	Fabric	70	70	S
			J	180	378				Gd	Fabric	48	60	S
			J	180	378				Gd	Fabric	55	75	N
	240		J	181	379				Gd	Fabric	180	90	W
	241		J	178	378				Gd	Fabric	178	75	W
64			J	07170	26306	Newry Railway Tunnel	N22A		Gd				
			J	07170	26306		N22B		Coarse Gd				
			J	07170	26306		N22C		Porphy Gd				
65			J	07112	26595		N23		Medium-coarse gd				
67			J	07096	26817		N24						
68			J	08001	23831	Cloghoge Roundabout North	(N)C12(A)		Coarse mafic gd	Fabric	150	60	SW
			J	08001	23831				Coarse mafic gd	Fabric	149	85	SW
			J	08001	23831				Gd vein	Vein orientation	145	80	SW
			J	08001	23831		(N)C12B						
	315		J	0795	2395				Coarse Gd	Fabric	160	90	
			J	0795	2395				Coarse Gd	Shear Zone	162	75	W
69			J	07975	23869		(N)C13		Coarse mafic gd				
70			J	07964	23887		NC14		Felsic gd				
			J	07964	23887		NC15		Porphyritic diorite				
			J	07964	23887		NC16		Felsic gd/porph diorite contact				
			J	07954	23890		NC17		Porphyritic diorite				
71			J	07921	23973		NC18		Host rock screen	Xenolith orientation	47	85	NW
	317		J	0790	2405				Gd	Shear Zone	180	40	W
			J	0790	2405				Gd	Fabric	30	90	
		MRC 58	J	070?	240			MRC 58	Gd				
72			J	04180	29061		N25(A)		Coarse gd				
			J	04129	29099		N25B		Coarse gd				
	373		J	041	291				Granite	Fabric	50	75	S
			J	041	291				Granite	Fabric	30	75	S
			J	041	291				Aplite vein	Vein Orientation	5	65	E
			J	041	291				Coarse Granite	Fabric	50	90	
			J	041	291				Coarse Granite	Fabric	50	75	E
	374		J	043	290				Coarse Granite	Fabric	45	90	
			J	043	290				Coarse Granite	Fabric	25	75	S
			J	043	290				Microgranite	Fabric	180	70	W
			J	043	290				Microgranite	Mineral lineation	270	70	
			J	043	290				Granite	Fabric	30	75	NW
	375		J	046	290				Granite	Fabric	29	45	NW
			J	046	290				Pegmatite	Vein Orientation	89	90	
	376		J	046	289				Fine Granite	Fabric	9	75	N
			J	046	289				Fine Granite	Mineral lineation	9	15	
			J	046	289				Fine Granite	Fabric	30	75	N
	377		J	047	289				Granite	Fabric	3	75	W
73			J	08149	24615		N26		Coarse bt gd				
	309		J	081	247				Gd	Fabric	100	75	S
74			J	08960	24250		N27(A)						
			J	08971	24205		N27B		Granite				
75			J	12039	26799		N28		Coarse hb bt gd				
76			J	10517	25924		N29		Hb bt gd				
77			J	11085	24743	Billys Road	N30(A)		hb gd	Fabric	260	20	N
			J	11085	24743				hb gd	Fabric	290	18	N
			J	11108	24736		N30B		hb gd	Fabric	255	60	N
78			J	11141	23536	Greenan Lough	N31		Coarse bt gd				
	356		J	113	234				Gd	Fabric	60	55	S
			J	113	234				Gd	Fabric	65	60	S
			J	113	234				Aplite sheet-Gd	Sheet Contact	25	25	NW
	358		J	1145	2335				Fine granite	Fabric	50	80	S
			J	1145	2335				Fine granite	Fabric	50	80	S
79			J	04826	25619	Camlough Mountain	C19						
80			J	04862	25425		C20		Fine gd				
	372		J	051	255				?Fine Gd	Fabric	60	65	N
			J	051	255				Gd	Fabric	60	65	N
81			J	06910	24274	Bernish Viewpoint	C21		Granitic pegmatite				
82			J	06928	24247		C22		Granitic pegmatite				
	320		J	071	240				Fine Granite-Coarse Gra	Internal Contact	80	90	
			J	071	240				Coarse Granite	Fabric	100	90	
	321		J	0705	2407				Coarse Granite	Fabric	120	70	N
			J	0705	2407				Coarse Granite	Fabric	100	90	
			J	0697	2400				Fine Granite-Fine Gran	Internal Contact	120	80	NE
			J	0697	2400				Fine Granite	Fabric	100	90	
86			J	00640	25223	Courtney Mountain	C26		Granite (+ mafic patches)				
	333		J	009	255				Granite	Fabric	20	80	E
			J	009	255				Granite	Fabric	20	80	E
			J	009	255				Granite	Fabric	20	90	
	334		J	007	254				Granite-felsic material	Internal Contact	150	80	E
			J	007	254				Granite	Fabric	40	80	N
			J	007	254				Granite	Fabric	30	80	E
	335		J	004	255				Felsic sheet-h.rock	Sheet Contact	70	90	

Locality							Sample			Structural data			
Loc. No.	Hurley Loc. No.	GSNI site	Irish Grid reference			Locality Name (if applicable)	Sample number	GSNI sample no.	Lithology	Measurement type	Strike	Dip	Direction of dip
			Grid	Easting	Northing								
	336		J	004	253				Granite	Fabric	10	80	NW
			J	004	253				Granite-felsic body	Internal Contact	15	? (steep)	NW
87			J	22741	41884	Doyles Close	T1		Fine gd				
			J	22741	41884				Satellite gd-h.rock	Satellite Contact	157	Uncertain	?
			J	22741	41884				C.rock	Bedding	72	72	N
			J	22741	41884				Satellite gd-h.rock	Satellite Contact	163	36	E
			J	22741	41884				Satellite gd-h.rock	Satellite Contact	178	80	E
			J	22741	41884				Satellite gd-h.rock	Satellite Contact	22	70	W
88			J	15390	38754	Kilty Hill	T2(A)		Fine gd				
			J	? −30m W of above			T2B		Porphyritic hb gd	Fabric	46	73	NW
89			J	17320	27534	Balludulany	T3		Gd				
			J	17325	27556				H.rock	Bedding	74	25	SE
			J	17325	27556				Satellite gd-h.rock	Satellite contact	168	67	E
90			J	17503	28367	Ballydoo Farm	T4(A)		Hb bt gd				
			J	17468	28321				Satellite gd-h.rock	Satellite contact	38	Uncertain	?
			J	17423	28359		T4B		Bt gd				
									H.rock	Bedding	33	60	SE
91			J	17723	28066	Leode Road Quarry	T5		Fine hb gd	Fabric	38	30	E
			J	17723	28066				C.rock	Bedding	25	48	E
			J	17723	28066				Satellite gd-h.rock	Satellite Contact	178	36	E
			J	17642	28119		T5B		Fine hb gd	Fabric			
			J	17642	28119				Satellite gd-h.rock	Satellite Contact	26	45	SE
		MRC 59	J	184	288			MRC 59	Hornfels and veinlet				
		MRC 368	J	2392	3892			MRC 368	m-co Fol gd (titanites?)				
	242		J	247	395				Gd	Fabric	100	90	N
	226		J	292	415				Gd	Fabric	62	78	S
	232		J	181	362				Gd	Fabric	45	80	S
	244		J	317	437				Gd	Fabric	85	75	N
	254		J	159	355				Gd	Fabric	30	70	N
			J	159	355				Gd	Fabric	22	72	N
	255		J	161	355				Gd	Fabric	30	70	N
	257		J	111	318				Bt Gd	Fabric	75	70	N
			J	111	318				Bt Gd	Fabric	90	70	N
	264		J	152	299				Hb bt gd (fine)	Fabric	180	60	S
			J	152	299				Hb bt gd (fine)	Fabric	174	60	S
	265		J	129	279				Bt Gd	Fabric	70	70	S
			J	129	279				Bt Gd	Fabric	60	70	S
			J	129	279				Bt Gd	Fabric	168	70	E
			J	129	279				Bt Gd	Fabric	140	Uncertain	
	267		J	143	295				Bt Gd	Fabric	150	Uncertain	S?
			J	143	295				Bt Gd	Fabric	125	90	N
	269		J	111	294				Bt Gd	Fabric	75	Uncertain	
	272		J	094	302				Bt Gd	Fabric	65	60	NW
	273		J	094	302				Gd	Fabric	68	60	N
			J	094	302				Gd	Fabric	62	45	NW
			J	094	302				Gd	Fabric	63	70	NW
	274		J	083	315				Bt Gd	Fabric	58	90	N
			J	083	315				Bt Gd	Fabric	30	40	S
			J	083	315				C.rock-Gd	Contact	60	Uncertain	
			J	083	315				Bt Gd	Fabric	62	75	N
			J	083	315				Host rock-Gd	Contact	58	75	N
	280								Bt Gd-fine qtz diorite	Contact	172	45	E
									Bt Gd-fine qtz diorite	Contact	175	55	E
									Fine Qtz diorite	Fabric	165	70	E
	281								?Bt gd	Fabric	147	70	E
									?Bt gd	Fabric	160	90	
	300		J	090	212				Gd	Fabric	40	90	
	302		J	092	219				Gd	Fabric	45	75	N
	303		J	0905	2195				Gd	Fabric	50	80	N
			J	0905	2195				Felsic dyke	Dyke Contact	35	90	
	312		J	0850	2350				Granite sheet	Fabric	90	90	
	313		J	059	251				Fine Gd-Porphyritic Gd	Internal Contact	25	80	S
			J	059	251				Fine Gd sheet	Fabric	100	75	N
	314		J	089	219				Fine Gd	Mainly Msfabric	70	80	N
	324		J	0600	2385				?Granite	Fabric	60	70	N
	343		J	020	255				Gd	Fabric	30	80	E
			J	020	255				Gd	Fabric	45	70	E
			J	020	255				?Gd	Shear Zone	165	55	NE
	352		J	090	257				Medium-Coarse Gd	Fabric	102	90	
			J	090	257				Medium-Coarse Gd	Fabric	120	65	W
			J	090	257				Medium-Coarse Gd	Fabric	110	75	N
			J	090	257				Dioritic enclave	Encl. Long axis	300	5	
			J	090	257				Dioritic enclave	Enclave fabric	120	70	N
	353		J	092	257				Gd	Fabric	120	75	N
			J	0920	2585				Gd	Fabric	150	75	E
	361		J	043	246				Granite sheet	Fabric	70	80	N
	363		J	045	248				Granite	Fabric	80	75	N
	365		J	043	250				Felsite-h.rock contact	Other Contact	110	45	N
			J	043	250				Felsite-h.rock contact	Other Contact	90	80	N
	366		J	041	246				Granite	Fabric	72	70	N
	367		J	040	245				Granite	Fabric	70	75	N
	370								Lampro dyke	Fabric	70	90	
	371		J	047	261				Microgranite	Vein Orientation	60	75	N
			J	047	261				Microgranite	Vein Orientation	80	15	N
			J	047	261				Coarse Gd	Fabric	60	60	S
			J	047	261				Coarse Granite	Fabric	60	90	
93			J	32750	46353	Slieve Croob			H.rock	Bedding	60	71	N
			J	32750	46353				H.rock	Bedding	56	71	N
			J	32750	46353				H.rock	Cleavage	64	81	N

Locality							Sample			Structural data			
Loc. No.	Hurley Loc. No.	GSNI site	Irish Grid reference			Locality Name (if applicable)	Sample number	GSNI sample no.	Lithology	Measurement type	Strike	Dip	Direction of dip
			Grid	Easting	Northing								
			J	32750	46353				H.rock	Cleavage	67	80	N
			J	32753	46456				H.rock	Joints	155	50	E
94			J	32067	47476				H.rock	Bedding	27	78	E
			J	32067	47476				H.rock	Bedding	38	80	E
			J	32067	47476				H.rock	Cleavage	10	90	
			J	32067	47476				H.rock	Cleavage	26	88	W
95			J	33922	40588				H.rock	Bedding	172	80	W
									H.rock	Cleavage	5	86	W
96			J	27717	44507				H.rock	Layering	50	82	W
97			J	25342	43429	Dehommed Mountain			H.rock	Bedding	81	84	N
			J	25342	43429				H.rock	Cleavage	86	78	N
98			J	21646	40785	Shannaghan Hill			H.rock	Layering	55	62	N
			J	21646	40785				H.rock	Cleavage	35	62	
99			J	32654	37445				H.rock	Layering	25	83	E
100			J	32902	37606				H.rock	Cleavage	24	87	E
101			J	30640	33671				H.rock	Cleavage	68	33	S
102			J	30378	33587				H.rock	Cleavage	60	53	S
			J	30378	33587				H.rock	Bedding	56	36	S
103			J	30333	33550				H.rock	Cleavage	76	58	S
104			J	32269	32437				H.rock	Cleavage	44	72	S
			J	32269	32437				H.rock	Cleavage	62	82	S
			J	32269	32437				H.rock	Bedding	65	79	N
			J	24222	10663				H.rock	Cleavage	60	54	S
106			J	21897	29020				H.rock	Bedding	95	55	S
			J	21897	29020				H.rock	Bedding	96	60	S
107			J	17543	29985				H.rock	Bedding	44	56	SE
			J	17543	29985				H.rock	Bedding	73	42	S
			J	17543	29985				H.rock	Joints	135	76	N
108			J	05984	33051				H.rock	Layering	20	87	W
			J	05984	33051				H.rock	Cleavage	62	76	N
			J	05984	33051				H.rock	Cleavage	62	75	N
			J	05984	33051				H.rock	Cleavage	96	66	N
109			J	17305	27509				H.rock	Bedding?	74	35	S
			J	17305	27509				H.rock	Bedding?	42	41	E
110			J	14499	23330				H.rock	Bedding	63	64	S
111			J	11454	20923	Clade Quarry			H.rock	Bedding	75	65	S
			J	11454	20923				H.rock	Bedding	65	55	S
			J	11454	20923				H.rock	Bedding	66	79	S
			J	11484	20831				H.rock	Bedding	56	50	S
			J	11484	20831				H.rock	Joints	152	62	E
			J	11484	20831				H.rock	Joints	130	90	
			J	11484	20831				H.rock	Joints	157	88	E
			J	11484	20831				H.rock	Joints	57	89	N
113			J	00816	25831				Bt granite				
			J	00816	25794				Bt granite	Ssfabric	49	74	
114			H	99905	25529	Belleeks			H.rock	Bedding	75	71	S
			H	99905	25529				H.rock	Bedding	80	85	S
			H	99905	25529				H.rock	Cleavage	68	70	S
115			H	87201	17978				H.rock	Bedding	37	83	W
116			H	89175	16171				H.rock	Bedding	45	88	S
			H	89175	16171				H.rock	Cleavage	50	89	S
117			H	95811	16604				H.rock	Bedding?	61	66	S
			H	95811	16604				H.rock	Bedding?	31	46	SE
118			H	95640	16390				H.rock	Bedding	44	62	S
			H	95640	16390				H.rock	Joints	131	90	
119			H	97125	15450	Silverbridge			H.rock	Bedding	70	77	S
120			H	97179	16046				H.rock	Bedding	45	85	S
121			H	96256	18766				H.rock	Bedding	40	60	E
122			H	96617	19941				H.rock	Bedding	2	80	E
			H	96617	19941				H.rock	Bedding	1	78	W
			H	96617	19941				H.rock	Cleavage	170	77	E
			H	96627	19977				H.rock	Bedding	12	81	W
123			H	99768	19007				Granite				
124			H	99325	21884				Hb granite	Fabric	10	86	E
125			H	99618	20916				Granite	Fabric	12	74	E
126			H	99814	20625				Bt hb granite	Fabric	144	90	
127			J	00603	22068				Granite sheet	Sheet contact	132	72	E
128			J	03496	15196				Coarse hb bt gd				
129			J	15951	35423				Hb gd				
130			J	24050	40540				Gd				
131			J	13942	32488				Coarse felsic gd				
132			J	07948	23878	Upper Motorway Terrace			Granite vein	Vein orientation	126	54	E
			J	07948	23878				Granite vein	Vein orientation	43	74	E
			J	07884	23980				Granite vein	Vein orientation	142	48	W
			J	07878	24007				Granite vein	Vein orientation	130	44	W
			J	07832	24070				Gd	Fabric	120	56	SW
133			J	08084	23274				Gd				
134			J	08146	24933				Porphyritic di/gd	Fabric	120	32	N
135			J	06759	29353				Gd				
136			J	06115	29961				Gd				
137			J	05838	32039				Bt gd	Fabric	44	31	E
138			J	08198	31500				Coarse gd				
139			J	14094	27815				Bt gd	Fabric	33	90	
140			J	30532	43634				Fine hb bt gd	Fabric	116	40	N
			J	30558	43673				Fine hb bt gd	Fabric	99	85	N
			J	30527	43684				Fine hb bt gd	Fabric	114	85	S
			J	30527	43684				Fine hb bt gd	Fabric	111	47	S
141			J	30611	43794				Mafic gd?				
142			J	27609	43221				Gd-h.rock	Contact	342	30	W

Locality							Sample			Structural data			
Loc. No.	Hurley Loc. No.	GSNI site	Irish Grid reference			Locality Name (if applicable)	Sample number	GSNI sample no.	Lithology	Measurement type	Strike	Dip	Direction of dip
			Grid	Easting	Northing								
143			J	27874	43566				Hb bt gd	Fabric	69	45	N
			J	27874	43566				Hb bt gd	Fabric	80	73	N
			J	27874	43566				Hb bt gd	Fabric	90	51	N
			J	27879	43583				Qtz diorite?	Fabric	59	85	N
			J	27879	43583				Qtz diorite-Gd	Internal contact?	127	75	S
			J	27879	43583				Hb bt gd	Fabric	74	84	N
144			J	24883	41627				Hb bt gd	Fabric	80	90	
			J	24883	41627				Qtz diorite?	Fabric			
145			J	32237	37392				Gd				
146			J	32502	37717				Qtz diorite?				
147			J	32865	37627				Felsite				
148			J	26357	33953				Hb gd	Fabric	74	72	S
			J	26357	33953				C.rock (xenolith)	Bedding (xeno)	178	77	E
			J	26357	33953				Qtz vein	Vein Orientation	166	55	W
149			J	25991	36580				Bt hb gd				
150			J	03650	24593	Camlough Quarry			C.rock	Bedding	42	58	N
			J	03650	24593				C.rock	Bedding	74	70	N
			J	03650	24593				C.rock	Bedding	62	85	S
			J	03650	24593				Granite sheet-h.rock	Contact	80	67	N
			J	03650	24593				Granite	Fabric	168	10	E
			J	03650	24593				Granite vein	Vein Orientation	63	75	N
			J	03650	24593				Palaeogene-h.rock	Contact	109	50	N
			J	03650	24593				H.rock	Bedding	110	76	N
151			J	32408	42359				Melodi	Fabric	164	73	E
			J	32408	42359				Melodi	Fabric	35	65	SE
			J	32492	42303				Gd vein	Vein Orientation	56	74	S
			J	32536	42261				Meladi	Fabric	20	80	E
			J	32536	42261				Meladi	Fabric	5	75	E
			J	32536	42261				Basalt vein				
			J	32536	42261				Basalt vein				
152			J	32829	41980				Melodioriote	Fabric	170	81	W
153			J	32789	42034				Gd vein	Vein orientation	38	65	NW
154			J	32473	42278				Granite vein	Vein orientation	62	65	SE
			J	32473	42278				Granite sheet	Sheet orientation	51	70	SE
155			J	30430	35436				Pegmatite-gd	Contact	170	60	E
			J	30430	35436				Gd	Fabric	35	86	SE
156			J	31243	35029				Infilled fractures?	Fractures	148	88	NE
			J	31243	35029				Infilled fractures?	Fractures	152	87	NE
			J	31243	35029				H.rock	Bedding	50	50	SE
			J	31243	35029				H.rock	Bedding	38	62	SE
			J	31243	35029				Qtz porphery-c.rock	Contact	85	37	N
			J	31243	35029					Bedding	24	60	SE
157			J	14608	25140	Aughnagon Quarry (2)			H.rock	Bedding	25	69	E
			J	14608	25140				Infilled fractures?	Fractures	126	81	NE
			J	14423	25143				Gd-h.rock	Contact	55	42	SE
			J	14423	25143				H.rock	Bedding	55	42	SE
			J	14423	25143				Gd	Msfabric	48	80	SE
			J	14423	25143				Gd	Msfabric	56	82	SE
158			J	11221	27100				Bt hb gd				
159			J	29924	44702				Coarse bt hb gd				
	306		J	08600	23600	Dublin Road Bridge			H.rock	Bedding	120	Uncertain	N
	307		J	09000	24000				H.rock	Bedding	80	80	S
	308		J	08800	23800				H.rock	Cleavage	110	80	N
	308		J	08800	23800				H.rock	Bedding	112	80	N
	310		J	08150	24100				H.rock	Cleavage	50	60	S
	310		J	08150	24100				H.rock	Bedding	50	50	S
	311		J	08250	24050				H.rock	Bedding	142	80	NE
	311		J	08250	24050				H.rock	Bedding	140	80	N
	311		J	08250	24050				H.rock	Bedding	135	75	N
	311		J	08250	24050				H.rock	Bedding	140	75	NE
	311		J	08250	24050				H.rock	Bedding	135	50	NE
	311		J	08250	24050				H.rock	Bedding	140	75	NE
	311		J	08250	24050				H.rock	Bedding	5	39	NW
	311		J	08250	24050				H.rock	Cleavage	100	80	N
	312		J	08500	23500				H.rock	Bedding	90	80	N
	312		J	08500	23500				H.rock	Cleavage	90	85	N

Appendix 2A: Major and trace element geochemistry results (see fig. 4.6 for sample locations)

	XRFS	XRFS	XRFS	XRFS	XRFS	XRFS	XRFS	XRFS	XRFS	XRFS	XRFS	XRFS	XRFS	XRFS	XRFS	XRFS	XRFS	XRFS	XRFS	XRFS	XRFS	XRFS	XRFS	LOI
Sample name	SiO_2	TiO_2	Al_2O_3	Recalc FeO	Mn_3O_4	MgO	CaO	Na_2O	K_2O	P_2O_5	SO_3	Cr_2O_3	SrO	ZrO_2	BaO	NiO	CuO	ZnO	PbO	V_2O_5	HfO_2	F	Cl	LOI
	%	%	%	%	%	%	%	%	%	%	%	%	%	%	%	%	%	%	%	%	%	%	%	%
S2	47.01	1.93	14.98	6.63	0.17	8.93	8.61	2.63	3.11	1.03	<0.1	0.05	0.17	0.05	0.22	0.03	0.00	0.01	0.00	0.05	0.00	0	0	1.70
S3	42.33	2.85	8.65	8.03	0.19	14.58	10.90	0.58	4.44	1.49	0	0.10	0.03	<0.02	0.50	0.04	0.00	0.01	0.00	0.07	0.00	0.2	0	0.67
S4	51.56	1.50	15.11	6.32	0.14	6.95	7.84	3.07	4.64	1.07	0	0.03	0.22	0.03	0.46	0.02	0.02	0.01	0.00	0.04	0.00	0	0	1.13
S6	44.08	2.47	9.63	7.73	0.21	13.02	11.14	1.01	3.03	1.47	0	0.07	0.10	0.02	0.37	0.04	0.00	0.01	0.00	0.06	0.00	0.2	0	0.98
S7	57.74	1.17	15.83	4.53	0.11	4.41	4.52	3.79	4.52	0.62	0	0.02	0.12	0.08	0.22	0.01	0.00	<0.01	0.00	0.03	0.00	0	0	2.59
S8	44.42	2.24	13.21	8.35	0.17	7.88	8.90	2.52	3.00	1.44	0.2	0.03	0.19	0.02	0.31	0.02	0.02	0.01	0.00	0.06	0.00	0.1	0	0.98
S9	43.47	2.00	10.79	7.86	0.22	12.96	10.83	1.27	2.36	1.34	0	0.08	0.16	<0.02	0.30	0.03	0.03	0.01	0.00	0.05	0.00	0.2	0	0.76
S11	46.79	1.90	14.84	6.58	0.17	8.92	8.68	2.56	3.10	1.02	0	0.04	0.17	0.05	0.24	0.02	0.01	0.01	0.00	0.05	0.00	0.1	0	0.79
S16	56.83	1.02	15.83	4.23	0.12	6.19	5.00	3.71	3.18	0.49	0.1	0.04	0.08	0.04	0.14	0.02	0.00	<0.01	0.00	0.03	0.00	0	0	1.17
S17	54.39	1.13	15.18	4.77	0.11	6.26	5.19	3.46	4.36	0.69	0	0.04	0.13	0.04	0.28	0.02	0.02	<0.01	0.00	0.03	0.00	0	0	1.85
S19	54.34	0.83	13.17	4.59	0.16	6.36	10.33	3.13	3.17	0.64	0	0.04	0.10	0.05	0.15	0.01	0.02	<0.01	0.00	0.03	0.00	0	0	0.88
S21	55.88	1.22	15.48	4.79	0.11	4.74	5.52	3.56	5.23	0.75	0	0.02	0.16	0.06	0.29	0.01	0.01	0.01	0.01	0.03	0.00	0	0	0.98
S22	71.31	0.24	14.40	0.95	0.03	0.74	1.54	3.59	4.55	0.06	0	0.01	0.03	<0.02	0.11	0.00	0.00	<0.01	0.00	<0.01	0.00	0	0	0.93
S24	55.68	1.17	15.76	4.61	0.10	4.98	5.80	3.61	4.62	0.70	0	0.03	0.16	0.05	0.27	0.01	0.01	<0.01	0.00	0.03	0.00	0	0	1.16
S25	56.06	1.15	15.52	4.48	0.11	4.35	5.39	3.57	4.76	0.67	0	0.02	0.16	0.06	0.25	0.01	0.00	<0.01	0.00	0.03	0.00	0	0	0.82
S26	62.02	0.54	17.68	2.36	0.04	1.88	2.23	4.01	6.31	0.27	0	<0.01	0.13	0.06	0.23	0.00	0.01	<0.01	0.00	0.02	0.00	0	0	0.85
S28B	55.49	1.24	15.92	4.93	0.13	5.44	6.01	3.74	4.21	0.69	0	0.03	0.16	0.06	0.23	0.01	0.00	0.01	0.00	0.03	0.00	0	0	0.76
S30	52.66	1.31	14.23	5.28	0.14	6.82	6.65	3.07	5.10	0.87	0	0.04	0.16	0.05	0.33	0.02	0.00	0.01	0.00	0.03	0.00	0	0	0.70
S32	55.92	1.16	16.07	4.93	0.13	5.37	6.45	3.96	3.19	0.66	0	0.03	0.13	0.07	0.20	0.02	0.00	0.01	0.00	0.03	0.00	0	0	0.39
S34	48.99	1.33	17.45	8.12	0.25	8.81	6.26	1.51	1.66	0.55	0.7	0.06	0.10	0.04	0.07	0.03	0.01	0.02	0.00	0.04	0.00	0	0	1.47
S35	56.21	1.39	16.52	4.71	0.13	3.49	4.37	4.11	5.49	0.78	0	0.01	0.12	0.11	0.24	0.00	0.01	0.01	0.01	0.03	0.00	0	0	0.58
S38	54.58	1.20	14.28	4.92	0.12	6.94	6.65	2.99	5.06	0.75	0	0.05	0.14	0.05	0.29	0.02	0.00	0.01	0.01	0.03	0.00	0	0	0.53
S39	53.83	1.13	14.49	5.84	0.14	7.39	7.53	3.49	2.32	0.73	0	0.04	0.15	0.04	0.16	0.02	0.00	0.01	0.00	0.03	0.00	0	0	0.76
S40	56.12	1.17	15.35	4.67	0.12	5.92	6.19	3.62	3.96	0.61	0	0.03	0.14	0.04	0.20	0.02	0.00	<0.01	0.00	0.03	0.00	0	0	0.35
S41	55.93	1.19	15.64	4.88	0.13	5.82	6.47	3.72	3.50	0.62	0	0.03	0.13	0.04	0.19	0.02	0.00	0.01	0.01	0.03	0.00	0	0	0.49
R1B	63.91	0.73	14.91	2.88	0.08	3.17	3.95	3.87	3.53	0.20	0	0.02	0.05	0.03	0.11	0.00	0.00	<0.01	0.00	0.02	0.00	0	0	0.99
R4B	68.96	0.49	15.49	2.23	0.06	1.84	1.24	4.16	3.23	0.16	0	<0.01	0.03	0.03	0.08	0.00	0.00	<0.01	0.00	0.01	0.00	0	0	1.25
N1A	64.72	0.72	15.97	2.83	0.09	2.23	3.15	4.05	3.29	0.24	0	<0.01	0.05	0.03	0.08	0.00	0.00	<0.01	0.00	0.01	0.00	0	0	1.03
C1	71.64	0.26	14.66	1.13	0.05	0.75	1.57	3.76	4.02	0.12	0	<0.01	0.02	0.02	0.08	0.00	0.00	<0.01	0.00	<0.01	0.00	0	0	1.30
C2D	65.30	0.62	16.54	2.70	0.09	2.11	2.96	4.70	2.68	0.27	0	<0.01	0.05	0.03	0.08	0.00	0.00	<0.01	0.00	0.01	0.00	0	0	1.47
NTS1	77.06	0.06	12.78	0.33	0.01	<0.05	0.69	2.98	6.27	<0.01	0	<0.01	<0.01	<0.02	<0.02	0.00	0.00	<0.01	0.00	<0.01	0.00	0	0	0.39
C3A	68.21	0.45	15.21	2.13	0.08	1.88	1.06	3.24	5.95	0.20	0	<0.01	0.02	0.02	0.08	0.00	0.00	0.01	0.00	<0.01	0.00	0	0	1.82
C3C	71.82	0.18	14.06	0.83	0.05	0.62	1.94	2.89	4.46	0.08	0	<0.01	<0.01	<0.02	0.05	0.00	0.00	<0.01	0.00	<0.01	0.00	0	0	3.64
R3A	74.79	0.22	13.74	0.78	0.02	0.62	1.67	3.57	4.07	0.06	0	<0.01	0.03	<0.02	0.10	0.00	0.00	<0.01	0.00	<0.01	0.00	0	0	0.65
R5A	61.85	0.84	15.65	3.52	0.10	4.46	4.55	3.90	3.16	0.26	0	0.03	0.06	0.03	0.11	0.02	0.00	<0.01	0.00	0.02	0.00	0	0	0.94
N5C	68.01	0.61	15.35	2.44	0.08	2.05	2.12	4.12	3.31	0.19	0	<0.01	0.03	0.03	0.07	0.00	0.00	<0.01	0.00	0.01	0.00	0	0	1.53
N7	67.66	0.56	15.56	2.25	0.08	1.89	2.40	4.28	3.09	0.17	0	<0.01	0.04	<0.02	0.07	0.00	0.00	<0.01	0.00	0.01	0.00	0	0	1.17
N8	66.76	0.68	16.05	2.67	0.09	1.99	3.19	4.34	2.87	0.22	0	<0.01	0.04	0.03	0.08	0.00	0.00	<0.01	0.00	0.02	0.00	0	0	0.96
N9	65.87	0.84	15.52	3.04	0.11	2.40	1.77	3.74	3.97	0.25	0	<0.01	0.04	0.03	0.09	0.00	0.00	<0.01	0.00	0.02	0.00	0	0	1.67
N10	66.62	0.66	15.74	2.66	0.09	2.01	3.05	4.28	2.99	0.22	0	<0.01	0.05	0.03	0.08	0.00	0.00	<0.01	0.00	0.01	0.00	0	0.2	1.20
C5	71.79	0.36	15.24	1.50	0.05	1.08	1.73	4.27	3.32	0.12	0	<0.01	0.03	0.02	0.09	0.00	0.00	<0.01	0.00	<0.01	0.00	0	0.1	0.96
C6	71.11	0.33	14.88	1.42	0.05	0.99	1.47	3.97	3.45	0.11	0	<0.01	0.02	0.02	0.10	0.00	0.00	<0.01	0.00	<0.01	0.00	0	0	0.90
C7	71.53	0.34	15.31	1.38	0.05	0.91	1.47	4.28	3.22	0.11	0	<0.01	0.02	0.03	0.09	0.00	0.00	<0.01	0.00	<0.01	0.00	0	0	1.28
C8	70.46	0.35	15.13	1.47	0.07	1.45	1.53	4.20	3.58	0.10	0	<0.01	0.02	<0.02	0.07	0.00	0.00	<0.01	0.00	0.01	0.00	0	0	1.41
N11A	68.80	0.50	16.38	2.05	0.05	1.36	2.38	4.36	3.14	0.15	0	<0.01	0.03	0.02	0.10	0.00	0.00	<0.01	0.00	0.01	0.00	0	0	1.13
N12	67.38	0.57	16.37	2.36	0.08	1.74	1.95	4.13	3.60	0.19	0	<0.01	0.04	0.02	0.08	0.00	0.00	<0.01	0.00	0.01	0.00	0	0	1.45
N13	67.08	0.58	15.35	2.48	0.08	1.88	2.88	4.16	2.91	0.19	0	<0.01	0.04	0.03	0.07	0.00	0.00	<0.01	0.00	0.01	0.00	0	0	0.98
N14	66.78	0.68	15.88	2.56	0.09	2.12	2.81	4.00	3.55	0.20	0	<0.01	0.05	0.03	0.08	0.00	0.00	<0.01	0.00	0.01	0.00	0	0	1.19
N15	66.05	0.68	16.05	2.79	0.08	2.04	3.29	4.24	2.84	0.22	0	<0.01	0.04	0.03	0.08	0.00	0.00	<0.01	0.00	0.02	0.00	0	0	1.12
N16A	68.09	0.60	15.26	2.36	0.08	1.74	2.74	4.06	3.23	0.19	0	<0.01	0.03	0.03	0.09	0.00	0.00	<0.01	0.00	0.01	0.00	0	0	1.12
N16C	67.97	0.54	15.79	2.34	0.08	1.65	3.26	4.22	3.12	0.18	0	<0.01	0.03	0.02	0.08	0.00	0.00	<0.01	0.00	0.02	0.00	0	0	0.82
N17	66.49	0.60	15.73	2.42	0.08	1.75	3.12	4.04	3.38	0.19	0	<0.01	0.04	0.02	0.09	0.00	0.00	<0.01	0.00	0.01	0.00	0	0	0.86
R7A	67.31	0.53	15.68	2.28	0.07	1.77	3.07	4.18	2.69	0.16	0	<0.01	0.03	0.02	0.08	0.00	0.00	<0.01	0.00	0.01	0.00	0	0	1.19
N18	68.02	0.51	15.86	2.15	0.07	1.78	2.59	4.29	3.15	0.17	0	<0.01	0.03	0.02	0.08	0.00	0.00	<0.01	0.00	0.01	0.00	0	0	1.19
N19	68.61	0.46	15.74	2.00	0.06	1.54	2.62	3.99	3.39	0.18	0	<0.01	0.04	<0.02	0.09	0.00	0.00	<0.01	0.00	<0.01	0.00	0	0	1.10
R9	66.24	0.51	16.16	2.34	0.07	2.69	3.22	4.34	3.04	0.20	0	0.01	0.05	<0.02	0.10	0.00	0.00	<0.01	0.00	0.01	0.00	0	0	1.05
N20	67.69	0.49	15.72	2.19	0.07	1.58	1.93	4.29	3.26	0.21	0	<0.01	0.03	0.02	0.07	0.00	0.00	<0.01	0.00	0.02	0.00	0	0	1.49
N20C	68.97	0.46	15.39	2.13	0.07	1.67	2.65	3.98	3.34	0.15	0	0.01	0.03	0.02	0.08	0.00	0.00	<0.01	0.00	0.01	0.00	0	0	0.79
N21A	68.87	0.47	15.71	2.11	0.06	1.56	2.54	4.25	3.26	0.17	0	<0.01	0.03	0.02	0.09	0.00	0.00	<0.01	0.00	<0.01	0.00	0	0	1.05
C9	53.35	1.85	14.18	5.26	0.14	5.79	6.09	2.68	5.30	1.20	0	0.03	0.11	0.06	0.27	0.00	0.01	0.01	0.00	0.03	0.00	0.1	0	1.60
C11	72.18	0.30	14.64	1.03	0.03	1.75	0.87	4.29	3.61	0.13	0	<0.01	0.01	0.02	0.07	0.00	0.00	<0.01	0.00	<0.01	0.00	0	0	1.58
C11B	71.14	0.29	14.67	1.18	0.04	0.86	1.40	3.91	4.05	0.13	0	<0.01	0.02	0.02	0.08	0.00	0.00	<0.01	0.00	<0.01	0.00	0	0	1.23
C11C	72.71	0.26	14.68	1.09	0.04	0.84	1.10	4.22	3.89	0.12	0	<0.01	<0.01	<0.02	0.06	0.00	0.00	<0.01	0.00	<0.01	0.00	0	0	1.31
C11D	76.36	0.16	13.31	0.73	0.03	0.38	0.66	3.81	4.59	0.05	0	<0.01	<0.01	<0.02	<0.02	0.00	0.00	<0.01	0.00	<0.01	0.00	0	0	0.95
C11E	72.50	0.23	14.29	1.01	0.03	0.84	0.59	4.15	4.05	0.10	0	<0.01	<0.01	<0.02	0.14	0.00	0.00	<0.01	0.00	<0.01	0.00	0	0	1.36
C11F	73.70	0.19	14.41	0.86	0.04	0.62	0.68	3.99	4.48	0.08	0	<0.01	<0.01	<0.02	0.05	0.00	0.00	<0.01	0.00	<0.01	0.00	0	0	1.18
R10	64.63	0.70	15.11	2.72	0.07	2.95	3.38	3.86	3.69	0.18	0	0.02	0.05	0.04	0.10	0.00	0.00	<0.01	0.00	0.01	0.00	0	0	0.97
R11	65.02	0.73	15.30	2.82	0.08	3.17	3.50	3.68	3.85	0.21	0	0.02	0.05	0.04	0.11	0.00	0.00	<0.01	0.00	0.02	0.00	0	0	0.84
R12	66.79	0.61	15.42	2.50	0.07	2.62	2.52	3.85	3.71	0.15	0	0.01	0.05	0.03	0.10	0.00	0.00	<0.01	0.00	0.02	0.00	0	0	1.18
R13	67.01	0.61	15.19	2.52	0.07	2.47	2.82	3.78	3.71	0.16	0	0.01	0.04	0.04	0.10	0.00	0.00	<0.01	0.00	0.01	0.00	0	0	0.90
R14	67.24	0.61	15.48	2.50	0.07	2.40	3.26	4.13	3.22	0.16	0	0.01	0.04	0.03	0.10	0.00	0.00	<0.01	0.00	0.02	0.00	0	0	0.88
R15	67.64	0.55	14.96	2.28	0.07	2.35	1.82	3.63	3.83	0.14	0	0.02	0.03	0.03	0.08	0.00	0.00	<0.01	0.00	0.02	0.00	0	0	2.22
R16	66.96	0.47	15.69	2.13	0.06	2.27	3.18	4.27	2.91	0.18	0	<0.01	0.06	<0.02	0.12	0.00	0.00	<0.01	0.00	0.01	0.00	0	0	1.09
R17	66.67	0.45	15.25	2.11	0.06	2.20	2.95	4.04	3.13	0.18	0	0.01	0.04	0.02	0.11	0.00	0.00	<0.01	0.00	0.01	0.00	0	0	1.03
R18	67.54	0.56	15.19	2.44	0.06	2.49	2.77	3.71	3.65	0.14	0	0.02	0.04	0.03	0.11	0.00	0.00	<0.01	0.00	0.01	0.00	0	0	1.13
R19	65.34	0.73	15.20	2.89	0.08	3.14	3.35	3.82	3.58	0.18	0	0.02	0.04	0.04	0.10	0.01	0.00	<0.01	0.00	0.02	0.00	0.1	0	0.93
R20	63.88	0.79	15.51	3.19	0.09	3.65	4.19	3.86	3.37	0.23	0	0.02	0.06	0.03	0.11	0.01	0.00	<0.01	0.00	0.02	0.00	0.2	0	0.83
R21	60.77	0.85	15.96	3.68	0.10	4.55	5.32	4.03	2.37	0.25	0	0.03	0.07	0.03	0.10	0.01	0.00	<0.01	0.00	0.02	0.00	0	0	0.80
R22	65.70	0.64	15.30	2.62	0.07	2.61	3.33	3.98	3.05	0.16	0	0.02	0.04	0.03	0.09	0.00	0.00	<0.01	0.00	0.02	0.00	0	0	0.89

Appendix 2A: Major and trace element geochemistry results (see fig. 4.6 for sample locations)

	XRFS	XRFS	XRFS	XRFS	XRFS	XRFS	XRFS	XRFS	XRFS	XRFS	XRFS	XRFS	XRFS	XRFS	XRFS	XRFS	XRFS	XRFS	XRFS	XRFS	XRFS	XRFS	XRFS	LOI
Sample name	SiO_2	TiO_2	Al_2O_3	Recalc FeO	Mn_3O_4	MgO	CaO	Na_2O	K_2O	P_2O_5	SO_3	Cr_2O_3	SrO	ZrO_2	BaO	NiO	CuO	ZnO	PbO	V_2O_5	HfO_2	F	Cl	LOI
	%	%	%	%	%	%	%	%	%	%	%	%	%	%	%	%	%	%	%	%	%	%	%	%
R23	58.62	1.19	16.39	4.84	0.10	4.59	4.75	3.10	3.03	0.43	0	0.02	0.08	0.05	0.10	0.01	0.00	0.01	0.00	0.03	0.00	0	0	1.17
R24	60.19	1.16	16.03	3.85	0.09	2.90	3.48	3.96	5.23	0.43	0	0.01	0.06	0.11	0.14	0.00	0.00	<0.01	0.01	0.02	0.00	0	0	0.89
R26	60.91	0.91	15.67	3.74	0.10	4.76	4.98	3.75	2.70	0.25	0	0.03	0.06	0.03	0.08	0.01	0.00	0.01	0.00	0.02	0.00	0	0	0.80
R27	53.50	1.36	15.47	5.31	0.14	6.30	6.23	3.23	4.72	0.86	0	0.03	0.16	0.06	0.33	0.02	0.00	0.01	0.00	0.03	0.00	0	0	0.84
R28	66.95	0.34	16.91	1.39	0.03	1.63	1.76	4.85	3.40	0.12	0	<0.01	0.09	<0.02	0.14	0.00	0.00	<0.01	0.00	<0.01	0.00	0	0	1.59
R29	67.28	0.52	15.82	2.30	0.05	2.64	2.73	3.99	2.99	0.18	0	0.01	0.05	0.02	0.10	0.00	0.03	<0.01	0.00	0.02	0.00	0	0	1.24
N22A/B	66.59	0.50	15.74	2.19	0.07	1.70	3.18	4.27	3.05	0.17	0	<0.01	0.04	0.02	0.08	0.00	0.00	<0.01	0.00	0.01	0.00	0	0	0.98
N22C	67.07	0.50	15.52	2.19	0.07	1.77	2.61	4.08	3.28	0.17	0	<0.01	0.03	0.02	0.08	0.00	0.00	<0.01	0.00	0.01	0.00	0	0	1.17
N23 (2 pieces)	65.77	0.64	15.31	2.52	0.09	2.13	2.77	3.74	3.83	0.22	0	0.01	0.04	0.02	0.09	0.00	0.00	<0.01	0.00	0.02	0.00	0	0	1.24
N24 (2 pieces)	66.81	0.70	15.50	2.70	0.09	2.00	3.43	4.03	3.03	0.23	0	<0.01	0.04	0.03	0.07	0.00	0.00	<0.01	0.00	0.02	0.00	0	0	1.06
C12B	68.14	0.52	14.86	2.10	0.07	1.65	3.08	3.81	3.71	0.22	0	0.01	0.05	0.02	0.08	0.00	0.00	<0.01	0.00	0.01	0.00	0	0	1.37
C13	65.02	0.65	15.17	2.42	0.08	1.90	3.56	4.20	3.66	0.30	0	<0.01	0.05	0.03	0.10	0.00	0.00	<0.01	0.00	0.01	0.00	0	0	1.48
NC14	72.43	0.21	14.80	0.91	0.04	0.55	2.00	3.94	4.55	0.11	0	<0.01	0.02	<0.02	0.09	0.00	0.00	<0.01	0.00	<0.01	0.00	0	0	0.80
NC15	59.95	1.21	15.72	3.70	0.09	3.09	4.83	3.97	3.39	0.77	0	<0.01	0.10	0.04	0.15	0.00	0.00	0.01	0.00	0.02	0.00	0	0	1.06
NC16	66.87	0.72	15.49	2.42	0.07	1.81	3.34	4.15	3.48	0.42	0	0.01	0.07	0.03	0.11	0.00	0.00	0.01	0.00	0.01	0.00	0	0	0.77
N25	65.49	0.63	16.59	2.68	0.08	2.18	3.44	4.22	2.78	0.22	0	<0.01	0.04	0.03	0.07	0.00	0.00	<0.01	0.00	0.02	0.00	0	0	0.93
N26	69.68	0.39	15.36	1.71	0.05	1.23	1.60	3.91	3.77	0.12	0	<0.01	0.03	<0.02	0.08	0.00	0.00	<0.01	0.00	<0.01	0.00	0	0	1.13
N27	70.90	0.36	15.11	1.65	0.06	1.22	1.07	3.88	4.50	0.19	0	<0.01	0.01	0.02	0.09	0.00	0.00	<0.01	0.00	<0.01	0.00	0	0	1.07
N27B	72.14	0.25	14.34	1.04	0.04	0.70	0.83	3.83	4.40	0.11	0	<0.01	0.01	<0.02	0.07	0.00	0.00	<0.01	0.00	<0.01	0.00	0	0	1.17
N28	66.74	0.66	16.00	2.69	0.09	2.07	2.74	4.21	3.12	0.20	0	<0.01	0.04	0.03	0.08	0.00	0.00	<0.01	0.00	0.01	0.00	0	0	1.30
N29	65.31	0.64	15.48	2.58	0.09	2.01	2.52	3.82	3.65	0.21	0	<0.01	0.04	0.02	0.09	0.00	0.00	<0.01	0.00	0.01	0.00	0	0	1.32
N30	63.27	0.86	15.82	3.28	0.10	2.79	3.51	3.57	3.04	0.21	0	0.01	0.04	0.02	0.07	0.00	0.00	<0.01	0.00	0.02	0.00	0	0	1.26
N30B	69.54	0.37	15.08	1.66	0.06	1.32	1.47	3.90	3.86	0.11	0	<0.01	0.03	<0.02	0.08	0.00	0.00	<0.01	0.00	<0.01	0.00	0	0	0.83
N31	69.56	0.37	15.07	1.66	0.06	1.31	1.47	3.96	3.87	0.12	0	<0.01	0.02	<0.02	0.09	0.00	0.00	<0.01	0.00	0.01	0.00	0	0	1.10
C19	68.66	0.47	16.00	1.76	0.06	1.17	1.71	4.02	4.39	0.15	0	<0.01	0.02	0.02	0.09	0.00	0.00	<0.01	0.00	0.01	0.00	0	0	1.44
C20	68.91	0.43	15.55	1.96	0.06	1.44	2.41	4.13	3.41	0.13	0	<0.01	0.03	0.02	0.08	0.00	0.00	<0.01	0.00	0.01	0.00	0	0	0.92
C21	70.57	0.34	13.60	2.25	0.07	0.12	1.15	3.54	5.81	0.05	0	<0.01	<0.01	0.08	0.10	0.00	0.00	0.01	0.00	<0.01	0.00	0	0	0.79
C26	67.13	0.66	15.43	2.35	0.05	1.62	1.25	4.29	3.32	0.22	0	<0.01	0.03	0.03	0.09	0.00	0.00	0.01	0.00	0.01	0.00	0	0	2.24
T1	66.35	0.49	16.02	1.99	0.05	1.54	3.22	4.22	3.14	0.21	0	<0.01	0.06	0.02	0.12	0.00	0.00	<0.01	0.00	0.01	0.00	0	0	0.74
T2	66.40	0.48	15.97	2.24	0.06	2.04	3.68	4.44	2.54	0.16	0	0.01	0.05	0.02	0.07	0.00	0.00	<0.01	0.00	0.02	0.00	0	0	0.71
T2B	68.01	0.37	15.72	1.80	0.06	1.50	2.15	4.27	3.09	0.12	0	<0.01	0.04	<0.02	0.09	0.00	0.00	<0.01	0.00	<0.01	0.00	0	0	0.95
T3	67.91	0.42	15.79	1.95	0.05	1.04	2.20	4.30	3.63	0.22	0	<0.01	0.03	0.03	0.09	0.00	0.00	0.03	0.00	0.01	0.00	0	0	1.13
T4	66.30	0.47	15.68	2.23	0.07	2.42	0.51	4.92	3.10	0.15	0	0.01	0.02	0.02	0.06	0.00	0.00	<0.01	0.00	0.01	0.00	0	0	2.19
T4B	67.15	0.44	16.18	2.13	0.07	1.90	1.71	3.78	3.56	0.15	0	0.01	0.05	0.02	0.11	0.00	0.00	<0.01	0.00	0.01	0.00	0	0	1.62
T5	67.61	0.40	15.46	1.85	0.04	1.50	2.21	3.95	3.25	0.14	0	<0.01	0.03	<0.02	0.09	0.00	0.00	<0.01	0.00	0.01	0.00	0	0	1.66
T5B	67.68	0.40	15.56	1.86	0.05	1.65	2.60	4.01	3.29	0.14	0	<0.01	0.03	0.02	0.10	0.00	0.00	<0.01	0.00	<0.01	0.00	0	0	1.42
MRC 363	52.44	1.28	14.10	5.54	0.14	6.59	7.02	3.04	4.59	0.88	0	0.03	0.18	0.04	0.34	0.02	0.01	0.01	0.00	0.04	0.00	0	0	0.67
MRC 364	60.28	0.87	15.62	3.64	0.11	4.38	4.42	3.70	3.34	0.29	0	0.03	0.08	0.04	0.13	0.01	0.00	<0.01	0.00	0.02	0.00	0.1	0	1.16
MRC 365	64.40	0.70	15.08	2.68	0.06	2.86	3.72	3.90	3.33	0.19	0	0.01	0.05	0.04	0.10	0.00	0.00	<0.01	0.00	0.01	0.00	0	0	0.98
MRC 366	64.42	0.56	16.47	2.54	0.07	2.67	4.01	4.58	2.13	0.20	0	0.01	0.06	<0.02	0.08	0.00	0.00	<0.01	0.00	0.02	0.00	0	0	1.04
MRC 367	67.02	0.45	16.30	1.87	0.06	1.79	3.05	4.41	2.97	0.16	0	<0.01	0.05	<0.02	0.09	0.00	0.00	<0.01	0.00	0.01	0.00	0	0	0.76
MRC 368	65.76	0.45	16.18	2.07	0.06	1.88	3.50	4.61	2.25	0.18	0	<0.01	0.05	0.02	0.08	0.00	0.00	<0.01	0.00	0.01	0.00	0	0	0.79
MRC 369	66.52	0.46	15.63	2.05	0.06	1.65	2.80	4.14	3.07	0.14	0	<0.01	0.04	0.02	0.08	0.00	0.00	<0.01	0.00	0.01	0.00	0	0	1.17
MRC 370	69.18	0.38	15.40	1.69	0.05	1.25	1.89	4.05	3.32	0.13	0	<0.01	0.03	<0.02	0.08	0.00	0.00	0.01	0.00	0.01	0.00	0	0	1.39
MRC 371	67.33	0.54	15.48	2.13	0.07	1.52	3.03	4.12	3.39	0.16	0	<0.01	0.03	0.02	0.08	0.00	0.00	<0.01	0.00	0.01	0.00	0	0	0.89
MRC 372	69.94	0.28	15.10	1.18	0.05	0.78	1.46	3.92	4.36	0.13	0	<0.01	0.01	0.02	0.08	0.00	0.00	<0.01	0.00	<0.01	0.00	0	0	1.16
MRC 437	67.01	0.48	15.97	2.06	0.05	1.63	3.34	4.41	2.71	0.17	0	0.01	0.05	<0.02	0.10	0.00	0.00	<0.01	0.00	0.01	0.00	0	0	0.83
MRC 438	66.97	0.43	15.77	2.01	0.05	2.18	2.68	4.11	3.26	0.16	0	0.01	0.05	<0.02	0.11	0.00	0.00	<0.01	0.00	0.01	0.00	0	0	1.44
MRC 439	61.17	0.80	15.52	3.36	0.09	4.03	4.27	3.80	3.59	0.26	0	0.02	0.07	0.04	0.12	0.01	0.00	<0.01	0.00	0.02	0.00	0	0	0.82
MRC 440	67.22	0.46	15.85	2.01	0.06	1.70	2.91	4.13	3.02	0.14	0	<0.01	0.04	0.02	0.08	0.00	0.00	<0.01	0.00	0.01	0.00	0	0	0.85
MRC 441	67.36	0.41	15.78	1.87	0.06	1.75	2.84	4.04	3.51	0.15	0	<0.01	0.05	<0.02	0.13	0.00	0.00	<0.01	0.00	0.01	0.00	0	0	0.79
MRC 442	67.57	0.46	16.03	1.96	0.06	1.58	2.87	4.40	2.75	0.14	0	<0.01	0.04	0.02	0.07	0.00	0.00	<0.01	0.00	0.01	0.00	0	0	1.05
MRC 443	67.06	0.48	15.73	2.11	0.06	1.93	2.45	3.96	3.69	0.18	0	0.01	0.05	0.02	0.12	0.00	0.00	<0.01	0.00	0.01	0.00	0	0	1.13
MRC 444	67.11	0.46	15.88	2.07	0.07	1.71	2.95	4.06	3.13	0.14	0	<0.01	0.04	0.02	0.08	0.00	0.00	<0.01	0.00	0.01	0.00	0	0	0.70
MRC 445	66.48	0.44	15.79	1.99	0.05	1.64	2.89	4.14	3.21	0.16	0	<0.01	0.05	0.02	0.11	0.00	0.00	<0.01	0.00	<0.01	0.00	0	0	0.75
MRC 447	67.01	0.51	15.55	2.19	0.07	1.41	2.35	4.37	3.67	0.22	0	<0.01	0.03	0.03	0.08	0.00	0.00	<0.01	0.00	0.01	0.00	0	0	0.91
MRC 448	64.90	0.71	15.61	2.70	0.09	2.19	3.49	4.43	3.31	0.29	0	<0.01	0.06	0.03	0.09	0.00	0.00	<0.01	0.00	0.02	0.00	0	0	0.66
MRC 449	64.27	0.73	15.60	2.72	0.08	2.18	3.61	4.10	3.39	0.29	0	<0.01	0.06	0.03	0.11	0.00	0.00	<0.01	0.00	0.02	0.00	0	0	0.97
MRC 450	63.79	0.70	15.83	2.84	0.09	2.31	3.74	4.29	3.29	0.30	0	<0.01	0.06	0.03	0.11	0.00	0.00	<0.01	0.00	0.02	0.00	0	0	0.97
MRC 452	64.12	0.72	15.59	2.78	0.08	2.25	3.85	4.28	3.28	0.32	0	<0.01	0.07	0.03	0.09	0.00	0.00	<0.01	0.00	0.02	0.00	0	0	0.56
MRC 453	64.63	0.68	16.45	2.63	0.08	2.08	2.81	4.06	3.57	0.24	0	<0.01	0.05	0.03	0.08	0.00	0.00	<0.01	0.00	0.02	0.00	0	0	1.25
MRC 454	63.69	0.75	15.68	2.86	0.08	2.41	3.55	4.16	3.33	0.35	0	<0.01	0.07	0.03	0.10	0.00	0.00	<0.01	0.00	0.01	0.00	0	0	1.14
MRC 455	56.95	0.75	13.97	3.56	0.10	5.50	5.36	3.43	1.90	0.25	0	0.04	0.02	<0.02	0.07	0.02	0.00	<0.01	0.00	0.02	0.00	0	0	6.28

Appendix 2B: Trace element geochemistry results (see fig. 4.6 for sample locations)

	ICP-MS Li	ICP-MS Be	ICP-MS B	ICP-MS P	ICP-MS Ti	ICP-MS V	ICP-MS Cr	ICP-MS Mn	ICP-MS Co	ICP-MS Ni	ICP-MS Cu	ICP-MS Zn	ICP-MS Ga	ICP-MS As	ICP-MS Se	ICP-MS Rb	ICP-MS Sr
	mg/kg	mg/kg	mg/kg	mg/kg	mg/kg	mg/kg	mg/kg	mg/kg	mg/kg	mg/kg	mg/kg	mg/kg	mg/kg	mg/kg	mg/kg	mg/kg	mg/kg
Detection Limit:	2	0.4	30	100	50	3	2	6	0.1	5	2	6	1	0.2	4	0.4	4
Sample name																	
S2	28	2.2	<30	3883	11083	240	253	1124	41.7	169	52	98	18	3.6	0	101.6	1435
S3	12	0.6	<30	5789	16155	356	583	1247	61.7	294	10	103	14	2.2	7	139.3	318
S4	13	2.8	<30	4576	8998	207	196	993	33.9	113	92	89	15	<0.2	0	121.6	1921
S6	25	1.5	<30	5905	13962	324	401	1389	59.8	253	61	106	11	3.0	0	100.7	839
S7	26	6.6	<30	2388	6072	137	106	727	22.7	78	68	76	20	11.1	0	157.8	1079
S8	25	2.0	<30	5945	12241	247	129	1150	46.5	116	212	126	19	6.8	0	128.6	1617
S9	36	1.3	<30	4355	9833	228	426	1297	48.0	225	245	128	11	2.5	4	86.0	1252
S11	29	3.0	<30	3886	11240	245	255	1168	42.3	169	102	101	17	3.3	0	112.9	1459
S16	26	2.8	<30	1772	6119	132	212	809	25.3	135	39	68	19	1.9	0	95.0	773
S17	26	3.9	<30	3656	7012	146	203	775	29.2	127	77	76	17	2.7	0	125.9	1274
S19	23	6.1	<30	2503	4449	137	194	1109	24.5	106	165	71	16	2.1	0	77.9	911
S21	23	5.4	<30	3027	6253	138	108	759	23.6	72	74	76	18	7.1	4	155.6	1403
S22	18	2.5	<30	273	1445	23	28	232	3.9	9	8	22	12	2.9	0	106.4	373
S24	24	3.9	<30	2989	5452	127	122	622	24.3	87	83	74	18	5.6	0	130.5	1258
S25	24	5.4	<30	2604	5565	118	94	770	21.4	68	37	70	19	9.2	0	155.2	1340
S26	17	5.6	<30	1128	3432	73	45	305	7.0	19	117	39	21	4.0	0	146.9	1268
S28B	22	5.5	<30	3226	7583	169	163	909	28.4	112	26	84	20	1.7	0	113.1	1420
S30	15	3.2	<30	3806	8023	186	239	967	33.0	131	85	85	17	2.1	0	148.6	1408
S32	15	3.4	<30	2791	4366	111	106	841	25.0	93	49	76	17	2.4	0	72.8	1118
S34	41	1.4	33	2285	6229	218	366	1681	44.3	194	138	135	21	1.8	0	56.3	882
S35	35	11.2	38	3315	7090	111	55	790	20.9	48	92	90	19	16.9	0	236.5	1079
S38	17	5.7	<30	2911	6988	158	259	858	31.4	158	68	75	15	7.9	0	173.1	1321
S39	18	4.6	<30	2828	5189	137	219	958	34.1	157	78	85	17	4.0	0	67.3	1309
S40	17	2.6	<30	2418	5219	113	158	770	26.5	124	89	72	20	2.8	0	116.7	1174
S41	18	4.0	<30	2183	5066	120	153	842	28.7	122	69	73	16	5.1	0	98.2	1135
R1B	32	2.7	<30	788	4389	90	107	531	15.1	63	21	49	17	13.0	0	154.2	508
R4B	56	2.6	<30	673	2964	56	36	380	8.9	17	9	56	16	1.3	0	117.2	339
N1A	52	3.0	<30	824	4416	82	47	655	12.3	24	20	59	18	0.3	0	104.2	529
C1	44	5.4	<30	469	1534	25	19	312	3.6	<5	9	43	22	1.0	0	150.4	231
C2D	57	3.2	<30	1660	3802	69	37	638	11.0	21	17	73	18	0.5	0	92.3	500
NTS1	5	2.3	<30	<100	388	3	23	96	0.4	<5	<2	16	14	0.5	0	140.5	42
C3A	90	5.0	<30	1114	2828	42	37	614	8.9	20	2	88	23	0.5	0	206.7	297
C3C	35	3.5	<30	321	1194	20	13	378	2.8	<5	4	42	19	0.2	0	209.0	148
R3A	24	1.7	<30	400	1444	23	21	157	4.2	11	3	14	15	1.5	0	115.8	341
R5A	27	2.6	<30	1202	5194	113	165	693	20.8	103	10	58	16	3.7	0	105.2	643
N5C	48	2.7	<30	811	3700	62	34	553	9.6	16	13	55	18	0.3	0	95.0	375
N7	55	2.3	<30	955	3395	56	25	523	8.9	16	14	50	17	0.8	0	94.5	399
N8	53	2.8	<30	1067	4156	69	34	594	11.4	21	16	59	17	1.2	0	87.0	449
N9	63	2.5	<30	1517	5329	85	38	786	13.1	23	25	66	18	1.1	0	116.2	463
N10	51	2.6	<30	920	3877	68	38	644	10.8	20	14	63	17	0.6	0	93.1	453
C5	59	2.6	<30	523	2084	30	36	371	4.4	6	8	42	17	<0.2	0	106.9	314
C6	65	2.1	<30	486	2090	30	34	355	4.5	7	4	44	17	0.2	0	111.7	312
C7	55	2.2	<30	641	2139	30	24	342	4.2	6	14	40	18	0.5	0	104.4	315
C8	31	2.6	<30	638	2142	45	32	433	6.8	14	9	44	19	0.2	0	107.7	253
N11A	43	2.4	<30	611	3075	58	29	352	7.9	14	15	47	18	1.7	0	109.9	400
N12	68	2.7	32	956	3779	67	37	600	9.7	18	13	55	18	0.7	0	120.7	449
N13	64	2.8	<30	1119	3852	74	61	634	10.7	19	15	57	18	0.7	0	100.5	427
N14	63	2.3	<30	866	4085	71	42	643	10.8	21	19	54	18	0.3	0	101.1	463
N15	50	2.6	<30	1049	4063	77	40	605	11.0	22	21	58	17	1.6	0	86.3	437
N16A	53	2.6	<30	854	3627	65	46	570	9.6	17	15	53	19	1.0	0	91.8	388
N16C	50	2.0	<30	1011	3225	65	55	546	9.2	17	19	51	18	1.2	0	100.5	392
N17	48	2.8	<30	974	3672	71	42	569	10.0	18	16	52	18	0.9	0	95.0	432
R7A	63	2.0	<30	861	3254	66	39	488	9.5	20	14	49	17	0.9	0	90.1	384
N18	64	2.3	<30	931	3169	58	44	467	8.2	12	14	50	17	1.2	0	94.6	400
N19	61	2.3	<30	878	2853	56	34	440	7.5	14	8	46	18	1.0	0	103.3	415
R9	54	2.8	<30	577	3069	69	75	526	11.5	43	4	49	16	0.3	0	100.9	496
N20	63	2.7	33	952	2915	54	26	500	7.6	10	12	62	18	1.1	0	107.6	359
N20C	70	3.2	<30	739	2849	56	67	497	8.8	16	16	54	18	0.8	0	111.0	341
N21A	79	3.2	42	638	2833	55	29	442	7.9	13	12	52	16	0.7	0	98.3	391
C9	64	4.1	<30	5183	11292	181	181	1075	28.5	45	89	97	22	<0.2	0	128.8	985
C11	74	3.9	<30	1242	1869	31	18	193	3.7	7	5	40	18	0.2	0	109.2	186
C11B	51	3.3	<30	931	1772	32	23	308	4.8	6	6	48	18	0.2	0	149.8	256
C11C	43	4.4	<30	372	1539	27	29	280	3.7	<5	8	47	21	0.8	0	159.8	198
C11D	22	3.6	<30	251	1049	16	31	184	2.0	<5	5	25	15	0.4	0	179.6	64
C11E	53	4.3	<30	267	1306	19	13	253	3.0	<5	6	41	16	0.3	0	146.3	150
C11F	77	4.6	<30	370	1143	18	16	272	2.7	<5	5	36	19	0.3	0	181.1	131

Appendix 2B: Trace element geochemistry results (see fig. 4.6 for sample locations)

	ICP-MS Li	ICP-MS Be	ICP-MS B	ICP-MS P	ICP-MS Ti	ICP-MS V	ICP-MS Cr	ICP-MS Mn	ICP-MS Co	ICP-MS Ni	ICP-MS Cu	ICP-MS Zn	ICP-MS Ga	ICP-MS As	ICP-MS Se	ICP-MS Rb	ICP-MS Sr
	mg/kg	mg/kg	mg/kg	mg/kg	mg/kg	mg/kg	mg/kg	mg/kg	mg/kg	mg/kg	mg/kg	mg/kg	mg/kg	mg/kg	mg/kg	mg/kg	mg/kg
Detection Limit:	2	0.4	30	100	50	3	2	6	0.1	5	2	6	1	0.2	4	0.4	4
Sample name																	
R10	42	3.5	<30	689	4307	87	106	525	13.7	56	19	44	14	5.8	0	141.0	449
R11	44	2.9	35	916	4402	90	124	591	14.5	61	21	47	16	6.6	0	136.6	468
R12	40	3.5	37	713	3700	74	93	536	12.6	49	13	44	18	0.8	0	143.2	488
R13	54	2.1	<30	765	3549	75	93	492	11.7	46	10	41	14	1.0	0	137.4	416
R14	41	2.5	<30	902	3468	70	77	510	11.7	42	10	44	16	1.5	0	123.0	414
R15	58	2.2	<30	614	3324	70	97	485	11.1	43	6	55	18	0.7	0	128.0	336
R16	43	2.4	<30	907	2825	64	73	412	10.9	42	13	46	16	1.5	0	88.3	543
R17	40	2.4	<30	787	2718	64	84	432	10.6	41	21	45	16	1.7	0	99.8	489
R18	31	2.2	<30	583	3244	70	89	431	12.0	48	9	41	15	1.3	0	121.4	405
R19	33	2.9	<30	805	4307	91	115	555	14.8	59	25	55	15	4.6	0	143.7	419
R20	27	2.0	<30	904	4678	104	125	596	17.5	70	17	53	16	2.6	0	118.7	526
R21	23	1.7	<30	1257	4996	116	170	684	21.1	96	3	61	17	5.3	0	73.6	617
R22	31	2.8	<30	735	3735	75	86	485	12.9	51	14	50	16	2.4	0	117.9	397
R23	42	4.7	<30	1757	7318	179	155	748	27.1	91	77	83	21	2.1	0	127.7	722
R24	39	7.5	44	2104	6955	126	84	643	16.5	52	58	70	20	10.1	0	278.9	588
R26	33	2.8	<30	1158	5426	118	179	700	22.9	96	40	96	17	7.9	0	111.7	564
R27	28	3.8	<30	3647	8181	188	216	981	31.1	125	29	88	18	2.3	0	137.0	1373
R28	28	3.4	<30	479	2146	48	50	272	7.7	33	3	22	17	1.3	0	112.7	827
R29	40	2.8	<30	827	3245	74	78	337	13.7	49	258	30	18	0.5	4	125.8	562
N22A/B	34	2.2	<30	747	2985	61	49	474	9.4	21	9	53	19	<0.2	0	100.1	440
N22C	42	2.4	<30	795	2956	57	46	479	9.4	22	12	52	17	0.8	0	104.6	353
N23 (2 pieces)	45	2.5	<30	829	4020	73	62	612	11.1	20	19	55	18	0.8	0	103.8	433
N24 (2 pieces)	43	2.8	<30	1032	4254	76	55	620	12.0	22	27	58	17	0.5	0	100.9	439
C12B	53	4.0	<30	993	3228	61	66	455	9.7	26	14	51	15	0.4	0	134.3	562
C13	42	3.4	<30	1107	3952	70	51	549	10.6	25	6	57	19	0.5	0	128.6	499
NC14	26	4.1	<30	633	1318	24	30	241	3.3	5	3	32	19	<0.2	0	161.3	309
NC15	64	2.8	<30	3298	7152	106	72	652	16.4	46	36	84	17	<0.2	0	105.0	916
NC16	57	3.3	<30	1793	4268	63	51	513	10.2	27	39	68	18	<0.2	0	138.2	604
N25	64	2.7	<30	685	3856	78	55	515	11.4	22	28	65	19	0.7	0	99.7	477
N26	41	2.8	<30	530	2262	45	43	319	6.5	13	14	40	17	0.6	0	117.9	301
N27	44	3.8	<30	801	2165	36	29	380	5.5	9	5	61	19	<0.2	0	174.7	244
N27B	36	4.6	<30	805	1598	27	26	264	4.3	6	26	38	19	<0.2	0	195.1	199
N28	62	2.0	<30	887	3894	72	45	620	11.6	21	59	66	17	0.2	0	97.2	427
N29	68	2.9	<30	923	4049	76	51	662	12.0	22	16	63	17	0.8	0	119.9	463
N30	70	2.2	<30	986	5180	109	64	645	17.1	35	20	62	18	0.4	0	107.5	430
N30B	47	2.1	<30	732	4352	78	53	528	11.5	22	14	55	15	0.7	0	96.2	471
N31	44	3.4	<30	466	2289	44	36	400	6.9	12	5	45	16	<0.2	0	120.9	324
C19	31	2.1	<30	589	2904	51	18	365	7.7	8	6	59	18	0.7	0	133.3	332
C20	52	2.6	<30	534	2526	51	38	397	7.9	16	9	49	17	0.5	0	118.4	355
C21	13	3.1	<30	294	2148	7	21	516	1.2	<5	4	79	24	0.5	0	193.7	57
C26	48	3.5	<30	1057	3857	68	46	348	9.5	20	3	103	19	1.6	0	132.7	353
T1	44	2.6	<30	783	3048	56	32	390	8.7	21	20	46	18	1.4	0	113.8	618
T2	22	2.0	<30	750	2794	62	68	379	10.9	34	21	53	18	0.9	0	78.8	443
T2B	43	3.9	<30	592	2415	55	47	465	8.8	25	17	60	20	2.3	0	122.1	441
T3	33	2.7	<30	1261	2869	49	24	444	8.7	14	28	269	19	2.0	0	150.4	413
T4	63	1.2	<30	623	3012	63	71	530	9.5	37	4	40	17	2.9	0	92.1	288
T4B	32	1.7	<30	602	2842	60	67	486	10.5	39	4	57	20	1.0	0	115.7	537
T5	29	2.6	<30	529	2445	50	46	319	8.8	28	46	47	18	3.7	0	101.4	387
T5B	26	2.2	<30	465	2388	48	33	358	8.7	27	33	73	15	1.3	0	110.6	363
MRC 364	23	3.4	<30	1164	5172	111	147	696	20.2	104	18	67	16	1.5	0	121.4	666
MRC 365	31	2.5	36	730	4300	90	101	425	14.5	65	18	52	15	7.1	0	140.7	497
MRC 366	44	2.9	<30	978	3287	72	79	474	12.7	60	18	54	17	0.8	0	82.7	543
MRC 367	52	3.1	<30	703	2721	54	41	383	9.0	32	6	47	18	1.0	0	115.6	485
MRC 368	63	3.4	<30	788	2874	62	42	429	10.1	32	8	54	18	1.0	0	102.1	546
MRC 369	58	3.1	<30	895	3041	63	41	476	9.6	24	9	57	19	0.5	0	125.3	460
MRC 370	50	3.3	<30	639	3505	63	35	543	9.5	21	12	57	18	0.8	0	118.4	411
MRC 371	64	5.0	36	534	1724	31	21	369	4.3	7	10	55	20	0.3	0	186.2	256
MRC 372	53	4.3	32	594	2466	50	28	372	6.6	21	33	97	20	2.2	0	130.3	373
MRC 437	45	3.2	<30	753	2825	57	34	375	8.6	23	6	54	18	0.3	0	91.1	506
MRC 438	46	2.1	37	745	2540	53	66	358	9.3	38	10	47	16	1.1	0	106.1	476
MRC 439	34	2.7	49	958	4890	104	138	674	19.3	88	21	57	16	2.9	0	136.3	649
MRC 440	66	3.2	<30	578	2734	55	37	446	8.4	20	47	53	17	0.9	0	108.2	401
MRC 441	46	2.5	<30	756	2447	51	51	379	8.4	28	8	50	18	0.5	0	111.8	500
MRC 442	55	3.7	<30	630	2727	54	25	414	8.0	16	15	48	17	1.8	0	95.3	413
MRC 443	42	2.4	42	808	2858	58	57	387	9.7	32	9	50	17	1.0	0	139.9	508
MRC 444	65	2.7	<30	619	2780	57	33	470	8.3	23	11	51	17	1.0	0	111.4	431

Appendix 2B: Trace element geochemistry results (see fig. 4.6 for sample locations)

	ICP-MS Li mg/kg	ICP-MS Be mg/kg	ICP-MS B mg/kg	ICP-MS P mg/kg	ICP-MS Ti mg/kg	ICP-MS V mg/kg	ICP-MS Cr mg/kg	ICP-MS Mn mg/kg	ICP-MS Co mg/kg	ICP-MS Ni mg/kg	ICP-MS Cu mg/kg	ICP-MS Zn mg/kg	ICP-MS Ga mg/kg	ICP-MS As mg/kg	ICP-MS Se mg/kg	ICP-MS Rb mg/kg	ICP-MS Sr mg/kg
Detection Limit:	2	0.4	30	100	50	3	2	6	0.1	5	2	6	1	0.2	4	0.4	4
Sample name																	
MRC 445	59	1.6	32	665	2688	53	34	366	8.4	25	13	46	17	0.3	0	103.5	500
MRC 447	68	3.7	<30	1025	3075	56	34	494	8.2	21	21	66	19	0.7	0	129.5	343
MRC 448	71	2.1	<30	1183	4497	82	52	642	13.1	33	11	73	21	5.3	0	113.8	599
MRC 449	50	3.1	<30	1285	4284	76	49	567	12.7	39	10	60	17	1.3	0	100.8	618
MRC 450	54	2.5	<30	1311	3950	78	50	609	12.6	29	22	62	17	1.1	0	102.0	553
MRC 452	56	3.1	<30	1409	4466	79	52	576	12.8	33	10	61	19	13.9	0	104.6	643
MRC 453	18	2.2	<30	908	4078	76	38	532	12.1	24	10	49	19	0.8	0	101.2	520
MRC 454	38	2.8	<30	1427	4517	81	54	570	13.2	34	15	67	17	1.0	0	102.0	639
MRC 455	47	1.5	<30	1228	4492	107	263	676	22.9	155	16	66	14	2.0	0	50.9	252

	ICP-MS Y	ICP-MS Zr	ICP-MS Nb	ICP-MS Mo	ICP-MS Ag	ICP-MS Cd	ICP-MS Sn	ICP-MS Sb	ICP-MS Cs	ICP-MS Ba	ICP-MS La	ICP-MS Ce	ICP-MS Pr	ICP-MS Nd	ICP-MS Sm	ICP-MS Eu	ICP-MS Gd
	mg/kg	mg/kg	mg/kg	mg/kg	mg/kg	mg/kg	mg/kg	mg/kg	mg/kg	mg/kg	mg/kg	mg/kg	mg/kg	mg/kg	mg/kg	mg/kg	mg/kg
Detection Limit:	0.1	3	0.1	0.2	0.2	0.1	1	0.1	0.05	5	0.6	4	0.3	1	0.2	0.1	0.1
Sample name																	
S2	34.5	130	27.3	0.6	<0.2	0.1	2	0.6	3.17	1740	64.5	149	20.7	81	14.3	3.3	10.4
S3	25.7	64	13.6	<0.2	<0.2	0.1	<1	0.1	2.80	4016	44.1	109	14.8	66	12.3	2.8	9.2
S4	23.9	60	11.7	0.5	<0.2	0.2	3	<0.1	2.40	3889	59.4	120	15.7	61	10.4	3.3	8.0
S6	31.7	81	11.9	0.3	<0.2	0.1	1	0.2	2.54	3063	54.2	127	17.4	74	13.6	2.9	10.1
S7	21.6	203	21.0	17.7	<0.2	<0.1	3	0.7	8.71	1774	65.8	121	15.1	55	8.9	2.1	6.4
S8	30.6	77	15.9	1.4	<0.2	0.1	4	0.3	4.84	2653	76.7	165	21.2	85	14.1	3.1	10.0
S9	26.4	66	12.3	0.5	<0.2	0.1	2	0.3	3.00	2343	51.4	115	15.8	68	11.7	2.9	8.9
S11	32.5	166	25.8	0.7	<0.2	<0.1	2	0.5	3.41	1935	61.5	144	19.0	78	13.1	3.1	9.8
S16	17.8	232	16.2	0.4	<0.2	<0.1	1	0.3	2.78	1189	56.3	110	12.8	47	6.9	1.9	5.1
S17	21.9	155	14.9	0.8	<0.2	0.1	2	0.2	3.61	2560	67.1	126	15.8	60	10.0	2.6	7.2
S19	29.5	160	9.3	1.1	<0.2	0.1	2	0.1	2.38	1248	55.3	112	14.9	58	10.3	2.3	8.3
S21	22.0	243	17.7	2.9	<0.2	0.1	2	0.5	7.26	2354	58.1	118	14.3	53	9.2	2.4	6.5
S22	8.1	82	8.5	0.3	<0.2	<0.1	<1	0.5	3.09	941	18.3	40	3.6	12	2.0	0.6	1.6
S24	19.4	238	12.9	1.7	<0.2	0.1	2	0.3	5.49	2090	49.8	92	11.8	45	7.5	2.0	5.6
S25	20.6	222	14.4	2.1	<0.2	<0.1	2	0.6	8.02	2231	56.2	103	13.6	49	8.4	2.2	6.3
S26	17.5	462	18.7	0.6	0.2	<0.1	2	0.2	6.20	2103	48.5	94	10.1	35	5.7	1.9	4.3
S28B	23.4	218	19.2	0.5	<0.2	0.1	3	0.1	3.29	1989	71.7	138	17.3	64	10.4	2.5	7.5
S30	23.1	151	17.1	0.4	<0.2	0.1	2	<0.1	3.73	2836	59.6	117	15.0	57	9.8	2.5	7.5
S32	21.4	75	8.9	0.6	<0.2	<0.1	1	<0.1	1.85	1571	54.4	100	13.2	49	8.0	2.1	6.1
S34	23.0	113	10.2	1.0	<0.2	<0.1	<1	0.1	3.13	587	41.2	83	10.4	41	7.8	2.5	5.8
S35	26.6	608	32.9	1.4	<0.2	<0.1	5	0.9	15.63	1942	70.4	154	17.1	63	10.5	2.3	7.5
S38	21.7	212	15.5	1.8	<0.2	0.1	3	0.4	7.84	2544	55.6	114	13.4	53	9.0	2.4	6.8
S39	21.7	120	8.6	0.9	<0.2	<0.1	1	0.1	2.71	1349	54.0	103	13.5	52	8.5	2.0	6.4
S40	20.5	170	11.0	0.7	<0.2	0.1	1	0.2	3.12	1660	52.4	99	12.5	46	7.5	2.0	5.8
S41	19.7	116	9.9	1.1	<0.2	<0.1	1	0.2	4.31	1549	51.9	102	12.5	47	7.7	2.0	5.7
R1B	18.1	45	15.1	3.9	<0.2	<0.1	2	0.6	7.54	852	46.7	87	10.2	37	5.7	1.2	4.5
R4B	8.9	79	7.4	<0.2	<0.2	<0.1	2	0.2	6.31	675	23.1	41	4.6	15	3.0	0.8	2.4
N1A	14.7	42	10.7	2.3	<0.2	<0.1	2	<0.1	4.62	718	40.4	72	7.9	28	4.9	1.2	3.9
C1	9.1	62	9.5	<0.2	<0.2	0.1	4	0.1	4.12	658	23.7	42	4.6	17	2.8	0.7	2.3
C2D	14.0	61	10.6	0.2	<0.2	<0.1	3	<0.1	2.45	631	45.2	77	8.8	31	5.4	1.2	4.1
NTS1	2.5	49	3.1	0.3	<0.2	<0.1	<1	<0.1	2.21	131	11.1	19	1.8	4	0.7	0.1	0.5
C3A	7.2	88	11.2	<0.2	<0.2	0.2	4	<0.1	3.21	705	30.5	54	5.9	20	3.0	0.8	2.1
C3C	11.4	46	10.4	<0.2	<0.2	0.1	4	<0.1	5.16	484	22.0	39	4.5	16	3.0	0.6	2.5
R3A	7.6	97	6.0	<0.2	<0.2	<0.1	<1	<0.1	3.57	997	25.6	43	4.5	14	2.2	0.6	1.7
R5A	16.6	108	12.7	1.0	<0.2	<0.1	2	0.5	4.83	997	41.2	74	9.2	33	5.6	1.4	4.4
N5C	14.9	70	10.4	0.4	<0.2	<0.1	2	<0.1	3.83	604	40.3	72	7.9	27	4.7	1.1	3.8
N7	12.4	57	9.4	0.2	<0.2	<0.1	2	0.9	3.32	569	26.7	49	5.7	20	3.4	1.0	2.9
N8	16.1	56	11.6	0.5	<0.2	<0.1	3	<0.1	3.38	601	34.6	68	7.8	28	5.1	1.2	4.1
N9	23.3	92	18.6	0.6	<0.2	<0.1	3	0.1	4.48	857	39.8	88	10.3	36	6.2	1.5	5.1
N10	13.9	60	10.8	0.4	<0.2	<0.1	2	<0.1	2.79	635	34.3	66	7.1	25	4.1	1.1	3.3
C5	8.7	77	7.1	0.3	<0.2	<0.1	1	<0.1	4.20	731	28.2	48	5.0	18	2.9	0.8	2.2
C6	8.2	141	6.6	0.3	<0.2	<0.1	1	<0.1	4.29	823	27.5	51	5.1	17	2.6	0.7	2.1
C7	9.1	172	7.8	<0.2	<0.2	<0.1	2	<0.1	3.52	772	26.5	51	4.7	16	2.6	0.7	2.0
C8	12.4	106	11.0	<0.2	<0.2	<0.1	2	<0.1	1.66	615	18.6	36	3.8	14	2.6	0.6	2.6
N11A	8.1	154	6.7	0.4	<0.2	<0.1	1	<0.1	4.71	838	23.6	44	4.6	17	2.6	0.8	2.3
N12	15.3	172	11.2	0.3	<0.2	<0.1	2	0.1	8.22	670	36.3	64	7.8	29	4.8	1.3	3.9
N13	13.6	182	10.1	0.5	<0.2	<0.1	2	<0.1	2.91	601	38.6	74	7.4	25	4.3	1.1	3.4
N14	19.4	160	13.1	0.4	<0.2	0.1	2	<0.1	4.70	712	31.5	71	8.1	31	5.7	1.4	4.8
N15	16.0	161	10.8	0.3	1.0	<0.1	3	<0.1	4.05	626	34.9	70	7.6	27	4.7	1.1	3.9
N16A	16.3	170	11.3	0.4	<0.2	<0.1	2	<0.1	3.45	756	33.1	66	7.1	26	4.6	1.1	3.8
N16C	7.8	148	8.2	0.5	<0.2	<0.1	2	<0.1	3.78	662	30.2	54	5.1	16	2.3	0.8	1.9
N17	14.3	159	9.9	0.8	<0.2	<0.1	1	<0.1	3.86	772	32.1	64	6.7	24	4.1	1.1	3.5
R7A	11.5	129	7.5	<0.2	<0.2	<0.1	2	<0.1	5.25	692	32.3	61	6.1	22	3.6	0.9	2.9
N18	12.5	138	8.2	0.4	<0.2	<0.1	1	<0.1	3.83	647	22.4	45	4.9	17	3.3	0.8	3.0
N19	9.5	141	6.7	0.3	<0.2	<0.1	1	<0.1	3.50	815	31.0	58	5.6	19	3.3	0.9	2.6
R9	9.7	147	6.0	<0.2	<0.2	<0.1	1	<0.1	3.03	844	23.2	48	5.2	20	3.3	0.9	2.7
N20	9.2	159	8.0	<0.2	<0.2	<0.1	1	<0.1	3.93	618	19.1	39	4.1	15	2.8	0.8	2.4
N20C	11.0	156	7.9	0.5	<0.2	<0.1	2	<0.1	3.72	675	25.8	56	5.2	18	3.5	0.9	2.8
N21A	10.5	157	7.8	<0.2	<0.2	<0.1	2	0.1	4.45	688	25.7	52	5.3	19	3.1	0.8	2.6
C9	23.3	359	25.3	1.5	0.3	0.1	3	<0.1	1.65	2286	103.9	232	27.1	101	14.2	3.3	9.2
C11	8.0	146	8.3	<0.2	<0.2	<0.1	3	<0.1	2.21	565	30.6	58	6.1	20	3.3	0.8	2.6
C11B	9.4	144	8.5	<0.2	<0.2	<0.1	3	<0.1	2.87	639	31.7	60	6.0	22	3.7	0.8	2.7
C11C	10.4	129	9.4	0.3	<0.2	<0.1	3	0.1	3.04	548	23.4	44	4.6	16	3.1	0.7	2.5
C11D	15.8	70	6.6	0.3	<0.2	<0.1	3	<0.1	5.18	116	19.1	42	4.7	16	3.6	0.4	3.1
C11E	8.3	96	8.4	<0.2	<0.2	<0.1	4	<0.1	2.57	1193	18.4	35	3.7	14	2.6	0.6	2.2
C11F	8.3	93	8.6	<0.2	<0.2	<0.1	3	<0.1	3.76	441	21.5	41	4.4	15	2.9	0.7	2.3

	ICP-MS Y	ICP-MS Zr	ICP-MS Nb	ICP-MS Mo	ICP-MS Ag	ICP-MS Cd	ICP-MS Sn	ICP-MS Sb	ICP-MS Cs	ICP-MS Ba	ICP-MS La	ICP-MS Ce	ICP-MS Pr	ICP-MS Nd	ICP-MS Sm	ICP-MS Eu	ICP-MS Gd
	mg/kg	mg/kg	mg/kg	mg/kg	mg/kg	mg/kg	mg/kg	mg/kg	mg/kg	mg/kg	mg/kg	mg/kg	mg/kg	mg/kg	mg/kg	mg/kg	mg/kg
Detection Limit:	0.1	3	0.1	0.2	0.2	0.1	1	0.1	0.05	5	0.6	4	0.3	1	0.2	0.1	0.1
Sample name																	
R10	16.5	253	14.6	2.0	<0.2	0.1	2	0.6	6.03	858	45.5	90	9.8	33	5.3	1.2	4.3
R11	17.8	264	14.8	1.5	<0.2	0.1	2	0.6	6.09	911	42.3	89	9.7	34	5.5	1.2	4.4
R12	15.4	214	12.0	0.3	<0.2	<0.1	1	0.1	5.20	857	34.8	77	7.4	26	4.6	1.0	3.7
R13	13.0	217	11.9	0.4	<0.2	<0.1	2	0.1	5.51	866	34.2	70	7.1	27	3.9	0.9	3.5
R14	14.6	181	11.4	1.4	<0.2	<0.1	1	0.1	5.34	813	37.5	70	7.8	26	4.4	1.0	3.5
R15	15.3	202	15.2	1.1	<0.2	<0.1	2	0.2	4.37	675	38.4	74	8.8	30	5.1	0.9	3.6
R16	8.6	132	6.0	0.3	<0.2	<0.1	1	0.2	2.84	977	30.7	52	5.8	21	3.3	1.0	2.5
R17	10.0	131	6.1	0.4	<0.2	<0.1	1	<0.1	4.70	953	27.8	51	5.8	21	3.6	0.8	2.8
R18	12.9	193	11.2	2.4	<0.2	<0.1	2	0.1	4.68	923	29.7	57	6.6	24	4.4	0.9	3.1
R19	16.9	205	14.5	1.2	<0.2	<0.1	2	0.6	6.77	825	41.3	78	9.1	33	5.1	1.1	4.1
R20	17.4	214	13.9	1.3	<0.2	<0.1	2	0.2	4.81	846	42.2	84	9.7	35	5.5	1.2	4.3
R21	14.9	194	10.9	0.7	<0.2	<0.1	1	0.3	3.08	805	36.5	72	8.2	30	5.0	1.4	3.9
R22	14.6	216	12.9	0.4	<0.2	<0.1	1	0.2	4.25	695	30.6	61	7.1	27	4.6	1.0	3.5
R23	23.6	350	18.2	2.6	<0.2	<0.1	2	0.2	8.83	805	48.4	102	12.1	46	7.9	1.8	6.3
R24	27.5	763	38.0	4.4	<0.2	0.1	4	0.8	16.95	1142	72.7	165	17.8	66	10.7	1.7	7.0
R26	17.0	246	13.6	2.3	<0.2	<0.1	2	0.7	7.17	677	38.9	75	9.0	33	5.6	1.3	4.3
R27	23.3	375	17.0	0.6	0.3	<0.1	1	0.2	4.86	2830	60.3	125	14.9	60	10.0	2.5	7.2
R28	5.4	106	4.3	0.9	<0.2	<0.1	<1	<0.1	6.59	1275	20.8	33	3.6	13	2.1	0.7	1.5
R29	9.7	135	6.6	14.8	<0.2	<0.1	<1	<0.1	8.16	939	20.2	40	4.5	16	3.1	0.9	2.6
N22A/B	9.4	137	6.7	0.7	<0.2	<0.1	1	<0.1	3.13	749	25.7	44	5.0	20	3.3	0.9	2.7
N22C	10.9	153	9.4	0.6	<0.2	<0.1	2	<0.1	4.22	684	23.2	45	4.8	17	3.3	0.8	2.6
N23 (2 pieces)	19.9	161	13.4	0.8	<0.2	<0.1	2	<0.1	3.39	786	30.0	63	8.3	32	6.3	1.3	5.0
N24 (2 pieces)	17.4	183	13.3	3.1	<0.2	<0.1	2	<0.1	2.89	601	39.8	78	8.9	32	5.7	1.3	4.4
C12B	9.8	135	9.8	0.6	<0.2	<0.1	2	0.1	4.89	722	36.5	63	7.0	24	4.0	0.9	2.7
C13	12.1	144	12.8	0.6	<0.2	<0.1	2	<0.1	4.03	828	51.5	87	9.6	33	5.1	1.1	3.6
NC14	8.4	104	7.4	0.3	<0.2	<0.1	3	<0.1	3.07	734	30.2	52	5.7	19	3.4	0.8	2.3
NC15	16.0	243	21.2	0.8	<0.2	0.1	2	<0.1	3.08	1192	79.5	150	17.1	63	8.8	2.0	5.8
NC16	12.4	192	13.8	0.6	<0.2	<0.1	3	<0.1	3.99	854	53.8	99	11.1	40	6.3	1.4	4.0
N25	14.0	160	8.7	0.4	<0.2	<0.1	2	<0.1	3.84	608	33.3	62	7.1	26	5.0	1.1	3.8
N26	7.9	106	6.8	0.6	<0.2	<0.1	1	<0.1	3.80	698	23.3	41	4.3	15	2.8	0.7	2.1
N27	9.3	157	8.8	0.2	<0.2	<0.1	4	<0.1	8.67	722	26.1	46	5.0	17	3.4	0.7	2.5
N27B	10.2	128	9.4	0.6	<0.2	<0.1	3	<0.1	6.36	623	27.0	46	5.2	19	3.3	0.7	2.5
N28	14.4	158	10.6	0.9	<0.2	0.1	2	<0.1	3.61	687	35.3	67	7.6	27	4.5	1.1	3.7
N29	15.0	177	12.0	0.5	<0.2	<0.1	2	0.1	5.71	762	36.4	72	8.0	29	5.0	1.1	3.9
N30	13.9	139	9.9	0.4	<0.2	<0.1	2	0.1	8.06	600	37.2	69	7.6	27	5.0	1.1	3.8
N30B	15.8	139	11.6	0.7	<0.2	<0.1	2	0.1	4.82	788	32.7	67	8.1	30	5.4	1.2	4.2
N31	8.8	109	8.2	<0.2	<0.2	<0.1	2	<0.1	4.22	719	22.3	43	4.3	16	3.0	0.6	2.3
C19	6.5	146	8.0	<0.2	<0.2	<0.1	1	<0.1	3.31	752	24.5	43	4.4	15	2.5	0.5	1.8
C20	9.4	121	7.7	0.3	<0.2	<0.1	1	<0.1	5.04	659	27.2	47	5.2	18	3.3	0.8	2.5
C21	41.9	584	32.6	1.9	<0.2	0.1	3	<0.1	5.52	847	61.6	121	14.0	53	10.5	1.8	9.1
C26	8.9	143	12.5	0.3	<0.2	<0.1	2	0.2	4.12	689	35.5	66	7.6	25	4.1	0.9	2.7
T1	9.2	143	6.6	0.5	<0.2	<0.1	1	0.1	2.90	1042	34.3	61	6.7	25	3.8	1.0	2.8
T2	10.2	149	5.6	0.3	<0.2	<0.1	1	0.1	4.18	663	26.9	48	5.4	19	3.4	0.8	2.7
T2B	8.7	142	5.4	<0.2	<0.2	<0.1	2	0.1	3.79	924	25.9	48	5.2	19	3.4	0.9	2.6
T3	13.5	254	14.2	0.3	<0.2	0.3	3	0.2	4.09	918	43.5	79	8.4	29	5.1	1.2	3.8
T4	7.7	170	7.3	<0.2	<0.2	<0.1	1	0.6	1.78	617	19.9	36	4.0	14	2.5	0.7	1.9
T4B	10.0	156	7.0	<0.2	<0.2	<0.1	1	<0.1	5.40	976	27.6	48	5.3	20	3.4	0.9	2.5
T5	6.5	132	6.0	1.0	<0.2	0.1	1	0.1	4.86	748	21.5	39	4.2	15	2.4	0.7	1.9
T5B	8.0	125	5.8	0.2	<0.2	0.1	1	0.1	5.36	789	22.7	41	4.7	17	2.9	0.7	2.2
MRC 364	17.7	254	15.2	0.6	<0.2	0.1	1	0.2	4.14	1021	51.7	102	11.6	41	6.8	1.5	5.0
MRC 365	13.7	256	12.6	2.4	<0.2	<0.1	1	0.7	6.36	878	38.0	76	8.4	31	4.9	1.1	3.6
MRC 366	9.2	129	6.4	0.2	<0.2	<0.1	1	<0.1	2.67	697	23.8	44	5.2	20	3.5	0.9	2.7
MRC 367	7.4	111	5.5	0.2	<0.2	<0.1	1	<0.1	4.90	790	20.9	37	4.2	15	2.7	0.7	2.0
MRC 368	8.0	140	6.1	0.3	<0.2	<0.1	1	<0.1	4.18	669	26.5	48	5.0	18	3.0	0.8	2.2
MRC 369	10.7	146	7.6	0.3	<0.2	0.1	2	<0.1	7.02	761	27.7	50	5.5	19	3.6	1.0	2.9
MRC 370	14.6	156	12.5	0.3	<0.2	0.1	2	0.1	4.57	699	32.0	63	7.2	26	4.4	1.1	3.4
MRC 371	8.6	148	8.4	<0.2	<0.2	0.1	4	0.1	6.69	740	27.1	49	5.3	19	3.8	0.9	2.6
MRC 372	9.5	131	8.3	0.3	<0.2	0.2	2	<0.1	6.86	679	23.0	43	4.6	16	2.9	0.8	2.4
MRC 437	11.2	130	7.2	0.7	<0.2	<0.1	1	<0.1	2.41	862	28.6	55	6.2	23	3.9	1.0	3.1
MRC 438	7.8	127	5.5	0.5	<0.2	<0.1	<1	<0.1	3.19	941	22.3	42	4.7	16	3.1	0.8	2.2
MRC 439	17.5	234	13.5	3.9	<0.2	0.1	2	0.3	5.73	1063	47.5	94	10.5	39	6.5	1.4	4.7
MRC 440	8.8	115	6.3	0.9	<0.2	<0.1	2	<0.1	4.27	694	20.1	37	4.3	16	2.9	0.8	2.4
MRC 441	8.4	124	5.7	0.3	<0.2	<0.1	<1	<0.1	2.80	1097	27.7	47	5.5	19	3.3	0.8	2.5
MRC 442	9.0	128	6.9	<0.2	<0.2	<0.1	<1	0.1	5.18	541	25.0	46	5.0	17	3.1	0.8	2.3
MRC 443	9.3	122	6.6	0.4	<0.2	<0.1	1	<0.1	3.90	965	27.1	50	5.6	21	3.8	0.9	2.7
MRC 444	9.4	130	6.0	0.2	<0.2	<0.1	2	<0.1	3.66	702	28.0	51	5.4	19	3.5	0.8	2.5

	ICP-MS Y	ICP-MS Zr	ICP-MS Nb	ICP-MS Mo	ICP-MS Ag	ICP-MS Cd	ICP-MS Sn	ICP-MS Sb	ICP-MS Cs	ICP-MS Ba	ICP-MS La	ICP-MS Ce	ICP-MS Pr	ICP-MS Nd	ICP-MS Sm	ICP-MS Eu	ICP-MS Gd
	mg/kg	mg/kg	mg/kg	mg/kg	mg/kg	mg/kg	mg/kg	mg/kg	mg/kg	mg/kg	mg/kg	mg/kg	mg/kg	mg/kg	mg/kg	mg/kg	mg/kg
Detection Limit:	0.1	3	0.1	0.2	0.2	0.1	1	0.1	0.05	5	0.6	4	0.3	1	0.2	0.1	0.1
Sample name																	
MRC 445	8.8	134	6.1	0.2	<0.2	<0.1	1	<0.1	4.36	934	26.8	48	5.3	19	3.1	0.9	2.4
MRC 447	12.0	192	10.5	0.3	<0.2	<0.1	2	<0.1	4.61	675	35.1	64	7.2	26	4.4	1.0	3.3
MRC 448	13.2	190	12.7	0.4	<0.2	0.3	2	0.2	2.94	804	46.5	86	9.3	33	5.0	1.2	3.6
MRC 449	14.5	196	13.1	0.9	<0.2	0.1	2	0.1	3.04	868	63.1	109	11.3	38	5.9	1.3	4.2
MRC 450	12.3	179	10.1	0.5	<0.2	<0.1	2	0.2	2.44	837	35.3	68	7.8	27	4.8	1.1	3.4
MRC 452	13.3	223	13.0	0.8	<0.2	0.1	2	0.3	3.55	815	47.0	90	10.0	35	5.6	1.3	3.9
MRC 453	14.9	168	10.9	0.5	<0.2	<0.1	2	<0.1	2.67	762	34.6	68	7.8	28	5.1	1.2	3.9
MRC 454	12.0	218	12.2	0.6	<0.2	<0.1	2	<0.1	2.58	847	43.0	83	9.2	33	5.0	1.3	3.6
MRC 455	14.6	126	8.8	<0.2	<0.2	<0.1	<1	1.6	1.22	618	22.7	46	5.5	22	4.2	1.1	3.5

	ICP-MS Tb mg/kg	ICP-MS Dy mg/kg	ICP-MS Ho mg/kg	ICP-MS Er mg/kg	ICP-MS Tm mg/kg	ICP-MS Yb mg/kg	ICP-MS Lu mg/kg	ICP-MS Hf mg/kg	ICP-MS Ta mg/kg	ICP-MS W mg/kg	ICP-MS Tl mg/kg	ICP-MS Pb mg/kg	ICP-MS Bi mg/kg	ICP-MS Th mg/kg	ICP-MS U mg/kg
Detection Limit:	0.05	0.05	0.05	0.05	0.05	0.05	0.05	0.1	0.1	1	0.1	0.7	0.1	0.6	0.05
Sample name															
S2	1.43	7.54	1.3	3.7	0.5	2.93	0.44	4.7	1.2	<1	0.2	12.1	<0.1	5.3	1.91
S3	1.17	5.99	1.0	2.7	0.4	2.03	0.28	2.4	0.6	<1	0.3	4.1	<0.1	3.9	1.00
S4	1.00	5.38	0.9	2.5	0.3	2.02	0.29	2.1	0.5	<1	0.3	23.9	<0.1	3.6	1.08
S6	1.36	7.02	1.3	3.4	0.5	2.63	0.37	3.1	0.5	<1	0.2	5.4	<0.1	5.3	1.51
S7	0.86	4.69	0.8	2.4	0.3	2.10	0.30	6.2	1.1	36	0.4	32.7	<0.1	21.6	6.23
S8	1.27	6.80	1.2	3.3	0.4	2.52	0.35	3.3	0.7	<1	0.3	13.0	<0.1	15.3	4.15
S9	1.17	6.20	1.0	2.7	0.4	2.10	0.31	2.6	0.6	<1	0.2	6.5	<0.1	5.0	1.85
S11	1.28	7.11	1.3	3.4	0.5	2.79	0.40	5.2	1.1	<1	0.3	11.2	<0.1	5.2	1.83
S16	0.66	3.65	0.6	1.8	0.3	1.51	0.24	6.0	0.9	6	0.4	12.6	0.2	9.4	2.41
S17	0.93	4.80	0.8	2.3	0.3	1.87	0.28	4.7	0.7	<1	0.4	33.7	<0.1	9.4	2.35
S19	1.16	6.36	1.1	3.2	0.5	2.87	0.41	5.3	0.4	<1	0.2	26.7	<0.1	6.7	2.17
S21	0.87	4.72	0.8	2.4	0.3	2.03	0.29	7.0	0.9	2	0.3	30.5	<0.1	18.4	5.44
S22	0.26	1.52	0.3	0.9	0.2	1.00	0.16	3.1	1.0	<1	0.2	26.9	<0.1	19.3	5.10
S24	0.73	4.08	0.7	2.0	0.3	1.71	0.27	6.4	0.6	1	0.3	24.5	<0.1	11.4	4.21
S25	0.80	4.48	0.8	2.2	0.3	1.83	0.31	6.1	0.8	2	0.3	32.8	<0.1	15.8	5.24
S26	0.60	3.45	0.6	1.9	0.3	2.00	0.31	12.6	1.1	6	0.2	33.7	<0.1	47.8	8.63
S28B	0.92	5.08	0.9	2.4	0.3	2.04	0.33	5.7	0.9	<1	0.3	26.2	<0.1	8.2	2.32
S30	0.91	5.08	0.9	2.3	0.3	1.92	0.31	4.4	0.8	<1	0.3	31.9	<0.1	7.5	2.21
S32	0.78	4.52	0.8	2.1	0.3	1.85	0.26	2.2	0.4	<1	0.1	19.1	<0.1	4.6	1.59
S34	0.78	4.90	0.9	2.5	0.4	2.35	0.37	3.2	0.5	<1	0.2	8.5	<0.1	4.0	1.34
S35	0.97	5.34	1.0	2.8	0.4	2.49	0.38	15.5	1.8	3	0.5	43.3	<0.1	36.1	11.43
S38	0.86	4.75	0.8	2.2	0.3	1.84	0.28	6.2	0.8	2	0.5	34.0	<0.1	16.7	4.87
S39	0.79	4.54	0.8	2.2	0.3	1.85	0.28	3.6	0.5	<1	0.1	18.0	<0.1	9.4	2.96
S40	0.75	4.22	0.8	2.0	0.3	1.69	0.27	4.5	0.6	<1	0.2	22.4	<0.1	8.9	2.89
S41	0.74	4.25	0.8	2.0	0.3	1.72	0.25	3.3	0.5	<1	0.2	20.7	<0.1	10.0	3.20
R1B	0.58	3.48	0.7	1.8	0.3	1.59	0.23	1.6	1.1	2	0.6	20.5	0.1	21.5	4.79
R4B	0.33	2.01	0.4	0.9	0.1	0.84	0.13	2.4	0.7	2	0.4	16.4	<0.1	7.8	2.26
N1A	0.52	2.97	0.5	1.5	0.2	1.23	0.19	1.4	0.7	<1	0.4	19.6	<0.1	10.0	2.40
C1	0.31	1.71	0.3	0.8	0.1	0.85	0.12	1.8	1.2	<1	0.5	29.2	0.3	10.5	1.25
C2D	0.53	3.09	0.5	1.3	0.2	0.96	0.13	1.7	0.7	<1	0.3	15.2	<0.1	8.9	1.91
NTS1	0.07	0.36	<0.1	0.2	<0.1	0.37	0.06	2.7	0.2	<1	0.2	44.0	<0.1	19.9	4.32
C3A	0.24	1.45	0.3	0.7	0.1	0.63	0.10	2.6	1.0	<1	0.4	35.9	0.2	11.0	3.11
C3C	0.38	2.08	0.4	1.0	0.1	0.95	0.14	1.7	1.1	<1	0.5	39.7	0.2	11.3	2.93
R3A	0.23	1.37	0.3	0.7	0.1	0.76	0.13	3.2	0.7	<1	0.1	18.9	<0.1	15.4	3.29
R5A	0.57	3.44	0.6	1.6	0.2	1.46	0.22	2.9	0.8	<1	0.3	17.5	<0.1	12.3	2.71
N5C	0.50	3.00	0.5	1.4	0.2	1.37	0.19	2.2	0.9	<1	0.2	20.2	0.1	10.8	2.87
N7	0.40	2.40	0.4	1.2	0.2	1.12	0.17	1.9	0.7	<1	0.3	20.6	<0.1	8.3	2.40
N8	0.52	3.27	0.6	1.5	0.2	1.37	0.21	1.8	0.9	<1	0.3	19.5	<0.1	9.7	2.01
N9	0.69	4.30	0.8	2.4	0.3	2.20	0.31	2.8	1.7	<1	0.4	21.5	0.1	11.8	3.41
N10	0.46	2.74	0.5	1.3	0.2	1.22	0.18	1.9	0.8	<1	0.4	20.5	<0.1	13.0	1.93
C5	0.30	1.68	0.3	0.8	0.1	0.83	0.13	2.4	0.7	<1	0.3	23.2	<0.1	10.2	3.08
C6	0.28	1.66	0.3	0.8	0.1	0.77	0.13	3.8	0.6	<1	0.3	24.7	<0.1	11.7	1.57
C7	0.31	1.85	0.4	1.0	0.2	0.94	0.19	4.6	0.7	<1	0.3	26.9	<0.1	12.8	1.51
C8	0.36	2.14	0.4	1.1	0.2	1.19	0.18	3.5	1.2	9	0.2	26.6	<0.1	9.5	3.01
N11A	0.29	1.73	0.3	0.8	0.1	0.84	0.13	3.9	0.6	5	0.3	17.7	0.1	8.2	2.18
N12	0.52	3.16	0.6	1.6	0.2	1.30	0.20	4.7	0.9	<1	0.4	17.9	0.2	11.6	3.36
N13	0.44	2.78	0.5	1.4	0.2	1.27	0.19	4.7	0.8	<1	0.2	20.5	<0.1	11.9	3.26
N14	0.63	3.98	0.7	1.9	0.3	1.69	0.24	4.2	1.2	<1	0.3	20.4	<0.1	7.8	2.63
N15	0.52	3.21	0.6	1.6	0.2	1.45	0.22	4.2	0.9	<1	0.2	18.5	0.1	8.9	2.24
N16A	0.51	3.16	0.6	1.6	0.2	1.45	0.22	4.6	0.9	<1	0.3	20.9	<0.1	11.0	2.28
N16C	0.24	1.43	0.3	0.8	0.1	0.81	0.14	4.0	0.5	<1	0.2	20.3	0.1	12.9	4.23
N17	0.47	2.91	0.5	1.4	0.2	1.25	0.19	4.1	0.8	<1	0.2	19.7	<0.1	9.3	2.44
R7A	0.38	2.32	0.4	1.1	0.2	1.01	0.15	3.4	0.6	1	0.2	20.5	<0.1	11.2	1.91
N18	0.40	2.50	0.5	1.2	0.2	1.03	0.15	3.6	0.8	<1	0.2	18.1	<0.1	8.3	2.85
N19	0.34	2.10	0.4	0.9	0.2	0.84	0.14	3.8	0.6	<1	0.2	19.4	<0.1	13.8	2.11
R9	0.35	1.97	0.4	1.0	0.1	0.81	0.12	4.1	0.4	<1	0.2	15.8	<0.1	8.4	2.06
N20	0.32	1.89	0.3	0.9	0.1	0.88	0.13	4.3	0.6	<1	0.2	18.2	0.1	11.5	2.95
N20C	0.37	2.16	0.4	1.1	0.2	1.02	0.17	4.3	0.7	<1	0.2	21.2	<0.1	11.6	2.20
N21A	0.32	2.10	0.4	1.0	0.2	0.97	0.15	4.2	0.7	<1	0.2	20.8	0.1	10.8	1.63
C9	1.02	5.52	0.9	2.2	0.3	1.77	0.25	9.7	1.3	<1	0.4	19.1	<0.1	13.2	2.90
C11	0.34	1.89	0.3	0.8	0.1	0.66	0.12	4.2	0.6	<1	0.2	20.2	2.3	15.4	1.86
C11B	0.36	2.00	0.3	0.9	0.1	0.79	0.13	4.1	0.5	<1	0.2	27.2	0.2	15.8	2.38
C11C	0.36	2.10	0.4	1.0	0.2	0.95	0.14	3.9	0.9	<1	0.2	25.0	0.2	11.9	4.65
C11D	0.49	2.97	0.6	1.5	0.2	1.55	0.23	2.8	0.4	<1	0.4	38.2	0.1	20.8	2.56
C11E	0.29	1.67	0.3	0.8	0.1	0.70	0.13	2.9	0.9	<1	0.2	24.2	<0.1	12.1	2.34
C11F	0.30	1.65	0.3	0.8	0.1	0.75	0.12	3.1	1.0	<1	0.4	31.2	<0.1	18.8	2.92

	ICP-MS Tb mg/kg	ICP-MS Dy mg/kg	ICP-MS Ho mg/kg	ICP-MS Er mg/kg	ICP-MS Tm mg/kg	ICP-MS Yb mg/kg	ICP-MS Lu mg/kg	ICP-MS Hf mg/kg	ICP-MS Ta mg/kg	ICP-MS W mg/kg	ICP-MS Tl mg/kg	ICP-MS Pb mg/kg	ICP-MS Bi mg/kg	ICP-MS Th mg/kg	ICP-MS U mg/kg
Detection Limit:	0.05	0.05	0.05	0.05	0.05	0.05	0.05	0.1	0.1	1	0.1	0.7	0.1	0.6	0.05
Sample name															
R10	0.55	3.34	0.6	1.7	0.2	1.54	0.25	6.9	1.1	2	0.4	19.9	<0.1	26.0	4.16
R11	0.61	3.61	0.7	1.7	0.3	1.69	0.25	7.1	1.2	3	0.4	19.0	<0.1	24.6	4.27
R12	0.48	3.03	0.5	1.6	0.2	1.48	0.22	5.9	1.0	1	0.3	13.6	<0.1	20.6	3.27
R13	0.44	2.79	0.5	1.3	0.2	1.21	0.19	6.2	0.9	1	0.3	15.8	<0.1	22.6	3.68
R14	0.46	2.87	0.5	1.5	0.2	1.38	0.22	5.2	0.9	9	0.3	15.0	<0.1	19.7	3.02
R15	0.54	3.16	0.6	1.7	0.3	1.64	0.23	5.8	1.2	6	0.5	17.5	<0.1	22.2	5.27
R16	0.32	1.91	0.3	0.8	0.1	0.82	0.13	3.6	0.5	<1	0.4	20.0	<0.1	6.7	1.65
R17	0.38	2.04	0.4	1.0	0.1	0.90	0.14	3.8	0.6	<1	0.5	24.1	0.1	8.3	1.68
R18	0.46	2.63	0.5	1.4	0.2	1.35	0.19	5.4	0.8	<1	0.4	15.5	<0.1	16.5	3.60
R19	0.57	3.40	0.6	1.8	0.3	1.68	0.26	5.8	1.1	1	0.6	21.6	0.1	18.4	4.07
R20	0.62	3.61	0.7	1.8	0.3	1.69	0.24	5.9	1.0	2	0.5	20.3	<0.1	17.1	2.00
R21	0.55	3.06	0.6	1.6	0.2	1.50	0.22	5.1	0.8	<1	0.3	20.4	<0.1	9.4	2.31
R22	0.48	2.91	0.6	1.5	0.2	1.48	0.20	5.9	0.9	<1	0.5	16.7	<0.1	16.0	2.28
R23	0.85	4.95	0.9	2.5	0.4	2.34	0.34	9.2	1.0	<1	0.5	14.7	<0.1	17.8	3.64
R24	0.98	5.46	1.0	3.0	0.4	2.92	0.41	19.3	2.4	3	0.9	34.7	<0.1	45.4	9.74
R26	0.61	3.46	0.7	1.9	0.3	1.78	0.26	6.8	1.0	3	0.5	18.4	0.1	15.7	5.27
R27	0.92	5.03	0.9	2.5	0.3	2.10	0.31	9.1	0.9	3	0.5	21.2	<0.1	7.2	2.33
R28	0.20	1.13	0.2	0.6	<0.1	0.52	0.08	3.0	0.3	3	0.4	11.1	<0.1	7.5	2.26
R29	0.34	1.98	0.4	1.0	0.2	0.95	0.14	4.0	0.5	17	0.4	9.6	<0.1	6.6	1.65
N22A/B	0.35	1.92	0.4	1.0	0.1	0.88	0.15	3.6	0.5	<1	0.5	20.3	<0.1	7.3	2.58
N22C	0.35	2.11	0.4	1.2	0.2	1.14	0.16	4.3	0.9	<1	0.4	21.1	<0.1	9.1	2.87
N23 (2 pieces)	0.70	4.11	0.8	2.2	0.3	1.86	0.25	4.3	1.3	<1	0.5	21.8	<0.1	7.7	2.55
N24 (2 pieces)	0.61	3.50	0.7	1.9	0.3	1.78	0.25	5.1	1.1	<1	0.5	20.3	<0.1	11.8	3.41
C12B	0.37	2.04	0.4	1.1	0.1	0.94	0.14	4.0	0.7	<1	0.6	28.0	0.1	18.3	5.22
C13	0.46	2.50	0.5	1.3	0.2	1.27	0.18	4.0	1.0	<1	0.5	22.5	<0.1	10.9	4.15
NC14	0.29	1.65	0.3	0.8	0.1	0.80	0.12	3.1	0.7	<1	0.6	30.1	<0.1	10.6	3.49
NC15	0.69	3.48	0.6	1.7	0.2	1.38	0.19	6.1	1.1	<1	0.5	22.5	<0.1	11.4	3.27
NC16	0.48	2.54	0.5	1.2	0.2	1.04	0.15	4.9	0.9	<1	0.6	27.0	<0.1	11.5	2.96
N25	0.50	2.91	0.5	1.5	0.2	1.24	0.17	4.2	0.8	<1	0.4	17.9	<0.1	7.3	2.37
N26	0.27	1.57	0.3	0.9	0.1	0.86	0.14	3.0	0.6	2	0.4	21.6	<0.1	8.7	2.46
N27	0.33	1.83	0.4	0.9	0.1	0.84	0.13	4.2	0.7	2	0.7	29.5	2.5	8.3	2.30
N27B	0.34	1.84	0.4	1.1	0.2	0.99	0.16	4.0	0.9	<1	0.7	61.6	196.3	10.8	4.23
N28	0.48	2.77	0.6	1.6	0.2	1.46	0.22	4.3	0.9	<1	0.5	20.1	0.2	8.9	2.25
N29	0.51	3.06	0.6	1.7	0.3	1.69	0.26	4.9	1.0	<1	0.5	23.5	0.3	12.3	2.97
N30	0.52	2.85	0.6	1.8	0.2	1.37	0.24	3.8	0.7	<1	0.5	16.4	0.2	9.0	2.05
N30B	0.54	3.24	0.6	1.8	0.3	1.64	0.25	3.8	1.0	<1	0.4	18.9	0.1	8.0	2.01
N31	0.29	1.70	0.4	1.0	0.1	0.98	0.14	3.2	0.8	2	0.4	26.3	<0.1	8.8	2.66
C19	0.22	1.30	0.3	0.8	0.1	0.79	0.14	4.2	0.7	3	0.6	26.3	<0.1	9.3	2.78
C20	0.33	1.87	0.4	1.0	0.1	0.98	0.14	3.6	0.6	<1	0.4	21.8	<0.1	10.0	1.79
C21	1.28	8.10	1.8	5.3	0.8	5.26	0.86	14.2	1.7	1	0.7	26.5	<0.1	14.2	3.49
C26	0.35	1.88	0.4	1.1	0.2	0.97	0.16	4.2	0.9	3	0.5	25.4	0.3	14.2	4.70
T1	0.33	1.83	0.4	1.0	0.1	0.88	0.14	4.1	0.5	<1	0.4	16.1	0.2	9.0	3.08
T2	0.35	1.97	0.4	1.1	0.2	0.98	0.14	4.0	0.4	<1	0.3	19.5	<0.1	8.2	2.77
T2B	0.34	1.85	0.4	0.9	0.1	0.87	0.15	4.1	0.5	<1	0.4	24.4	0.1	9.7	3.43
T3	0.51	2.83	0.5	1.5	0.2	1.31	0.21	6.4	1.1	<1	0.6	47.8	0.3	13.4	4.41
T4	0.27	1.46	0.3	0.8	0.1	0.80	0.12	4.8	0.5	2	0.4	7.0	0.2	9.3	2.05
T4B	0.35	2.05	0.4	1.1	0.2	0.97	0.15	4.4	0.6	<1	0.5	13.7	0.2	8.4	1.75
T5	0.25	1.33	0.3	0.8	0.1	0.73	0.11	3.8	0.5	<1	0.4	22.0	0.2	8.9	3.55
T5B	0.30	1.72	0.3	0.9	0.1	0.82	0.13	3.5	0.5	1	0.4	34.6	0.1	8.5	2.88
MRC 364	0.67	3.81	0.7	1.9	0.3	1.76	0.27	7.1	0.9	<1	0.5	17.7	<0.1	19.2	3.57
MRC 365	0.49	2.89	0.6	1.5	0.2	1.39	0.20	7.0	0.8	1	0.6	21.0	0.1	19.5	4.56
MRC 366	0.37	1.99	0.4	1.0	0.2	0.93	0.16	3.6	0.4	<1	0.4	16.6	<0.1	5.2	1.05
MRC 367	0.27	1.47	0.3	0.8	0.1	0.74	0.10	3.3	0.4	<1	0.4	20.0	<0.1	7.6	1.92
MRC 368	0.30	1.67	0.3	0.8	0.1	0.79	0.11	3.9	0.5	<1	0.4	18.5	<0.1	7.8	1.69
MRC 369	0.43	2.36	0.4	1.2	0.2	1.06	0.14	4.0	0.7	<1	0.5	23.1	<0.1	9.2	3.08
MRC 370	0.47	2.90	0.6	1.6	0.2	1.69	0.23	4.6	1.1	<1	0.5	28.3	0.2	10.6	3.63
MRC 371	0.36	1.80	0.3	0.9	0.1	0.87	0.13	4.2	0.9	<1	0.6	36.2	0.3	12.9	1.76
MRC 372	0.34	1.92	0.4	1.1	0.2	1.08	0.15	3.6	0.7	2	0.4	28.9	0.8	9.1	2.87
MRC 437	0.44	2.39	0.4	1.2	0.2	1.09	0.15	3.7	0.7	<1	0.3	21.7	<0.1	8.6	1.70
MRC 438	0.32	1.71	0.3	0.9	0.1	0.77	0.10	3.6	0.5	<1	0.3	15.2	<0.1	7.1	2.17
MRC 439	0.63	3.54	0.7	1.9	0.3	1.76	0.25	6.2	0.9	13	0.4	17.9	<0.1	16.3	4.04
MRC 440	0.34	1.85	0.3	1.0	0.1	0.92	0.14	3.3	0.5	<1	0.4	22.8	0.2	6.9	2.31
MRC 441	0.33	1.78	0.3	0.9	0.1	0.78	0.12	3.5	0.5	<1	0.3	18.8	<0.1	6.8	1.86
MRC 442	0.31	1.75	0.3	0.9	0.1	0.85	0.14	3.6	0.5	<1	0.3	20.5	0.2	8.1	2.73
MRC 443	0.35	2.01	0.3	1.0	0.1	0.83	0.13	3.5	0.5	<1	0.4	17.6	<0.1	7.7	1.55
MRC 444	0.35	1.92	0.4	1.0	0.1	0.95	0.13	3.7	0.5	<1	0.4	19.8	<0.1	8.4	2.41

	ICP-MS Tb mg/kg	ICP-MS Dy mg/kg	ICP-MS Ho mg/kg	ICP-MS Er mg/kg	ICP-MS Tm mg/kg	ICP-MS Yb mg/kg	ICP-MS Lu mg/kg	ICP-MS Hf mg/kg	ICP-MS Ta mg/kg	ICP-MS W mg/kg	ICP-MS Tl mg/kg	ICP-MS Pb mg/kg	ICP-MS Bi mg/kg	ICP-MS Th mg/kg	ICP-MS U mg/kg
Detection Limit:	0.05	0.05	0.05	0.05	0.05	0.05	0.05	0.1	0.1	1	0.1	0.7	0.1	0.6	0.05
Sample name															
MRC 445	0.33	1.81	0.3	0.9	0.1	0.80	0.12	3.8	0.5	<1	0.4	20.4	<0.1	8.3	2.22
MRC 447	0.44	2.52	0.5	1.3	0.2	1.25	0.18	5.1	0.8	<1	0.5	23.8	<0.1	11.4	3.52
MRC 448	0.47	2.63	0.5	1.4	0.2	1.35	0.21	5.3	0.9	<1	0.4	34.4	0.1	13.0	3.03
MRC 449	0.54	3.06	0.6	1.6	0.2	1.50	0.21	5.4	1.0	<1	0.4	22.3	0.1	15.9	2.69
MRC 450	0.45	2.60	0.5	1.3	0.2	1.20	0.20	4.6	0.7	<1	0.3	18.8	0.2	8.4	2.82
MRC 452	0.50	2.72	0.5	1.5	0.2	1.35	0.21	6.0	0.9	<1	0.4	26.0	0.3	14.6	3.95
MRC 453	0.50	3.11	0.6	1.7	0.2	1.53	0.21	4.4	0.9	<1	0.4	17.3	0.1	9.6	2.43
MRC 454	0.47	2.53	0.5	1.3	0.2	1.15	0.19	5.7	0.8	<1	0.4	19.6	<0.1	10.8	2.81
MRC 455	0.51	2.97	0.6	1.6	0.2	1.53	0.22	3.8	0.6	<1	0.2	8.3	<0.1	6.8	1.79

Appendix 3: Full geochronology results obtained by GSNI

	Sample Parameters						Radiogenic Isotope Ratios								Isotopic Ages					
Sample	Th/U	^{206}Pb* x10^{-13} mol	mol % ^{206}Pb*	Pb*/Pb$_c$	Pb$_c$ (pg)	^{206}Pb/^{204}Pb	^{208}Pb/^{206}Pb	^{207}Pb/^{206}Pb	% err	^{207}Pb/^{235}U	% err	^{206}Pb/^{238}U	% err	corr. coef.	^{207}Pb/^{206}Pb	±	^{207}Pb/^{235}U	±	^{206}Pb/^{238}U	±
(a)	(d)	(e)	(e)	(e)	(e)	(f)	(g)	(g)	(h)	(g)	(h)	(g)	(h)		(i)	(h)	(i)	(h)	(i)	(h)
MRC 363																				
z1	0.746	28.8634	99.94%	565	1.36	32166	0.235	0.055156	0.078	0.503513	0.185	0.066209	0.122	0.952	418.11	1.75	414.08	0.63	413.35	0.49
z2	0.755	18.4818	99.93%	469	1.05	26714	0.238	0.055137	0.095	0.504317	0.184	0.066337	0.11	0.915	417.37	2.12	414.62	0.63	**414.13**	**0.44**
z3	0.763	12.9511	99.93%	434	0.8	24707	0.24	0.055118	0.09	0.503676	0.175	0.066276	0.098	0.941	416.59	2	414.19	0.6	**413.76**	**0.39**
z5	0.724	4.9293	99.51%	65	2	3735	0.228	0.055085	0.111	0.503607	0.191	0.066307	0.091	0.935	415.25	2.48	414.14	0.65	**413.94**	**0.37**
z6	0.778	14.8428	99.71%	112	3.56	6308	0.245	0.055191	0.1	0.505143	0.193	0.066381	0.114	0.917	419.56	2.23	415.18	0.66	**414.39**	**0.46**
z4	0.761	14.4473	99.79%	152	2.55	8575	0.24	0.055296	0.053	0.505645	0.177	0.066322	0.117	0.98	423.77	1.19	415.52	0.6	**414.03**	**0.47**
MRC 364																				
z3	0.819	1.174	99.10%	36	0.87	2062	0.258	0.055047	0.204	0.501463	0.294	0.06607	0.149	0.768	413.72	4.55	412.69	1	**412.51**	**0.59**
z4	0.87	0.7035	98.98%	32	0.6	1810	0.273	0.054932	0.228	0.503484	0.295	0.066475	0.099	0.772	409.05	5.1	414.06	1	414.96	0.4
z7	1.173	0.3634	98.87%	31	0.34	1639	0.369	0.055039	0.265	0.503006	0.335	0.066282	0.11	0.732	413.48	5.92	413.74	1.14	413.78	0.44
z9	0.928	0.3108	97.89%	16	0.55	876	0.291	0.054979	0.443	0.500573	0.513	0.066034	0.115	0.684	410.98	9.9	412.09	1.74	**412.29**	**0.46**
z8	0.82	0.7345	90.87%	3	6.13	199	0.257	0.055005	0.711	0.501928	0.787	0.066182	0.184	0.508	412.01	15.9	413.01	2.67	**413.18**	**0.74**
MRC 365																				
z1	0.736	2.2039	99.49%	63	0.93	3601	0.231	0.055044	0.164	0.502781	0.24	0.066248	0.119	0.784	413.57	3.67	413.58	0.81	**413.59**	**0.48**
z3	0.753	0.6273	99.44%	57	0.29	3265	0.237	0.055131	0.142	0.503368	0.217	0.06622	0.094	0.873	417.1	3.18	413.98	0.74	**413.42**	**0.38**
z3	0.756	0.5541	97.84%	15	1.02	842	0.238	0.05511	0.404	0.502829	0.469	0.066174	0.101	0.711	416.26	9.02	413.62	1.59	**413.14**	**0.4**
z4	0.831	1.7169	99.55%	72	0.65	4007	0.261	0.055114	0.124	0.505574	0.198	0.066531	0.087	0.915	416.44	2.76	415.47	0.68	415.29	0.35
z5	0.79	0.7155	99.34%	49	0.39	2759	0.248	0.055098	0.171	0.503396	0.244	0.066263	0.107	0.8	415.8	3.83	414	0.83	**413.68**	**0.43**
MRC 366																				
z2	0.557	2.0692	99.40%	51	1.02	3089	0.175	0.05508	0.145	0.500993	0.286	0.065968	0.206	0.876	415.01	3.24	412.37	0.97	**411.9**	**0.82**
z3	0.473	1.5984	98.53%	20	1.97	1246	0.149	0.05507	0.263	0.500622	0.338	0.065932	0.143	0.676	414.58	5.88	412.12	1.14	**411.68**	**0.57**
z4	0.469	5.5589	98.88%	26	5.25	1614	0.147	0.055023	0.168	0.500583	0.329	0.065983	0.244	0.869	412.66	3.76	412.1	1.11	**412**	**0.98**
z5	0.588	4.0352	95.38%	6	16.25	392	0.185	0.055016	0.315	0.49466	0.386	0.06521	0.119	0.691	412.42	7.05	408.08	1.3	407.31	0.47
z9	0.557	1.6884	98.36%	18	2.32	1115	0.176	0.05514	0.24	0.501931	0.325	0.06602	0.147	0.73	417.45	5.35	413.01	1.1	**412.21**	**0.59**
MRC 367																				
z1	0.696	1.0872	98.98%	31	0.93	1778	0.219	0.055078	0.2	0.501062	0.266	0.065979	0.089	0.816	414.97	4.48	412.42	0.9	**411.97**	**0.35**
z2	0.551	2.4982	99.74%	117	0.54	6977	0.173	0.055051	0.1	0.501633	0.179	0.066087	0.085	0.96	413.84	2.23	412.81	0.61	412.62	0.34
z3	0.585	4.06	99.82%	167	0.62	9866	0.184	0.055059	0.092	0.501416	0.172	0.066049	0.085	0.973	414.16	2.05	412.66	0.58	**412.39**	**0.34**
z4	0.931	4.3101	99.83%	195	0.61	10620	0.293	0.055039	0.092	0.500867	0.173	0.066001	0.086	0.967	413.43	2.07	412.29	0.59	**412.09**	**0.34**
z5	0.88	2.7829	99.80%	162	0.47	8916	0.277	0.055028	0.129	0.500497	0.195	0.065965	0.091	0.839	412.97	2.89	412.04	0.66	**411.87**	**0.36**
MRC 369																				
z3	0.409	3.8943	99.81%	160	0.59	9968	0.128	0.054962	0.092	0.500947	0.174	0.066104	0.087	0.97	410.19	2.06	412.34	0.59	412.73	0.35
z4	0.734	5.7571	99.84%	204	0.75	11710	0.231	0.055012	0.093	0.499355	0.173	0.065834	0.087	0.96	412.3	2.07	411.27	0.59	**411.08**	**0.35**
z9	0.445	3.3378	99.74%	117	0.71	7203	0.14	0.054948	0.112	0.498514	0.197	0.0658	0.107	0.893	409.62	2.51	410.7	0.66	**410.89**	**0.43**
z5	0.449	4.5472	97.65%	12	9.1	770	0.141	0.055044	0.233	0.501917	0.347	0.066134	0.193	0.771	413.52	5.21	413	1.18	412.91	0.77
z8	0.435	1.9053	99.68%	93	0.5	5780	0.136	0.054873	0.247	0.502977	0.32	0.06648	0.166	0.651	406.55	5.52	413.72	1.09	415	0.67
z9	0.495	3.4037	97.64%	12	6.85	767	0.156	0.055044	0.212	0.499909	0.288	0.065869	0.099	0.835	413.52	4.74	411.64	0.97	**411.31**	**0.39**
z10	0.734	5.7571	99.84%	204	0.75	11710	0.231	0.055012	0.093	0.499338	0.173	0.065831	0.086	0.963	412.3	2.07	411.25	0.58	**411.07**	**0.34**
MRC 370																				
z3	0.366	10.2935	99.45%	53	4.7	3316	0.115	0.054994	0.095	0.49978	0.194	0.065911	0.108	0.958	411.49	2.13	411.55	0.66	**411.56**	**0.43**
z7	0.374	2.9678	99.63%	80	0.9	5034	0.118	0.055034	0.124	0.498873	0.213	0.065745	0.119	0.868	413.09	2.78	410.94	0.72	**410.56**	**0.47**
z8	0.351	4.8456	99.79%	141	0.83	8912	0.111	0.054999	0.109	0.49907	0.183	0.065812	0.088	0.916	411.66	2.43	411.07	0.62	**410.97**	**0.35**
z10	0.346	3.8835	99.84%	184	0.51	11661	0.109	0.055003	0.089	0.499041	0.172	0.065804	0.086	0.976	411.82	2	411.05	0.58	**410.92**	**0.34**
MRC 371																				
z1	0.506	3.0099	99.71%	106	0.71	6448	0.159	0.055033	0.106	0.498738	0.192	0.065728	0.103	0.915	413.09	2.37	410.85	0.65	**410.45**	**0.41**
z2	0.657	2.6867	99.71%	108	0.65	6331	0.207	0.054962	0.112	0.498439	0.212	0.065773	0.132	0.891	410.24	2.5	410.65	0.72	**410.72**	**0.53**
z5	0.555	1.9413	99.61%	79	0.62	4769	0.174	0.054964	0.116	0.499376	0.2	0.065894	0.101	0.906	410.29	2.6	411.28	0.68	411.46	0.4
z7	0.618	0.9341	99.48%	60	0.4	3555	0.194	0.054949	0.138	0.497893	0.231	0.065716	0.128	0.859	409.71	3.08	410.28	0.78	**410.38**	**0.51**
z9	0.512	1.2083	97.31%	11	2.77	678	0.161	0.055067	0.335	0.498379	0.409	0.06564	0.124	0.696	414.46	7.48	410.6	1.38	**409.92**	**0.49**
z10	0.459	0.8583	99.01%	30	0.7	1869	0.144	0.054932	0.214	0.497389	0.281	0.06567	0.095	0.795	408.98	4.78	409.93	0.95	**410.1**	**0.38**
MRC 372																				
z1	0.527	4.4246	97.64%	13	8.88	768	0.169	0.05476	0.208	0.426802	0.723	0.056527	0.673	0.958	401.9	4.65	360.9	2.2	354.56	2.32
z2	0.524	2.258	98.81%	25	2.25	1536	0.167	0.054835	0.17	0.452075	0.266	0.059794	0.14	0.821	404.96	3.81	378.73	0.84	374.45	0.51
z3	0.423	3.6157	99.33%	44	2.01	2737	0.134	0.054857	0.127	0.47213	0.214	0.062421	0.11	0.886	405.88	2.85	392.66	0.7	390.42	0.42
z4	0.483	2.7688	97.63%	12	5.59	764	0.156	0.054794	0.216	0.418313	0.327	0.05537	0.179	0.788	403.24	4.84	354.84	0.98	347.49	0.61
z5	0.42	1.9152	99.01%	30	1.58	1851	0.132	0.054816	0.169	0.477239	0.245	0.063144	0.101	0.842	404.2	3.77	396.18	0.8	394.8	0.39
z6	0.705	5.7356	98.86%	27	5.51	1586	0.223	0.054968	0.128	0.478922	0.213	0.063191	0.093	0.946	410.45	2.86	397.33	0.7	395.08	0.36
z7	0.456	4.3161	97.17%	10	10.43	641	0.146	0.054773	0.226	0.434341	0.301	0.057512	0.102	0.807	402.43	5.07	366.25	0.93	360.57	0.36
z1	0.606	2.4639	99.25%	41	1.54	2439	0.191	0.054843	0.158	0.48173	0.226	0.063706	0.087	0.859	405.36	3.53	399.26	0.75	398.21	0.33
z4	0.666	5.2136	99.89%	288	0.47	16780	0.21	0.054941	0.12	0.49388	0.187	0.065197	0.089	0.858	409.37	2.68	407.55	0.63	**407.23**	**0.35**
z1	0.349	1.8628	99.76%	120	0.37	7635	0.11	0.054901	0.12	0.478144	0.192	0.063165	0.092	0.881	407.69	2.68	396.8	0.63	394.93	0.35
z2	0.427	2.5509	99.65%	84	0.74	5235	0.135	0.054971	0.116	0.478519	0.196	0.063134	0.097	0.903	410.55	2.6	397.06	0.65	394.74	0.37
z4	0.522	2.1439	99.30%	43	1.25	2620	0.165	0.054919	0.15	0.474843	0.221	0.062709	0.087	0.881	408.42	3.35	394.53	0.72	392.16	0.33
z5	0.381	7.5207	99.87%	231	0.79	14476	0.121	0.054886	0.092	0.475261	0.179	0.062801	0.1	0.936	407.07	2.07	394.82	0.59	392.73	0.38

(a) z1, z2 etc. are labels for fractions composed of single zircon grains or fragments; all fractions annealed and chemically abraded after Mattinson (2005).

(d) Model Th/U ratio calculated from radiogenic 208Pb/206Pb ratio and 207Pb/235U age.

(e) Pb* and Pbc represent radiogenic and common Pb, respectively; mol % ^{206}Pb* with respect to radiogenic, blank and initial common Pb.

(f) Measured ratio corrected for spike and fractionation only.
Daly analyses, based on analysis of NBS-981 and NBS-982.

(g) Corrected for fractionation, spike, and common Pb; up to 1 pg of common Pb was assumed to be procedural blank: ^{206}Pb/^{204}Pb = 18.60 ± 0.80%; 207Pb/204Pb = 15.69 ± 0.32%; 208Pb/204Pb = 38.51 ± 0.74% (all uncertainties 1-sigma). Excess over blank was assigned to initial common Pb.

(h) Errors are 2-sigma, propagated using the algorithms of Schmitz and Schoene (2007) and Crowley et al. (2007).

(i) Calculations are based on the decay constants of Jaffey et al. (1971). 206Pb/238U and 207Pb/206Pb ages corrected for initial disequilibrium in ^{230}Th/^{238}U using Th/U [magma] = 3.

(j) Corrected for fractionation, spike, and blank Pb only.

Appendix 4: High Temperature Quartz Recrystallisation (HTQR) scores throughout the NIC

Sample	Site	Irish Grid Reference			HTQR score
		Grid	Easting	Northing	
N8	20	J	09229	26385	1
R7B	34	J	18128	33437	2
C5	23	J	02755	26310	2
R9	38	J	15097	34837	4
R4A	5	J	20062	33973	2
R1A	2	J	30431	35453	4
N4C	17	J	14423	25146	3
N11B	27	J	10126	32674	4
C9	41	J	05178	16385	0
T2B	88	J	15390	38754	1
T3	89	J	17320	27534	2
N20C	39	J	13592	31955	3
N31	78	J	11141	23536	3
R11B	45	J	32404	40149	2
R15	49	J	31672	40808	3
R23	57	J	33156	38363	1
R26	60	J	27372	43019	3
T2	88	J	15390	38754	0
C1	7	J	07860	22504	2
C2B	8	J	05545	22111	2
N7	19	J	10126	24878	2
N14	30	J	11623	28626	1
N18	35	J	15873	31380	2
MRC 364	14	J	2782	3315	2
MRC 365	2	J	3045	3545	4
MRC 366	3	J	2927	3694	2
MRC 367	15	J	2483	3360	2
MRC 368		J	2392	3892	2
MRC 369	5	J	2006	3395	1
MRC 370	17	J	1439	2515	2
MRC 371	18	J	1242	2982	1
MRC 372	7	J	0786	2251	1
MRC 58		J	070	240	1
MRC 60	2	J	304	354	4
MRC 61	150	J	037	246	2
MRC 62	17	J	145	251	4
MRC 63	17	J	145	251	3
MRC 65	10	J	066	319	2
MRC 66	10	J	066	319	2
MRC 67		J	187	344	1
MRC 68		J	204	354	1

Appendix 5: Sample orientation for AMS

Prior to extraction from the field AMS samples were marked so as to preserve the original strike and dip of one of the sample faces:

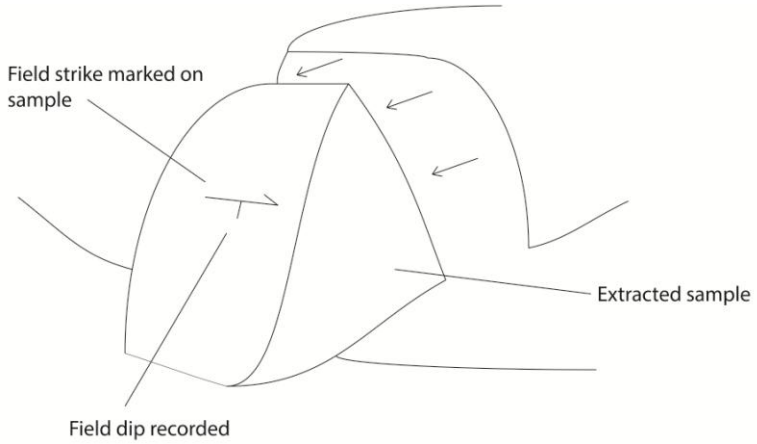

A second dip and strike orientation was marked on the sample to record its position on the drill table prior to extraction of a sub-sample core. The difference in orientation of this measurement from the previous was measured and recorded:

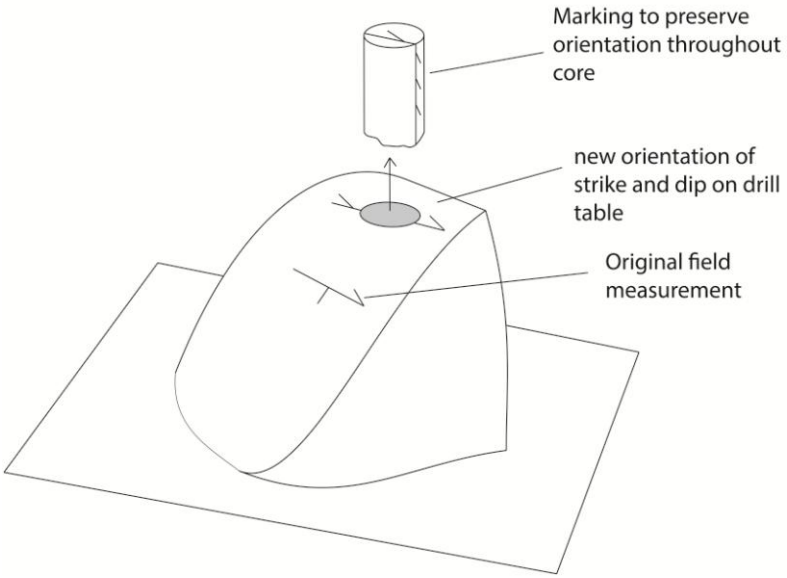

A final marking was made along the long axis of the core to record the strike angle and direction of dip of the drill table measurement. Hence, when the core was sawn into separate sub-cores, the orientation of the latter measurement and ultimately the field strike and dip could be derived.

Appendix 6: AMS data

	susceptibility data				K1 normalised with directions			K2 normalised with directions			K3 normalised with directions			Owens (1974) parameters					
Block	Kmean	K1	K2	K3	K1norm	dec	dip	K2norm	dec	dip	K3norm	dec	dip	L	F	M	Mu	H	Shape
C1	633.45	655.96	648.328	596.053	1.034	322.6	17.4	1.023	45.6	-21.3	0.943	88.5	62	1%	8%	0.1	8	9%	oblate
C2B	5141.23	5384.769	5157.052	4881.879	1.047	73.4	-29.4	1.003	87.2	59.9	0.951	346.8	6	4%	5%	0.8	40	10%	triaxial
C2C	1485.06	1537.884	1489.327	1427.983	1.032	74.7	-42.7	1.006	86.5	46.7	0.962	350.2	5.9	3%	4%	0.6	31	7%	oblate-triaxial
C2D	4354.18	4604.414	4341.526	4116.597	1.057	67.9	-40.9	0.997	102.8	43.4	0.946	354.5	18.3	6%	5%	1.2	50	11%	triaxial
C3A	663.38	670.1	665.098	654.936	1.01	153.8	19.3	1.002	288.3	63.4	0.988	57.4	17.5	1%	1%	0.6	32	2%	oblate-triaxial
C3B	919.96	927.553	922.379	909.945	1.008	254.7	-35.4	1.003	340.1	6.5	0.989	241.1	53.8	1%	1%	0.4	21	2%	oblate-triaxial
C3C	623.65	629.086	622.363	619.5	1.009	236.9	-66.3	0.998	52.1	-23.6	0.993	322.9	1.8	1%	1%	2.1	64	2%	prolate-triaxial
C5	6513.66	6879.388	6597.024	6064.565	1.056	336.2	41.4	1.013	47.6	-19.8	0.931	118.7	42	4%	8%	0.5	28	12%	oblate-triaxial
C6	4026.72	4231.488	3975.66	3873.011	1.05	129.9	-41.9	0.987	182	34.4	0.963	69.7	29	6%	2%	2.7	70	9%	prolate-triaxial
C7	2858.44	3052.249	2853.33	2669.74	1.068	111.6	-50.8	0.998	147.1	33.6	0.934	44.8	17.8	7%	6%	1.1	47	13%	triaxial
C8	367.93	381.301	366.782	355.722	1.036	92.1	-27.6	0.997	46.3	53.1	0.967	349.6	-22.4	4%	3%	1.3	53	7%	triaxial
C11A	139.08	139.985	138.74	138.528	1.007	87.2	-15.4	0.997	69.8	73.9	0.996	356	-4.6	1%	0%	6.0	81	1%	prolate
C11B	2408.83	2482.516	2436.419	2307.542	1.028	232.6	-26.4	1.012	327.5	-9.8	0.96	256.1	61.5	2%	5%	0.3	17	7%	oblate
C11C	122.15	124.923	122.917	118.62	1.022	292.8	8.1	1	25.2	16.4	0.978	177.6	71.6	2%	2%	1.0	45	4%	triaxial
C11D	80.85	82.333	80.984	79.233	1.018	45.6	4.3	1.002	136.8	15.6	0.98	300.6	73.8	2%	2%	0.8	38	4%	triaxial
C11E	410.93	416.494	412.125	404.182	1.013	222.3	7.4	1.003	307.4	-33.5	0.984	323.3	55.5	1%	2%	0.5	28	3%	oblate-triaxial
C11F	127.99	129.458	129.049	125.467	1.012	151.7	-40.2	1.007	100.7	36.7	0.98	34.5	-28.4	0%	3%	0.2	10	3%	oblate
NC12B	15011.55	16250.58	14765.15	14018.9	1.082	77.2	68.9	0.984	13.7	-9.7	0.935	106.9	-18.5	10%	5%	2.0	63	15%	prolate-triaxial
NC13	17035.74	18018.488	16635.18	16453.55	1.058	285.1	-37	0.977	347.9	31.2	0.966	230.3	37.4	8%	1%	7.7	83	9%	prolate
C19	377.76	390.407	376.89	365.998	1.033	93.7	-31.9	0.998	35.3	40.1	0.969	339.3	-33.6	4%	3%	1.2	51	6%	triaxial
C20	7413.53	8396.079	7189.419	6655.085	1.133	273.1	42.2	0.97	336.7	-26.1	0.898	45.4	36.6	16%	7%	2.3	66	23%	prolate-triaxial
C21	3204.02	3286.698	3246.986	3078.368	1.042	87	36.3	1.028	299.2	49.1	0.93	9.5	-16.3	1%	5%	0.2	13	7%	oblate
C22	2770.49	2865.006	2831.241	2615.212	1.034	269	-88.5	1.022	97.1	-1.5	0.944	7.1	-0.2	1%	8%	0.2	9	9%	oblate
NC12A	18817.89	19918.248	18652.83	17882.58	1.056	269.4	19.4	0.991	9.7	26.9	0.952	148.1	55.8	6%	4%	1.7	59	10%	prolate-triaxial
N1A	3353.33	3571.043	3347.669	3141.288	1.064	325.1	25.9	0.999	54	-2.4	0.937	139.1	64	7%	6%	1.1	47	13%	triaxial
N1B	3488.23	3647.037	3493.557	3324.103	1.044	279.7	26.8	1.003	11.2	3	0.953	107.1	63	4%	5%	0.8	40	9%	triaxial
N2	747.12	797.355	775.488	668.526	1.064	48.1	-1.7	1.038	125.8	82	0.898	318.4	7.8	3%	14%	0.2	10	17%	oblate
N3	1353.75	1519.116	1394.082	1148.062	1.116	80.5	-5.7	1.034	22.5	79.3	0.851	349.6	-9	8%	18%	0.5	24	27%	oblate-triaxial
N4A	52.24	54.142	51.562	51.012	1.037	24.1	-22.9	0.988	97.5	34	0.976	321.1	47	5%	1%	4.0	76	6%	prolate
N4B	145.6	151.248	146.298	139.253	1.028	41.1	-34.8	1.008	96.1	39.5	0.964	336.1	31.2	2%	4%	0.5	24	6%	oblate-triaxial
N4C	101.53	104.262	100.983	99.429	1.027	219.7	32.1	0.994	67.9	54.6	0.979	138.3	-13.4	3%	2%	2.1	65	5%	prolate-triaxial
N5A	8018.32	8377.084	8102.545	7575.342	1.045	120.4	15.6	1.011	4.3	57.6	0.944	38.8	-27.6	3%	7%	0.5	27	10%	oblate-triaxial
N5C	7168.53	7450.779	7264.754	6790.046	1.039	134.4	15.8	1.014	15.7	59.5	0.947	52.1	-25.4	3%	7%	0.4	21	9%	oblate-triaxial
N5D	5933.02	6208.692	5943.814	5646.552	1.046	287.8	-22.1	1.002	7.7	23.1	0.952	236.5	57	4%	5%	0.9	41	9%	triaxial
N7	5780.42	6105.608	5818.589	5417.067	1.056	93.4	24.1	1.007	266.2	65.7	0.938	2.2	2.7	5%	7%	0.7	36	12%	triaxial
N8	6019.96	6447.764	6078.727	5533.383	1.071	250.8	20.6	1.009	346.3	14.3	0.92	108.7	64.5	6%	9%	0.7	35	15%	oblate-triaxial
N9	7131.66	7557.663	7166.746	6670.563	1.059	104.4	-26.9	1.005	166.9	42.4	0.936	35.9	35.8	5%	7%	0.8	38	12%	triaxial
N10	7499.23	8005.697	7695.996	6796.001	1.064	242.2	10.8	1.025	336.3	20.5	0.91	126	66.6	4%	12%	0.3	19	15%	oblate
N11A	8032.01	8800.615	8006.006	7289.403	1.096	125.5	-58.1	0.997	44.2	5.4	0.908	317.5	-31.3	10%	9%	1.1	48	19%	triaxial
N11B	1484.51	1609.2	1474.729	1369.601	1.084	88.6	-61.5	0.994	56.6	24.7	0.922	332.9	-13.3	9%	7%	1.3	52	16%	triaxial
N12	3928.04	4079.361	3942.492	3762.256	1.037	74.1	-7.7	1.004	354.1	52.3	0.959	338.4	-36.6	3%	5%	0.7	36	8%	triaxial
N13	9650.54	10404.381	9838.721	8708.527	1.063	70.8	40.4	1.029	278.9	46	0.907	353.5	-14.4	6%	12%	0.5	27	18%	oblate-triaxial
N14	4834.4	5031.236	4968.839	4503.123	1.04	262.9	-16.5	1.028	342	32.6	0.932	195.6	52.5	1%	10%	0.1	8	11%	oblate
N15	6380.07	6968.28	6523.205	5648.724	1.085	285	-4.1	1.021	12.8	28.1	0.894	202.6	61.6	6%	13%	0.5	27	19%	oblate-triaxial
N16A	8576.44	8926.378	8627.365	8175.582	1.039	131.2	-2.1	1.007	43.5	47.1	0.954	39.2	-42.9	3%	5%	0.7	34	9%	oblate-triaxial
N16B	4663.51	4728.497	4683.012	4579.01	1.014	144.6	-33.6	1.004	79.9	32.7	0.981	21.7	-39.3	1%	2%	0.4	23	3%	oblate-triaxial
N16C	8947.51	9185.317	9126.024	8531.183	1.024	269.3	-2.7	1.018	356.7	43.8	0.958	182.1	46.1	1%	6%	0.1	5	7%	oblate
N17	7774.99	8341.298	7862.207	7121.461	1.07	107	2.7	1.014	331.3	86.2	0.916	17.1	-2.7	6%	10%	0.6	30	15%	oblate-triaxial
N18	13175.12	14030.136	13566.64	11928.57	1.065	320.3	-20.5	1.03	33.8	37.1	0.905	252.8	45.8	3%	13%	0.3	15	16%	oblate
N19	8200.99	8413.668	8284.257	7905.042	1.026	104.1	63.7	1.01	356.7	8.4	0.964	82.7	-24.7	2%	5%	0.3	19	6%	oblate
N20A	7503.01	8417.825	7585.379	6505.813	1.121	129.6	-14.8	1.01	60.8	53.8	0.868	30	-32.1	11%	14%	0.8	38	25%	triaxial
N20C	5889.23	6661.068	6046.823	4959.794	1.128	117.8	-1.3	1.026	30.7	66.8	0.846	27.3	-23.2	10%	18%	0.6	30	28%	oblate-triaxial
N21A	9343	9917.735	9555.85	8555.412	1.061	121.2	-13.7	1.023	56.5	60.3	0.916	24.4	-25.8	4%	11%	0.4	20	15%	oblate-triaxial
N21B	14229.04	15559.313	14829.26	12298.56	1.094	141.5	-6.3	1.042	61.7	58.1	0.864	47.7	-31.1	5%	18%	0.3	16	23%	oblate
N22A	5889.81	5878.876	5262.655	5027.905	1.091	87.4	2.6	0.976	351.4	66.3	0.934	358.5	-23.5	12%	4%	2.8	70	16%	prolate-triaxial
N22B	5554.81	6120.275	5371.207	5172.941	1.102	216.8	-27.3	0.967	273.2	47.1	0.931	144.3	30.3	14%	4%	3.8	75	17%	prolate
N22C	3258.17	3567.85	3177.108	3029.565	1.094	105	1.9	0.975	3	81.1	0.93	15.3	-8.7	12%	5%	2.6	69	16%	prolate-triaxial
N23	4250.32	4719.838	4201.515	3829.595	1.111	121.6	-10.6	0.989	192.3	60.3	0.9	37.2	27.4	12%	9%	1.4	54	21%	triaxial
N24	5561.32	6196.831	5373.896	5113.229	1.105	113.6	-24.2	0.966	84.9	62.9	0.929	18.4	-11.5	14%	4%	3.7	75	18%	prolate
N25A	1319.11	1420.244	1307.247	1229.837	1.076	218.2	13.9	0.991	354	71	0.932	124.9	12.8	9%	6%	1.5	55	14%	prolate-triaxial
N25B	4770.94	5111.355	4782.963	4418.507	1.071	212.9	24.3	1.002	345.3	56.2	0.927	112.4	22	7%	8%	0.9	42	14%	triaxial
N26	3267.85	3554.661	3307.981	2940.906	1.085	102.6	25.5	1.012	271.7	64	0.903	10.5	4.3	7%	11%	0.7	34	18%	oblate-triaxial
N27A	172.83	174.988	172.964	170.544	1.012	161.9	-59.1	1.001	90.8	11	0.987	6.9	-28.4	1%	1%	0.8	39	3%	triaxial
N27B	324.31	329.008	324.491	319.42	1.015	357.3	52.2	0.999	26.5	-34.1	0.986	106.5	14.3	2%	1%	1.2	51	3%	triaxial
N28	7781.83	8189.954	7897.115	7258.422	1.052	282.2	-48	1.014	31	-16.2	0.934	313.9	37.4	4%	8%	0.5	26	12%	oblate-triaxial
N29	3821.89	3989.192	3926.208	3550.281	1.042	76.2	-6.3	1.026	159.3	47.7	0.932	351.8	41.6	2%	9%	0.2	9	11%	oblate
N30A	2495.6	2603.388	2525.105	2358.312	1.043	72.6	18.6	1.012	311.2	57.2	0.946	352	-25.9	3%	7%	0.5	25	10%	oblate-triaxial
N30B	11380.38	12088.192	11597.3	10455.66	1.062	91.9	4.1	1.018	350.2	70.5	0.92	3.3	-19	4%	10%	0.5	24	14%	oblate-triaxial
N31	7065.37	7835.34	7079.618	6281.153	1.107	95.9	10.2	1.002	216.3	70.4	0.891	2.9	16.6	10%	11%	0.9	43	22%	triaxial
R1A	1673.79	1788.359	1702.241	1530.782	1.068	25.4	-53.5	1.017	68.1	28.6	0.914	326.2	20.8	5%	10%	0.5	27	15%	oblate-triaxial
R1B	2001.01	2141.348	2061.05	1800.63	1.07	337.3	-57.1	1.03	55.2	7.7	0.9	320.4	31.7	4%	13%	0.3	17	17%	oblate
R2A	416.21	420.924	414.633	413.064	1.011	280.1	-39.9	0.996	347.8	24.3	0.992	235.3	40.3	2%	0%	4.0	76	2%	prolate
R2B	44230.49	46383.887	44532.73	41774.86	1.048	211.9	-16.3	1.006	244.1	71	0.945	124.7	9.6	4%	6%	0.7	35	10%	oblate-triaxial
R3B	382.75	390.757	389.472	368.02	1.021	72.7	-8.6	1.018	18.2	75.3	0.961	340.9	-11.8	0%	6%	0.1	4	6%	oblate
R4A	7016.42	7216.769	7087.688	6744.817	1.028	333.1	-17.5	1.01	79.5	-41.9	0.961	46	42.9	2%	5%	0.4	21	7%	oblate-triaxial
R4B	6407.39	6653.763	6370.271	6198.127	1.038	149.2	35.8	0.994	277.9	40.9	0.968	36	28.6	4%	3%	1.7	60	7%	prolate-triaxial
R5A	387.5	392.171	389.725	380.604	1.012	146.3	54.2	1.006	16.7	24.7	0.982	94.8	-24.2	1%	2%	0.3	15	3%	oblate
R5B	515.77	520.909	516.863	509.548	1.01	177.3	52.2	1.002	38.2	30.4	0.988	115.7	-20.3	1%	1%	0.6	29	2%	oblate-triaxial
R6	3799.22	4210.404	4099.415	3087.846	1.108	56.9	-1.6	1.073	135.4	82	0.819	327.1	7.9	3%	25%	0.1	8	29%	oblate
R7A	4107.57	4198.436	4168.285	3955.997	1.022	287.4	-49.3	1.014	118.8	-40.2	0.964	24	-5.6	1%	5%	0.2	9	6%	oblate
R7B	5733.72	5913.283	5845.686	5442.203	1.03	143.9	-22	1.019	192.2	58.7	0.951	62.9	21.1	1%	7%	0.2	9	8%	oblate
R8	2897.24	3013.548	2896.199	2781.969	1.042	327.9	25.6	0.998	45.6	-23.8	0.96	98.6	53.7	4%	4%	1.2	49	8%	triaxial
R9	3164.99	3653.155	3345.106	2496.719	1.154	183.1	-7.2	1.057	264.1	51.4	0.789	98.7	37.7	10%	27%	0.4	20	36%	oblate
R10	1392.99	1447.538	1410.276	1321.161	1.039	161.4	11.3	1.012	351.9	78.5	0.949	71.8	-2	3%	6%	0.4	23	9%	oblate-triaxial
R11A	986.1	1032.195	995.904	930.21	1.047	154.5	37.6	1.01	8	47.2	0.943	78.3	-17.3	4%	7%	0.6	29	10%	oblate-triaxial
R11B	935.51	967.582	938.428	900.524	1.035	166.7	40.7	1.003	18	44.8	0.963	91.2	-16.2	3%	4%	0.8	38	7%	triaxial
R12	244.91	249.6	246.783	238.342	1.019	155.7	31.9	1.008	359.1	55.8	0.973	72.6	-10.9	1%	3%	0.3	19	5%	oblate
R13	496.89	507.802	502.529	480.329	1.023	43.4	62.5	1.011	18.3	-25.3	0.966	113.1	-10.2	1%	5%	0.3	14	6%	oblate
R14	798.36	820.476	814.766	759.835	1.028	177.9	13	1.02	30.2	74.8	0.952	89.8	-7.9	1%	7%	0.1	6	8%	oblate
R15	631.46	661.656	630.708	602.027	1.043	153.3	19	1.001	333.8	71	0.955	63.4	-0.1	4%	5%	0.9	43	9%	triaxial
R16	1951.99	2038.033	2007.538	1810.4	1.044	160.8	-19.7	1.028	171.2	70	0.928	72	3.5	2%	10%	0.2	9	12%	oblate
R17	654.28	674.176	656.908	631.746	1.03	137.5	-21.4	1.005	125.7	68.2	0.966	45.9	-4	3%	4%	0.6	33	6%	oblate-triaxial
R18	4278.2	4890.373	4249.389	3694.831	1.141	204.8	60.4	0.993	33.5	29.4	0.866	121.4	-3.7	15%	13%	1.2	49	28%	triaxial
R19	291.92	300.779	297.853	277.114	1.03	42.8	-16.4	1.02	104.2	58.4	0.949	321.1	26.2	1%	7%	0.1	8	8%	oblate
R20	410.05	418.756	410.379	401.01	1.021	70.1	60.9	1.001	7.6	-14.4	0.978	104.4	-24.7	2%	2%	0.9	42	4%	triaxial

	susceptibility data				K1 normalised with directions			K2 normalised with directions			K3 normalised with directions			Owens (1974) parameters					
Block	Kmean	K1	K2	K3	K1norm	dec	dip	K2norm	dec	dip	K3norm	dec	dip	L	F	M	Mu	H	Shape
R21	910.19	931.078	902.408	897.077	1.022	138.9	74.7	0.992	1.1	11.5	0.986	89.1	-10	3%	1%	4.6	78	4%	prolate
R22	552.99	579.273	557.649	522.058	1.047	194.9	23.6	1.008	61.6	57.5	0.944	114.5	-21	4%	6%	0.6	32	10%	oblate-triaxial
R23A	5257.14	5345.88	5244.199	5181.353	1.017	319.6	-13.1	0.998	60.3	-38.5	0.985	34.4	48.5	2%	1%	1.5	56	3%	prolate-triaxial
R23B	885.03	897.693	882.543	874.839	1.014	304.2	20.2	0.997	26.5	-20.7	0.989	74.5	60.4	2%	1%	1.9	62	3%	prolate-triaxial
R24	9427.08	10035.046	9522.106	8724.083	1.064	342.1	49.1	1.01	331.7	-40.5	0.926	66.1	-5.2	5%	8%	0.6	33	14%	oblate-triaxial
R25	981.21	1023.984	1002.646	917.01	1.043	125.8	-54.5	1.022	101	32.9	0.935	18.8	-11.8	2%	9%	0.3	14	11%	oblate
R26	1001.95	1040.795	1016.035	949.023	1.039	99.1	-36.7	1.014	74.5	50.6	0.947	359.8	-12.2	3%	7%	0.4	21	9%	oblate-triaxial
R27	500.73	506.33	499.414	496.456	1.011	215.4	-77.9	0.997	85.5	-7.8	0.991	354.3	-9.1	1%	1%	2.4	67	2%	prolate-triaxial
R28	1643.71	1704.928	1682.24	1543.96	1.042	102.3	-60.8	1.025	54.4	20.5	0.933	332.1	-19.8	2%	9%	0.2	10	11%	oblate
R29	310.24	335.467	311.768	283.482	1.051	106.7	-42.2	1.002	50.7	31.7	0.946	343	-31.5	5%	6%	0.9	41	11%	triaxial
T1	11630.95	12038.43	11823.89	11030.53	1.035	63.8	61.4	1.017	333.5	0.2	0.948	63.3	-28.6	2%	7%	0.3	15	9%	oblate
T2A	674.48	702.14	675.89	645.403	1.039	50.4	1.9	1.002	318.1	51.2	0.959	321.9	-38.8	4%	4%	0.9	42	8%	triaxial
T2B	116.28	118.641	117.384	112.821	1.02	61.6	-28.3	1.009	19.9	54.2	0.97	320.3	-20.1	1%	4%	0.3	16	5%	oblate
T3	5197.05	5307.802	5250.215	5033.133	1.021	208.5	-16.3	1.01	138.7	49.8	0.969	106.5	-35.6	1%	4%	0.3	15	5%	oblate
T4A	134.14	136.495	133.249	132.669	1.018	283.8	-42.5	0.993	23.6	-10.5	0.989	304.5	45.6	2%	0%	5.7	80	3%	prolate
T4B	154.11	156.155	153.609	152.579	1.013	270.9	-17.2	0.997	358.2	8.8	0.99	242.1	70.5	2%	1%	2.4	68	2%	prolate-triaxial
T5A	149.53	153.801	150.922	143.861	1.029	0.5	-26.7	1.009	71.4	33	0.962	300.8	45.1	2%	5%	0.4	22	7%	oblate-triaxial
T5B	173.29	178.487	175.788	165.597	1.029	359.7	-32.6	1.015	74.3	22.6	0.956	316.2	48.5	1%	6%	0.2	14	7%	oblate

References

Anderson, E., 1936, The dynamics of the formation of cone-sheets, ring-dykes and cauldron-subsidence: Proceedings of the Royal Society of Edinburgh, v. 56, p. 128-157.

Anderson, E. D., Hitzman, M. W., Monecke, T., Bedrosian, P. A., Shah, A. K., and Kelley, K. D., 2013, Geological analysis of aeromagnetic data from southwestern Alaska: Implications for exploration in the area of the Pebble porphyry Cu-Au-Mo deposit: Economic Geology, v. 108, no. 3, p. 421-436.

Anderson, P., 1950, Antiferromagnetism. Theory of superexchange interaction: Physical Review, v. 79, no. 2, p. 350.

Anderson, T., 2004, Southern Uplands–Down–Longford Terrane: The geology of Northern Ireland–Our natural foundation, p. 41-60.

Annen, C., 2009, From plutons to magma chambers: Thermal constraints on the accumulation of eruptible silicic magma in the upper crust: Earth and Planetary Science Letters, v. 284, no. 3, p. 409-416.

-, 2011, Implications of incremental emplacement of magma bodies for magma differentiation, thermal aureole dimensions and plutonism–volcanism relationships: Tectonophysics, v. 500, no. 1, p. 3-10.

Annen, C., Blundy, J., and Sparks, R., 2006, The genesis of intermediate and silicic magmas in deep crustal hot zones: Journal of Petrology, v. 47, no. 3, p. 505-539.

Aranguren, A., Cuevas, J., Tubia, J., Román-Berdiel, T., Casas-Sainz, A., and Casas-Ponsati, A., 2003, Granite laccolith emplacement in the Iberian arc: AMS and gravity study of the La Tojiza pluton (NW Spain): Journal of the Geological Society, v. 160, no. 3, p. 435-445.

Arbaret, L., Diot, H., Bouchez, J. L., Lespinasse, P., and de Saint-Blanquat, M., 1997, Analogue 3D simple-shear experiments of magmatic biotite subfabrics, Granite: from segregation of melt to emplacement fabrics, Springer, p. 129-143.

Archanjo, C. J., Trindade, R. I., Bouchez, J. L., and Ernesto, M., 2002, Granite fabrics and regional‐scale strain partitioning in the Seridó belt (Borborema Province, NE Brazil): Tectonics, v. 21, no. 1, p. 3-1-3-14.

Atherton, M., and Ghani, A., 2002, Slab breakoff: a model for Caledonian, Late Granite syn-collisional magmatism in the orthotectonic (metamorphic) zone of Scotland and Donegal, Ireland: Lithos, v. 62, no. 3, p. 65-85.

Atherton, M. P., 1993, Granite magmatism: Journal of the Geological Society, v. 150, no. 6, p. 1009-1023.

Aydin, A., and Nur, A., 1982, Evolution of pull-apart basins and their scale independence: Tectonics, v. 1, no. 1, p. 91-105.

Baranov, V., and Naudy, H., 1964, Numerical calculation of the formula of reduction to the magnetic pole: Geophysics, v. 29, no. 1, p. 67-79.

Barnes, R., Anderson, T., and McCurry, J., 1987, Along-strike variation in the stratigraphical and structural profile of the Southern Uplands Central Belt in Galloway and Down: Journal of the Geological Society, v. 144, no. 5, p. 807-816.

Bateman, R., 1984, On the role of diapirism in the, segregation, ascent and final emplacement of granitoid magmas: Tectonophysics, v. 110, no. 3, p. 211-231.

-, 1985, Aureole deformation by flattening around a diapir during in situ ballooning: the Cannibal Creek granite: The Journal of Geology, p. 293-310.

Beamish, D., Kimbell, G., Stone, P., and Anderson, T., 2010, Regional conductivity data used to reassess Early Palaeozoic structure in the Northern Ireland sector of the Southern Uplands–Down–Longford terrane: Journal of the Geological Society, v. 167, no. 4, p. 649-657.

Beausoleil, N., Lavallee, P., Yelon, A., Ballet, O., and Coey, J., 1983, Magnetic properties of biotite micas: Journal of applied physics, v. 54, no. 2, p. 906-915.

Benn, K., 1994, Overprinting of magnetic fabrics in granites by small strains: numerical modelling: Tectonophysics, v. 233, no. 3, p. 153-162.

Besser, P., Morrish, A., and Searle, C., 1967, Magnetocrystalline anisotropy of pure and doped hematite: Physical Review, v. 153, no. 2, p. 632.

Blake, S., and Fink, J., 2000, On the deformation and freezing of enclaves during magma mixing: Journal of Volcanology and Geothermal Research, v. 95, no. 1, p. 1-8.

Bluck, B., 1985, The Scottish paratectonic Caledonides: Scottish Journal of Geology, v. 21, no. 4, p. 437-464.

Blumenfeld, P., and Bouchez, J.-L., 1988, Shear criteria in granite and migmatite deformed in the magmatic and solid states: Journal of Structural Geology, v. 10, no. 4, p. 361-372.

Böhnel, H., McIntosh, G., and Sherwood, G., 2002, A parameter characterising the irreversibility of thermomagnetic curves: Physics and Chemistry of the Earth, Parts A/B/C, v. 27, no. 25, p. 1305-1309.

Borradaile, G., and Henry, B., 1997, Tectonic applications of magnetic susceptibility and its anisotropy: Earth-Science Reviews, v. 42, no. 1, p. 49-93.

Bouchez, J. L., 1997, Granite is never isotropic: an introduction to AMS studies of granitic rocks, Granite: from segregation of melt to emplacement fabrics, Springer, p. 95-112.

Boudreau, A., Love, C., and Prendergast, M., 1995, Halogen geochemistry of the Great Dyke, zimbabwe: Contributions to Mineralogy and Petrology, v. 122, no. 3, p. 289-300.

Bouillin, J.-P., Bouchez, J.-L., Lespinasse, P., and Pecher, A., 1993, Granite emplacement in an extensional setting: an AMS study of the magmatic structures of Monte Capanne (Elba, Italy): Earth and Planetary Science Letters, v. 118, no. 1, p. 263-279.

Bowen, N., 1919, Crystallization-differentiation in igneous magmas: The Journal of Geology, p. 393-430.

Broome, H. J., 1990, Generation and interpretation of geophysical images with examples from the Rae Province, northwestern Canada shield: Geophysics, v. 55, no. 8, p. 977-997.

Brown, G., 1979, Geochemical and geophysical constraints on the origin and evolution of Caledonian granites: Geological Society, London, Special Publications, v. 8, no. 1, p. 643-651.

Brown, G., Thorpe, R., and Webb, P., 1984, The geochemical characteristics of granitoids in contrasting arcs and comments on magma sources: Journal of the Geological Society, v. 141, no. 3, p. 413-426.

Brown, M., 2013, Granite: From genesis to emplacement: Geological Society of America Bulletin, v. 125, no. 7-8, p. 1079-1113.

Brown, P., Ryan, P., Soper, N., and Woodcock, N., 2008, The newer granite problem revisited: a transtensional origin for the early Devonian Trans-Suture suite: Geological Magazine, v. 145, no. 02, p. 235-256.

Brun, J., Gapais, D., Cogne, J., Ledru, P., and Vigneresse, J., 1990, The Flamanville granite (northwest France): an unequivocal example of a syntectonically expanding pluton: Geological Journal, v. 25, no. 3-4, p. 271-286.

Brun, J., and Pons, J., 1981, Strain patterns of pluton emplacement in a crust undergoing non-coaxial deformation, Sierra Morena, Southern Spain: Journal of Structural Geology, v. 3, no. 3, p. 219-229.

Burchardt, S., Tanner, D., and Krumbholz, M., 2012, The Slaufrudalur pluton, southeast Iceland—An example of shallow magma emplacement by coupled cauldron subsidence and magmatic stoping: Geological Society of America Bulletin, v. 124, no. 1-2, p. 213-227.

Burg, J.-P., and Vigneresse, J.-L., 2002, Non-linear feedback loops in the rheology of cooling-crystallizing felsic magma and heating-melting felsic rock: Geological Society, London, Special Publications, v. 200, no. 1, p. 275-292.

Butler, R. F., 1992, Paleomagnetism: magnetic domains to geologic terranes, Blackwell Scientific Publications Boston.

Butler, R. F., and Banerjee, S. K., 1975, Theoretical single-domain grain size range in magnetite and titanomagnetite: Journal of Geophysical Research, v. 80, no. 29, p. 4049-4058.

Calhoun, B., 1954, Magnetic and electric properties of magnetite at low temperatures: Physical Review, v. 94, no. 6, p. 1577.

Cañón-Tapia, E., 1996, Single-grain versus distribution anisotropy: a simple three-dimensional model: Physics of the Earth and Planetary Interiors, v. 94, no. 1, p. 149-158.

Caricchi, L., Annen, C., Rust, A., and Blundy, J., 2012, Insights into the mechanisms and timescales of pluton assembly from deformation patterns of mafic enclaves: Journal of Geophysical Research: Solid Earth (1978–2012), v. 117, no. B11.

Carmichael, I. S., 2002, The andesite aqueduct: perspectives on the evolution of intermediate magmatism in west-central (105–99 W) Mexico: Contributions to Mineralogy and Petrology, v. 143, no. 6, p. 641-663.

Chapman, R. W., and CHAPMAN, C. A., 1940, Cauldron subsidence at Ascutney Mountain, Vermont: Geological Society of America Bulletin, v. 51, no. 2, p. 191-211.

Chernicoff, C. J., Richards, J. P., and Zappettini, E. O., 2002, Crustal lineament control on magmatism and mineralization in northwestern Argentina: geological, geophysical, and remote sensing evidence: Ore Geology Reviews, v. 21, no. 3, p. 127-155.

Chew, D., and Stillman, C., 2009, Late Caledonian orogeny and magmatism: The Geology of Ireland, p. 143-173.

Clemens, J., 1998, Observations on the origins and ascent mechanisms of granitic magmas: Journal of the Geological Society, v. 155, no. 5, p. 843-851.

Clemens, J., and Mawer, C., 1992, Granitic magma transport by fracture propagation: Tectonophysics, v. 204, no. 3, p. 339-360.

Clemens, J., Petford, N., and Mawer, C., 1997, Ascent mechanisms of granitic magmas: causes and consequences: MINERALOGICAL SOCIETY SERIES, v. 8, p. 145-172.

Cloos, H., 1925, Einführung in die tektonische Behandlung magmatischer Erscheinungen (granittektonik): spezieller teil. Das Riesengebirge in Schlesien; bau, bildung und oberflächengestaltung, Gebrüder Borntraeger.

Clough, C. T., Maufe, H. B., and Bailey, E. B., 1909, The cauldron-subsidence of Glen Coe, and the associated igneous phenomena: Quarterly Journal of the Geological Society, v. 65, no. 1-4, p. 611-678.

Cogné, J., 1988, Strain-induced AMS in the granite of Flamanville and its effects upon TRM acquisition: Geophys. J, v. 92, p. 445-453.

Cogné, J., and Perroud, H., 1988, Anisotropy of magnetic susceptibility as a strain gauge in the Flamanville granite, NW France: Physics of the earth and planetary interiors, v. 51, no. 4, p. 264-270.

Coleman, D. S., Gray, W., and Glazner, A. F., 2004, Rethinking the emplacement and

evolution of zoned plutons: Geochronologic evidence for incremental assembly of the Tuolumne Intrusive Suite, California: Geology, v. 32, no. 5, p. 433-436.

Conder, J. A., Wiens, D. A., and Morris, J., 2002, On the decompression melting structure at volcanic arcs and back-arc spreading centers: Geophysical Research Letters, v. 29, no. 15, p. 17-11-17-14.

Cook, D., and Weir, J., 1980, The stratigraphical setting of the Cairnsmore of Fleet Pluton, Galloway: Scottish Journal of Geology, v. 16, no. 2-3, p. 125-141.

Cook, S., Corner, R., Groves, P., and Grealish, G., 1996, Use of airborne gamma radiometric data for soil mapping: Soil Research, v. 34, no. 1, p. 183-194.

Cooper, M., Crowley, Q., Hollis, S., Noble, S., and Henney, P., 2013, AU–Pb age for the Late Caledonian Sperrin Mountains minor intrusions suite in the north of Ireland: timing of slab break-off in the Grampian terrane and the significance of deep-seated, crustal lineaments: Journal of the Geological Society, v. 170, no. 4, p. 603-614.

Cooper, M., and Johnson, T., 2004, Chapter 5: Late Palaeozoic Intrusives, *in* Mitchell, W., ed., The geology of Northern Ireland: our natural foundation, Geological Survey of Northern Ireland, Belfast, p. 61-68.

Crawford, A., Falloon, T., and Eggins, S., 1987, The origin of island arc high-alumina basalts: Contributions to Mineralogy and Petrology, v. 97, no. 3, p. 417-430.

Cruden, A., and McCaffrey, K., 2001, Growth of plutons by floor subsidence: implications for rates of emplacement, intrusion spacing and melt-extraction mechanisms: Physics and Chemistry of the Earth, Part A: Solid Earth and Geodesy, v. 26, no. 4, p. 303-315.

Cruden, A. R., 1990, Flow and fabric development during the diapiric rise of magma: The Journal of Geology, p. 681-698.

-, 1998, On the emplacement of tabular granites: Journal of the Geological Society-London, v. 155, no. 5, p. 853-862.

D'lemos, R., Brown, M., and Strachan, R., 1992, Granite magma generation, ascent and emplacement within a transpressional orogen: Journal of the Geological Society, v. 149, no. 4, p. 487-490.

Daly, R. A., 1903, The mechanics of igneous intrusion: American Journal of Science, no. 88, p. 269-298.

-, 1933, Igneous rocks and the depths of the earth: containing some revised chapters of" Igneous rocks and their origin"(1914), McGraw-Hill Book Company, Incorporated.

Dankers, P., 1981, Relationship between median destructive field and remanent coercive forces for dispersed natural magnetite, titanomagnetite and hematite: Geophysical Journal International, v. 64, no. 2, p. 447-461.

Davis, P., and Evans, M., 1976, Interacting single-domain properties of magnetite intergrowths: Journal of Geophysical Research, v. 81, no. 5, p. 989-994.

de Boer, C. B., Dekkers, M. J., and van Hoof, T. A., 2001, Rock-magnetic properties of TRM carrying baked and molten rocks straddling burnt coal seams: Physics of the Earth and Planetary Interiors, v. 126, no. 1, p. 93-108.

de la Roche, H., 1964, Sur l'expression graphique des relations entre la composition chimique et la composition minéralogique quantitative des roches cristallines. Presentation d'un diagramme destiné à l'étude chimo-minéralogique des massifs granitiques ou grano-dioritiques. Application aux Vosges cristallines: Sciences de la Terre, v. 9, p. 293-337.

de Saint Blanquat, M., Horsman, E., Habert, G., Morgan, S., Vanderhaeghe, O., Law, R., and Tikoff, B., 2011, Multiscale magmatic cyclicity, duration of pluton construction, and the paradoxical relationship between tectonism and plutonism in continental arcs: Tectonophysics, v. 500, no. 1, p. 20-33.

Debon, F., and Le Fort, P., 1988, A cationic classification of plutonic rocks and their magmatic associations: principles, methods, applications: Bulletin de Minéralogie, v. 111, p. 493-510.

Debon, F., and Lemmet, M., 1999, Evolution of Mg/Fe ratios in late Variscan plutonic rocks from the external crystalline massifs of the Alps (France, Italy, Switzerland): Journal of Petrology, v. 40, no. 7, p. 1151-1185.

Deer, W., 1966, Howie. RA and Zussman, J., 1966. An Introduction to the Rock Forming Minerals, Longman, London.

Dehls, J., Cruden, AR, and Vigneresse, J.-L., 1998, Fracture control of late Archean pluton emplacement in the northern Slave Province, Canada: Journal of Structural Geology, v. 20, no. 9, p. 1145-1154.

Dempsey, C., 1990, Halliday, AN and Meighan, IG, 1990. Combined Sm-Nd and Rb-Sr isotope systematic,., in the Donegal granitoids and their petrogenetic implications: Geol. Mag, v. 127, p. 75-80.

Dewey, J., and Strachan, R., 2003, Changing Silurian–Devonian relative plate motion in the Caledonides: sinistral transpression to sinistral transtension: Journal of the Geological Society, v. 160, no. 2, p. 219-229.

Djouadi, M.-T., and Bouchez, J.-L., 1992, Structure étrange du granite du Tesnou (Hoggar, Algérie): Comptes rendus de l'Académie des sciences. Série 2, Mécanique, Physique, Chimie, Sciences de l'univers, Sciences de la Terre, v. 315, no. 10, p. 1231-1238.

Douce, A. E. P., 1999, What do experiments tell us about the relative contributions of crust and mantle to the origin of granitic magmas?: Geological Society, London, Special Publications, v. 168, no. 1, p. 55-75.

Dunlop, D., 1971, Magnetic properties of fine-particle hematite: Ann. Geophys, v. 27, no. 3, p. 269-293.

-., 1986, Hysteresis properties of magnetite and their dependence on particle size: A test of pseudo-single-domain remanence models: Journal of Geophysical Research: Solid Earth (1978–2012), v. 91, no. B9, p. 9569-9584.

Dunlop, D. J., and Özdemir, Ö., 2001, Rock magnetism: fundamentals and frontiers, Cambridge University Press.

Dunlop, D. J., Stacey, F. D., and Gillingham, D. E., 1974, The origin of thermoremanent magnetization: Contribution of pseudo-single-domain magnetic moments: Earth and Planetary Science Letters, v. 21, no. 3, p. 288-294.

Egan, F. W., 1872, Explanatory memoir to Sheet 48, Mem. Geol. Surv. Ireland.

Egan, H., 1881, Explanatory memoir to Sheets 60, 61 and part of 71, Mem. Geol. Surv. Ireland.

-., 1873, Explanatory Memoir to Sheet 47: Mem. Geol. Surv. Ireland.

Eichelberger, J. C., 1975, Origin of andesite and dacite: evidence of mixing at Glass Mountain in California and at other circum-Pacific volcanoes: Geological Society of America Bulletin, v. 86, no. 10, p. 1381-1391.

Eichelberger, J. C., Izbekov, P. E., and Browne, B. L., 2006, Bulk chemical trends at arc volcanoes are not liquid lines of descent: Lithos, v. 87, no. 1, p. 135-154.

Emeleus, C. H., Troll, V. R., Chew, D. M., and Meade, F. C., 2012, Lateral versus vertical emplacement in shallow-level intrusions? The Slieve Gullion Ring-complex revisited: Journal of the Geological Society, v. 169, no. 2, p. 157-171.

England, R., 1990, The identification of granitic diapirs: Journal of the Geological Society, v. 147, no. 6, p. 931-933.

Ewart, A., Milner, S., Duncan, A., and Bailey, M., 2002, The Cretaceous Messum igneous complex, SW Etendeka, Namibia: reinterpretation in terms of a downsag-cauldron subsidence model: Journal of Volcanology and Geothermal Research, v. 114, no. 3, p. 251-273.

Fabian, K., Shcherbakov, V., and McEnroe, S., 2013, Measuring the Curie temperature: Geochemistry, Geophysics, Geosystems, v. 14, no. 4, p. 947-961.

Farina, F., Stevens, G., and Villaros, A., 2012, Multi-batch, incremental assembly of a dynamic magma chamber: the case of the Peninsula pluton granite (Cape Granite Suite, South Africa): Mineralogy and Petrology, v. 106, no. 3-4, p. 193-216.

Farner, M. J., Lee, C.-T. A., and Putirka, K. D., 2014, Mafic–felsic magma mixing limited by reactive processes: A case study of biotite-rich rinds on mafic enclaves: Earth and Planetary Science Letters, v. 393, p. 49-59.

Fernandez, A. N., and Gasquet, D. R., 1994, Relative rheological evolution of chemically contrasted coeval magmas: example of the Tichka plutonic complex (Morocco): Contributions to Mineralogy and Petrology, v. 116, no. 3, p. 316-326.

Ferré, E. C., Galland, O., Montanari, D., and Kalakay, T. J., 2012, Granite magma migration and emplacement along thrusts: International Journal of Earth Sciences, v. 101, no. 7, p. 1673-1688.

Ferris, J., Johnson, A., and Storey, B., 1998, Form and extent of the Dufek intrusion, Antarctica, from newly compiled aeromagnetic data: Earth and Planetary Science Letters, v. 154, no. 1, p. 185-202.

Fowler, M., Henney, P., Darbyshire, D., and Greenwood, P., 2001, Petrogenesis of high Ba–Sr granites: the Rogart pluton, Sutherland: Journal of the Geological Society, v. 158, no. 3, p. 521-534.

Frost, T. P., and Mahood, G. A., 1987, Field, chemical, and physical constraints on mafic-felsic magma interaction in the Lamarck Granodiorite, Sierra Nevada, California: Geological Society of America Bulletin, v. 99, no. 2, p. 272-291.

Gaillot, P., de Saint-Blanquat, M., and Bouchez, J.-L., 2006, Effects of magnetic interactions in anisotropy of magnetic susceptibility: Models, experiments and implications for igneous rock fabrics quantification: Tectonophysics, v. 418, no. 1, p. 3-19.

Galadí-Enríquez, E., Galindo-Zaldívar, J., Simancas, F., and Expósito, I., 2003, Diapiric emplacement in the upper crust of a granitic body: the La Bazana granite (SW Spain): Tectonophysics, v. 361, no. 1, p. 83-96.

Gamble, J., 1979, Some relationships between coexisting granitic and basaltic magmas and the genesis of hybrid rocks in the Tertiary central complex of Slieve Gullion, northeast Ireland: Journal of Volcanology and Geothermal Research, v. 5, no. 3, p. 297-316.

Gamble, J., Meighan, I., and McCormick, A., 1992, The petrogenesis of Tertiary microgranites and granophyres from the Slieve Gullion Central Complex, NE Ireland: Journal of the Geological Society, v. 149, no. 1, p. 93-106.

Gapais, D., and Barbarin, B., 1986, Quartz fabric transition in a cooling syntectonic granite (Hermitage Massif, France): Tectonophysics, v. 125, no. 4, p. 357-370.

Gilbert, G., 1877, Report on the geology of the Henry Mountains: U.S. Geogr. Geol. Survey of the Rocky Mountains Region.

Gillespie, M., and Styles, M., 1999, BGS rock classification scheme, Volume 1. Classification of igneous rocks.

Glazner, A. F., and Bartley, J. M., 2006, Is stoping a volumetrically significant pluton emplacement process?: Geological Society of America Bulletin, v. 118, no. 9-10, p. 1185-1195.

-, 2008, Reply to comments on “Is stoping a volumetrically significant pluton emplacement process?”: Geological Society of America Bulletin, v. 120, no. 7-8, p. 1082-1087.

Glazner, A. F., Bartley, J. M., Coleman, D. S., Gray, W., and Taylor, R. Z., 2004, Are plutons assembled over millions of years by amalgamation from small magma chambers?: GSA today, v. 14, no. 4/5, p. 4-12.

Gleizes, G., Nédélec, A., Bouchez, J. L., Autran, A., and Rochette, P., 1993, Magnetic susceptibility of the Mont-Louis andorra ilmenite-type granite (Pyrenees): A new tool for the petrographic characterization and regional mapping of zoned granite plutons: Journal of Geophysical Research: Solid Earth (1978–2012), v. 98, no. B3, p. 4317-4331.

Goodenough, J. B., 1968, Localized vs collective descriptions of magnetic electrons: Journal of Applied Physics, v. 39, no. 2, p. 403-411.

Grantham, D., 1928, The petrology of the Shap Granite: Proceedings of the Geologists' Association, v. 39, no. 3, p. 299-IN211.

Grasty, R., 1975, Uranium measurement by airborne gamma-ray spectrometry: Geophysics, v. 40, no. 3, p. 503-519.

Grégoire, V., Darrozes, J., Gaillot, P., Nédélec, A., and Launeau, P., 1998, Magnetite grain shape fabric and distribution anisotropy vs rock magnetic fabric: a three-dimensional case study: Journal of Structural Geology, v. 20, no. 7, p. 937-944.

Grégoire, V., de Saint Blanquat, M., Nédélec, A., and Bouchez, J. L., 1995, Shape anisotropy versus magnetic interactions of magnetite grains: experiments and application to AMS in granitic rocks: Geophysical Research Letters, v. 22, no. 20, p. 2765-2768.

Grout, F., 1945, Scale models of structures related to batholiths: American Journal of Science, v. 243A, p. 260-284.

Grove, T., Parman, S., Bowring, S., Price, R., and Baker, M., 2002, The role of an H2O-rich fluid component in the generation of primitive basaltic andesites and andesites from the Mt. Shasta region, N California: Contributions to Mineralogy and Petrology, v. 142, no. 4, p. 375-396.

GSNI, 1997, Geological map of Northern Ireland, Solid Geology (Second Edition): Keyworth, scale 1:250 000.

-, 2007, Tellus project overview. Available from <http://www.bgs.ac.uk/gsni/tellus/overview/>. [21st September 2007].

Guillope, M., and Poirier, J., 1979, Dynamic recrystallization during creep of single-crystalline halite: An experimental study: Journal of Geophysical Research: Solid Earth (1978–2012), v. 84, no. B10, p. 5557-5567.

Guineberteau, B., Bouchez, J.-L., and Vigneresse, J.-L., 1987, The Mortagne granite pluton (France) emplaced by pull-apart along a shear zone: Structural and gravimetric arguments and regional implication: Geological Society of America Bulletin, v. 99, no. 6, p. 763-770.

Gunn, P., Maidment, D., and Milligan, P., 1997, Interpreting aeromagnetic data in areas of limited outcrop: AGSO Journal of Australian Geology and Geophysics, v. 17, p. 175-186.

Hall, A., 1996, Igneous Petrology (2nd Edition), Addison Wesley, New York.

Halliday, A., Aftalion, M., van Breemen, O., and Jocelyn, J., 1979, Petrogenetic significance of Rb-Sr and U-Pb isotopic systems in the 400 Ma old British Isles granitoids and their hosts: Geological Society, London, Special Publications, v. 8, no. 1, p. 653-661.

Halliday, A., Stephens, W., Hunter, R., Menzies, M., Dickin, A., and Hamilton, P., 1985, Isotopic and chemical constraints on the building of the deep Scottish lithosphere: Scottish Journal of Geology, v. 21, no. 4, p. 465-491.

Hargraves, R., Johnson, D., and Chan, C., 1991, Distribution anisotropy: the cause of AMS in igneous rocks?: Geophysical Research Letters, v. 18, no. 12, p. 2193-2196.

Harker, A., 1909, The natural history of igneous rocks Methneu: London. 344p.

Harry, W., and Richey, J., 1963, Magmatic pulses in the emplacement of plutons: Geological Journal, v. 3, no. 2, p. 254-268.

Hartstra, R., 1982, High-temperature characteristics of a natural titanomagnetite: Geophysical Journal International, v. 71, no. 2, p. 455-476.

He, B., Xu, Y.-G., and Paterson, S., 2009, Magmatic diapirism of the Fangshan pluton, southwest of Beijing, China: Journal of Structural Geology, v. 31, no. 6, p. 615-626.

Hecht, L., and Vigneresse, J., 1999, A multidisciplinary approach combining geochemical, gravity and structural data: implications for pluton emplacement and zonation: Geological Society, London, Special Publications, v. 168, no. 1, p. 95-110.

Higgins, M. D., 2006, Quantitative textural measurements in igneous and metamorphic petrology, Cambridge University Press Cambridge.

Hildreth, W., and Moorbath, S., 1988, Crustal contributions to arc magmatism in the Andes of central Chile: Contributions to Mineralogy and Petrology, v. 98, no. 4, p. 455-489.

Hirose, K., 1997, Melting experiments on lherzolite KLB-1 under hydrous conditions and generation of high-magnesian andesitic melts: Geology, v. 25, no. 1, p. 42-44.

Holder, M., 1979, An emplacement mechanism for post-tectonic granites and its implications for their geochemical features, Origin of granite batholiths, Springer, p. 116-128.

Holdsworth, R., Tavarnelli, E., and Clegg, P., 2002, The nature and regional significance of structures in the Gala Group of the Southern Uplands terrane, Berwickshire coast, southeastern Scotland: Geological Magazine, v. 139, no. 06, p. 707-717.

Hopkinson, J., 1889, Magnetic and other physical properties of iron at a high temperature: Philosophical Transactions of the Royal Society of London. A, p. 443-465.

Hrouda, F., Jelínek, V., and Zapletal, K., 1997, Refined technique for susceptibility resolution into ferromagnetic and paramagnetic components based on susceptibility temperature-variation measurement: Geophysical Journal International, v. 129, no. 3, p. 715-719.

Hubert, A., Schafer, R., Hubert, A., and Schafer, R., 1998, Magnetic domains, Springer.

Huppert, H. E., and Sparks, R. S. J., 1988, The generation of granitic magmas by intrusion of basalt into continental crust: Journal of Petrology, v. 29, no. 3, p. 599-624.

Hutton, D., 1982, A tectonic model for the emplacement of the Main Donegal Granite, NW Ireland: Journal of the Geological Society, v. 139, no. 5, p. 615-631.

Hutton, D., and Alsop, G., 1996, The Caledonian strike-swing and associated lineaments in NW Ireland and adjacent areas: sedimentation, deformation and igneous intrusion patterns: Journal of the Geological Society, v. 153, no. 3, p. 345-360.

Hutton, D., and McErlean, M., 1991, Silurian and Early Devonian sinistral deformation of the Ratagain granite, Scotland: constraints on the age of Caledonian movements on the Great Glen fault system: Journal of the Geological Society, v. 148, no. 1, p. 1-4.

Hutton, D., and Reavy, R., 1992, Strike-slip tectonics and granite petrogenesis: Tectonics, v. 11, no. 5, p. 960-967.

Hutton, D. H., 1988, Granite emplacement mechanisms and tectonic controls: inferences from deformation studies: Transactions of the Royal Society of Edinburgh: Earth Sciences, v. 79, no. 2-3, p. 245-255.

-, 1992, Granite sheeted complexes: evidence for the dyking ascent mechanism: Geological Society of America Special Papers, v. 272, p. 377-382.

-, 1997, Syntectonic granites and the principle of effective stress: a general solution to the space problem?, Granite: from segregation of melt to emplacement fabrics, Springer, p. 189-197.

Hutton, D. H., and Siegesmund, S., 2001, The Ardara Granite: reinflating the balloon hypothesis: Zeitschrift der Deutschen Geologischen Gesellschaft, p. 309-323.

Hutton, J., 1788, Theory of the Earth; or an Investigation of the Laws observable in the Composition, Dissolution, and Restoration of Land upon the Globe: Transactions of the Royal Society of Edinburgh, v. 1, no. 02, p. 209-304.

Ingram, G. M., and Hutton, D. H., 1994, The Great Tonalite Sill: Emplacement into a contractional shear zone and implications for Late Cretaceous to early Eocene tectonics in southeastern Alaska and British Columbia: Geological Society of America Bulletin, v. 106, no. 5, p. 715-728.

Ising, G., 1942, On the magnetic properties of varved clay. Ark. Mat. Astron. Fys.. v. 29A, p. 1-37.

Nolan, J., 1877, Explanatory memoir to Sheet 70, Mem. Geol. Surv. Ireland.

Jacques, J., and Reavy, R., 1994, Caledonian plutonism and major lineaments in the SW Scottish Highlands: Journal of the Geological Society, v. 151, no. 6, p. 955-969.

Jerram, D. A., and Higgins, M. D., 2007, 3D analysis of rock textures: quantifying igneous microstructures: Elements, v. 3, no. 4, p. 239-245.

John, B. E., and Stünitz, H., 1997, Magmatic fracturing and small-scale melt segregation during pluton emplacement: evidence from the Adamello massif (Italy), Springer.

Johnson, A. M., and Pollard, D. D., 1973, Mechanics of growth of some laccolithic intrusions in the Henry mountains, Utah, I: field observations, Gilbert's model, physical properties and flow of the magma: Tectonophysics, v. 18, no. 3, p. 261-309.

Keaney, A., McKinley, J., Graham, C., Robinson, M., and Ruffell, A., 2013, Spatial statistics to estimate peat thickness using airborne radiometric data: Spatial Statistics, v. 5, p. 3-24.

Kelemen, P. B., and Dick, H. J., 1995, Focused melt flow and localized deformation in the upper mantle: juxtaposition of replacive dunite and ductile shear zones in the Josephine peridotite, SW Oregon: Journal of Geophysical Research: Solid Earth (1978–2012), v. 100, no. B1, p. 423-438.

Kemp, A., 1987, Tectonic development of the Southern Belt of the Southern Uplands accretionary complex: Journal of the Geological Society, v. 144, no. 5, p. 827-838.

Kerr, A. D., and Pollard, D. D., 1998, Toward more realistic formulations for the analysis of laccoliths: Journal of Structural Geology, v. 20, no. 12, p. 1783-1793.

Khan, M. A., 1962, The anisotropy of magnetic susceptibility of some igneous and metamorphic rocks: Journal of Geophysical Research, v. 67, no. 7, p. 2873-2885.

King, J., Banerjee, S. K., Marvin, J., and Özdemir, Ö., 1982, A comparison of different magnetic methods for determining the relative grain size of magnetite in natural materials: some results from lake sediments: Earth and Planetary Science Letters, v. 59, no. 2, p. 404-419.

Kingsley, L., 1931, Cauldron subsidence of the Ossipee Mountains: American Journal of Science, no. 128, p. 139-168.

Kistler, R., Chappell, B., Peck, D., and Bateman, P., 1986, Isotopic variation in the Tuolumne intrusive suite, central Sierra Nevada, California: Contributions to Mineralogy and Petrology, v. 94, no. 2, p. 205-220.

Kittel, C., 1946, Theory of the structure of ferromagnetic domains in films and small particles: Physical Review, v. 70, no. 11-12, p. 965.

Knipe, R., and Needham, D., 1986, Deformation processes in accretionary wedges—examples from the SW margin of the Southern Uplands, Scotland: Geological Society, London, Special Publications, v. 19, no. 1, p. 51-65.

Koyaguchi, T., and Kaneko, K., 1999, A two-stage thermal evolution model of magmas in continental crust: Journal of Petrology, v. 40, no. 2, p. 241-254.

Kryza, R., Schaltegger, U., Oberc-Dziedzic, T., Pin, C., and Ovtcharova, M., 2014, Geochronology of a composite granitoid pluton: a high-precision ID-TIMS U–Pb zircon study of the Variscan Karkonosze Granite (SW Poland): International Journal of Earth Sciences, v. 103, no. 3, p. 683-696.

Lagroix, F., and Borradaile, G. J., 2000, Magnetic fabric interpretation complicated by inclusions in mafic silicates: Tectonophysics, v. 325, no. 3, p. 207-225.

Le Bas, M., and Streckeisen, A., 1991, The IUGS systematics of igneous rocks: Journal of the Geological Society, London, v. 148, p. 825-833.

Le Maitre, R. W., 2002, Igneous Rocks: A Classification and Glossary of Terms: A Classification and Glossary of Terms: Recommendations of the International Union of Geological Sciences, Subcommission on the Systematics of Igneous Rocks, Cambridge University Press.

Leake, B., 1978, Granite emplacement: the granites of Ireland and their origin: Crustal evolution in NW Britain and adjacent regions. Geol. J. Spec. Issue, no. 10, p. 221-248.

Leggett, J., 1987, The Southern Uplands as an accretionary prism: the importance of analogues in reconstructing palaeogeography: Journal of the Geological Society, v. 144, no. 5, p. 737-751.

Leggett, J., McKerrow, W., Morris, J., Oliver, G., and Phillips, W., 1979, The north-western margin of the Iapetus Ocean: Geological Society, London, Special Publications, v. 8, no. 1, p. 499-512.

Lipman, P. W., 2007, Incremental assembly and prolonged consolidation of Cordilleran magma chambers: Evidence from the Southern Rocky Mountain volcanic field: Geosphere, v. 3, no. 1, p. 42-70.

Lister, G., and Dornsiepen, U., 1982, Fabric transitions in the Saxony granulite terrain: Journal of Structural Geology, v. 4, no. 1, p. 81-92.

Lonsdale, K., 1937, Diamagnetic and paramagnetic anisotropy of crystals: Reports on Progress in Physics, v. 4, no. 1, p. 368.

Lowrie, W., 1990, Identification of ferromagnetic minerals in a rock by coercivity and unblocking temperature properties: Geophysical Research Letters, v. 17, no. 2, p. 159-162.

Lowrie, W., and Fuller, M., 1971, On the alternating field demagnetization characteristics of multidomain thermoremanent magnetization in magnetite: Journal of Geophysical Research, v. 76, no. 26, p. 6339-6349.

Lynne, B. Y., and Campbell, K. A., 2004, Morphologic and mineralogic transitions from opal-A to opal-CT in low-temperature siliceous sinter diagenesis, Taupo Volcanic Zone, New Zealand: Journal of Sedimentary Research, v. 74, no. 4, p. 561-579.

Magee, C., Briggs, F., and Jackson, C. A., 2013, Lithological controls on igneous intrusion-induced ground deformation: Journal of the Geological Society, v. 170, no. 6, p. 853-856.

Mahan, K. H., Bartley, J. M., Coleman, D. S., Glazner, A. F., and Carl, B. S., 2003, Sheeted intrusion of the synkinematic McDoogle pluton, Sierra Nevada, California: Geological Society of America Bulletin, v. 115, no. 12, p. 1570-1582.

Mann, P., Hempton, M. R., Bradley, D. C., and Burke, K., 1983, Development of pull-apart basins: The Journal of Geology, p. 529-554.

Marsh, B. D., 1982, On the mechanics of igneous diapirism, stoping, and zone melting: American Journal of Science, v. 282, no. 6, p. 808-855.

Martelet, G., Truffert, C., Tourlière, B., Ledru, P., and Perrin, J., 2006, Classifying airborne radiometry data with Agglomerative Hierarchical Clustering: A tool for geological mapping in context of rainforest (French Guiana): International Journal of Applied Earth Observation and Geoinformation, v. 8, no. 3, p. 208-223.

Martín-Hernández, F., and Hirt, A. M., 2003, The anisotropy of magnetic susceptibility in biotite, muscovite and chlorite single crystals: Tectonophysics, v. 367, no. 1, p. 13-28.

Martins, H. C., Sant'Ovaia, H., Abreu, J., Oliveira, M., and Noronha, F., 2011, Emplacement of the Lavadores granite (NW Portugal): U/Pb and AMS results: Comptes Rendus Geoscience, v. 343, no. 6, p. 387-396.

McBirney, A. R., 2007, Igneous petrology, Jones & Bartlett Learning.

McBirney, A. R., and Murase, T., 1984, Rheological properties of magmas: Annual Review of Earth and Planetary Sciences, v. 12, p. 337.

McCaffrey, K., 1992, Igneous emplacement in a transpressive shear zone: Ox Mountains igneous complex: Journal of the Geological Society, v. 149, no. 2, p. 221-235.

McCaffrey, K., and Petford, N., 1997, Are granitic intrusions scale invariant?: Journal of the Geological Society, v. 154, no. 1, p. 1-4.

McKenzie, D., 1984, The generation and compaction of partially molten rock: Journal of Petrology, v. 25, no. 3, p. 713-765.

Meighan, I., and Neeson, J., 1979, The Newry igneous complex, county Down: Geological Society, London, Special Publications, v. 8, no. 1, p. 717-722.

Meighan, I. G., Hamilton, M., Gamble, J., Ellam, R., and Cooper, M., The Caledonian Newry Complex, NE Ireland: New U-Pb ages, a sub-surface extension and magmatic epidote, *in* Proceedings 46th Irish Geological Research Meeting, abstract, Irish Journal of Earth Sciences2003.

Miles, A., Graham, C., Hawkesworth, C., Gillespie, M., Dhuime, B., and Hinton, R., 2013, Using zircon isotope compositions to constrain crustal structure and pluton evolution: the Iapetus Suture Zone granites in Northern Britain: Journal of Petrology, p. egt065.

Miller, J. S., 2008, Assembling a pluton… one increment at a time: Geology, v. 36, no. 6, p. 511-512.

Miller, R. B., and Paterson, S. R., 1994, The transition from magmatic to high-temperature solid-state deformation: implications from the Mount Stuart batholith, Washington: Journal of Structural Geology, v. 16, no. 6, p. 853-865.

-, 1999, In defense of magmatic diapirs: Journal of Structural Geology, v. 21, no. 8, p. 1161-1173.

-, 2001, Construction of mid-crustal sheeted plutons: examples from the north Cascades, Washington: Geological Society of America Bulletin, v. 113, no. 11, p. 1423-1442.

Miller, R. B., Paterson, S. R., and Matzel, J. P., 2009, Plutonism at different crustal levels: Insights from the~ 5–40 km (paleodepth) North Cascades crustal section, Washington: Geological Society of America Special Papers, v. 456, p. 125-149.

Mishra, D., 2011, Gravity and magnetic methods for geological studies, BS Publications and CRC Press, USA.

Molyneux, S., and Hutton, D., 2000, Evidence for significant granite space creation by the ballooning mechanism: the example of the Ardara pluton, Ireland: Geological Society of America Bulletin, v. 112, no. 10, p. 1543-1558.

-, 2000, Evidence for significant granite space creation by the ballooning mechanism: the example of the Ardara pluton, Ireland: Geological Society of America Bulletin, v. 112, no. 10, p. 1543-1558.

Morfin, S., Sawyer, E. W., and Bandyayera, D., 2014, The geochemical signature of a felsic injection complex in the continental crust: Opinaca Subprovince, Quebec: Lithos, v. 196, p. 339-355.

Morgan, S., Law, R., and de Saint Blanquat, M., 2013, Forceful emplacement of the Eureka Valley–Joshua Flat–Beer Creek composite pluton into a structural basin in eastern California; internal structure and wall rock deformation: Tectonophysics, v. 608, p. 753-773.

Morrish, A., and Yu, S., 1955, Dependence of the coercive force on the density of some iron oxide powders: Journal of Applied Physics, v. 26, no. 8, p. 1049-1055.

Morrish, A. H., 1994, Canted antiferromagnetism: hematite.

Mrazec, L., 1927, Les plis diapirs et le diapirienne en general: Inst. Geol. Roumanie, Comptes-rendus, v. 6, p. 226-272.

Murphy, F., and Hutton, D., 1986, Is the Southern Uplands of Scotland really an accretionary prism?: Geology, v. 14, no. 4, p. 354-357.

Myers, J. S., 1975, Cauldron subsidence and fluidization: mechanisms of intrusion of the Coastal Batholith of Peru into its own volcanic ejecta: Geological Society of America Bulletin, v. 86, no. 9, p. 1209-1220.

Néel, L., 1948, Magnetic properties of ferrites: ferrimagnetism and antiferromagnetism: Ann. Phys, v. 3, p. 137.

Neeson, J. C., 1984, The geology and geochemistry of the Newry igneous complex, Northern Ireland [Unpublished PhD thesis]: Queen's University, Belfast.

Neilson, J., Kokelaar, B., and Crowley, Q., 2009, Timing, relations and cause of plutonic and volcanic activity of the Siluro-Devonian post-collision magmatic episode in the Grampian Terrane, Scotland: Journal of the Geological Society, v. 166, no. 3, p. 545-561.

Nockolds, S. R., 1940, The Garabal Hill-Glen Fyne igneous complex: Quarterly Journal of the Geological Society, v. 96, no. 1-4, p. 451-511.

Oldershaw, W., 1974, The Lochnagar granitic ring complex, Aberdeenshire: Scottish Journal of Geology, v. 10, no. 4, p. 297-309.

Oliver, G., and Leggett, J., 1980, Metamorphism in an accretionary prism: prehnite-pumpellyite facies metamorphism of the Southern Uplands of Scotland: Transactions of the Royal Society of Edinburgh: Earth Sciences, v. 71, no. 04, p. 235-246.

Oliver, G. J., Wilde, S. A., and Wan, Y., 2008, Geochronology and geodynamics of Scottish granitoids from the late Neoproterozoic break-up of Rodinia to Palaeozoic collision: Journal of the Geological Society, v. 165, no. 3, p. 661-674.

O'reilly, W., 1984, Rock and mineral magnetism, Blackie Glasgow.

Owens, W., 1974, Mathematical model studies on factors affecting the magnetic anisotropy of deformed rocks: Tectonophysics, v. 24, no. 1, p. 115-131.

Owens, W., and Bamford, D., 1976, Magnetic, seismic, and other anisotropic properties of rock fabrics: Philosophical Transactions of the Royal Society of London. Series A, Mathematical and Physical Sciences, v. 283, no. 1312, p. 55-68.

Parman, S. W., and Grove, T. L., 2004, Harzburgite melting with and without H2O: Experimental data and predictive modeling: Journal of Geophysical Research: Solid Earth (1978–2012), v. 109, no. B2.

Paterson, S. R., and Fowler Jr, T. K., 1993, Re-examining pluton emplacement processes: Journal of Structural Geology, v. 15, no. 2, p. 191-206.

Paterson, S. R., Fowler Jr, T. K., Schmidt, K. L., Yoshinobu, A. S., Yuan, E., and Miller, R. B., 1998, Interpreting magmatic fabric patterns in plutons: Lithos, v. 44, no. 1, p. 53-82.

Paterson, S. R., Pignotta, G. S., and Vernon, R. H., 2004, The significance of microgranitoid enclave shapes and orientations: Journal of Structural Geology, v. 26, no. 8, p. 1465-1481.

Paterson, S. R., and Vernon, R. H., 1995, Bursting the bubble of ballooning plutons: A return to nested diapirs emplaced by multiple processes: Geological Society of America Bulletin, v. 107, no. 11, p. 1356-1380.

Paterson, S. R., Vernon, R. H., and Tobisch, O. T., 1989, A review of criteria for the identification of magmatic and tectonic foliations in granitoids: Journal of structural geology, v. 11, no. 3, p. 349-363.

Pauling, L., 1938, The nature of the interatomic forces in metals: Physical Review, v. 54, no. 11, p. 899.

Petford, N., 1996, Dykes or diapirs?: Geological Society of America Special Papers, v. 315, p. 105-114.

-, 2003, Rheology of granitic magmas during ascent and emplacement: Annual Review of Earth and Planetary Sciences, v. 31, no. 1, p. 399-427.

Petford, N., Cruden, A., McCaffrey, K., and Vigneresse, J.-L., 2000, Granite magma formation, transport and emplacement in the Earth's crust: Nature, v. 408, no. 6813, p. 669-673.

Petronis, M., O'Driscoll, B., Stevenson, C., and Reavy, R., 2012, Controls on emplacement of the Caledonian Ross of Mull Granite, NW Scotland: Anisotropy of magnetic susceptibility and magmatic and regional structures: Geological Society of America Bulletin, p. B30362. 30361.

-, 2012, Controls on emplacement of the Caledonian Ross of Mull Granite, NW Scotland: Anisotropy of magnetic susceptibility and magmatic and regional structures: Geological Society of America Bulletin, p. B30362. 30361.

Petrovský, E., and Kapička, A., 2006, On determination of the Curie point from thermomagnetic curves: Journal of Geophysical Research: Solid Earth (1978–2012), v. 111, no. B12.

Pfeiffer, H., and Schüppel, W., 1994, Temperature dependence of the magnetization in fine particle systems and the Hopkinson effect. Application to barium ferrite powders: Journal of magnetism and magnetic materials, v. 130, no. 1, p. 92-98.

Picard, D., Arbaret, L., Pichavant, M., Champallier, R., and Launeau, P., 2013, The rheological transition in plagioclase-bearing magmas: Journal of Geophysical Research: Solid Earth, v. 118, no. 4, p. 1363-1377.

Pitcher, W.S., 1979, The nature, ascent and emplacement of granitic magmas: Journal of the Geological Society, v. 136, no. 6, p. 627-662.

-., 1997, The nature and origin of granite, Springer.

Pitcher, W. S., Berger, A. R., and Spencer, M. O., 1972, The geology of Donegal: a study of granite emplacement and unroofing, Wiley-Interscience New York.

Plissart, G., Diot, H., Monnier, C., Mărunţiu, M., and Berger, J., 2012, Relationship between a syntectonic granitic intrusion and a shear zone in the Southern Carpathian-Balkan area (Almăj Mountains, Romania): Implications for late Variscan kinematics and Cherbelezu granitoid emplacement: Journal of structural geology, v. 39, p. 83-102.

Pons, J., Barbey, P., Nachit, H., and Burg, J.-P., 2006, Development of igneous layering during growth of pluton: the Tarçouate Laccolith (Morocco): Tectonophysics, v. 413, no. 3, p. 271-286.

Potter, D. K., and Stephenson, A., 1988, Single-domain particles in rocks and magnetic fabric analysis: Geophysical Research Letters, v. 15, no. 10, p. 1097-1100.

Pownall, J. M., Waters, D. J., Searle, M. P., Shail, R. K., and Robb, L. J., 2012, Shallow laccolithic emplacement of the Land's End and Tregonning granites, Cornwall, UK: Evidence from aureole field relations and PT modeling of cordierite-anthophyllite hornfels: Geosphere, v. 8, no. 6, p. 1467-1504.

Rabillard, A., Jolivet, L., Arbaret, L., Laurent, V., Bessiere, E., and Menant, A., Granitoids and extensional shear zones in the Aegean Sea (Greece), interactions during Metamorphic Core Complexes formation, *in* Proceedings EGU General Assembly Conference Abstracts2014, Volume 16, p. 5146.

Radhakrishnamurty, C., and Likhite, S., 1970, Hopkinson effect, blocking temperature and Curie point in basalts: Earth and Planetary Science Letters, v. 7, no. 5, p. 389-396.

Ramberg, H., 1981, The role of gravity in orogenic belts: Geological Society, London, Special Publications, v. 9, no. 1, p. 125-140.

Ramsay, J. G., 1989, Emplacement kinematics of a granite diapir: the Chindamora batholith, Zimbabwe: Journal of Structural Geology, v. 11, no. 1, p. 191-209.

Raposo, M. I. B., Chaves, A. O., Lojkasek-Lima, P., D'Agrella-Filho, M. S., and Teixeira, W., 2004, Magnetic fabrics and rock magnetism of Proterozoic dike swarm from the southern São Francisco Craton, Minas Gerais State, Brazil: Tectonophysics, v. 378, no. 1, p. 43-63.

Ratajeski, K., Glazner, A. F., and Miller, B. V., 2001, Geology and geochemistry of mafic to felsic plutonic rocks in the Cretaceous intrusive suite of Yosemite Valley, California: Geological Society of America Bulletin, v. 113, no. 11, p. 1486-1502.

Reid Jr, J. B., Evans, O. C., and Fates, D. G., 1983, Magma mixing in granitic rocks of the central Sierra Nevada, California: Earth and Planetary Science Letters, v. 66, p. 243-261.

Reid, M., 2003, Timescales of magma transfer and storage in the crust: Treatise on geochemistry, v. 3, p. 167-193.

Reubi, O., and Blundy, J., 2009, A dearth of intermediate melts at subduction zone volcanoes and the petrogenesis of arc andesites: Nature, v. 461, no. 7268, p. 1269-1273.

Reynolds, D. L., 1934, The eastern end of the Newry Igneous Complex: Quarterly Journal of the Geological Society, v. 90, no. 1-4, p. 585-636.

Reynolds, D. L., 1936, The two monzonitic series of the Newry Complex: Geological Magazine, v. 73, no. 08, p. 337-364.

-, Granitisation of hornfelsed sediments in the Newry granodiorite of Goraghwood quarry, Co. Armagh, *in* Proceedings Proceedings of the Royal Irish Academy. Section B: Biological, Geological, and Chemical Science1942, JSTOR, p. 231-267.

-., 1943, The South-Western End of the Newry Igneous Complex. A Contribution towards the Petrogenesis of the Granodiorites Read 23 June, 1943 [Plates XXI and XXII]: Quarterly Journal of the Geological Society, v. 99, no. 1-4, p. 205-246.

Reynolds, J. M., 2011, An introduction to applied and environmental geophysics, John Wiley & Sons.

Richey, J.E, 1928, Structural relations of the Mournes Granites (Northern Ireland): Quaternary Journal of the Geological Society of London, v. 83, p. 653.

-., 1932, II.—Tertiary Ring Structures in Britain: Transactions of the Geological Society of Glasgow, v. 19, no. 1, p. 42-140.

Roberts, W., and Ahlblom, B., 1978, A nucleation criterion for dynamic recrystallization during hot working: Acta Metallurgica, v. 26, no. 5, p. 801-813.

Rochette, P., 1987, Magnetic susceptibility of the rock matrix related to magnetic fabric studies: Journal of Structural Geology, v. 9, no. 8, p. 1015-1020.

Rochette, P., Jackson, M., and Aubourg, C., 1992, Rock magnetism and the interpretation of anisotropy of magnetic susceptibility: Reviews of Geophysics, v. 30, no. 3, p. 209-226.

-, 1992, Rock magnetism and the interpretation of anisotropy of magnetic susceptibility: Reviews of Geophysics, v. 30, no. 3, p. 209-226.

Roni, E., Westerman, D. S., Dini, A., Stevenson, C., and Rocchi, S., 2014, Feeding and growth of a dyke–laccolith system (Elba Island, Italy) from AMS and mineral fabric data: Journal of the Geological Society, v. 171, no. 3, p. 413-424.

Rubin, J. N., Henry, C. D., and Price, J. G., 1993, The mobility of zirconium and other "immobile" elements during hydrothermal alteration: Chemical Geology, v. 110, no. 1, p. 29-47.

Ruprecht, P., Bergantz, G. W., Cooper, K. M., and Hildreth, W., 2012, The crustal magma storage system of Volcán Quizapu, Chile, and the effects of magma mixing on magma diversity: Journal of Petrology, v. 53, no. 4, p. 801-840.

Saltus, R., Hill, P., Connard, G., Hudson, T., and Barnett, A., 1999, Building a magnetic view of Alaska, [Open-file report] U.S. Geological Survey.

Sawka, W., Chappell, B., and Kistler, R., 1990, Granitoid compositional zoning by side-wall boundary layer differentiation: evidence from the Palisade Crest Intrusive Suite, central Sierra Nevada, California: Journal of Petrology, v. 31, no. 3, p. 519-553.

Sawyer, E., 1996, Melt segregation and magma flow in migmatites: implications for the generation of granite magmas: Geological Society of America Special Papers, v. 315, p. 85-94.

Schetselaar, E. M., Chung, C.-J. F., and Kim, K. E., 2000, Integration of Landsat TM, Gamma-Ray, Magnetic, and Field Data to Discriminate Lithological Units in Vegetated: Remote Sensing of Environment, v. 71, no. 1, p. 89-105.

Schetselaar, E. M., Harris, J., Lynds, T., and de Kemp, E., 2007, Remote Predictive Mapping 1. Remote Predictive Mapping (RPM): A Strategy for Geological Mapping of Canada's North: Geoscience Canada, v. 34, no. 3.

Schulmann, K., Mlčoch, B., and Melka, R., 1996, High-temperature microstructures and rheology of deformed granite, Erzgebirge, Bohemian Massif: Journal of Structural Geology, v. 18, no. 6, p. 719-733.

Schwerdtner, W., 1990, Structural tests of diapir hypotheses in Archean crust of Ontario: Canadian Journal of Earth Sciences, v. 27, no. 3, p. 387-402.

Searle, M., Cottle, J., Streule, M., and Waters, D., 2010, Crustal melt granites and migmatites along the Himalaya: melt source, segregation, transport and granite emplacement mechanisms: Geological Society of America Special Papers, v. 472, p. 219-233.

Shan, Y., Lin, G., Li, Z., and Suen, H., 2004, Continuous restoration of deformed shapes through the construction of a reverse displacement gradient and its application to granite emplacement in central North China: Journal of structural geology, v. 26, no. 1, p. 71-85.

Sibson, R. H., 1994, Crustal stress, faulting and fluid flow: Geological Society, London, Special Publications, v. 78, no. 1, p. 69-84.

Simancas, J. F., Galindo-Zaldívar, J., and Azor, A., 2000, Three-dimensional shape and emplacement of the Cardenchosa deformed pluton (Variscan Orogen, southwestern Iberian Massif): Journal of Structural Geology, v. 22, no. 4, p. 489-503.

Simpson, C., and Aust, K., 1972, Grain boundary migration: Surface Science, v. 31, p. 479-497.

Smith, J., 2004, Determining the size and shape of blocks from linear sampling for geotechnical rock mass classification and assessment: Journal of structural geology, v. 26, no. 6, p. 1317-1339.

Smithies, R., and Champion, D., 2000, The Archaean high-Mg diorite suite: links to tonalite–trondhjemite–granodiorite magmatism and implications for early Archaean crustal growth: Journal of Petrology, v. 41, no. 12, p. 1653-1671.

Solano, J., Jackson, M., Sparks, R., Blundy, J., and Annen, C., 2012, Melt segregation in deep crustal hot zones: a mechanism for chemical differentiation, crustal assimilation and the formation of evolved magmas: Journal of Petrology, v. 53, no. 10, p. 1999-2026.

Soper, N., 1986, The Newer Granite problem: a geotectonic view: Geological Magazine, v. 123, no. 03, p. 227-236.

Soper, N., Strachan, R., Holdsworth, R., Gayer, R., and Greiling, R., 1992, Sinistral transpression and the Silurian closure of Iapetus: Journal of the Geological Society, v. 149, no. 6, p. 871-880.

Soper, N., and Woodcock, N., 2003, The lost Lower Old Red Sandstone of England and Wales: a record of post-Iapetan flexure or Early Devonian transtension?: Geological Magazine, v. 140, no. 06, p. 627-647.

Soper, N. t., and Woodcock, N., 1990, Silurian collision and sediment dispersal patterns in southern Britain: Geological Magazine, v. 127, no. 06, p. 527-542.

Spector, A., and Grant, F., 1970, Statistical models for interpreting aeromagnetic data: Geophysics, v. 35, no. 2, p. 293-302.

Stavrev, P., and Gerovska, D., 2000, Magnetic field transforms with low sensitivity to the direction of source magnetization and high centricity: Geophysical Prospecting, v. 48, no. 2, p. 317-340.

Stephens, W., 1992, Spatial, compositional and rheological constraints on the origin of zoning in the Criffell pluton, Scotland: Geological Society of America Special Papers, v. 272, p. 191-200.

Stephens, W., and Halliday, A., 1984, Geochemical contrasts between late Caledonian granitoid plutons of northern, central and southern Scotland: Transactions of the Royal Society of Edinburgh: Earth Sciences, v. 75, no. 02, p. 259-273.

Stevenson, C., 2004, Granite emplacement and magma flow in contrasting tectonic environments using AMS [Unpublished PhD thesis]: University of Birmingham.

-., 2009, The relationship between forceful and passive emplacement: The interplay between tectonic strain and magma supply in the Rosses Granitic Complex, NW Ireland: Journal of Structural Geology, v. 31, no. 3, p. 270-287.

Stevenson, C. T., Hutton, D. H., and Price, A. R., 2006, The Trawenagh Bay Granite and a new model for the emplacement of the Donegal Batholith: Transactions of the Royal Society of Edinburgh: Earth Sciences, v. 97, no. 04, p. 455-477.

Stevenson, C. T., O'Driscoll, B., Holohan, E. P., Couchman, R., Reavy, R. J., and Andrews, G. D., 2008, The structure, fabrics and AMS of the Slieve Gullion ring-complex, Northern Ireland: testing the ring-dyke emplacement model: Geological Society, London, Special Publications, v. 302, no. 1, p. 159-184.

Stevenson, C. T., Owens, W. H., Hutton, D. H., Hood, D. N., and Meighan, I. G., 2007a, Laccolithic, as opposed to cauldron subsidence, emplacement of the Eastern Mourne pluton, N. Ireland: evidence from anisotropy of magnetic susceptibility: Journal of the Geological Society, v. 164, no. 1, p. 99-110.

Stevenson, C. T., Owens, W. H., and Hutton, D. H., 2007b, Flow lobes in granite: The determination of magma flow direction in the Trawenagh Bay Granite, northwestern Ireland, using anisotropy of magnetic susceptibility: Geological Society of America Bulletin, v. 119, no. 11-12, p. 1368-1386.

Stewart, M., Strachan, R., Martin, M., and Holdsworth, R., 2001, Constraints on early sinistral displacements along the Great Glen Fault Zone, Scotland: structural setting, U–Pb geochronology and emplacement of the syn-tectonic Clunes tonalite: Journal of the Geological Society, v. 158, no. 5, p. 821-830.

Stipp, M., StuÈnitz, H., Heilbronner, R., and Schmid, S. M., 2002, The eastern Tonale fault zone: a 'natural laboratory'for crystal plastic deformation of quartz over a temperature range from 250 to 700 C: Journal of Structural Geology, v. 24, no. 12, p. 1861-1884.

Stone, P., and Evans, J., A comparison of the Skiddaw and Manx groups (English Lake District and Isle of Man) using neodymium isotopes, *in* Proceedings Proceedings of the Yorkshire Geological and Polytechnic Society1997, Volume 51, Geological Society of London, p. 343-347.

Stone, P., and Merriman, R., 2004, Basin thermal history favours an accretionary origin for the Southern Uplands terrane, Scottish Caledonides: Journal of the Geological Society, v. 161, no. 5, p. 829-836.

Streckeisen, A., 1976, To each plutonic rock its proper name: Earth-Science Reviews, v. 12, no. 1, p. 1-33.

Sullivan, W., Boyd, A., and Monz, M., 2013, Strain localization in homogeneous granite near the brittle–ductile transition: A case study of the Kellyland fault zone, Maine, USA: Journal of Structural Geology, v. 56, p. 70-88.

Tarling, D., and Hrouda, F., 1993, Magnetic anisotropy of rocks, Springer.

Tarney, J., and Jones, C., 1994, Trace element geochemistry of orogenic igneous rocks and crustal growth models: Journal of the Geological Society, v. 151, no. 5, p. 855-868.

Tatsumi, Y., 1982, Origin of high-magnesian andesites in the Setouchi volcanic belt, southwest Japan, II. Melting phase relations at high pressures: Earth and Planetary Science Letters, v. 60, no. 2, p. 305-317.

-, 1986, Formation of the volcanic front in subduction zones: Geophysical Research Letters, v. 13, no. 8, p. 717-720.

Taubeneck, W. H., 1967, Petrology of Cornucopia tonalite unit, Cornucopia stock, Wallowa mountains, northeastern Oregon: Geological Society of America Special Papers, v. 91, p. 1-54.

Thirlwall, M., 1981, Implications for Caledonian plate tectonic models of chemical data from volcanic rocks of the British Old Red Sandstone: Journal of the Geological Society, v. 138, no. 2, p. 123-138.

Thompson, A. B., 1999, Some time-space relationships for crustal melting and granitic intrusion at various depths: Geological Society, London, Special Publications, v. 168, no. 1, p. 7-25.

Thompson, R., and Oldfield, F., 1986, Environmental magnetism, Springer.

Tripathi, K., Sen, K., and Dubey, A., 2012, Modification of fabric in pre-Himalayan granitic rocks by post-emplacement ductile deformation: insights from microstructures, AMS, and U–Pb geochronology of the Paleozoic Kinnaur Kailash Granite and associated Cenozoic leucogranites of the South Tibetan Detachment zone, Himachal High Himalaya: International Journal of Earth Sciences, v. 101, no. 3, p. 761-772.

Uyeda, S., Fuller, M., Belshe, J., and Girdler, R., 1963, Anisotropy of magnetic susceptibility of rocks and minerals: Journal of Geophysical Research, v. 68, no. 1, p. 279-291.

van den Eeckhout, B., Grocott, J., and Vissers, R., 1986, On the role of diapirism in the segregation, ascent and final emplacement of granitoid magmas—discussion: Tectonophysics, v. 127, no. 1, p. 161-166.

Vance, J. A., 1961, Zoned granitic intrusions—an alternative hypothesis of origin: Geological Society of America Bulletin, v. 72, no. 11, p. 1723-1727.

Vernon, R., 2000, Review of microstructural evidence of magmatic and solid-state flow: Visual Geosciences, v. 5, no. 2, p. 1-23.

Vernon, R., and Paterson, S., 1993, The Ardara pluton, Ireland: deflating an expanded intrusion: Lithos, v. 31, no. 1, p. 17-32.

Vigneresse, J. L., 1990, Use and misuse of geophysical data to determine the shape at depth of granitic intrusions: Geological Journal, v. 25, no. 3-4, p. 249-260.

Vigneresse, J. L., Barbey, P., and Cuney, M., 1996, Rheological transitions during partial melting and crystallization with application to felsic magma segregation and transfer: Journal of Petrology, v. 37, no. 6, p. 1579-1600.

Vonsovskii, S. V. e., and Hardin, R., 1974, Magnetism, Wiley New York.

Walker, F., 1924, A marginal modification of the Ballachulish granite: Geological Magazine, v. 61, no. 12, p. 550-554.

Wang, T., Wang, X., and Li, W., 2000, Evaluation of multiple emplacement mechanisms: the Huichizi granite pluton, Qinling orogenic belt, central China: Journal of Structural Geology, v. 22, no. 4, p. 505-518.

Weinberg, R. F., 1996, Ascent mechanism of felsic magmas: news and views: Geological Society of America Special Papers, v. 315, p. 95-103.

Weinberg, R. F., 1999, Mesoscale pervasive felsic magma migration: alternatives to dyking: Lithos, v. 46, no. 3, p. 393-410.

Weinberg, R. F., Sial, A., and Mariano, G., 2004, Close spatial relationship between plutons and shear zones: Geology, v. 32, no. 5, p. 377-380.

Weinberg, R. F., Mark, G., and Reichardt, H., 2009, Magma ponding in the Karakoram shear zone, Ladakh, NW India: Geological Society of America Bulletin, v. 121, no. 1-2, p. 278-285.

White, S., 1976, The effects of strain on the microstructures, fabrics, and deformation mechanisms in quartzites: Philosophical Transactions of the Royal Society of London. Series A, Mathematical and Physical Sciences, v. 283, no. 1312, p. 69-86.

Wilson, B. M., 1989, Igneous petrogenesis a global tectonic approach, Springer.

Bond, W. L., 1957, Physical properties of crystals: Their representation by tensors and matrices: JF Nye: Clarendon Press, Oxford, 322 pp., Pergamon.

Wu, F.-y., Jahn, B.-m., Wilde, S., and Sun, D.-y., 2000, Phanerozoic crustal growth: U–Pb and Sr–Nd isotopic evidence from the granites in northeastern China: Tectonophysics, v. 328, no. 1, p. 89-113.

Yan, D.-P., Zhou, M.-F., Zhao, D., Li, J.-W., Wang, G.-H., Wang, C.-L., and Qi, L., 2011, Origin, ascent and oblique emplacement of magmas in a thickened crust: An example from the Cretaceous Fangshan adakitic pluton, Beijing: Lithos, v. 123, no. 1, p. 102-120.

Yang, J.-H., Chung, S.-L., Wilde, S. A., Wu, F.-y., Chu, M.-F., Lo, C.-H., and Fan, H.-R., 2005, Petrogenesis of post-orogenic syenites in the Sulu Orogenic Belt, East China: geochronological, geochemical and Nd–Sr isotopic evidence: Chemical Geology, v. 214, no. 1, p. 99-125.

Yoder, H., 1973, Contemporaneous basaltic and rhyolitic magmas: American Mineralogist, v. 58, no. 3-4, p. 153-171.

Yoshinobu, A. S., and Girty, G. H., 1999, Measuring host rock volume changes during magma emplacement: Journal of Structural Geology, v. 21, no. 1, p. 111-116.

Young, S. W., 1976, Petrographic textures of detrital polycrystalline quartz as an aid to interpreting crystalline source rocks: Journal of Sedimentary Research, v. 46, no. 3.

Žák, J., Verner, K., Klomínský, J., and Chlupáčová, M., 2009, “Granite tectonics” revisited: insights from comparison of K-feldspar shape-fabric, anisotropy of

magnetic susceptibility (AMS), and brittle fractures in the Jizera granite, Bohemian Massif: International Journal of Earth Sciences, v. 98, no. 5, p. 949-967.

Zener, C., 1951, Interaction between the d-shells in the transition metals. II. Ferromagnetic compounds of manganese with perovskite structure: Physical Review, v. 82, no. 3, p. 403.

Zhu, Y., Sun, S., Gu, L., Ogasawara, Y., Jiang, N., and Honma, H., 2001, Permian volcanism in the Mongolian orogenic zone, northeast China: geochemistry, magma sources and petrogenesis: Geological Magazine, v. 138, no. 02, p. 101-115.

Zibra, I., 2012, Syndeformational granite crystallisation along the Mount Magnet Greenstone Belt, Yilgarn Craton: evidence of large-scale magma-driven strain localisation during Neoarchean time: Australian Journal of Earth Sciences, v. 59, no. 5, p. 793-806.